Sheffield Hallam University

A Sheffield Hallam University thesis

00814

ProQuest Number: 10701256

ProQuest 10701256

FATIGUE CRACK GROWTH IN

IRON SILICON ALLOYS

by

W GEARY

A thesis submitted to the Council for
National Academic Awards in partial
fulfilment for the Degree of:

DOCTOR OF PHILOSOPHY
IN METALLURGY

Collaborating Establishment:-   Sponsoring Establishment:-

Sheffield Laboratories   Department of Metallurgy
Swinden House   Sheffield City Polytechnic
British Steel Corporation   SHEFFIELD
ROTHERHAM
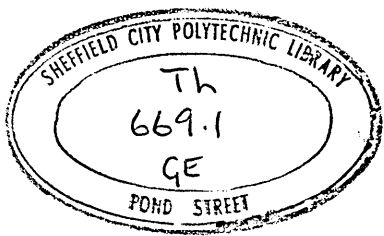
It seems to me an art comprising great knowledge, for I know of no art or activity whatever, excluding the sciences and painting, that does not need this as its principal member. Therefore, in my opinion, if it were not for the nobility of the material, I would say that the smith working in iron should justly take precedence over the goldsmith because of the great benefit that he brings.

<div style="text-align: right;">Vannoccio Biringuccio 1540</div>

CONTENTS

Preface

All the work reported in this thesis was carried out during the period for which the candidate was registered for a higher degree.

In accordance with the regulations for PhD in Industrial Metallurgy, a full course in Metallurgical Process and Management was successfully completed. The details of the course are given below:-

MODULE 1

Process Metallurgy

Mechanical Metallurgy

Advanced Thermodynamics

MODULE 2

Accountancy

Micro-economics and Financial Control

Computational Methods and Operational Research

MODULE 3

Powder Metallurgy

High Strength Steels

Heat Treatment and Transformations

Atmospheric Pollution and Control

Corrosion Resistant and High Temperature Alloys

Automatic and Computer Control

MODULE 4

Industrial Case Studies

One of the case studies, which is related to the current research work, is attached with the thesis, as Appendix 1.

The candidate's performance during the above mentioned courses was assessed by means of written examinations and continuous assessment of specific assignments.

Acknowledgements

The author is heavily indebted to Mr P Leggett, Mr F Walker,
and Dr P James for their continuous support, encouragement
and advice throughout the duration of the work.

Grateful appreciation is also expressed to the technical
staff of the Department of Metallurgy and British Steel
Corporation, Swinden Laboratories whose services were
invaluable. Special thanks are due to Dr I M Austen
and Mr C Lindley.

The author would also like to express his gratitude to
Dr A W D Hills, Head of Department of Metallurgy,
for provision of facilities for the work. Sincere
gratitude is also due to Dr M J May, Research Manager,
for provision of facilities at Swinden Laboratories.

ABSTRACT

Fatigue Crack Propagation in Iron-Silicon Alloys

by

W Geary 1985

A technique for accurately monitoring fatigue crack growth
at near threshold growth rates has been established. The
characteristics of near threshold fatigue crack growth of
a number of iron-silicon alloys has been quantitatively and
qualitatively investigated. Relationships have been
established relating the stress intensity factor, ΔK, and
the fatigue crack growth rate da/dN. At fatigue crack
growth rates approaching threshold the material has shown
some microstructural sensitivity and this has been related
to the stress intensity factor and the yield stress.

A relationship has been shown to exist between the value
of the threshold stress intensity factor and the inverse root
of the grain size, $d^{-\frac{1}{2}}$, for each of the alloys investigated.
A model for near threshold fatigue crack growth has been
proposed and includes the contributions made by grain
size and crack tip plasticity.

This work has also shown that fatigue crack closure plays
an important role in the micromechanisms of fatigue crack
growth near the threshold at low R ratio s. A number of
mechanisms have been identified: crack closure due to
the presence of oxidation products on fracture surfaces
in tests conducted in air, and closure due to the presence
of fatigue fretting, facet contact and a contribution
of mixed mode opening.

INTRODUCTION

Little is currently known about the micromechanisms of fatigue crack propagation at near threshold growth rates. It is important from a design point of view that engineering and metallurgical data of this sort are provided to allow design of components and selection of materials capable of withstanding a large number of cycles at low stress intensity factor ranges for lifetimes up to 10^{12} cycles.

Most studies of fatigue crack propagation have confirmed that the crack growth rate da/dN is a function of the alternating stress intensity factor, ΔK, through the power law expression da/dN = $C(\Delta K)^n$. The expression, however, over estimates the growth rate as ΔK approaches ΔK_{Th}.

Much work has been done on near threshold fatigue crack growth on a wide variety of materials. However, the majority of data has been obtained on complex alloy systems of direct industrial application. These complex, multiphase, industrial alloys are not ideally suited to the task of determining the basic mechanisms occurring at low fatigue crack growth rates. An iron silicon, single phase, system was considered ideal for the purpose of assessing the effects of variations in grain size on near threshold fatigue crack growth. It was intended during this work to determine the effects of variations in grain size on ΔK_{Th} levels in terms of the micromechanisms of deformation and fracture occurring at the crack tip.

It is known that in pure iron homogeneous wavy slip occurs

and that a change to more planar slip is caused by the

addition of silicon to iron. Screw dislocations tend to

remain on the (110) planes rather than moving by cross slip

onto other planes as in pure iron.

Restricted slip systems are produced in the iron silicon

alloys. It was intended during this research to examine

the effects of restricted slip systems on near threshold

fatigue crack growth rates and the interrelationships

between slip behaviour, crack tip plasticity and grain size.

This was to be achieved by the production of a series of iron

silicon alloys and the use of thermomechanical treatments to

produce a variable grain size. A number of compact

tension fatigue specimens were to be tested in tension –

tension fatigue, and monitored by a sensitive technique

to produce data relating the effects of grain size and

solute concentration to the near threshold fatigue crack

growth of these alloys.

1   REVIEW OF LITERATURE

1.1   STRESS DISTRIBUTION AROUND CRACKS AND CRACK TIP PLASTICITY

1.1.1   INTRODUCTION

The primary variable which dictates whether and at what rate fatigue crack propagation occurs under variable loading conditions is the stress configuration immediately adjacent to the crack tip.

A great deal of work has been concentrated on the solution of elastic and elastic/plastic boundary conditions of statically and cyclically loaded cracks. A comprehensive review of stress and strain distributions around cracks is given in the standard texts[1],[2].

Using the stress co-ordinate system shown in Figure 1 after Rice[3], the elastic stress distribution around a geometric stress concentration under Mode 1 opening is given by Figure 2 (a). Under plane strain conditions where no through thickness relaxation can occur, σ_{zz} arises in order to maintain elastic strain continuity. In plane stress the value of σ_{zz} is zero and the distribution of σ_{xx} is diminished as contraction is allowed in the Z direction. The edge of a body, in essentially plane strain, will be in plane stress and the distribution is shown in Figure 2 (b).

The elastic distribution around a crack in Mode 1 opening has been given by Irwin[4].

$$\begin{pmatrix} \sigma_{xx} \\ \tau_{xy} \\ \sigma_{yy} \end{pmatrix} = K_I \ (2\pi r)^{-\frac{1}{2}} \ \text{Cos}(\theta/2) \begin{pmatrix} 1 - \text{Sin}(\theta/2) \ \text{Sin}(3\theta/2) \\ \text{Sin}(\theta/2) \ \text{Cos}(3\theta/2) \\ 1 + \text{Sin}(\theta/2) \ \text{Sin}(\theta/2) \end{pmatrix} \qquad - 1$$

$\tau_{xz} = \tau_{yz} = 0 \ \sigma_z = 0$ Generalised plane stress

$\sigma_z = \nu(\sigma_x + \sigma_y)$ Plane strain

K_I is the stress intensity factor for Mode I type opening and is simply related to the elastic energy release rate. Other equations exist for Modes II and III openings, incorporating the respective stress intensity factors K_{II} and K_{III}.

Once determined, the stress intensity parameter K allows comparison of crack tip elastostatics independent of specimen geometry, crack length or applied stress.

If the ideal case of a crack of length 2a situated in an infinite body subject to a stress σ_a in Mode I opening is considered then the stress intensity at the crack tip is defined as

$$K_I = \sigma_a \ \sqrt{\pi a} \qquad\qquad - 2$$

In a cracked body of finite dimensions this equation is modified by a dimensionless geometric parameter, Y, to allow for specific boundary conditions.

$$K_I = Y \ \sigma_a \ \sqrt{\pi a} \qquad\qquad - 3$$

When a body containing a crack is stressed elastically, it is possible to produce high stresses at the crack tip which may locally exceed the material's yield stress to produce a plastic zone. The occurrence of plasticity under plane

2

strain conditions causes σ_{xx} to rise at a much greater rate than would be expected in order to maintain continuity of the elements (Figure 3).

A simple estimation of the size of the plastic zone at the head of the crack under plane strain conditions is given by Irwin[4].

The elastic stress distribution shown in Figure 4 (a) is altered by an amount of yielding, Figure 4 (b), which is small compared with the crack length and the dimensions of the body. The plastic zone is considered to extend a small distance ahead of the crack tip. Within this zone the tensile stress σ_{yy} is equal to the yield stress.

An underestimate of the plastic zone size, ω, can be obtained by equating σ_{yy} with the yield stress (σ_{ys}), Figure 4 (c). This is an underestimate as the stress depicted by the shaded area $\sigma_{yy} = \sigma_{ys}$ and

$$\sigma_{yy} = \frac{K_I}{\sqrt{2\pi r}} \qquad - 4$$

is available for further yielding.

The magnitude of r_y is then given by:-

$$r_y = \frac{K_I^2}{2\pi \sigma_{ys}^2} \qquad - 5$$

The shaded area can be shown to be equal to half the total area under the curve up to $r = r_y$ and it has been conventional to equate w to a first approximation as:-

$$W = 2r_y = \frac{K_I^2}{\pi \sigma_{ys}^2} \qquad\qquad - 6$$

The plane strain plastic zone is reduced to 1/3 to account for the effects of triaxiality on yielding and therefore the plane strain plastic zone size is given by:-

$$W = \frac{1}{3\pi} \left(\frac{K_I}{\sigma_{ys}}\right)^2 \qquad\qquad - 7$$

The elastic stress distribution ahead of a crack can be described by a modified stress intensity factor, K^*, where:-

$$K^* = \sigma \sqrt{[\pi(a + r_y)]} \qquad\qquad - 8$$

1.1.2   CYCLIC PLASTIC ZONE FORMATION

It is assumed (see Figure 5) that the central region of a thick test piece deforms under plane strain conditions; local yielding occurs around the crack tip; high constraints are set up and a triaxial stress state is developed.

For a given crack opening displacement the plastic zone size in plane stress is much larger than for plane strain because yielding spreads under a shear stress component which incorporates the full value of the local tensile stress. The strain gradient in plane strain immediately ahead of the crack is steep and crack extension is easier to achieve.

Figure 6 shows a schematic stress displacement curve for the region immediately ahead of the crack tip during a stress cycle. The specimen is unloaded from the peak of

the tensile stroke, the local stresses at the crack tip
unloaded elastically and then become compressive. Some
reverse plastic flow is then obtained when the compressive
stresses become equal to the flow stress in compression.
The amount of reversed flow at zero overall displacement
is given by the amount of flow corresponding to a material
with a flow stress $2\sigma_{ys}$. Then the reversed plastic zone
size can be estimated from:-

$$W = \frac{1}{3\pi}\left(\frac{\Delta K}{2\sigma_{ys}}\right)^2 \qquad\qquad - 9$$

The stress distribution produced by the displacement curve,
Figure 6, is indicated in Figure 7 (c), when a cracked
body is loaded by a system of stresses proportional to L,
and the loading parameter is reduced by a quantity ΔL to the
lower level L-ΔL. On unloading a new reversed plastic
zone is formed embedded in the plastic zone accompanying
the original loading.

In practice complete reversal of the load is prevented by
the intervention of crack closure.

1.2 EXPERIMENTAL EVIDENCE OF PLASTICITY

Crack tip plasticity, as characterised by linear elastic
fracture mechanics, is a prerequisite for fatigue crack
growth and a number of workers have investigated this
plasticity experimentally.

Surface techniques [5-7] of plastic zone measurement will
refer effectively to plane stress conditions whilst internal
methods [6-11] may refer to a state of stress anywhere

5

between plane strain and plane stress, being dependent upon loading and geometrical considerations.

Evidence of the effect of state of stress on zone shape and magnitude has been provided by several techniques [8], [6].

Weiss and Meyerson [5] using two surface measurement techniques showed that the size and shape of the plastic zone produced by fully reversed bending fatigue is virtually unpredictable but in general they observed zones smaller than theoretically predicted. They suggest that local micro-structural conditions such as the heterogeneous pre-cipitiation of carbides in austenitic steels, at the crack tip control the spread of plasticity.

Hahn et al [8] verified the existence of two distinct regions of plasticity surrounding a fatigue crack. Etch pitting techniques revealed a region of highly strained material adjacent to the crack, sharply delineated from a lightly strained region spreading further into the bulk of the material, indicating the presence of cyclic and mono-tonic plastic zones.

Dislocation structures that exist around propagating fatigue cracks have been the subject of investigation by a number of workers [12], [10], [11]. The majority of this work has been carried out on f.c.c. materials where dislocation structures are found to exist as cell substructures and loops dependent upon ΔK, strain amplitude and stacking fault energy.

Other investigations[5] have been carried out using resistivity techniques and metallographic studies involving linear analysis of the deformed material. Results suggested that plastic zone sizes and shapes are controlled by local microstructural conditions at the crack tip rather than stress intensity~~factor~~ range . Electron channeling contrast techniques have also been used to investigate cyclic deformation and subcell formation in fatigue crack propagation of a variety of materials[13].

1.3 INTERMEDIATE RANGE FATIGUE CRACK GROWTH

1.3.1 MODELS

It is now widely recognised that fatigue crack growth rate, da/dN, can be related to the alternating stress intensity factor ($\Delta K = K_{max} - K_{min}$) by the simple power law:-

$$\frac{da}{dN} = C(\Delta K_I)^n \qquad\qquad - 10$$

where C and n are constants[14].

This equation gives an adequate, but not complete, description of behaviour for mid-range growth rates, (ie approximately $10^{-6} - 10^{-3}$ mm/cycle for air). At higher growth rates when K_{max} approaches K_{IC}, the fracture toughness, equation 10 underestimates the propagation rate[15], whereas at lower growth rates it is found to be conservative as ΔK approaches the threshold ΔK, ΔK_{Th} , below which fatigue crack growth cannot be detected. (see Figure 8)

It has been suggested[16],[17] that at high growth rates the

final acceleration to instability occurs at some critical value of K_{max} and is consistent with the linkage of independantly initiated facets. The model developed for pearlite/martensite structures suggested that as a fatigue crack encountered a band of martensite a smaller plastic zone is produced, due to the higher yield stress, the tensile stress is therefore higher and the martensite band cleaves. As K_{max} increases more cleavage takes place and the uncleaved ligaments fail by tearing or accelerated fatigue crack growth and the static modes of failure become increasingly self sustaining.

Other models have also been produced involving static failure mode variables but taking into account cleavage failure modes[18, 19].

Robinson et al[20], working on α titanium, found the fatigue fracture process involved the formation of faceted regions, primarily ΔK controlled, and their interconnection by local plastic tearing (primarily K_{max} controlled). The mechanism was seen as a discontinuous process on a microscopic scale. Some grains, dependent upon their crystallographic orientation, fractured to produce faceted regions.

Crack growth by this faceting process will be restrained due to the presence of unbroken interconnected ligaments, and those ligaments will in turn be subjected to increasing stresses caused by the fracture of the surrounding material. It was suggested that any factor, such as low R ratio,

that increased the difficulty of attaining a sufficient tensile stress level to cause ligament failure would reduce the overall growth rate.

Knott[21], [22] has suggested a model based upon the coalecence of microvoids formed around MnS inclusions (Figure 9). The mechanism proposed suggested that inclusions near a sharp crack are subject to increased strains. Voids form at low plastic strains because the MnS particles are bonded very poorly to the ferrite matrix. Void growth is limited until they are subjected to higher plastic strains and triaxial stresses which are concentrated in the region of the crack tip. The growth mechanism entails the growth of the crack, by an opening and blunting mode, and propagation to the nearest void.

Attempts have been made to describe region 'C' fatigue crack growth where equation 10 is not applicable. Typical of these equations is[23] –

$$\frac{da}{dN} = A \left[\frac{\Delta K^4}{\sigma_{UTS}^2 (K_c^2 - K_{max}^2)} \right]^{0.73} \qquad - 11$$

where A = A numerical constant which varies slightly with
     the material

     K_c = Fracture toughness

which describes fatigue crack propagation as K_{max} approaches the fracture toughness in pearlitic structures.

Others[24] have proposed models based on the formation of striations, the work hardening of material ahead of the

crack tip[25], the propagation rate as a function of loading
parameters and material properties such as elastic modulus
and cyclic yield stress:-

$$\frac{da}{dN} = \frac{\Delta K^2}{\alpha \pi E \, \sigma_{yc} \, \varepsilon_F} \qquad - 12$$

where α = A material constant having a value between 1 and 2

E = Elastic modulus of the material

σ_{yc} = Cyclic yield stress of the material

ε_F = A fracture strain term

and
$$\frac{da}{dN} = +\beta \left(\frac{K^2_{max} - K^2_{min}}{K_{IC}^2} + \text{In} \, \frac{K_{IC}^2 - K^2_{max}}{K_{IC}^2 - K^2_{min}} \right) \qquad - 13$$

where β is a material constant.

1.3.2 MECHANISMS

It has been widely reported[26] that at low ΔK values,
approaching threshold, and at high K_{max} values approaching
K_{IC} fatigue crack growth is sensitive to microstructure.
The mechanism of growth in the intermediate fatigue crack
growth range has been established by many workers[16], [27], [28]
as striation growth[29], [30], [31], [32] and the Paris equation
is obeyed in this range[16], [33], [31], [34]. Research has shown
that each striation is produced by one cycle although every
cycle does not necessarily produce one striation[35].

Laird[36] and others[37] considered the production of ductile
striations involves the alternate blunting and re-
sharpening of the crack tip, as shown by Figure 13, and
growth controlled by the local crack tip alternating plastic

deformation[24]. Others have considered a shear decohesion model appropriate in this growth regime (see Figure 14).

McMillan and Pelloux[37] proposed a plastic blunting mechanism for the production of striations which is supported by the data produced by other workers[38]. Striation spacings have been shown to correspond closely with macroscopic fatigue crack growth rates[38],[8], however, ductile fracture modes and cleavage have been found to be associated with striations[22].

Others[39] have postulated that a transition from structure sensitive to structure insensitive growth occurs in the intermediate growth regime. Results indicated that the relationship between the plastic zone size and the grain size, or some controlling microstructural parameter, was a controlling factor in this transition.

Gerberich et al[40] have shown that where combined ductile and brittle modes of fracture are observed then the constant, C, in the Paris relationship depends in a complex way on the stress intensity required to nucleate cleavage:-

$$\frac{da}{dN} = \frac{\Delta K^4}{C \, \sigma_{ys}^2 \left[\dfrac{1}{1 + 8/\pi \, \text{Sec}^{-1}(K_{max}/K_{nucl})^{\frac{1}{2}}} - \dfrac{1}{3} \right]^2} \qquad -14$$

where C = a constant dependent upon grain size

K_{nucl} = the stress intensity required to nucleate cleavage

11

1.3.3   MEAN STRESS EFFECTS

1.3.3.1   INTRODUCTION

Whilst it has been shown that fatigue crack growth is insensitive to changes in mechanical parameters such as frequency, waveform[41] and thickness[42] early investigations on a number of materials[43] have shown constants n and c in the Paris relationship may be influenced by intermediate fatigue crack growth rates[44].

However, most investigations[45], [34], [46] have shown the effect of mean stress to be negligible in the intermediate fatigue crack growth range, growth being primarily dependant upon the alternating stress intensity where growth appears to be controlled by the amount of crack opening per cycle[29] and is dependent upon the crack tip plasticity and ultimately on the elastic modulus[30]. A marked influence of mean stress has been observed at high fatigue crack growth rates approaching K_{IC} and also at growth rates approaching threshold (Figure 15).

Irving and Kurzfeld[47] have shown for tests carried out in vacuum, on quenched and tempered steel, that no influence of mean stress is present at low values of ΔK, however, some influence is observed at higher values. In contrast, Ohta et al[48], working on stainless steel found a influence of R ratio at all values of ΔK.

A number of workers have indicated that the influence of R ratio on fatigue crack propagation may be partly

explained by the mechanism of fracture. Investigations have shown that as the mean stress increases the proportion of cleavage increases and the overall propagation rate accelerates. Richie and Knott[49] have found that provided the fracture mechanism was normal ductile propagation, producing striations, mean stress had no effect and growth depended on ΔK only and the occurrence of periods of either void coalescence or intergranular fracture lead to mean stress sensitivity.

A factor of ten difference in crack growth rates between R ratios of 0.34 and 0.85 has been reported[44] in cold rolled mild steel; this was attributed to the presence of residual stresses introduced as a result of cold working.

Frost et al[43] reported the influence of mean stress levels in an Al 5.5% Zn alloy to be attributable to the presence of hard intermetallic impurities in the alloy causing periods of fast fracture accompanying normal fatigue crack growth.

Static modes of failure have been reported by a number of workers[45], [50] to account for R ratio effects, and in the absence of these static modes, growth rates are insensitive to mean stress levels.

Work on a high nitrogen steel[51] tested near the ductile brittle transition temperature and a temper embrittled steel[49] suggested that cleavage 'bursts' occur at a critical value

of maximum stress intensity factor, K_{max}.

It has been shown for negative R ratio tests[52] that the compression portion of the loading cycle does not significantly affect crack growth rates except when tensile residual stresses are present. It was also indicated that the transition from a ductile mode normal to the crack direction to a shear type mode at 45° to the propagation directions (see Figure 16) occurred at growth rates of 2×10^{-7} to 7.3×10^{-7} mm/cycle for all R values in aluminium alloy sheet, but is dependent upon thickness.

1.4   NEAR THRESHOLD CRACK GROWTH MODELS

A considerable amount of work has been carried out in recent years to determine the mode of failure and nature of near threshold fatigue crack growth. It has been suggested[29] that facet formation observed in the threshold region may be the result of small scale reversed plasticity ie a mode of growth resembling stage I occurring on a grain to grain basis. Although unlike stage I, cracks do not in general form on the primary slip plane it is clear from the large deviations out of the macro-scopic crack growth plane that an element of shear mode growth is involved.

Other workers have produced dislocation models for fatigue crack growth at low stress intensities[12, 53]. Hornbogen et al[12] proposed a dislocation model based upon the relationships between plastic zone sizes and grain sizes. The model is shown schematically in Figure 10. The cyclic

14

plastic zone is approximated by δ_f, the static plastic zone size by δ_s and the grain size by D.

$$\delta_s = \frac{1}{6\pi}\left(\frac{K_{max}}{\sigma_{ys}}\right)^2 \qquad - 15$$

and

$$\delta_f = \frac{1}{8\pi}\left(\frac{\Delta K}{\sigma_{ys}}\right)^2 \qquad - 16$$

where σ_{ys} is the yield stress of the material.

When $\delta_f < \delta_s < D$. Dislocations are nucleated at the crack tip and travel to the interior of the grain until the external stress has exceeded the yield stress.

When $\delta_f < D < \delta_s$. Dislocations pile up at the grain boundary under static stress and cross slip out of one plane becomes more likely than in the previous stage. The size of the pile up in this case is limited to the grain size.

When $D < \delta_f < \delta_s$. As δ_s is larger than δ_f dislocations are nucleated in two or more grains ahead of the moving crack. The size of the pile up is limited by the grain size; additional cross slip and nucleation of slip at grain boundaries.

Sadanada et al[53] introduced a model based on the minimum ΔK required to cause the nucleation of a dislocation at the crack tip,

$$\Delta K_{min} = \frac{2\pi\rho\tau_t}{\cos\theta/2 \, \sin\theta/2 \, \cos\theta/2} \qquad - 17$$

15

where ρ = Distance between dislocation and crack.

τ_t = Total stress necessary to nucleate and move a dislocation from the crack tip.

θ = Crystallographic orientation of the slip system with respect to the crack plane.

The model suggested that the threshold ΔK is nearly independent of all material properties except elastic modulus.

A number of workers have tried to relate the fatigue threshold ΔK to the R ratio.

Masounave and Bailon[54] suggested a relationship of the form,

$$\Delta K_{Th} = \Delta K_o (1 - R) \qquad\qquad - 18$$

where ΔK_o is the stress intensity factor at R = O. This relationship predicts that ΔK_{Th} is a linear function of R only. Other workers[55] have suggested an adaption of this,

$$\Delta K_{Th} = K_o (1 - R)^\gamma \qquad\qquad - 19$$

where γ is a constant.

The data from a number of sources appears to fit an expression of this form.

Davenport and Brook[56] have suggested that a simple power law relationship does not exist and proposed the expression

$$\Delta K_{Th} = \Delta K_o \sqrt[3]{\frac{(K_c - K_{max})(1 - R)}{(K_c - \Delta K_o)}} \qquad\qquad - 20$$

16

which predicts a decreasing threshold ΔK with
increasing R ratio. This equation can be approximated to
the Klesnil and Lukas relationship[55] with exponent 0.33
when K_{max} is equal to $\Delta K_{Th(o)}$ and has been demonstrated
to be appropriate to 0.15% C 1.5% Mn steels.

A model proposed by Schmidt and Paris[168] related the crack
closure phenomena to load ratio effects at the threshold:-

for low load ratio:- $\quad \Delta K_{Th} = K_{max} - K_{min} = K_{max} (1 - R)$ — 21

$$= (K_{CL} + \Delta K_o)(1 - R)$$

for high load ratio:- $K_{max} = \dfrac{\Delta K_{Th}}{1 - R} = \dfrac{\Delta K_o}{1 - R}$ — 22

where ΔK_o = Stress intensity range above K_{CL} necessary to
produce crack growth at the threshold.

$\quad K_{CL}$ = Stress intensity necessary to open crack.

The relationship predicted an R ratio cutoff point above
which threshold ΔK was unaffected by R ratio. The
theory fitted the data for a number of materials.

A model based upon strain controlled fracture criterion
and effective stress intensity factor, ΔK_{eff}

$$\frac{da}{dN} = \frac{2^{1+n}(1 - \nu^2)^{1+n}(\Delta K_{eff}^2 - \Delta K_{cTh}^2)}{4\alpha(1 + n)\pi\sigma_{yc}^{1-n}(E)^{1+n}\varepsilon_f^{1+n}}$$ — 23

where n = Cyclic strain hardening exponent

$\quad \sigma_{yc}$ = Cyclic yield stress

$\quad \varepsilon_f$ = True fracture strain

$\quad \alpha$ = A constant describing the state of stress

17

$$\Delta K_{c\ Th} = \text{Minimum value of } \Delta K_{Th}$$

and has been applied to low alloy steels[57].

A simple model proposed by Masounave et al[55] to explain the grain size effect produced in the near threshold region is based on the microscopic crack path morphology. This model is also the basis of one produced by Priddle[59]. Near threshold facture surfaces are characterised by considerable zig-zag deviations of the fatigue crack from the plane normal to the principal stress. The magnitude of the deviations is greater in coarse grained material than in fine (Figure 11). Fracture mechanics theory applies to a crack which is assumed to grow perpendicular to the principal stress. In practice the ΔK value is lower than that predicted from the stress intensity calibration. Crack deviation away from the plane of maximum tensile stress leads to a reduction in K_I and and increase in K_{II} stress intensity components (Figure 12). Further reduction in ΔK arises due to an increase in the real crack surface area compared to that obtained from macroscopic measurements.

Modelling crack growth, particularly near the threshold is difficult since the influence of microstructure on mode I/mode II growth must be considered. It is even more complex if the crack is advancing in a discontinuous manner, held up at various points along its leading edge by microstructural obstacles. McEvily[60] has proposed a model where growth is related to the crack opening displacement with a modification to take into account

18

the contributions of static modes of separation in the growth process,

$$\frac{da}{dN} = \frac{A}{\sigma_{ys}E} \left(\Delta K - \Delta K_{Th(R)} \right)^2 \left(1 + \frac{\Delta K}{K_c - K_{max}} \right) \qquad - 24$$

where $\Delta K_{Th(R)} = \sqrt{\frac{1 - R}{1 + R}} \, \Delta K_{Th(o)}$ $\qquad - 25$

σ_{ys} = Yield Stress

E = Youngs Modulus

A = A material constant depending upon material and environment

K_c = Fracture Toughness

Others[61], [62] have attempted to include a component to take into account crack closure effects (see Section 1.5.3.7) on the unloading part of fatigue cycle. This has lead to the formation of further equations:-

$$\frac{da}{dN} = C^1 (\Delta K_{eff})^{m^1} \qquad - 26$$

where ΔK_{eff} is the effective ΔK and is equal to K_{max} - K opening.

The relationship between $\frac{da}{dN}$ and K_{eff} has been shown to be linear for low carbon steels[61].

Tanaka[63] has proposed an empirical relationship taking into account microstructure , material strength, fracture toughness and specimen thickness, for ductile steels in the intermediate to threshold range:-

$$\frac{da}{dN} = 1.700 \times 10^{-4}(\Delta K/103.6)^m - 10^6 \qquad - 27$$

and

$$\Delta K_{Th} = 163.6(5.88 \times 10^{-3})^{1/m} \qquad - 28$$

Other relationships have been determined for brittle steels. Petit and co workers[64] have proposed a relationship which describes crack propagation from the threshold to intermediate rate and include an environmental constant.

$$\frac{da}{dN} = e(R, \alpha) \left[\left(1 - \frac{K_{Th}}{K_{max}} \right)^\alpha \frac{K_{max}}{K_{Th}} \right]^m \qquad - 29$$

where m is a constant depending upon the environment.

Further models attempt to include terms describing the critical crack root radius, the strain distribution and the plastic zone size:-

$$\Delta K_{Th} = E \, \varepsilon_f \sqrt{2\pi \, \rho_{min}} \qquad - 30$$

where ρ_{min} = Critical crack root radius

E = Youngs Modulus

ε_f = Real fracture strain.

1.5 FATIGUE THRESHOLDS

1.5.1 INTRODUCTION

Little is currently known about the micromechanisms of fatigue crack progagation at near threshold growth rates. It is important from a design point of view that engineering

20

and metallurgical data of this type is provided to allow design of components and materials[65], capable of withstanding high frequency low amplitude loading for lifetimes up to 10^{12} cycles.

Most studies of fatigue crack propagation have confirmed that the crack growth rate da/dN is a function of the alternating stress intensity ΔK through the power law expression,

$$da/dN = C(\Delta K)^n \qquad\qquad - 10$$

The expression, however, overestimates the growth rate as ΔK approaches ΔK_{Th}.

It is well established[17], [33], [66] that a threshold for fatigue crack propagation does exist. However, the exact nature of this threshold has yet to be adequately described. The micromechanisms of low growth rate fatigue are complex and a study of the literature[67] indicates that at least 10 different propagation modes are claimed to occur. Other than metallurgical variables there are a number of factors which may lead to an increase in threshold:- crack tip blunting, bifurcation, closure and residual stresses.

1.5.2   <u>MEAN STRESS EFFECTS</u>

1.5.2.1   <u>INTRODUCTION</u>

The influence of mean stress is often expressed in terms of load ratio, R, (= K_{min}/K_{max}), while it is known that

there is little influence of load ratio in the mid-range, growth rates near the threshold have been identified as being sensitive to load ratio (Figure 17)

It has been widely reported[65-76] that decreasing the load ratio, increasing grain size[20] and increasing the intersititial alloying content all produce significant reductions in fatigue crack propagation rates at low ΔK.

Cooke et al[17] noted that the threshold fatigue crack growth behaviour was dominated by the R ratio such that K_{max} rather than ΔK controlled the kinetics; K_{max} at the threshold remained relatively constant over the range of R values. Others have observed K_{max} control on threshold values up to specific values above which threshold values tended to be ΔK controlled.

Richie found the increased dependence of ΔK_{Th} on strength[12] was less marked at high R ratios (Figure 18). McEvily et al[77] working on Ti-6Al-4V has found reasonable comparison of results with an expression of the form,

$$K_{Th} = \sqrt{\frac{1 - R}{1 + R}}\, K_{Th(o)} \qquad\qquad - 31$$

where $K_{Th(o)}$ is the threshold at R = O

Many other attempts have been made to relate the threshold ΔK to mean stress, one by Radhakrishnan[78] appears to fit experimental data for steels and aluminium alloys:-

$$\log (\Delta K)_{Th} = \left(-\frac{1.25}{n} + 1.14 \right) + 0.7 \log(1 - R) \qquad - 32$$

where n is a constant.

The load ratio dependence on near threshold growth, however, is found to be lower with increasing temperature[68] and inert environments[37], [46], [77].

Experiments carried out on En 24 and Ti-6Al-4V in vacuum[46] indicated that near threshold crack propagation rates and the value of ΔK_{Th} were completely independent of load ratio. This lack of R dependence for tests in inert conditions has been confirmed for low alloy martensitic steels tested in vacuum[47].

Other studies of Ti-6Al-4V show that for tests in vacuum the dependence of the threshold on mean stress is markedly reduced though not eliminated[79] the value of the threshold was significantly higher than in air.

These results indicate that the effect of load ratio on near threshold fatigue crack propagation rate may be attributed, in part, to some environmental interaction. The lack of load ratio effect on higher, mid-range growth rates is consistent with this since the environment may be unable to keep pace with the crack velocity.

More recent explanations of the load ratio effect have centred around the phenomenon of crack closure[68-70] which suggests that as the R ratio is decreased then a value of R is reached where the crack closes as the minimum of the stress cycle is approached. The crack closure,

occuring at positive loads above K_{min}, reduces the effective ΔK applied and therefore produces a higher value of ΔK_{Th}.

1.5.3   MICROSTRUCTURAL FACTORS

1.5.3.1   MATERIAL STRENGTH

Investigations have indicated that fatigue crack propagation in metals is largely independent of yield strength[67] and Lindley and Richards have found that raising the strength level by an order of magnitude does not affect the crack growth rate, over the mid-range, by more than a factor of two or three[80].

The effect of material strength on intermediate growth rates has been investigated by Dowse and Richards[81], working on low alloy steel weldments.   They observed a marked reduction of crack propagation rate when a crack reached the hardened heat affected zone of the weld and con-sidered this to be due to a reduction in the plastic zone size.   No difference in crack propagation mechanism was observed between parent metal and heat affected zone.

However, at near threshold levels, material strength has been observed to have a large effect on the value of the threshold, ΔK_{Th}[79] (see Figures 18, 19).   In low strength ferrite-pearlite steels, values of threshold have been observed to decrease significantly with increasing strength[58], [176], [82].   A large effect has been observed for high strength martensitic steels where the controlling measure of strength was the cyclic rather

than the monotonic yield strength[29]. Coarse grained precipitation hardened ferritic microstructures significantly lower growth rates near the threshold and have a more pronounced effect than higher strength bainitic or martensitic structures[83]. The effects of yield strength on ΔK_{Th} have been summarised for a number of steels (see Figure 20).

The effect of strength on near-threshold crack propagation behaviour is significantly less at high R values[29]. Varying the strength in low strength steels may involve variations in the ferrite grain size which also has a strong effect on near-threshold behaviour[58], [19], [34].

The effect of tempering temperature has been investigated for a low alloy steel[85] and a peak value of threshold ΔK obtained as a function of tempering temperature (as the tempering temperature is raised then the U.T.S and the yield strength decrease continuously) (see Figure 21). The threshold is then dependent on strength level on one side of the maxima and a characteristic material parameter on the other. Therefore a suitable combination is required to give the optimum threshold value. Results showed that a coarse grain size and lath martensite gives inferior thresholds compared with a mixture of plate martensite and lath martensite formed in finer grained material.

The dependence of ΔK_{Th} on strength may be due to a number of factors, such as - larger plastic zones in lower strength material may retard crack growth.

Alternatively higher strength steels may be more susceptible
to the effects of hydrogen, due to higher equilibrium
solubility of hydrogen.

1.5.3.2   GRAIN SIZE EFFECTS AND CRACK TIP PLASTICITY

1.5.3.2.1   INTRODUCTION

It has been shown that grain refining can be beneficial in
raising the fatigue limit or the endurance strength of
materials[86]. Most studies at intermediate growth rates
have shown that grain size has little effect. However,
a number of studies on titanium alloys and steels indicate
that a grain size effect is present at higher growth rates
[67] (see Figure 22).

At very low growth rates an effect has also been shown to
exist. Several workers[57], [29], [87], [88] have observed an
improved resistance to near threshold propagation with
an increase in grain size (see Figure 23).

A number of investigators[89] have reported a linear
relationship between threshold and grain size, whilst
others[58], [61] have shown the threshold value to vary
linearly with the square root of the grain size.

Robinson and Beevers[20] have reported an order of magnitude
decrease in near threshold growth rates in α Titanium after
coarsening the grain size from 20 to 200 μm. Similar
effects have been observed in Ti-6Al-4V. A marked increase
in threshold ΔK values has also been observed in a range
of low strength steels by increasing the ferrite grain

26

size, [58], [90], [76]. In these studies material strength was not controlled and the effect of grain coarsening may have been masked by a decrease in material strength.

Comparisons of threshold stress intensity values as a function of grain size, at constant yield strength, have been made in high strength steels[29], [30], [72] and it has been determined that coarsening the prior austenite grain size by an order of magnitude led to a decrease in near threshold growth rate but left the threshold value unchanged; further data on low strength steels indicated a strong grain size affect on the normalised threshold[13].

An increase in the threshold of duplex structures with an increase in the grain size has been attributed to a decrease in notch sensitivity with a decrease in strength level. It was shown[26] that the martensitic phase was a barrier to crack growth and a crack could only propagate if the plastic zone size exceeded the size of the martensitic phase.

Masounave and Bailon[18] have shown a linear relationship to exist between the threshold stress intensity ΔK_{Th} and the grain size $d^{\frac{1}{2}}$(Figure 24) and produced an expression relating ΔK_{Th} to $d^{\frac{1}{2}}$.

$$\Delta K_{Th} = (1 - R) (\Delta K_{o} + K_{f}d^{\frac{1}{2}}) \qquad - 33$$

where ΔK_{o} = Threshold when R = 0

K_{f} = Factor dependent upon the local stress ahead of the crack.

27

The threshold ΔK has also been shown to vary linearly with the monotonic yield stress[89] and the mean stress[79]. Thompson[90] has suggested that the influence of grain size on fatigue, in a low carbon steel, may be correlated with the ease of cross slip of the system.

In contrast to other workers Robin et al[91] found no significant effect of grain size on the fatigue threshold, in aluminium alloy. Fracture surfaces consisted of flat facets separated by steps, the facets being approximately equal to the grain size. They determined that the relationship between the grain size and the plastic zone size was not significant in the transition from crystallographic type growth to non-crystalographic growth. Transition occurred at a constant growth rate independent of grain size.

Higo et al[92], working on Cu-Al alloys, have noted a regular increase in fatigue crack threshold with $d^{-\frac{1}{2}}$ which becomes more pronounces as the stacking fault energy is decreased (see Figure 25). The fatigue fracture surfaces showed a high proportion of intergranular facets at low ΔK levels. Their explanation suggested that a process depending on reversed dislocation movement at the crack tip was a function of the alternating plastic strain amplitude. Lower strains would be developed in higher yield strength material for a given ΔK; if a critical value of alternating plastic strain amplitude, $\Delta \varepsilon p$, were required to produce crack

growth then this would require a higher ΔK so that an increase of ΔK_{Th} with yield stress would be expected.

If a constant reversed plastic zone size were required to propagate a crack then ΔK_{Th} would vary in a linear manner with yield stress.

1.5.3.2.2   PLASTICITY EFFECTS

It has been observed by many workers[29] that the threshold condition is achieved when the reversed plastic zone size is of the order of the grain size.

Robinson et al[20] have noted the occurrence of grain orientation control when the reversed plastic zone size was approximately equal to the grain size.

Others[33] have shown that as the reversed plastic zone size exceeds the scale of the microstructure a growth mode occurs which is insensitive to microstructure, R ratio, and to a large extent environment. Where the reverse plastic zone size is smaller than the scale of the microstructure, stage I type growth occurs and this process tends to be K_{max} rather than ΔK dependant.

A number of workers[61], [67] have reported the transition from structure insensitive growth to structure sensitive growth to occur when the reversed plastic zone size was of the order of the grain size. The dislocation structure ahead of a crack and the effect of a change in grain size is schematically shown by Lindigkeit et al[93], [95] in Figure 26.

Taira et al[61] working on low carbon steel, showed that the ratio of the reversed plastic zone size, W_{rev}, to the grain size, d, to be of the order of 1.5 - 2. They proposed that the threshold condition is determined by whether the slip band near the crack tip propagated into an adjacent grain or not, and that the slip band propagation was governed by the ΔK at the slip band tip. It was suggested that the microscopic K could be approximated by:-

$$K^m = K - K_{fr}^* \qquad\qquad - 33$$

$$\text{where } K_{fr}^* = 2\sqrt{2}\ \sigma_{fr}^* \sqrt{\xi_F/\pi} \qquad\qquad - 34$$

and σ_{fr}^* = flow stress in the slip zone

ξ_F = size of the slip band zone in the forward direction

and thus $K = K^m + 2\sqrt{2}\ \sigma_{fr}^* \sqrt{\xi_F/\pi}$ $\qquad\qquad - 35$

and at the threshold

$$K_{Th} = K^m_{CVH} + 2\sqrt{2}\ \sigma_{fr}^* \sqrt{P2S/\pi} \qquad\qquad - 36$$

Gerberich et al[67] suggest that although the R.P.Z.S might be fundamental to the transition from microstructure sensitive to microstructure insensitive growth near the threshold, this zone was an order of magnitude smaller that the controlling microstructural parameter in Ti-6Al-4V. They also reported a poor correlation between the R.P.Z.S and ΔK_{Th} in steel.

These workers indicated that at the threshold, the stress distributions associated with the crack, which is a

semi-cohesive zone associated with the selective cleavage of the microstructure and the plastic zone, must be in equilibrium. An expression was derived for a central crack length 2c in an infinite plate:-

$$\pi\sigma - 2\sigma_{sc}\cos^{-1}\left(\frac{c}{a}\right) - 2(\sigma_{ys} - \sigma_{sc})\cos^{-1}\left(\frac{b}{a}\right) = 0 \qquad - 37$$

where σ = Applied stress

σ_{sc} = Stress in semi-cohesive zone

σ_{ys} = Yield stress in plastic zone

2c = Real crack size

2b = Real crack + semi-cohesive zone size

2a = Fictitious crack containing all three zones

The agreement with experimental results from a number of sources was reasonable, (see Figure 27).

1.5.3.3 EFFECT OF GRAIN BOUNDARY SEGREGATION

It is well known that grain boundary segregation can severely impair toughness of low alloy steels (temper embrittlement).

A study has been conducted[72] on the effects of impurity segregation on near threshold fatigue crack propagation, in an ultra high strength steel. (Tests were conducted at the same grain size and yield stress). It was determined that no difference in propagation rates was observed between the unembrittled and embrittled structures at mid-range growth rates. At near threshold levels, impurity induced embrittlement gave rise to vastly accelerated growth rates and a corresponding reduction in

31

ΔK_{Th} at both high and low R ratios.

This effect was accompanied by a significant increase in the proportion of intergranular fracture in the embrittled steel close to the threshold. This effect at low growth rates compares to little or no effect at intermediate rates.

1.5.3.4   EFFECT OF MATERIAL PURITY

It has been observed that crack propagation rates are considerably enhanced by the presence of impurities in steel (see Figure 28). Evans et al[94], working on En 24, showed a threefold decrease in propagation rates in high purity alloys compared with a standard commercial alloy, at near threshold ΔK.

Differences in growth rates were most apparent in the Paris regime; the growth data tending to converge near the threshold. Less convergence of data was observed in tests carried out in vacuum, however, differences in tempering temperature were also shown to affect growth rates.

1.5.3.5   MICROSTRUCTURE AND MECHANISMS

The importance of microstructural parameters in very low growth rate fatigue has been the subject of study by a number of workers and it is known that changes in the microstructure in, for example, weldments,[95] can lead to a considerable difference in growth rates. A decrease in the interlamellar spacing, in the absence of ferrite matrix hardening, increases the threshold values for

fatigue crack propagation in pearlitic steels[96].

Although it has been widely reported[24] that near threshold
fatigue crack propagation is sensitive to microstructure,
the precise mechanisms are not known. Macroscopically
a band of corrosion product is generally observed on
fracture surfaces in the area where growth rates have
been less than $10^{-6} - 10^{-7}$ mm/cycle[17], [46], [74]. This
indicates the presence of environmental action at near
threshold levels even in air.

Microscopically, near threshold growth has been termed
microstructurally sensitive[24], [27], [17], [37], [46] owing to the
presence of isolated planar, transgranular or intergranular
facets within a flat, ductile transgranular mode[17].
Secondary cracking and rough steps may also be present
and may be indicative of environmentally sensitive
fracture. The dependence of intergranular fracture on
ΔK and K_{max} at threshold is shown in Figure 29.

Work on iron carbon alloys[31] determined that failure at
low growth rates was preceeded by intergranular separation
of ferrite grains. Slip lines across these grains indicated
that slip has occurred within them after the passage of the
crack tip. These features were observed to occur when the
reversed plastic zone size was approximately equal to the
grain size.

The appearance of isolated intergranular facets[46] in
addition to ductile striations has been observed by a
number of workers[49]. It has been shown that rates of

growth in the near threshold region vary depending on the type of microstructure present. Fracture surfaces have been observed to be very irregular in appearance and contain many deviations from the primary fracture plane[20]. This scale of irregularity was found to increase with the scale of the microstructure, in agreement with the model proposed by Masounave et al[58]. The mechanism for the formation of these facets in the threshold region is thought to be the result of small scale plasticity, a pseudo stage I mode of growth occurring on a grain to grain basis.

Further investigations suggest that these facets, unlike stage I cracks, do not in general form on the primary slip plane; but is is clear from the deviations that an element of shear is involved.

Irving et al[9] suggested that the formation of fracture facets was aided by shear modes of failure rather than tensile mode I (Figure 12) which operates once the transition to structure insensitive growth has occurred. They conclude that structure sensitive growth consisted of facet formation in a pseudo stage I shear mechanism, coupled with an environmentally assisted failure of the inter-vening regions. It was proposed that a two stage mechanism existed; one part ΔK controlled (the formation of facets at and ahead of the crack tip) and the other K_{max} controlled (the inter-connection of these facets).

Experiments on ultra high strength steel[29] determined that fracture consisted of a flat transgranular mode

34

with isolated segments of intergranular separation. Others
have shown that fracture path topography is strongly
sensitive to the orientation of the grains through which
the crack front passed.

The threshold condition for microscopic fatigue cracks in
two phase microstructures, for example martensite/ferrite,
has been shown to be controlled by the martensite phase,
and a crack growth resistance term $K_{Th(m)}$ represents a
material characteristic. Smaller values of ΔK_1 compared
with $K_{Th(m)}$, will produce non propagating cracks in the
matrix. A further observation suggested that the crack
front near the threshold is moving in a discontinuous
manner with the front being held up at various points
by microstructural obstacles (second phase particles,
ligaments or improperly oriented colonies of grains).

The presence of static modes of failure during fatigue at
low growth rates has been seen to be as a result of
restricted slip systems[34], embrittlement and environmental
influences and it is known that control of the micro-
structure can lead to an improvement in threshold
behaviour[26].

Gerberich et al[67] considered a mixed mode of fracture at
near threshold growth rates where cleavage occurs in large
grains but not in some of the smaller ones. The resulting
ligament acts as a traction on the crack preventing
opening, thus reducing the ΔK at the crack tip.
Alternatively fracture may occur in those grains which
are most favourably orientated and those which are

unfavourably orientated remain as ligaments.

The dynamics of ligament fracture and static discontinuous fracture modes are among a number of variables which may influence very low crack growth rates; others may be crack blunting, crack branching and void formation.

1.5.3.6 THE BEHAVIOUR OF DISLOCATIONS

1.5.3.6.1 INTRODUCTION

It has been known for many years that dislocations play a significant part in the conditions for crack growth[98] and theories of their role are well developed[99], [100], [101].

Work in the early 1960's[102] on fatigue induced dislocation sub-structures in poly-crystalline aluminium showed even at low strains, large concentrations of dislocation loops were found in the vicinity of sub-grain boundaries.

Recent investigations have indicated the presence of dislocation tangles[103] and cell sub-structures[104], [105] adjacent to the crack tip. Katagiri et al[103] have noted in addition to a high density of dislocation tangles a change in sub-structure on lines radiating from the crack tip at 60° to the direction of crack growth. They suggested that the slip band/dislocation structure indicated a complex strain distribution occurring near lines of discontinuity in crystallographic orientation. Intense plastic flow was observed at the tip of the crack along the planes close to the plane of maximum elastic shear stress.

A number of models have assumed that crack growth is facilitated by the nucleation and motion of dislocations at the crack tip. It therefore follows that easier nucleation of dislocations enables crack growth to occur at lower ΔK with less crack tip blunting.

1.5.3.7 CRACK CLOSURE CONCEPTS

Recent theories of fatigue crack growth, particularly in the threshold region, have suggested an effect of crack closure[106] on threshold values.

It has been postulated that as the R ratio is decreased then a value of R is eventually reached where the crack begins to close as the minimum stress intensity of the load is approached. Crack closure reduces the effective ΔK applied to the specimen and so has the effect of raising the apparent threshold stress intensity measured for a given R ratio.

If closure does not occur then the R dependence of ΔK_{Th} disappears.

Alternatively the R ratio effect could be caused by the formation of oxide which acts to hold the crack open at low R ratios leading to a reduction of the effective ΔK applied to the crack and a consequent rise in the apparent ΔK_{Th}. This would also account for the lack of any effect in vacuum.

Work on fully pearlitic steels at low R values[107] has indicated the presence of oxide on the fracture surface

along with an increase in the surface roughness with increasing grain size. It is suggested that the residual plastic deformation present along the path of a growing crack leads to some closure of the crack surfaces at positive values of K_{min}. This leads to an effective reduction of ΔK (ie ΔK_{eff} < ΔK apparent) which is available to act as a crack driving force. At higher R values the crack remains open during the whole of the loading cycle and the role of crack closure disappears.

In oxidising conditions, closure could lead to enhanced corrosion debris formation within the crack tip region by repeated breaking and compacting of the oxide. This could cause increased contact between the crack surfaces thereby decreasing ΔK_{eff} and reducing the crack driving force. It was suggested that the effect of a finer grain size was to reduce roughness. The appearance of a mismatch of striation peaks has also been shown to lead to closure.

Further work on medium strength steels[108], aluminium alloys[109], titanium[110], and nimonic alloys[111] has shown a dependence of crack growth rate, at near threshold values, on crack closure occurring at low R ratios.

The magnitude of the closure effect has been estimated using the equation:-

$$\delta = \frac{K^2(1 - \nu^2)}{2E\ \sigma_{ys}} \qquad\qquad - 38$$

where σ_{ys} = The yield strength

      E   = Youngs Modulus

      δ = Crack opening displacement

This equation has been found to fit well with the size of oxide particles at the crack tip .

The closure phenomena may also be used to explain the effect of strength level on threshold. In higher strength steels, smaller plastic zones are formed ahead of the crack and therefore closure effects will be reduced, giving rise to lower ΔK threshold values, particularly at high stress ratios. If crack closure effects are reduced, then the amount of fretting corrosion products might also be expected to be reduced. The effective stress intensity range of the higher strength material will be closer to the applied ΔK giving higher crack growth rates.
and lower threshold values.

1.5.4   ENVIRONMENTAL ASPECTS OF FATIGUE CRACK GROWTH

1.5.4.1   INTRODUCTION

It has been observed[20], [33] that the stress intensity range, ΔK, required for crack growth in vacuum is very much greater than that required for air (Figure 30). It is therefore important that a complete understanding of the environmental effects in fatigue crack growth be obtained to enable the design engineer to evaluate requirements of components for service in other than vacuum conditions.

1.5.4.2 INFLUENCE OF MICROSTRUCTURE

Observations suggest that environments play an active role at low growth rates[20], [46], [112]. Many workers[47], [113], [114] have found large differences[46], [115], [116] in near threshold growth rates between hydrogen containing environments and vacuum (see Figure 31). Extensive tests carried out in other environments (sea-water[117], Nitrogen[115], 3% NaCl[57]) have also shown considerable differences.

In the intermediate growth range most workers have found little influence of environment[119], although some workers have noted an influence in this range[113], [91]. An increase in crack growth rates by up to a factor of 8 has been observed in aqueous solutions and a critical frequency was determined at which maximum environmental attack occurred [120].

In vacuum little detectable influence of R ratio on growth is observed at low ΔK values[47]. Research also suggests that there is little influence of water vapour on growth rates less than 10^{-5} mm/cycle in quenched and tempered steels. However, at higher ΔK values some influence of R ratio was apparent. Stewart[115] has suggested that the growth rate in an environmental species can be expressed by a simple relationship of the form:-

$$\left(\frac{da}{dN}\right)_{Total} = \frac{1}{f}\left(\frac{da}{dN}\right)_{evn} + \left(\frac{da}{dN}\right)_{mech} \qquad - 39$$

where f is the frequency of testing.

Reports suggest that at low ΔK values, growth becomes increasingly sensitive to K_{max} and under these conditions the influence of environment becomes more marked and non-continuum mechanisms - cleavage, intergranular fracture and void coalescence become operative.

Frandsen et al[8], observed a transition in failure mode from ductile transgranular fracture in vacuum to a mixed inter-granular and transgranular mode in hydrogen. A correlation was shown to exist between the increase in crack prop-agation rate caused by hydrogen and the proportion of intergranular fracture (Figure 32). The maxima correspond to the point where the forward yield plastic zone size is equal to the prior austenite grain size.

The appearance of the fracture surfaces at low growth rates has indicated that cracking mode changes from ductile to 'quasi cleavage'[94] and is consistent with a hydrogen related embrittlement mechanism [114], growth showing a time and maximum stress dependence analogous to stress corrosion cracking, the change in the fracture mode being associated with hydrogen enhancement of fatigue crack growth[121].

Stewart[79], working on two low alloy steels found little influence of environment (hydrogen) at stress intensities close to the threshold and noted that these results were inconsistent with the hypothesis that the effect of strength level and stress ratio on the threshold is as a result of hydrogen embrittlement. He further suggested that the build-up of corrosion products within

the crack by fretting in moist environments also has a marked effect on ΔK_{Th} values at low stress intensities.

Work on Cu-Al alloys[92] suggested that the occurrence of intergranular cracking could be associated with preferential oxidation effects at the crack tip. At low crack growth rates more time is available for preferential oxidation to occur along grain boundaries adjacent to the crack tip. At higher growth rates cracks will propagate more rapidly than oxidation down grain boundaries could occur, and the incidence of intergranular facet formation would fall.

1.5.4.3   MECHANISMS OF CRACK GROWTH IN ENVIRONMENTS

It has been proposed that the microstructural effects observed at near threshold stress intensities (for tests carried out in moist air[29]) could be due to the presence of hydrogen, a semi-qualitative model relating the contribution to fatigue crack propagation from the environmental effect of hydrogen, evolved from the crack tip surface reactions with moist air was proposed. It was also suggested that the observations of lower growth rates in coarser grained material will be due to the diffusion of hydrogen atoms to grain boundaries, ie - transport of hydrogen from crack surface into the metal through the motion of dislocations[122], [123] rather than diffusion[121]. However, the dumping and pickup of H_2 at the grain boundaries has been shown to be a fast process and is not rate limiting[122-123].

Investigators considered that hydrogen was transported on dislocations in Cottrell type atmospheres[124]. The presence of an atmosphere around a dislocation, however, may cause a drag on the dislocation thus reducing their mobility. The hydrogen may then be deposited at micro-structural locations such as grain boundaries, inclusions or microvoids. These locations may then be the critical paths for fracture.

It was further suggested[125] that since the dislocations are unable to travel from grain to grain, hydrogen carrying dislocations which approach grain boundaries will deposit their hydrogen at or near the grain boundaries where the hydrogen atoms are picked up by mobile dislocations emitted from sources in the adjoining grain. It is therefore possible for dislocations to transport hydrogen deep into the plastic zone even at ambient temperature[125].

The concentration of hydrogen atoms reacting at the grain boundaries was thought to be greatest when the maximum plastic zone size is of the order of the grain size. In coarser grained structures the plastic zone size remains small compared to the grain size until much higher stress intensities resulting in a reduced environmental influence.

The formation of microvoids ahead of the crack tip has been observed in ferrite[126] and the segregation of hydrogen to the grain boundaries contributes to the formation of cracks. The observance of the formation of secondary cracks in the elastic-plastic zone head of the crack tip

and their coalescence with the primary crack[84] leads to
the suggestion that crack propagation would only occur
when the local stress[127] exceeds that required to break
the Fe-H-Fe bond. The threshold is then a function of
this local critical stress.

Comparison of fatigue crack propagation data in air and
vacuum, for nickel based alloys[128], indicated that a
higher and more clearly defined threshold occurred in
vacuum; it was proposed that crack blunting resulted in
a rapid approach to a clearly defined threshold. Fatigue
crack propagation was observed to be reduced by slip
reversal. The effect of environment was to retard slip
reversal by oxide pinning of the dislocations. Oxidation
also reduced rewelding of the crack surfaces on unloading.

A model proposed by Lynch[129] suggested that surface lattice
distortion could hinder the nucleation and ingress of
dislocations at the surface since dislocations moving
in the first few atomic layers would be associated with
larger than normal lattice distortions. The effect of
an environmental species present at the crack tip would be
to increase the number of neighbouring atoms, through
chemisorption, and reduce the surface lattice distortion,
thus facilitating dislocation activity at the crack tip.
The model indicated that chemisorption of environments
(liquid metals, aqueous, moist air etc) could therefore
be responsible for enhanced growth rates. The effect
of frequency can be explained on the basis of the effect-
iveness of the environment in promoting crack growth and

is a time dependent process.

At higher crack growth rates the environmental effects
would be expected to disappear, as indicated by a marked
reduction in the proportion of fracture occurring by an
intergranular mechanism. At high cyclic frequencies
the hydrogen atoms will no longer be able to diffuse
sufficiently rapidly to keep pace with a crack tip which
is advancing at a high rate.

Recent investigations have focused on the phenomena of
crack closure and the part played by environmental species
at low growth rates. This is more fully discussed in
section 1.5.3.7.

1.5.4.4   KINETICS OF HYDROGEN EFFECT

Investigations have suggested that the kinetics of the
environmental effect are controlled by the diffusion
of hydrogen to the crack tip, dissociation to atomic
hydrogen at the clean metal surface adsorption into the
metal matrix and finally diffusion through the lattice to
the region of embrittlement. The rate limiting step is
variously thought to be the surface processes[130] and the
long range diffusion of hydrogen[131].

Others have suggested that the controlling mechanism
may be a critical concentration of hydrogen, ie the
applied stress intensity equals the threshold when the
equilibrium concentration of hydrogen at the crack tip
achieves a critical concentration.

1.6   THE FATIGUE CRACK GROWTH OF SILICON IRON

1.6.1   INTRODUCTION

Research on the fatigue crack growth of silicon iron,
particularly in the threshold region, is not common.
However, as a single phase system it is ideally suited
to threshold work and investigations into restricted slip
systems.

The addition of silicon to iron produces solute strength-
ening making it increasingly difficult for cross slip to
occur and restricting plastic deformation within the grains.
It has been reported[18] that additions of silicon to iron
increase crack propagation rates, Figure 33, and also
result in an increasing proportion of cleavage (silicon
decreasing the fracture stress) and that a change from
intergranular to transgranular propagation is observed[132].

The intensive slip band formation which is characteristic
of other materials in cyclic deformation has not been
observed in silicon iron[193]. Others have reported[134], [135]
that dislocations tend to remain on the (110) plane
rather than cross slip readily on to other types of plane
as in pure iron. This leads to an increase of fatigue
resistance, however this improvement cannot be ascribed
solely to the increased resistance to cross slip because
the yield stress of iron is also increased by the addition
of silicon, although other workers report that the yield
stress has little effect on threshold levels of silicon
iron[67].

Earlier work on Fe-Si single crystals[136], [137] indicated that cyclic cleavage is initiated by an increase in the rate of loading[138]. Further investigations[139] on the system have shown that the crack tip opening rate is the controlling factor in determining whether a crack propagates by a ductile or brittle mode. The critical crack opening rate at which the fracture mode changes is temperature dependent and an activation energy for the initiation of cleavage has been determined. The activation energy for dislocation glide agrees well with the activation energy for the transition from ductile to cleavage fracture.

Gerberich et al[140] have proposed a cyclic cleavage crack growth model based on that of Neumann[139] for crack growth in iron and some of its alloys. It was shown that a decrease of a factor of five in crack growth rate occurred on a reduction of temperature from R.T to 233 K in an iron 2% silicon alloy. The yield stress was shown to increase from 199 to 222 MPa over this range of temperature but it seems improbable that such a small increase in yield stress could have such a large effect on the growth rate.

At lower temperatures they reported a further increase in yield stress from 222 to 370 MPa, however this did not reduce the growth rate as might be expected. The cleavage mode became predominant and the trend in growth rates was reversed.

Similar behaviour was noted for Fe 2.5% Ni alloy where

growth rates were shown to increase by almost a factor of 30 as the temperature falls to 173 K which corresponds to an increase in yield strength 160 to 240 MPa.

Gerberich et al[67] noted that a 1% silicon addition to iron decreased the ductile/brittle transition temperature slightly while greater amounts of silicon increase it. Small additions of silicon produced solute softening and therefore the yield stress is actually lower than the pure iron at 173°K.

Neumann et al[141] stated that alternating activation of two intersecting slip planes results in crack growth and showed that in 'quasi-brittle' crack propagation in Fe-3% Si the activation energy for brittle crack initiation was equal to the activation energy of dislocation motion.

The low cycle fatigue of Cu-Al polycrystalline materials has been shown to produce 'cell substructures' ahead of the fatigue crack. Dislocation 'bands' and 'tangles' were observed parallel to the primary slip planes which is indicative of the planar dislocation arrays encountered in low stacking fault energy material. Dislocation bands occurred at all strain ranges; slip band coarsening occurred as the strain level was increased.

Recent work on grain orientated silicon iron[143] has suggested that the appearance of cleavage facets on the fatigue fracture surface is associated with inhomogeneous deformation along the crack front. Results indicated a reverse plastic displacement, δ_R, almost two orders of

magnitude larger than the growth rate and suggested that
the occurrence of crack closure provided a possible
explanation.

Further work on similar material[144] indicated that crack
growth occurred by means of slip occurring at the apex of
the crack tip; slip of upper and lower slip planes formed
new surfaces at the crack tip during the loading cycle,
crack closure occurred by means of reverse slip at the
apex during the unloading cycle. The deformation cycle
was found to coincide with the slip directions of the
material and deformation in the reverse direction was
found during the unloading cycle.

2 EXPERIMENTAL PROCEDURES

2.1 MATERIALS

High purity Japanese electrolytically refined iron melted in a Scotvac vacuum furnace under an atmosphere of argon together with small quantities of silicon was used to obtain the desired composition. Initially twelve 5 kg ingots were produced with silicon contents varying from 0 to 4%.

A further series of four ingots were subsequently produced containing small quantities of aluminium and nitrogen. It was hoped to produce a fine dispersion of aluminium nitrides in order to produce a degree of grain boundary pinning and retardation of grain growth.

A third series of eight ingots was produced to supplement the first in the mechanical working and heat treatment experiments.

2.1.1 CHEMICAL COMPOSITION

Tables 1, 2 and 3 show the chemical composition of the three series of material respectively. Analysis was determined using a combination of wet and X-ray analytical techniques on samples representative of the melt. The analysis of base materials is given in Table 4 and the analysis of residual and tramp elements for series 3 material is given in Table 5.

2.1.2 MECHANICAL WORKING AND HEAT TREATMENTS

The cast ingots, of initial dimensions approximately 230 x 60 x 60 mm, were cropped (to remove pipe) and skimmed to produce a surface suitable for rolling.

Conditions of plane strain at the crack tip are necessary to achieve a uniform crack front shape during propagation. It is known that under plane strain conditions, fatigue cracks tunnel ahead more rapidly than under plane stress conditions likely to be found at specimen surfaces. Only a small reduction was possible due to the constraint on specimen size and therefore little effect of orientation might be expected.

The cast structure in all cases was very coarse, the central sections of the ingots being coarse equiaxed grains up to 4 mm in diameter surrounded by columnar grains up to 20 mm in length.

Initial hot rolling treatments from 1000°C to a finished rolling temperature of 800°C were made to ingots IS00B, IS20B, IS30A, IS40A. Initially ingots were rolled with the maximum pass permitted by the mill (up to 13%). These treatments failed to produce the desired equiaxed grain structure. A final grain size of 2.6 mm was achieved in the case of ingot IS00B. The cast structure of ingot IS20B was only partially broken up by the treatment and little break up of the cast structure was

observed for ingots 1S30A and 1S40A.

The results of these experiments indicated the necessity for a cold or warm working treatment. An attempt to roll ingot 1S05B was made using the smallest available pass ($\cong$ 0.5%). This resulted in extensive cracking of the ingot surface, up to 5 mm deep.

Ingot 1S20A was hot rolled at 1050°C to 30 mm in thickness and a final 5 mm cold reduction to introduce sufficient strain energy to facilitate a grain refining heat treatment utilising this strain energy. Extensive cracking of the billet occurred on the first pass of 7% rendering the billet unusable. The cracking was identified as grain boundary decohesion.

Ingot 1S10B was rolled at 800°C employing passes of 2%. Cracking started to occur on the third pass and the experiment was terminated. The cracks were subsequently removed and the ingot re-rolled at 1000°C down to 30 mm and the final 5 mm rolled at 800°C. Again grain boundary decohesion occurred at small passes.

Ingot 1S10A was rolled at 1000°C down to 30 mm thickness and rolled to the finished size (25 mm) at 900°C and produced an equiaxed grain size of 0.760 mm. The effect of holding time on grain size was investigated to determine the presence, if any, of a critical holding time, in the γ loop, to produce grain refinement via the phase transformation ($\alpha - \gamma$). The results are shown in Figures 34 and 35.

The possibility of grain refinement by thermal cycling through the α - γ - α phase change was also investigated.

Ingot 1S20A was hot rolled at 1000°C down to 30 mm and rolled to 25 mm at 900°C and a final equiaxed grain size of 1.2 mm produced. The material was then cycled through the phase change up to five times, followed by an air cool. The results are shown in Figure 36.

It was considered that the lack of any tendency for this material to undergo grain refinement was due to the lack of fine second phase particles at the grain boundaries, and therefore no grain boundary pinning was evident. This was compounded by the use of high rolling temperatures required to avoid cracking during rolling. This also precluded the utilisation of strain energy in any heat treatment process.

2.1.2.1 ALUMINIUM TREATED CASTS

The addition of small quantities of aluminium powder together with a controlled amount of nitrogen (in stoichiometric ratio) was made to two casts with a view to forming a fine dispersion of aluminium nitrides (see Table 2) in order to facilitate grain refinement.

Ingots 1S05(2)A and 1S10(2)A were initially rolled to 30 mm flat at 1000°C and a finishing temperature of 900°C. The grain size achieved by this treatment was 1.4 mm and 1.6 mm respectively. A charpy specimen of each material was fractured in liquid nitrogen at -196°C and examined in

53

the SEM. No evidence of a fine dispersion of aluminium nitrides was observed. Subsequent examination of thin foils confirmed that no fine dispersion was present at the grain boundaries.

2.1.2.2 UPSET FORGING

In view of the large grain size and the restricted amount of deformation possible, by rolling, to achieve the finished specimen size, it was considered that a hot forging and rolling programme was required to obtain a greater proportion of deformation than by rolling alone. A number of trials were carried out to obtain the optimum conditions to produce a fine grain size. The final treatment involved the upset forging, to 50% deformation, in one pass at 1150°C followed by forging down to 27 mm flat and a final roll pass at 900°C to the finished size (25 mm).

Individual specimen blanks were subsequently heat treated at a series of temperatures and times to produce a uniform, varied grain size.

2.2. GRAIN SIZE MEASUREMENTS

Grain size measurements were made using a mean linear intercept technique[145]. The method entails the measurement of the chord length defined by the intersection of a random straight line, by the grain boundaries on the plane of the polish. The mean linear intercept is then defined

as $\bar{d}$ where:-

$$\bar{d} = \frac{\ell}{n} \qquad - 40$$

where ℓ is the length of the random line on the planar
surface, and n is the number of grain boundary inter-
sections on this line. The mean linear intercept is
clearly less than the true grain size since it includes
sectioning effects. The true mean diameter, $\bar{D}$, is then
defined as:-

$$\bar{D} = 1.75\bar{d} \qquad - 41$$

The standard deviation of the mean is defined as:-

$$\sigma\bar{d} = \frac{\sigma d}{\sqrt{N}} \qquad - 42$$

Where N is the number of observations made and σ_d is the
standard deviation of the individual measurements. The
relative error is then given by:-

$$\alpha = \frac{\sigma\bar{d}}{d} \qquad - 43$$

The error of the individual intercept is given by:-

$$\frac{\sigma d}{\sigma} = 0.7 \qquad - 44$$

and therefore the relative error is:-

$$\alpha = \frac{0.7}{\sqrt{N}} \qquad - 45$$

The grain size was determined in three directions to ensure
that any non-uniformity of the grains was taken into

consideration; determinations being made on broken test specimens in each case. The results of grain size measurements are given in Table 6.

2.3   TENSILE PROPERTIES

Tensile properties were obtained from test pieces of the geometry shown in Figure 37, machined from broken fatigue test specimens. The specimens were taken from positions indicated on Figure 38. It was considered that the removal of specimens from this position would negate the possibility of any influence of prior cyclic strain. The specimens were necessarily taken from a direction perpendicular to the applied stress in fatigue. Any differences in tensile properties due to the influence of orientation resulting from such a procedure were considered small since microstructual evidence did not indicate the presence of any prefered orientation effects (see section 3.10).

The tests were carried out on a 500 kg capacity Instron universal testing machine (Model 1104). An Instron strain gauge extensometer, attached to the specimen, was used to obtain accurate values of proof stress. These results together with percentage elongation, reduction in cross-sectional area and the tensile strength are shown in Table 7. Large discrepancies between individual specimens from the same compact tension specimen may be as a result of the small ratio between tensile specimen diameter and grain size. This would result in small differences in microstructure having a disproportionate effect on tensile properties. These variations in the determination of

tensile properties are also reflected in the calculation of plastic zone sizes (see table 9).

2.4 TEST PIECE PREPARATION

All fatigue crack growth tests were carried out using compact tension test pieces of a geometry shown in Figure 38. All specimen surfaces were ground finished and the faces metallographically polished to ensure ease of observation. Test piece dimensions were accurately determined before testing.

2.5   CRACK GROWTH MEASURING TECHNIQUE

2.5.1   INTRODUCTION

The study of fatigue crack growth, and near threshold crack growth rates in particular, requires a sensitive and accurate technique for monitoring such growth. The correlation of fatigue crack growth rates with loading variables and metallographic features requires precise experimental procedures.

A fatigue crack growth monitoring technique must be capable of fulfilling the following requirements:-

(i)   Be capable of operation over the long term periods necessary for threshold testing.

(ii)   Not require visual accessiblity to the test piece so that tests can be conducted under vacuum or other environments.

(iii)   Must be capable of resolving small increments of crack growth.

(iv)   Provide continuous measurement of crack length representative of the complete test piece thickness.

A number of experimental techniques have been used including ultrasonic and acoustic emission[146] and X ray diffraction techniques[147] but the DC potential drop technique best fits the above requirements[148-151]. This technique was used in this investigation. It must be noted that this technique provides no information about the shape of the crack front, because the PD response is measured across

the notch and averaged through the thickness, or any deflection of the crack from the plane perpendicular to the applied stress.

Essentially the technique involves passing a constant current through a cracked test piece under load, and measuring the potential difference across the crack. As the crack length increases, the area of uncracked ligament decreases, its resistance increases and the potential difference across the crack increases. The potential increase (V) is measured; from this and the known reference potential the crack length to test piece width can be determined.

2.5.2 CALIBRATION OF PD TECHNIQUE

In a current carrying body a disturbance in the potential field will exist around a discontinuity such as a crack. This is measured as the potential difference across the crack. If the body has homogeneous electrical properties and the current passing and temperature are held constant then there will be a unique relationship between the crack length and the potential difference across the crack for a given test peice geometry.

Calibrations may be produced theoretically, involving a solution of Laplace's equation:-

$$\nabla^2(\phi) = 0 \qquad\qquad\qquad - 46$$

where ∇ is the Laplacian operator ϕ is the steady electrical potential or experimentally either by producing electrical analogues[150] or by fatigue marking of real samples. In this investigation an experimental technique was used and

is described below.

Theoretical calibrations involving a solution to Equation 42 which describes the electrical potential field in a geometry of specific boundary conditions for a specific test piece geometry are not easily applicable to complex test piece geometry although finite element analysis methods have been used[152] and compare closely with those provided by experimental calibration for compact tension specimens.

2.5.3   EXPERIMENTAL CALIBRATION

Experimental calibrations may be made using thin foil analogues or by fatigue marking of real specimens and are conveniently represented in the form of variation of potential V/Vo with dimensionless crack length a/w.

Calibration was performed on test pieces identical to those used in threshold testing. Test piece surfaces were metalographically polished and marked at 1 mm intervals. As the fatigue crack reached each successive scribe mark the load was either raised or lowered to produce a marking on the fracture surface corresponding to the load change. Using this technique the position of the crack front can be fixed with respect to the potential associated with it. This procedure is continued until an a/w ratio of 0.75 is exceeded.

In practice this procedure did not produce a sufficiently

well marked fracture surface, a problem which was overcome by interrupting the tests for periods to allow a film of oxide to form on the surface thus allowing easier identification of changes in load along the crack front.

Crack length measurements were averaged over values measured at 0, 25, 50, 75, 100% of the test piece thickness. The numerical average is taken as the characteristic crack length for subsequent analysis.

The calibration is represented by the dimensionless plot of the potential ratio V/V_0 against dimensionless crack length a/W. This is shown in Figure 39. A computer program was then used to determine the best fit to the data points.

It has been shown[153], for a number of steels, that this calibration technique for compact tension specimens is unique to a high degree of accuracy and is independent of size and thickness provided that the current lead separation is in proportion to the test piece size. This was the case in this investigation.

2.6   EXPERIMENTAL TEST EQUIPMENT AND TESTING PROCEDURE

All tests were carried out on a 25 kN capacity Dartec electrohydraulic fatigue machine. The fatigue specimen is shown connected schematically in Figure 40.

The test pieces were held at a constant temperature, to within $\pm 0.5^{\circ}C$, using a West Guardian proportional temperature controller with a heating element soldered to the

top face of the specimen. The chromel/alumel control thermocouple was attached to a point 2 mm from the upper surface of the specimen to ensure thermal cycling did not occur. The actual temperature in the region of the crack was determined by a chromel/alumel thermocouple spot welded to the front face 2 mm from the crack and was recorded on either a Comark 5000 digital thermometer or a Comark 1605 electronic thermometer.

The test piece was electrically insulated from the machine by using tufnol annuli in the loading collets. During testing a perspex chamber surrounds the specimen to exclude draughts. Humidity is maintained at 35% ± 15%.

Soft iron wires 0.02 mm in diameter and coated in PTFE were spot welded to the test specimen 1 mm either side of the notch to sense the potential (the use of soft iron wires precludes the possibility of pin heating, due to the thermal emf associated with Fe/Cu junctions - 12 $\mu V/^{o}C$, introducing significant error). Potential wires were twisted throughout their length to avoid magnetic field interference. The Fe/Cu junction was embedded in an aluminium block heat sink to ensure no temperature difference existed between the junctions. Epoxy resin was used to add mechanical strength to the spot welds on iron wires and thermocouples. These details are shown in Figure 41.

Because small changes in potential corresponding to small

changes in crack growth must be accurately measured in a signal considerably larger, the majority of the signal must be suppressed so the more sensitive range of the microvolt meter can be used. This was achieved using a Time Electronics 2003S DC voltage calibrator, which provides a controlled dc signal with an absolute accuracy of ± 0.25 μV and a stability of less than 10 ppm/hr at constant temperature and a temperature coefficient of less than 30 ppm/^{O}C. It was powered by batteries as a precaution against earth loops.

A Keithley 155 microvoltmeter was used to measure the remainder of the signal. The accuracy of this instrument is $\pm 1\%$ of full scale deflection with low term drift (<0.5 μV/24 hrs) and noise (<0.03μV rms) characteristics. The potential difference readings were recorded by a Servoscribe 1s chart recorder.

All signal leads were constructed from low noise coaxial cable with minimum loop area to prevent pickup from external electrical and magnetic sources.

The constant current supply was a Farnell F2111 15/30T feedback controlled unit and ammeter providing a maximum continuous output of 30A. This unit has low ripple and noise and low temperature sensitivity (0.005%/^{O}C) characteristics required for long term stable operation. To avoid heating effects the current was supplied to the specimen via 50 amp DC rated copper cable and two copper contacts soldered such that the ratio of current lead

separation to test piece width was maintained at O.3.

2.7   DATA ANALYSIS

The potential difference technique described produces data
in the form of potential versus time plots. A computer
program was utilised which produces crack growth data from
the following inputs:

(1)   Specimen name

(2)   Material

(3)   Environment

(4)   Stress ratio

(5)   Frequency

(6)   Waveform

(7)   Testpiece width

(8)   Testpiece thickness

(9)   Load range

(1O)   Time interval between readings

(11)   Values of V/Vo.

The output from the program is tables giving values of V/Vo,
time (mins), crack length (mm), cycles, ΔK, and da/dN. The
program also contains graphics facilities and plots of 'a'
against 'N' and log (da/dN) against log (ΔK) may be produced.
The stress intensity factors determined in the program
are calculated from the following equations:

$$K_{max} = \frac{YP_{max}}{BW^{\frac{1}{2}}} \qquad\qquad - 47$$

$$\Delta K = \frac{Y \Delta P}{B W^{\frac{1}{2}}}$$

where Y is the specimen compliance function

    P is the load

    B is the specimen breadth

    W is the specimen width.

The compliance function for compact tension specimens is given by[115] :-

$$Y = 29.6(a/w)^{\frac{1}{2}} - 185.5(a/w)^{\frac{3}{2}} + 655.7(a/w)^{\frac{5}{2}}$$
$$- 1017(a/w)^{\frac{7}{4}} + 638.9(a/w)^{\frac{9}{2}} \qquad - 49$$

2.8   THRESHOLD TESTING

A fatigue crack was initiated from the notch using an R ratio of 0.2 and high loads to ensure a straight crack front. This also serves to counter the possibility of notch effects. Crack initiation on both sides of the test piece was observed before threshold testing commenced.

Once a growing fatigue crack had been initiated the loads were successively reduced in increments of 10% (of the maximum load) until no further growth could be detected in 10^7 cycles[56]. After each load reduction the crack was allowed to grow for a length exceeding at least twice the plastic zone size at that load[73]. This procedure ensures that the results are independent of stress history[154]. Figure 42 is a schematic example of the load reduction sequence. Fatigue cracks were grown up to a maximum of a/W = 0.7, the limit of the linear portion of the

calibration curve.

2.9 ACCURACY OF THE POTENTIAL DROP TECHNIQUE

Current and test piece temperature fluctuations result in
a certain amount of noise and drift of the measured
potential across a crack of given length. Included in
this noise and drift is a contribution from the potential
measuring circuitry and is given in the specification of
the equipment. The cumulative effect of these sources
of error may be experimentally determined from a drift
test where the equipment is left running for 24 hours
below the fatigue threshold.

These tests were carried out at the start of every
experiment, firstly to allow the specimen temperature
and equipment to stabilize and secondly to determine the
amount of drift. These tests confirmed that the measured
potential remained constant to within $\pm0.5\mu V$. If it is
assumed that the total error is a simple addition of the
individual errors then the crack length may be estimated
to an absolute accuracy of about 1%. This is confirmed
by the measurement of known points on the fracture surface
during calibration tests.

A more complete analysis of the errors involved in this
technique is given in the literature. Druce &
Booth have confirmed that crack lengths can be estimated
to within ±0.2 mm. An absolute value of crack length may
be estimated with an accuracy of 1%. This corresponds to

an error in the compliance function Y of ±2% at a/W = O.7.

The error in the loads P and ΔP, determined from the
operating manual, were within a value of ±2%. Therefore
an estimate of the overall accuracy of the stress intensity
would be ±4% (ie±(2 + 2)).

2.10   RESIDUAL STRESS MEAURESMENTS

2.10.1   INTRODUCTION

It has been accepted for many years that stresses of
considerable magnitude may be produced by cooling metals
from high temperatures. These stresses are introduced
by a transformation of phase (from austenite to ferrite
for example) and also by temperature gradients set up in
the component.

Residual surface stresses may also be produced by grinding
[155-157] and these may have a considerable effect on fatigue
compressive residual stresses are advantageous in reducing
crack growth rates.

2.10.2   RESIDUAL STRESS MEASUREMENT TECHNIQUE

The method used to determine the residual stresses was the
centre hole drilling technique. A strain gauge rosette
(see Figure 43) was mounted on the surface of the specimen
and a small hole was made in the surface through the
centre (Figure 44) of the strain gauge relieving part of
the surface residual stress produced by machining. When
the hole is made the stress existing at the edge of the

hole is reduced to zero and the stress field around the hole is modified. The strain gauge measurements are then used to determine the residual stresses.

The hole in the rosette is machined by an air/alumina powder mixture which is directed on to the surface of the sample by an eccentrically mounted rotating jet[158]. The technique ensured stress-free drilling. A hole 1.8-1.9 mm deep is produced.

The residual stresses present can then be determined from:[159]

$$\frac{\sigma_1}{\sigma_2} = -\left(\frac{E}{2}\right) \left(\frac{1}{K} \left[\frac{\varepsilon_1 + \varepsilon_3}{1-\nu K_2/K_1} \pm \frac{1}{1+ K_2/K_1} \sqrt{(\varepsilon_3 - \varepsilon_1)^2 + (\varepsilon_1 - \varepsilon_3) - 2\varepsilon_2{}^2}\right]\right) \qquad - 50$$

where σ_1 and σ_1 = principle stresses

   E   = Young's modulus

   $1/K_1$ = Constant dependent upon hole diameter

   $\nu K_2/K_1$ = Poisson's ratio

   $\varepsilon_1, \varepsilon_2, \varepsilon_3$ = Related strains, ie final reading minus original reading for each of the three strain gauges.

The direction of the most positive principal stress measured from gauge one can be determined from:-

$$\alpha = \tfrac{1}{2}\tan^{-1}\left[\frac{(\varepsilon_1 + \varepsilon_3) - 2\varepsilon_2}{\varepsilon_3 - \varepsilon_1}\right] \qquad - 51$$

The accuracy of the technique is considered to be not greater than ±10%[160-161].

2.11   METALLOGRAPHY

2.11.1   OPTICAL MICROSCOPY

Initial metallographic examination and grain size deter-
minations (etched in 2% nital) were carried out on Vickers
fifty five and Carl Zeiss Ultraphot optical microscopes.
Investigation of crack profiles and microhardness deter-
minations were carried out on a Reichart (Mef) microscope.

2.11.2   ELECTRON MICROSCOPY

A Phillips 500 scanning electron microscope was used for
the majority of fracture surface examination. Little
prior preparation was required. However a number of
oxidised surfaces were gold coated to improve conductivity.
The EDAX facility was used for examination and analysis
of inclusions.

Taking measurements from the SEM micrometer stage controls
enabled crack lengths to be determined to within ± 0.05 mm.
By referring to the computer print-out of the test results
it was possible to collate fractographic details with
corresponding stress intensity values and growth rates.

Quantitative fractography was performed by taking fract-
ographs of the surface and tracing the elements of
transgranular, or intergranular, fracture onto a sheet
of tracing paper. The relative proportion of constituents
on the fracture surface could then be estimated using
an Optimax facility. The direct use of Fractographs for

this purpose was discounted due to a lack of optical contrast between trans and intergranular fracture. The estimated accuracy of this technique for 95% confidence limits was approximately ±10%.

Thin foil examination of the area immediately ahead of the crack was achieved by spark eroding a 3 mm column of material along the plane of the crack. A number of discs were then cut from the column to ensure a foil was produced immediately ahead of the crack within the plastic zone. Discs were ground down to 0.1 mm, and polished and thinned using a Struers unit. Thinning was carried out using a solution of 10% perchloric acid in alcohol at a flow rate setting of 6 and 70 volts. The temperature was maintained at $-40^{\circ}C$ during the operation.

Examination of foils was made using JEOL 100 Cx and AEI 1000 KV transmission electron microscopes. The use of the 1000 KV machine allowed the examination of thicker sections of material which are more representative of the bulk material.

2.12   TEXTURE DETERMINATIONS

Primary and secondary recrystallisation textures for this material have been examined using Siemens X-ray apparatus.

Typically specimens, taken from a fractured fatigue test piece, 25 x 20 x 5 mm were used in the etched condition. The specimens were mounted on the goniometer and subjected

to a to and fro movement; to improve statistical averaging by increasing the number of grain samples, rotation about the axis perpendicular to the specimen and a rotation about an orthogonal axis was also used.

3   EXPERIMENTAL RESULTS

3.1   INTRODUCTION

In order to achieve the proposed objectives of this research
several series of fatigue threshold tests have been carried
out to investigate specific metallurgical and com-
positional variables on near threshold fatigue crack growth.

Five series of high purity Japanese electrolytically
refined iron containing small quantities of silicon of
nominal value 0%, 0.5%, 1.0%, 1.5% and 2.0% were produced.
These alloys were subsequently, forged and rolled under
controlled conditions and finally heat treated to produce
a uniformly variable grain size. Details of these processes
and techniques have been described in Section 2.
Fatigue specimens for 0% and 2.0% silicon alloys were
produced from series 1 material. Specimens from materials
nominal silicon content of 0.5%, 1.0% and 1.5% were produced
from series 3 material. Examination of tables 1 and 3 show
that the composition of both materials is essentially the
same. Differences in high temperature thermomechanical
treatments of these alloys produced changes in grain size,
however, it is considered that the influence on fatigue
data associated with different thermomechanical treatments
is small, due to the high temperature of deformation, the
limited reductions possible and the evidence of texture
determinations.

3.2   FATIGUE CRACK GROWTH RATE RESULTS

3.2.1   THRESHOLD GROWTH RESULTS

Load reduction fatigue threshold tests were carried out,
as described in Section 2, at a constant stress ratio of
0.2 ($\pm 4\%$) and the effect of metallurgical and com-
positional variables established.   In each specimen the
degree of crack front bowing was observed and in no
case did the maximum crack length exceed the minimum crack
length by more than 0.5%W.   This was considered to have a
negligable effect on crack growth characteristics.

Figures 45 to 65 show the near threshold fatigue crack
growth data obtained during the experimental programme.
Figures 66 to 70 are the superimposed threshold data for
each series of alloys.   It can be seen that all specimens
exhibit a sharp fall in fatigue crack propagation rates as
the threshold stress intensity, ΔK_{Th}, is approached.

Series 1 material, pure. iron, Figure 66, exhibits threshold
behaviour at growth rates up to 10^{-6} mm/cycle.   A sharp
transition from region B to A is observed only in the case
of specimen 1500(1)A2. ΔK values taken at a growth rate
of 1 x 10^{-7} mm/cycle reflect an increase in threshold
behaviour from 10.2 $MNm^{-3/2}$ to 10.8 $MNm^{-3/2}$ with a
corresponding increase in the grain size from 195 μm to
237 μm.

Series 2 material, 0.5% silicon alloys, Figure 67, again
shows the growth rate to diminish asymptotically toward

the stress intensity axis. Values of threshold increase from 11.9 MNm$^{-3/2}$ to 13.2 MNm$^{-3/2}$ with corresponding increase in the grain size from 110 μm to 276 μm.

Series 3 material 1.0% silicon alloys, Figure 68, again shows well defined threshold values. A larger variation in threshold ΔK values is observed in this case, for an equivalent change in grain size, than for series 1 and 2 alloys. A decreasing value of threshold ΔK is observed from 15.4 MNm$^{-3/2}$ to 13.7 MNm$^{-3/2}$ with a corresponding increase in grain size from 154 μm to 292 μm. The effect of increasing grain size producing a decrease in the threshold ΔK is contrary to the effect observed in Series 1 and 2 alloys.

Series 4 material, 1.5% silicon alloy, Figure 69, again shows well defined values of threshold ΔK. The effect of increasing grain size is, in common with series 3 alloys, to reduce the threshold ΔK from 16.1 MNm$^{-3/2}$ to 11.1 MNm$^{-3/2}$, for a change in grain size from 246 μm to 395 μm.

Series 5 material, 2.0% silicon alloy, Figure 70 clearly indicates thresholds are again present in this alloy. A strong effect of grain size on the threshold stress intensity range was apparent. An increase in grain size from 395 μm to 621 μm was associated with a corresponding decrease in threshold values from 13.8 MNm$^{-3/2}$ to 9.9 MNm$^{-3/2}$. Table 8 shows the fatigue crack threshold ΔK values at threshold for all specimens. The relationship between the fatigue

threshold stress intensity, ΔK_{Th}, and the square root of the grain size has been found to approximate to a straight line and the data for all specimens is plotted on Figure 71.

3.3   GRAIN SIZE AND COMPOSITIONAL EFFECTS

It is clear from a consideration of Figure 71 that as the silicon content of the material is increased from 0 to 2% then the slope of the line becomes increasingly positive with each increment of silicon.   At 0.5% silicon content the grain size has a limited effect on the threshold behaviour.   The result of an addition of silicon is to increase the effect of a change in grain size up to at least 2% silicon.

3.4 INTERMEDIATE GROWTH RESULTS

In addition to the near threshold growth results, results
have been obtained in the region where the Paris
relationship is approximately applicable. Some convergence
of growth rates was observed in most cases above 1×10^{-5}
mm/cycle. A sharp transition of growth rates between
regimes A and B can also be seen in a number of curves.

3.5 PLASTIC ZONE SIZES

Table 9 shows the values of the monotonic and cyclic plastic
zone sizes determined from the following equations:

$$W_{rev} = \frac{1}{3\pi}\left(\frac{\Delta K}{2\sigma_{ys}}\right)^2 \qquad\qquad - 52$$

$$W_{mono} = \frac{1}{3\pi}\left(\frac{K_{max}}{\sigma_{ys}}\right)^2 \qquad\qquad - 53$$

The values of yield stress in this case were substituted by
0.1% proof stress since no yield stress was observed
during tensile testing.

It has been suggested that the cyclic plastic zone at the
threshold is approximately equal to the grain size to
within an order of magnitude. Table 9 shows that this
is the case with the exception of specimen 1S15(3)B2 and
all the series 5 specimens. Average values of cyclic
plastic zone sizes are a factor of 3 to 8 smaller than the
grain size for alloy series 1 to 4. However, the cyclic
plastic zone sizes for the alloy series 5 material are a

factor of approximately 10-20 smaller than the grain size at threshold.

3.6 STRAIN HARDENING EXPONENTS

The tensile data obtained in section 2.3 were used to determine values of the strain hardening exponent, n. The true stress and true strain were determined from the following equations:-

$$\sigma = S(e+1) \text{ and } \varepsilon = \ln(e+1)$$

where s is the engineering stress

   are e is the engineering strain

An approximate strain hardening exponent, n, has been determined from the tensile data using equation

$$\sigma_T = K\varepsilon_T^n \qquad\qquad\qquad - 54$$

where σ_T is the effective stress

     ε_T is the effective strain

      K is the strength coefficient.

The strain hardening coefficient is plotted against solute concentration in Figure 72. Although the errors involved in the determination of the strain hardening coefficient are large, the trend indicates a lowering of the strain hardening coefficient coincident with increasing silicon content.

3.7 TEM RESULTS

Results of the examination of approximately 10 foils in each series of material did not show, conclusively, the presence of voids formed at the grain boundaries within the plastic zone of the fatigue crack.

Evidence was present of high dislocation densities and sub boundary formation in series 4 and 5 material (Figure 73). The presence of mechanical twins within the plastic zone was also observed at these higher silicon contents (Figures a and b). This behaviour was not observed in series 1, 2 and 3 material.

3.8 FRACTOGRAPHY

Macroscopic examination of the fatigue fracture surfaces, from specimens used to produce the threshold data, revealed the presence of oxide corrosion products on areas of the surface corresponding to low growth rate areas. Visual examination suggested that there was no discernable difference in the quantity of corrosion product from specimen to specimen.

SEM examination of some surfaces was obscured by the presence of these corrosion products which reduced resolution. It was therefore necessary to produce a thin gold coating on these surfaces to overcome this.

3.8.1 QUALITATIVE FRACTOGRAPHY

Examples of fatigue fracture surfaces near the fatigue threshold are given in Figures 74 to 85. The

macroscopic crack propagation direction is indicated by an arrow in each case and the point at which the threshold condition is achieved is marked. Any influence of position through the specimen thickness on the mode of failure was negated by examining only the central, plane strain, section of each specimen.

An example of series 1 material is shown in Figure 74. In this case the fracture is almost entirely intergranular over the whole cyclic stress intensity factor range.

An example of series 2 material is given in Figures 75 and 76. The series is micrographs are taken along the direction of propagation from the threshold ΔK. Again a high proportion of intergranular propagation is present together with some cleavage cracking.

Figure 77 illustrates the transformation in fracture mode from near threshold growth rates where a high proportion of intergranular fracture is present to a higher stress intensity range where the surface is almost entirely a rough, cleavage mode for series 2 material.

Discrete areas of transgranular fracture occur at irregular intervals throughout the low growth rate regime (Figure 78). These segments of transgranular failure are approximately the order of the grain size, however, in some instances they may cross up to 4 consecutive grains.

Examples of series 3 material are shown in Figures 79 to 81. In this higher silicon alloy (nominally 1.0%) an increased

contribution of transgranular failure with a fibrous appearance is observed.

Examples of series 4 material are shown in Figures 82 and 83. The fracture surface at the threshold ΔK is composed, almost entirely, of transgranular fracture.

Series 5 material, shown in Figures 84 and 85, shows the fracture at all stress intensity ranges to be completely transgranular with occasional isolated areas of cleavage. The macroscopic fractograph (Figure 86) shows the crack path to be channelled to some degree with obvious 'ridge and valley' features running parallel to the macroscopic growth direction.

Figures 86 and 90 show examples of fracture surfaces at ΔK above the threshold. With the exception of the series 1 material, all crack propagation tends toward a wholly cleavage fracture as the stress intensity range is increased to levels corresponding to region B of the fatigue crack growth curve.

Figure 88b illustrates the presence of isolated facets of cleavage present at high stress intensity levels in series 4 and 5 material.

Figures 89 and 90 illustrate a form of 'crack channeling' which occurs in the high silicon material, series 4 and 5. These features run parallel to the macroscopic direction of propagation. The width of these 'channels' is greater, by more than an order of magnitude, than the crack growth

rate at that point. The intervals of the features observed in Figure 90b are also an order of magnitude greater than the corresponding crack propagation rate.

3.8.2 CRACK BRANCHING AND SECONDARY CRACKING

The occurrence of secondary cracking and crack branching was found to be a common feature in all specimens and at stress intensities throughout the range.

Widespread intergranular crack branching was observed in series 1 and 2 materials over the whole range of stress intensity factors (Figures 91 and 92). Extensive crack branching was also found to be common in series 3, 4 and 5 materials at both threshold ΔK levels and at higher ΔK. (Figure 93)

Figure 94a illustrates that secondary cracking present at near threshold ΔK occurs intergranularly and transgranularly whilst at higher stress intensity ranges cracking is entirely transgranular as is the main crack (Figure 94b).

As expected, the intergranular cracks are almost independent of the microscopic crack growth direction. The transgranular secondary cracks, however, tend to form on a plane perpendicular to the crack growth direction at threshold and growth rates up to 1×10^{-4} mm/cycle. Figure 95 shows the profile of a crack of series 1 material and shows the main intergranular crack with major intergranular secondary cracking and the presence of some minor transgranular cracking.

The complex crack path produced by intergranular propagation is illustrated in Figure 95b. In the following the grain boundaries the crack may deviate from the macroscopic crack growth direction by up to 120°. This must necessarily lead to a change in the crack opening mode from mode I to a mode containing a contribution of mode II and mode III opening. The length of the main fatigue crack (ie, not including secondary cracks) had been measured, in profile, and results show that the microscopic length of an intergranular crack may exceed the length of the macro- scopic crack by up to 110%. The corresponding value for a crack propagating in a 50/50 intergranular/transgranular mode is 65% and for a wholly transgranular crack is 30%. The significance of this crack path deviation is discussed in Section 4.

As well as considerable quantities of crack branching and crack path deviation in the intergranular mode, it was noted that transgranular failure was also sensitive to the presence of grain boundaries as illustrated in Figure 96a and b. This is also associated with considerable surface roughness both at near threshold ΔK and higher levels.

3.8.3 STRIATIONS

It has been reported by a great many workers that the most commonly observed feature in the region where the Paris relationship is obeyed is the striation, formed by

the incremental advance of a crack every fatigue cycle.

Fatigue crack propagation at intermediate ΔK values used in this research is of a rough, featureless trans- granular mode and striations have not been observed in the low silicon material. However, in series 4 and 5 these features have been observed (Figure 97a and b). The features observed in Figure 97 running perpendicular to the macroscopic crack growth direction have been measured on the SEM and have been found to occur at an interval of approximately 8×10^{-5} mm. The corresponding fatigue crack growth rate at this point is of the order of 1×10^{-5} to 1×10^{-4} mm/cycle. This would suggest that each 'ridge' was formed by the advance of the crack during one loading cycle.

3.8.4 FATIGUE FRETTING

Examination of fracture surface revealed the widespread presence of material which appeared to have detached from the fatigue surface. This loose material was present both at near threshold and high growth rates and was assoicated with the transgranular portion of failure. The dimensions of these detached particles was up to 0.1 mm^2 (Figure 98a and b).

In areas of fracture containing a high proportion of transgranular fracture associated with a smaller quantity of intergranular fracture, intergranular facets have been observed with a rough surface, illustrated in Figure 99a and b.

This damage may be as a result of loose particles or oxides being compressed into the surface at the minimum of the loading cycle, K_{min}. The presence of oxide particles or fatigue debris is clearly shown trapped between the crack surfaces on Figure 95.

3.8.5 QUANTITATIVE METALLOGRAPHY

The results of quantitative metallography are summaried in Figure 100. The proportion of intergranular fracture was determined with the use of an optimax facility the basis of measurement being contrast between transgranular and intergranular feature, and is plotted against the stress intensity range, ΔK. The transition in each case corresponds approximately to the point where propagation changes from near threshold behaviour to behaviour associated with the Paris regime.

3.9 RESIDUAL STRESS RESULTS

Using the centre hole drilling technique described earlier, two measurements were taken to determine the surface residual stress introduced by machining.

Changes in the results due to chemical composition and grain size have been ignored and will contribute to the errors involved in the measurement.

TEST PIECE	σ_{max}	σ_{min}	α^o	TREATMENT
A	+98 Nmm^{-2}	−7Nmm^{-2}	−29	NONE
B	+17 Nmm^{-2}	−5Nmm^{-2}	−37	STRESS RELIEVED

Test piece A was tested as machined and B was stress relieved at 600 for 1 hour followed by air cool. A positive sign indicates a tensile stress and a negative sign indicates a compressive stress.

It is concluded from these results that a stress relief treatment is sufficient to reduce residual stresses to an insignificant level.

3.10   TEXTURE RESULTS

The results of investigations into the possible presence of a preferred orientation in these materials proved negative. Specimens from each material series were examined. The resultant pole figures showed a random orientation and it was concluded that no significant texture was present.

4   DISCUSSION

4.1   INTRODUCTION

The object of this research has been to study the pheno-
mena associated with fatigue crack growth thresholds and
near threshold crack propagation rates. Particular
emphasis has been placed on the role of metallurgical
variables in determining the threshold condition and the
kinetics of the crack growth process. In this section the
results and observations reported in Section 3 will be
discussed with respect to the physical processes of low
crack growth rate and threshold behaviour in iron-silicon
based alloys. A mechanistic description of the effect of
each variable and the effect of the interaction of
variables together and their effect on the crack growth
process will be evaluated.

4.2   THE CONCEPT OF FATIGUE THRESHOLD

The fatigue threshold is defined as the stress intensity range
at which the crack growth rate is zero. In practice
zero crack growth rate is immeasurable and therefore must
be replaced by some minimum growth rate, below which
crack growth can be considered to be insignificant. This
then provides an adequate estimate of the threshold stress
intensity range if the crack growth rate diminishes
asymptotically towards the ΔK axis.

The threshold may occur as a result of crack growth rates
being unable to decrease below the lattic spacing per
cycle. However, macroscopic growth rates of less than one

lattice spacing per cycle are possible where crack growth
is not occurring every cycle or is occurring discontinuously
across the crack front.

A number of the fatigue crack growth models reviewed in
Section 1 suggested that the threshold was a fixed material
parameter. It has become clear in this research that
variables, other than ΔK, may affect the value of the
threshold. Metallurgical variables and residual stress
distributions have some influence in this area.

4.3   FATIGUE CRACK GROWTH FRACTOGRAPHY

The characteristics of fatigue crack pro-
pagation in iron-silicon based alloys, described in
Section 3, have also been reported by other workers[132].
The relationships, obtained in this research, between the
stress intensity range and the proportion of transgranular
fracture is shown in Figure 100 for stress intensity ranges
from threshold to a level where crack growth data can be
approximated by the Paris relationship. The results
indicate that crack growth near the threshold occurs by a
wholly intergranular nature in pure iron and as the silicon
content and the yield stress is increased then the mode
of failure at threshold changes to a mixed transgranular/
intergranular mode. The proportion of transgranular mode
occurring increases with each increment of silicon added.
A wholly transgranular mode of fracture is achieved for the
series 5 alloys which contain approximately 2% silicon.

Figure 100 clearly shows, for the 3 alloys considered, that increasing values of ΔK above the threshold produce an increase in the proportion of transgranular fracture and a sharp transition is apparent which corresponds to the interaction of grain size and cyclic plastic zone size. This is discussed in greater detail in section 4.4.

4.3.1   MODEL OF NEAR THRESHOLD GROWTH

The mode of propagation in these materials will depend upon the relative energies required for the crack to propagate in an intergranular or transgranular manner. Any factor which increases the energy of transgranular propagation or decreases the energy required for the decohesion of the grain boundaries will promote an increased proportion of intergranular fracture. It might also be expected that an increase in the proportion of embrittling elements at grain boundaries or an increase in solution strengthening within the grain would lead to an increase in the susceptibility to intergranular cracking. It was apparent in regions of low crack growth that the fracture path and the surface topography were strongly influenced by the orientations of the grains through which the crack front passed. The crack front may progress in a discontinuous manner, whilst the measured growth rate is an average value over many grains of random orientation along the crack front. Thus a grain which is favourably orientated will favour rapid growth along the grain boundary but will find that crack extension is retarded by slower growth in less favourably

orientated grains. Growth in the less favourably orientated gains will tend to accelerate as a result of a build up of stress intensity factor range on the remaining ligament. Fracture of the remaining ligament will occur and will be essentially ΔK controlled.

The modelling of the near threshold fatigue crack propagation is complex when growth is occurring in a discontinuous manner as described above. This is compounded if the crack is progressing in a mixed opening mode. The results of fractography, shown in Section 3, show that this is the case and the consequences are described in Section 4.5.

4.4 PLASTICITY AND GRAIN SIZE EFFECTS ON THRESHOLD

4.4.1 INTRODUCTION

The action of silicon as a solid solution strengthener in iron is well documented. The addition of silicon to iron, in this research, leads to an increase in 0.1% proof stress as increasing quantities of silicon are added as shown in Table 7. An increase in the yield stress, or proof stress, of the material produces a decrease in the cyclic plastic zone size, ω, described by:-

$$\omega = \frac{1}{3\pi} \left(\frac{\Delta K}{2\sigma_{ys}} \right)^2 \qquad\qquad -55$$

It is important to note that the scatter observed in experimentally determined values of 0.1% PS will necessarily lead to considerable scatter of the calculated values of the cyclic plastic zone size, ω.

An increase in the material yield strength, σ_{ys}, has been shown experimentally to reduce the plastic zone size and constrain the zone to particular, favourable slip systems. It is suggested that the strain hardening exponent of this material may also be significant in characterising the plastic zone shape. Hahn et al[163] first suggested that the strain hardening exponent, n, has an important influence on crack extension. From experimental observation they showed that the width of the yielded zone, ℓn, was proportional to the strain hardening exponent, n^2, providing that the true stress true strain curve was of the form:-

$$\sigma_T = K\varepsilon_T^{\ n} \qquad\qquad - 56$$

This is shown schematically in Figure 101. The experimentally determined values of n are shown as a function of silicon concentration in Figure 72.

It has been widely reported that the occurrence of microstructurally sensitive growth will occur when the plasticity associated with a propagating fatigue crack approaches the microstructure element size[118]. As a result fewer slip systems are operable resulting in dislocation pile ups and discontinuities at grain boundaries. Alternative fracture mechanisms might then be expected to occur. The size of the monotonic and cyclic plastic zones have been derived theoretically from consideration of the stresses acting ahead of the crack and are known to be a function of ΔK, K_{max} and the yield stress.

Analysis of the form of the plastic zones in the region of crack tips have shown that its size and shape is dependent upon a number of other variables other than those stated above. Microstructural effects and strain hardening may also be significant parameters.

The results reported in section 3 have shown that the calculated values of plastic zone sizes are of the order of magniture of the grain size at threshold for series 1-4 alloys. The use of tensile data obtained from these specimens to calculate values of plastic zone sizes (see section 2.3) necessarily produces large errors in values of plastic zone sizes. However it is considered that these values are of the correct order.

Examination of the results shown in Figure 100 indicate a sharp transition in propagation mode from intergranular to transgranular as the stress intensity range, ΔK, is increased from threshold values. The cyclic plastic zone size corresponds more closely to the material grain size at this transition than at the threshold stress intensity value. This transitional behaviour has also been observed in hydrogen assisted fatigue crack propagation in martensitic steels[113].

This behaviour is interpreted as follows:-

At large values of stress intensity range, ΔK in the intermediate growth regime, the cyclic plastic zone size is much larger than the corresponding micro structural cell size. A large number of slip systems are operable over many grains and the resulting fracture is transgranular. As the stress intensity range is reduced no significant effect becomes apparent until the cyclic

plastic zone size becomes approximately equal to the grain size. Propagation then becomes sensitive to the presence of grain boundaries and intergranular cracking predominates. Dislocations move along the preferred slip plane and pile up at the grain boundary and act as stress concentrators.

The lack of an intergranular/transgranular transition in series 1 material may be associated with the presence of embrittling elements at the grain boundaries. These may be associated with the segregation of impurity elements to grain boundaries or the sweeping in of hydrogen to the grain boundaries which reduces their cohesive strength.

The proportion of intergranular fracture occurring at threshold stress intensity ranges is also shown in Figure 100. This effect, of increasing transgranular failure with increasing silicon content, is considered to be due to the constraint imposed upon the plastic zone by the solid solution strengthening effect of silicon on the strain hardening characteristics described earlier.

As the zone becomes constrained to the planes of maximum shear stress at 45° to the applied stress, as a result of strain hardening, the number of grain boundaries encountered within the zone is diminished, which results in a reduced liklihood of intergranular fracture. This effect is best illustrated in series 5 alloys where little intergranular failure is present at threshold levels and corresponds to the greatest effect of the strain

hardening coefficient.

4.4.2 GRAIN SIZE EFFECTS

4.4.2.1 INTRODUCTION

The effect of refining the grain size can be beneficial in raising the fatigue limit or the endurance strength of planar slip materials. The effect of grain size on fatigue crack propagation has been observed to be negligible in most cases at intermediate growth rates[87]. The majority of research into the effects of grain size on the fatigue crack growth threshold, on a wide variety of materials, has concluded that an increase in the grain size is beneficial in increasing threshold values.

The results of this research, shown in Figure 71, have indicated that a linear relationship exists between the threshold, ΔK_{Th}, and the inverse root of the grain size, $d^{-1/2}$. These results may be expressed by a relationship of the form

$$\Delta K_{Th} = \Delta K_{Th(o)} + Kd^{\pm 1/2} \qquad - 57$$

where $\Delta K_{Th(o)} = \Delta K_{Th}$ at R = O $\qquad - 58$

which suggests that the sensitivity of the threshold to the grain size is diminished at higher R values.

The effect of grain size on threshold behaviour in series 1 and 2 alloys showed an increasing value of threshold ΔK with increasing grain size, producing a beneficial

93

result in terms of threshold behaviour. For material series 3, 4 and 5 the reverse is the case, threshold values decrease with a coarser grain size. This type of behaviour has been observed in copper-aluminium alloys[89]. This effect is discussed in detail in section 4.5.

4.5   CRACK CLOSURE AND CRACK DEFLECTION PHENOMENA

It is considered that the effects of crack closure and crack deflection are of considerable importance in this work. These phenomena are discussed in detail in the following sections.

4.5.1   CRACK CLOSURE

There has recently been considerable interest in the mechanisms of fatigue crack closure, particularly at very low stress intensity factor ranges approaching the threshold stress intensity range, ΔK_{Th}, below which cracks remain dormant or grow at experimentally undetectable rates. The presence of crack closure occuring at stress intensity factors greater than k_{min} produces an effective stress intensity factor range less than the applied stress intensity factor range. It has been suggested that crack closure, particularly that associated with plasticity, is most prevalent under essentially plane stress conditions and yet at very low growth rates, approaching ΔK_{Th}, where plane strain conditions exist, Very significant effects of crack closure have been

observed (48, 60, 164, 165, 169, 170).

4.5.2   MICROMECHANISMS OF CRACK CLOSURE

A number of closure mechanisms may be considered to be relevant to the result of this research:-

(i)   That due to the presence of oxidation products on the fracture surface.

(ii)   That due to the presence of fretting.

(iii)   That due to facet contact.

(iv)   That due to mixed mode fracture.

4.5.3   OXIDATION PRODUCTS

The presence of oxide induced closure follows from the fact that during near threshold crack growth at low load ratio's in moist environments, corrosion products may build up at the crack tip, providing a mechanism for enhanced closure such that the crack is wedged open at stress intensities above K_{min}. The oxide build up is generally thought to be due to fretting effects. More oxide is formed than simple predictions from oxidation rates suggest. Evidence for the occurence of such a mechanism is common in the literature[106-111]. Suresh et al[166] noted that for low strength steels, tested in moist air (30% relative humidity) at R = 0.05, oxide films built up on the new fracture surfaces with a maximum thickness of twenty times that, expected on metallographically polished samples exposed to the same environment for similar periods. The mechanism is supported by the

95

observation that a clear relationship exists between the quantity of water present, the amount of corrosion debris produced and a consequent increase in threshold levels[79]. The quantities of corrosion product observed in this research, at near threshold growth rates, appeared to be consistent over the whole range of alloys and therefore it might be expected that additions of silicon or changes in the grain size might have little effect upon the quantity of oxide produced. However, a coarse grain size may lead to more roughness induced closure, more fretting and more oxide. The closure effect, promoted by these oxide deposits, might be expected to be enhanced by a mechanism of fretting oxidation in which the oxide layer is repeatedly broken up and compacted as closure occurs and fresh oxide is produced on the clean metal surface. At higher growth rates this might be expected to diminish due to the time dependance of oxide production.

4.5.4   FRETTING FATIGUE

The presence of debris, other than oxide, on the fatigue surfaces, in this research, at near threshold fatigue crack growth rates is consistent with a fatigue fretting mechanism. The debris may be formed as a result of rough fracture surfaces induced as a consequence of a large grain size and a significant quantity of mode II opening. This fretting debris would tend to wedge open the crack at stress intensity factors above K_{min} thus reducing the apparent ΔK and increasing the threshold values.

The apparent propensity for debris to form as a result of
rubbing of transgranular areas of fracture would suggest
that a greater degree of closure, by this mechanism, would
occur in material when a larger proportion of trans-
granular fracture is present at near threshold growth rates.
It might then be expected that threshold levels would
increase as a function of silicon content and this is in
fact the case at constant grain size. The observation of
"damaged" intergranular facets (Figure 99) is indicative
of the presence of fretting debris, either matrix or oxide,
or of some mismatch occurring between the crack surfaces.
At higher growth rates it might be expected that fretting
would become less significant as the fracture path becomes
less structure sensitive.

4.5.5   IRREGULAR, ROUGH FRACTURE SURFACES AND FACET CONTACT

The effects of crack closure might also be expected to arise
from an irregular or rough fracture surface morphology.
In instances where the scale of the roughness is com-
parable or greater than the crack opening displacements
and where there may be a significant contribution of mode
II displacement, crack closure may be promoted since
the crack may be wedged open at discrete contact points
along the crack faces. Damaged facets are evidence that
this may be occurring (figure 99). This is shown
diagramatically in Figure 102.

Roughness induced closure may provide an important in-
dication of the role of microstructure in influencing

near threshold crack growth behaviour, particularly where
a high proportion of intergranular failure is present. It
might also be expected that a coarser grain size, providing
a rougher fracture surface and therefore a greater tendency
toward closure would produce higher threshold values.

The data for alloys 1 and 2 would tend to support this
view where a large proportion of intergranular failure
is present and increasing grain size leads to an increase
in threshold stress intensity factor range. As the silicon
content is increased, producing a subsequent fall in the
proportion of intergranular and fatigue profile roughness
is observed it might be expected that this mechanism would
play a smaller role in the overall closure process. It
has been shown, in section 3.8.2 that the microscopic
crack profile length, at near threshold propagation rates,
exceeds the macroscopic crack profile length by 110% for
low silicon alloys and falls to approximately 30% in 2%
silicon alloys.

4.5.6   MODE II TYPE OPENING

The role of mode II opening displacements may be important
in view of the results obtained in section 3, to the extent
of fracture surface interference at near threshold levels.

Fatigue crack propagation at high growth rates, where
growth is transgranular, may be considered in terms of
intense localised shear deformation in flow bands near

the crack tip which results in the formation of new crack
surface by shear decohesion at the tip. When the crack and
its plastic zone are contained within one or two grain
diameters, growth is confined to one shear direction, with
one primary slip system in the direction of growth and a
tensile component normal to it. Such propagation,
essentially stage I growth, proceeds under a combination
of Mode I and Mode II displacements. The marked transition
from a mixed mode fracture to an entirely transgranular
mode, observed in this research, with the exception of
series 1 material, supports this model. Fatigue crack
growth above the transition is essentially stage II and
occurs in almost pure mode I, perpendicular to the principal
tensile stress.

At near threshold stress intensity factor ranges where the
reversed plastic zone size is of the order of the grain
size, fatigue crack growth takes place by a stage I mech-
anism and results in the typical mixed mode fracture surface
morphology observed in series 2, 3 and 4 material. This
coupled with mode II displacements would be expected to
generate high closure loads. A mode II displacement will
produce asymetry of deformation at the crack tip and
introduce a frictional stress between fracture surfaces
so that rubbing may occur. The crack surfaces can then
no longer be considered to be stress free planes and the
crack driving force will be reduced by the surface
contact.

At higher crack growth rates as the plastic zone size increases, the transition to stage II propagation and Mode I opening results in a flatter fracture surface morphology and more symetrical crack tip deformation due to the continuum deformation in the crack tip plastic zone once it encompasses many grains, such that closure would be expected to diminish. This view would tend to be confirmed by the fractographic evidence of this research and the microstructurally sensitive nature of growth at near threshold stress intensity factor ranges. This is supported by the diminishing proportion of intergranular failure at higher stress intensity factor ranges.

The presence of a mode II mechanism for near threshold crack advance with its associated propagation is relevant to the effects of grain size on threshold values. It has been shown that refining the grain size can be beneficial in raising the fatigue limit of materials. The effect of grain size has been shown to be negligible at intermediate growth rates for most materials[29]. However at near threshold growth rates most workers have observed higher thresholds occurring with a corresponding increase in grain size. Where this behaviour has been examined at both high and low R ratios it is significant that the effects of a large grain size are absent or reduced at higher R ratios. This would suggest that this may be due to the diminished effect of crack closure at high R levels.

4.5.7 CRACK DEFLECTION EFFECTS

Stress intensity factor range calculations for near thres-
hold fatigue crack growth usually assume that the crack
path is flat and mode I opening is predominent. However
it has been shown in this work that on a microscopic scale
the crack path is flat only in the higher silicon materials
and that considerable deviation of the crack occurs, from
a line perpendicular to the applied stress, in the lower
silicon materials.

It is suggested that such deviations of the crack will lead
to a reduction in the stress intensity factor range from
the apparent value. In addition the crack deflection will
produce a component of mode II type crack opening. The
effective stress intensity factor range may be conveniently
expressed by the expression:-

$$\Delta K_{eff} = \Delta K_{applied} - K_{deflection}$$

An increase in the grain size will lead to an increase
in the factor $K_{deflection}$, where intergranular crack
growth occurs, and will thus induce a reduction in the
effective stress intensity factor. An increase in the
measured threshold stress intensity factor range will be
observed. These observations agrees with the experimental
results obtained in this research.

It has been widely reported by many workers that values
of threshold stress intensity factor range are reduced
at high R ratio[88] This observation suggests that other
closure factors may be present since an increase in R ratio

would be unlikely to affect the proportion of crack deflection occurring at near threshold growth rates and therefore little effect on values of ΔK_{Th} would be observed.

It is suggested that some influence of both crack deflection and crack closure is present in these materials such that −

$$\Delta K_{eff} = \Delta K_{applied} - K_{deflection} - K_{closure}$$

however the relative contributions of the two phenomena are difficult to quantify.

4.6   SUMMARY

It is suggested that both crack deflection and crack closure play a part in determining the local driving force for growth processes occurring at near threshold growth rates. Section 4.5 has shown that both crack deflection and closure are likely to occur to a lesser degree as the growth rate is increased and the zone of reversed plasticity becomes very much greater than the grain size.

The presence of crack deflection and crack closure micro-mechanisms suggest that an increase in the grain size will lead to increased threshold values. This has been borne out by the results for series 1 and series 2 alloys.

As the silicon content and the proof stress is increased then crack deflection and closure become less significant effects because the constraint on the plastic zone produces a more planar crack path. In the 2% silicon material little deflection of the crack path is observed and it is reasonable to expect that there would be little effect of crack closure due to surface roughness and mode II opening. There may however be some contribution from oxidation products.

The sensitivity to grain size of the high silicon material, in the absence of crack closure and deflection, despite the lack of microstructure sensitive growth may be associated with an increase in proof stress in this material. This effect becomes less noticable and deflection and closure

micromechanisms become dominant at lower silicon levels.

This research suggests that at higher R ratios the effect
of crack closure on threshold behaviour would become small
and the threshold would then be controlled by grain size$^{-\frac{1}{2}}$
A regular change in the threshold with $d^{-\frac{1}{2}}$ might be expected.
Experiments carried out by other workers on copper-aluminium
alloys[89] at an R ratio of 0.5 have shown this to be the
case.

5   CONCLUSIONS

1   Pure iron and iron-silicon alloys up to 2% Silicon
have been observed to exhibit threshold stress
intensities.

2   Crack growth at the fatigue threshold stress intensity
proceeds by a wholly intergranular mechanism in pure
iron. As the yield stress is increased by additions
of silicon then the growth mode changes through a mixed
transgranular/intergranular mode to a wholly trans-
granular mode in the 2 per cent material.

3   A sharp transition in failure mode is observed when the
cyclic plastic zone size approximates to the grain
size (except in pure iron).

4   Constraint imposed upon the plastic zone due to the
effect of silicon on solid solution strengthening and
thus on strain hardening characteristics is thought to
lead to increased transgranular failure.

5   A linear relationship had been shown to exist between
threshold stress intensity range, ΔK_{Th} and the inverse
root of the grain size $d^{-\frac{1}{2}}$.

6   Crack closure is considered to play an important role
in the determination of fatigue thresholds and a
number of mechanisms have importance:-
(i)   The presence of oxide products on fracture
surfaces.

(ii)   Fretting of fracture surfaces.

(iii)   Facet contact between fracture surfaces.

(iv)   Mixed mode type opening.

7   Crack deviation from the plane perpendicular to the
     applied stress has been observed and is considered
     to lead to an increase in the measured value of the
     fatigue threshold. An increase in grain size can
     produce an increase in the value of fatigue threshold
     by this mechanism.

8   Micromechanisms of closure, fretting, rough fracture
     surfaces, facet contact and mode II opening are con-
     sidered to become increasingly operable as the grain
     size is increased.

9   At higher R ratio s it is suggested that the effect
     of closure on threshold behaviour becomes small and
     threshold values are then controlled by the grain size.

10   At near threshold propagation rates the fracture path
     is strongly influenced by grain orientation and growth
     occurs in a discontinuous manner. Favourably orientated
     grains failing first followed by failure of the
     remaining ligament.

6 <u>RECOMMENDATIONS FOR FURTHER WORK</u>

1   Fatigue crack closure, by a number of different mechanisms, has been proposed as an explanation for many of the results of this work. Crack closure may be measured directly by use of clip gauges attached to fatigue specimens and would allow a correlation to be drawn with closure mechanisms occuring on a macroscopic scale.

2   The proposal in this research that crack closure masks the effect of grain size on fatigue threshold behaviour may be substantiated by a series of tests carried out at a high R ratio where it is thought crack closure plays an insignificant role.

3   Auger electron spectroscopy (AES) is a technique sensitive to the first few atomic layers of fracture surfaces. It may be used on intergranular fracture surfaces to determine the extent of segregation of alloying elements and residual elements to grain boundaries. It is suggested that this facility would provide a useful insight into some of the mechanicms of failure encountered in this work.

4   Further work on other alloy systems and studies into material tempering characterisitcs, carbide morphology and residual elements on near threshold fatigue crack propagation and crack closure would provide

a more comprehensive picture of the mechanisms

observed in this work.

REFERENCES

1   J F KNOTT Fundamentals of Fracture Mechanics, Butterworth (1973) 234

2   S P TIMOSHENKO, J N GOODIER, Theory of elasticity, McGraw-Hill, New York (1971)

3   J R RICE Mechanics of crack tip deformation and extension by fatigue, ASTM STP 415 (1967) 247

4   G R IRWIN Fracture Mechanics, Structural Mechanics, Pergamon Press, New York (1960)

5   B WEISS, M R MAEYERSON Plastic zone formation and fatigue crack extension during high cyclic bending of steel, Eng. Fract. Mech. 3 (1971) 475

6   M CAVEL, D FOURNIER, A PINEAU Plastic zone sizes in fatigued specimens of INCO 718, MET TRANS 6 (1975) 2305

7   A OHTA, E SASAKI Plastic zone around fatigue cracks of pure iron in vacuum and dry air, ACTA MET 20 (1972) 657

8   G T HAHN, R G HOAGLAND, A R ROSENFIELD Local yielding attending fatigue crack growth, MET TRANS 3 (1972) 1189

9   C BATHIAS, R M PELLOUX Fatigue crack propagation in martensitic and austenitic stainless steels, MET TRANS 4 (1973) 1265

10   J GROSSKREUTZ, G G SHAW Fine subgrain structures adjacent to fatigue cracks, ACTA MET 20 (1972) 523

11   M A WILKINS, G C SMITH Dislocation structures near a propagating fatigue crack in a Al-0.5% Mg, ACTA MET 18 (1070) 1035

12   E HORNBOGEN, K H ZUM GAHR Microstructure and fatigue crack growth in a γ-Fe-Ni-Al alloy, ACTA MET 24 (1976) 581

13   D L DAVIDSON The study of fatigue mechanisms with electron channeling, ASTM STP 675 (1979) p 254

14   P C PARIS, F J ERDOGAN Basic Eng. 85 (1963) 528

15   W G CLARK Subcritical crack growth and its effect upon the fatigue characteristics of structural alloys, ENG FACT MECH 1 (1068) 385

16   C J BEEVERS, R J COOKE, J F KNOTT, R O RICHIE Some considerations of the influence of subcritical cleavage growth during fatigue crack propagation in steels, MET SCI 9 (1975) 119

17   R J COOKE, C J BEEVERS Slow fatigue crack propagation in pearlitic steels, MAT SCI AND ENG 13 (1974) 201

18   N R MOODY, W W GERBERICH Fatigue crack propagation in iron and two iron binary alloys at low temperatures, MAT SCI AND ENG 41 (1975) 271

19   D A CURRY Cleavage micromechanisms of crack extensions in steels, MET SCI, Aug/Sept (1980) 319

20   J L ROBINSON, C J BEEVERS The effects of load ratio, interstitial content and grain size on low stress fatigue crack propagation in α titanium

21   J F KNOTT Micromechanics of fibrous crack extension in engineering alloys.

22   R O RICHIE, R F SMITH, J F KNOTT Effects of thickness on fibrous fracture from a notch and on fatigue crack propagation in low strength steels, MET SCI 9 (1975) 485

23   P T HEALD, T C LINDLEY, C E RICHARDS The influence of stress intensity and microstructure on fatigue crack propagation in a 1% carbon steel, MAT SCI ENG 10 (1972) 235

24   B THOMKINS Plastic and elastic-plastic models for fatigue crack growth, Conf Proc. Churchill College, Cambridge, 4-6 April (1973) 174

25   J WEERTMAN Theory of fatigue crack growth based on a BSC crack theory with work hardening. INT. JOURN. FRACT 9 (1973) 125

26   H SUZUKI, A J McEVILY Microstructural effects on fatigue crack growth in low carbon steel, MET TRANS 10A (1979) 475

27   P E IRVING, C J BEEVERS Microstructural influences on fatigue crack growth in Ti-6AL-4V, MAT SCI and ENG 14 (1974) 229

28   J P BENSON, D V EDMONDS Microstructural effects on fatigue at intermediate and high crack growth rates in a low alloy steel, MAT SCI and ENG, 38 (1979) 179

29   R O RICHIE Influence of microstructure on near
     threshold fatigue crack propagation in ultra-high
     strength steel, MET SCI, Aug/Sept (1977) 368

30   R O RICHIE Effects of strength and grain size on near
     threshold fatigue crack growth in ultra-high
     strength steel, 'FRACT 77', Waterloo, Canada,
     June 19-24 2 (1977)

31   C R AITA, J WEERTMAN The effect of microstructure on
     fatigue crack propagation in iron carbon alloys,
     MET TRANS 10A (1979) 535

32   A J McEVILY, T L JOHNSON The role of cross slip in
     brittle fracture and fatigue, INT JOURN of FRACT
     MECH 3 (1967) 45.

33   P R IRVING, C J BEEVERS The effect of air and vacuum
     environments on fatigue crack growth rates in
     Ti-6AL-4V, MET TRANS 5 (1974) 391

34   J F KNOTT, R O RICHIE Effects of fracture mechanics
     on fatigue crack propagation, CONF. PROC. BSC
     Churchill, Cambridge 4-6 April (1973) 200

35   C E RICHARDS, T C LINDLEY The influence of stress
     intensity and microstructure on fatigue crack
     propagation in ferritic materials, ENG FRACT MECH
     4 (1972) 951

36   C LAIRD The influence of metallurgical structure
     on the mechanisms of fatigue crack propagation,
     ASTM STP (1967) 131

37   J C McMILLAN, R M N PELLOUX Fatigue crack propagation
     under program and random loads, STP 415 (1967) 505

38   C MASUDA, A OHTA, S NISHIJIMA, E SASAKI Fatigue
     striation in a wide range of crack propagation
     rates upto 70μm/cycle in a ductile structural steel,
     Journ of MAT SCI 15 (1980) 1663

39   G BIRKBECK, A E INCKLE, G W J WALDRON Aspects of
     stage II fatigue crack propagation in low carbon
     steel, Journ of MAT SCI 6 (1971) 319

40   W W GERBERICH, N MOODY Low temperature fatigue
     crack propagation, 'FRACT 77', Waterloo, Canada,
     3 (1977) 829

41   I M AUSTEN, E F WALKER Quantitative understanding of
     the effects of mechanical and environmental variables
     on corrosion fatigue crack growth behaviour, CONF. PROC
     INST of MECH ENG, IMECHE HQ, May (1977) C98/77

42   B K NEALE   An investigation into the effect of
      thickness on the fracture behaviour of compact
      tension specimens, INT. Journ of FRACT 14 (1978)
      203

43   N E FROST, L P POOK, K DENTON   A fracture mechanics
      analysis of fatigue crack growth data for various
      materials, ENG FRACT MECH 3 (1971) 109

44   S J MADDOX   The effect of mean stress on fatigue
      crack propagation - A literature review, INT Journ
      of FRACT 11 (1975) 389

45   T C LINDLEY, C E RICHARDS, R O RICHIE   The mechanics
      and mechanisms of fatigue crack growth in metals,
      CONF PROC Churchill, Cambridge

46   R J COOKE, P E IRVING, G S BOOTH, C J BEEVERS   The
      flow fatigue crack growth and threshold behaviour
      of a medium carbon alloy steel in air and vacuum,
      ENG FRACT MECH 7 (1975) 69

47   P E IRVING, A KURZFELD   Measurements of intergranular
      failure produced during fatigue crack growth in
      quenched and tempered steels, MET SCI 5 (1978) 495

48   A OHTA, M KOSUGE, E SASAKI   Fatigue crack closure
      over the range of stress ratios from -1 to 0.8
      down to threshold stress intensity level in HT 80
      steel and SUS 304 stainless steel,   INT Journ of
      FRACT. 14 (1978) 251

49   R O RICHIE, J F KNOTT   Mechanisims of faitgue crack
      growth in low alloy steel, ACTA MET 21 (1973) 639

50   C G GARRETT, J F KNOTT   On the influence of fatigue
      mechanisms of fatigue crack propagation in
      aluminium alloys, MET TRANS 6A (1975) 1663

51   R O RICHIE, K J BATHE   One the calibration of the
      electrical potential technique of monitoring crack
      growth using finite element methods, INT Journ of
      FRACT MECH 15 (1979) 47

52   C M HUDSON, J T SCARDINA   Effects of stress ratio
      on fatigue crack growth in 7075-T6 aluminium alloy
      sheet,   ENG FRACT MECH 1 (1969) 429

53   K SADANADA, P SHAHINIAN   Prediction of theoretical
      stress intensity for fatigue crack growth using a
      dislocation model, INT Journ of FRACT (1977) 585

54   J MASOUNAVE, J P BAILON   The dependance of the thres-
      hold stress intensity factor on the cyclic stress
      ratio in fatigue for ferritic-pearlitic steels,
      SCRIPTA MET 9 (1075) 723

55   M KLESNIL, P LUKAS   Effect of stress cycle asymmetry
      on fatigue crack growth, MAT SCI ENG 9 (1972) 231

56   R T DAVENPORT, R BROOK   The threshold stress intensity
      range in fatigue, FAT of ENG MAT and STRUCT 1 (1979)
      151

57   J C RADON   Fatigue crack growth in the threshold
      region, INT SYMP on FAT THRESHOLDS, Stockholm
      1-3 June (1981) Paper 4

58   J MASOUNAVE, J P BAILON   Effect of grain size on the
      threshold stress intensity factor in fatigue of
      ferritic steel, SCRIPTA MET 10 (1976) 165

59   E K PRIDDLE   The influence of grain size on the
      threshold stress intensity for fatigue crack growth
      in AlSl 316 stainless stainless steel, SCRIPTA MET
      12 (1978) 49

60   A J McEVILY   Current aspects of fatigue, MAT SCI
      Aug/Sept (1977) 274

61   A TAIRA, K TANAKA, M HOSHINA   Grain size effect on
      crack nucleation and growth in long life fatigue
      of low carbon steel, ASTM STP 675 (1979) p35

62   A CLERIVET, C BATHIAS   Study of crack tip opening
      under cycle loading taking into account the
      environment and load ratio, ENG FRACT MECH 12 (1979)
      599

63   K TANAKA   A correlation of ΔKT_h value with expontent,
      m, in the equation of fatigue crack growth in steels,
      INT Journ of FRACT 15 (1979) 58

64   J PETIT, J L MAILLARD   Environment and load ratio
      effects on fatigue crack propagation near threshold
      conditions, SCRIPTA MET 14 (1980) 163

65   F W NOBLE   The use of acoustic emmision for threshold
      determination in rigid polyurethane foam,   INT
      SYMP on FAT THRESHOLDS, Stockholm, 1-3 June (1981)
      Paper 1

66   L P POOK   Extensive study of low fatigue crack growth
      rates in A533 and A508 steels, ASTM STP 153 (1972)
      106

67   W W GERBERISH, N R MOODY   A review of fatigue fracture
      topography effects on threshold and growth mechanisms,
      ASTM STP 675 (1979) 292

68   P C PARIS, R J BUCCI, E T WESSEL, W G CLARK, T R MAGER
      Extension study of low fatigue crack growth rates in
      A533 and A508 steels, ASTM STP 515 (1972) 141

69   R J BUCCI, W G CLARK, P C PARIS Fatigue crack
      propagation growth rates under a wide variation of
      ΔK for an ASTM A157 grade F(T-1) steel. ASTM STP
      513 (1972) 177

70   R J BUCCI, P C PARIS, R W HERTZBERG, R A SCHMIDT,
      A F ANDERSON Fatigue threshold crack propagation
      in air and dry argon for a Ti-6AL-4V alloy, ASTM
      STP 513 (1972) 125

71   L P POOK, Practical implications of the fatigue
      crack growth threshold, MET SCI Aug/Sept (1977)
      382

72   R O RICHIE Influence of impurity segregation on
      temper embrittlement and on slow fatigue crack
      growth and threshold behaviour in 300 M high
      strength steel, MET TRANS 8A (1977) 1131

73   R J COOKE, C J BEEVERS The effect of load ratio
      on the threshold stresses of fatigue crack growth
      in medium carbon steel, ENG FRACT MECH 5 (1973)
      1061

74   E K PRIDDLE Fatigue crack growth in a high strength
      steel, "FRACT 77', Waterloo, Canada 2 (1977) 1249

75   M KLESNIL, P LUCAS Influence of strength and stress
      history on growth and stabilisation of fatigue cracks,
      ENG FRACT MECH 4 (1972) 77

76   J MASOUNAVE, J P BAILON Fatigue properties of plain
      carbon steels, PROC 2nd INT CONF on MECH BEHAVIOUR
      of MATERIALS, Boston (1976) 636

77   A J McEVILY, J GROEGER, On the threshold for fatigue
      crack growth, 'FRACT 77', Waterloo, Canada 2 (1977)

78   V M RADAKRISHNAN Quantifying the parameters in
      fatgiue crack propagation, ENG FRACT MECH 13 (1980)
      129

79   A T STEWART The influence of environment and stress
      ratio on fatigue crack growth at near threshold stress
      intensities in low alloy steels, 13 (1980) 463

80   T C LINDLEY, C E RICHARDS, R O RICHIE Mechanics and
      mechanisms of fatigue crack growth: A review -
      Metallurgia and Metal Forming 43 (1976) 268

81   K R DOWSE, C E RICHARDS Fatigue crack propagation
      through weld heat affected zones, MET TRANS 2
      (1971) 599

82   T C LINDLEY, C E RICHARDS Near threshold fatigue crack growth in materials used in the electrical supply industry, INT SYMP on FAT THERSHOLD, Stockholm, 1-3 June (1981) Paper 45

83   J P BENSON, D V EDMONDS Effect of microstructure on fatigue in threshold region in low alloy steel, MET SCI May (1978) 223

84   R RAJ, V K VARADAN The kinetics of hydrogen assisted crack growth, Mechanisms of Environ. sensitive cracking of Mat. Proc. Int. Conf. (1977) 426

85   G HAICHENG, J F KNOTT Effects of autenitisation temperature and tempering temperature on fatigue thresholds in a low alloy steel, INT SYMP on FAT THRESHOLDS, Stockholm, 1-3 June (1981) Paper 30

86   R W ARMSTRONG The influence of polycrystal grain size on several mechanical properties of materials, MET TRANS 1 (1970) 1169

87   M F CARLSON, R O RICHIE On the effect of prior austenite grain size on near threshold fatigue crack growth, SCRIPTA MET 11 (1977) 1113

88   R O RICHIE Near threshold fatigue crack porpagation in steels, INT MET REVIEWS 5/6 (1979) 205

89   Y HIGO, A C PICKARD, J F KNOTT Effects of grain size and stacking fault energy on fatigue crack propagation threshold in Cu-Al aluminium alloys, MET SCIENCE June (1981) 233

90   A W THOMPSON A comparison of yield and fatigue strength dependance on grain size, SCRIPTA MET 5 (1971) 859

91   C ROBIN, G ULUVINAGE Fatigue threshold in A2618A aluminium alloy, FAT of ENG MAT and STRUCT 3 (1980) 147

92   Y HIGO, A C PICKARD, J F KNOTT Effects of grain size and stacking fault energy on fatigue crack propagation thresholds in Cu-Al Aluminium alloys, MET SCI June (1981) 233

93   J LINDIGKEIT, G TERLINDE, A GYSLER, G LUTJERING The effect of grain size on the fatigue crack propagation behaviour of age hardened alloys in inert and corrosive environments, ACTA MET 27 (1979) 1717

94   P R V Evans, N B OWEN, B E HOPKINS The effect of purity on fatigue crack growth in a high strength steel, ENG FRACT MECH 3 (1971) 463

95   J KATAJISTO, A calculation of the threshold stress range of fatigue crack propagation in weldment, INT SYMP on FAT THRESHOLDS, Stockholm, 1-3 June (1981) paper 26.

96   P O W E KAO, J G BYRNE, Microstructural influences on fatigue crack propagation in pearlitic steels, INT SYMP on FAT THRESHOLDS, Stockholm, 1-3 June (1981) paper 22.

97   S E STANZL, High frequency fatigue crack growth and threshold behaviour in monocrystalline copper, SCRIPTA MET 14(1980) 749

98   P T HEALD, C ATKINSON, The influence of slip dislocations on the propagation of fracture from a crack tip, ACTA MET 15 (1967) 1617

99   K KATAGIRI, J AWARANI, A OMURA, K KOYANAGI, T SHIRAISHI, Dislocation structures around the crack tips in the early stage in fatigue of iron, ASTM STP 675 (1979) 106

100   D KUHLMANN-WILSDORF, C LAIRD, Dislocation behaviour in fatigue II. Friction stress and back stress as inferred from an analysis of hysteresis loops, MAT SCI and ENG 37 (1979) 111

101   D KUHLMANN-WILSDORF, C LAIRD, Dislocation behaviour in fatigue V. Breakdown of loop patches and formation of persistant slip bands and of dislocation cells, MAT SCI and ENG 46 (1080) 209

102   J C GROSSKREUTZ, P WALDON, Substructure and fatigue fracture in aluminium.

103   K KATIGIRI, J AWATANI, K KOYANAGI, Y ONISHI, M TSUJI, Dislocation structures adjacent to fatigue crack tips propagating at high rates in copper and 70/30 brass, MET TRANS 11 (1980) 2029

104   L M BROWN, Dislocation substructures and the initiation of crack by fatigue, MET SCI Aug/Sept (1977) 315

105   W A JOHNSON, N S STOLOFF, Microstructure and fatigue of a Ni, Cr, Al, Ta eutectic composite, MET TRANS 11 (1980) 307

106   A J CADMAN, C E NICHOLSON, R BROOK, Microstructural effects at and near the fatigue threshold, INT SYMP on FAT THRESHOLDS Stockholm, 1-3 June (1981) paper 34

107   G T GRAY, A W THOMPSON, J C WILLIAMS, D H STONE,
      Influence of microstructure on fatigue crack growth
      behaviour in fully pearlitic steels, INT SYMP on
      FAT THRESHOLDS, Stockholm, 1-3 June (1981)
      paper 28

108   J A LEWIS, Fatigue thresholds in medium strength
      steel, INT SYNP on FAT THRESHOLDS, Stockholm,
      1-3 June (1981) paper 32

109   K MINAKAWA, A J McEVILY, On near threshold fatigue
      crack growth in steels and Aluminium alloys, INT
      SYMP on FAT THRESHOLDS, Stockholm, 1-3 June
      (1981) paper 36

110   C W BROWN, G C SMITH, The effect of microstructure
      and texture on fatigue crack growth threshold in
      Ti-6Al-4V, INT SYMP on FAT THRESHOLDS, Stockholm,
      1-3 June (1981) paper 16

111   J BYRNE, T V DUGGAN, Fatigue crack growth in the
      threshold region, INT SYMP on FAT THRESHOLD,
      Stockholm, 1-3 June (1981) paper 4

112   R N WRIGHT, A S ARGON, Fatigue crack growth in Si-Fe,
      MET TRANS 1 (1970) 3065

113   J D FRANDSEN, H L MARCUS The correlation between
      grain size and plastic zone size for environmental
      hydrogen assisted fatigue crack propagation, SCRIPTA
      MET 9 (1975) 1089

114   R P SKELTON, J R HAIGH Fatigue crack growth rates and
      thresholds in steels under oxidising conditions,
      MAT SCI and ENG 36 (1978) 17

115   A T STEWART The effect of hydrogen on fatigue
      crack propagation in steels, Mechanimsm of
      Environment Sensitive Cracking of Mat. Proc.
      Int. Conf (1977) 400

116   J D FRANDSEN, N E PATON, H L MARCUS, The influence
      of low pressure hydrogen gas on crack growth in
      TD Nickel and TD Nichrome, SCRIPTA MET 7 (1973)
      409

117   E BARDAL, T BERGE, M GROVLEN, P J HAAGENSEN, B M FORRE,
      Measurements of very low corrosion fatigue crack
      growth rates in structural steel in artificial
      sea water, INT SYMP on FAT THRESHOLDS, Stockholm,
      1-3 June (1981) paper 30

118   J PETIT, A ZEGHLOUL, Gaseous environment effect on
      threshold level in high strength aluminium alloys,
      INT SYMP on FAT THRESHOLDS, Stockholm, 1-3 June
      (1981) paper 21

117

119   J R KENNEDY, P N ADLER, R L SCHULTE, Hydrogen
related fatigue fracture of Ti-6Al-4V, SCRIPTA MET
14 (1980) 299

120   J D ATKINSON, T C LINDLEY, The effect of frequency
and temperature on environmentally assisted fatigue
crack growth below Kiscc in steels, Conf. Proc.
INST MECH ENG HQ May (1977) C106/77

121   G F PITTINATO, Hydrogen enhanced fatigue crack growth
in Ti-6Al-4V, ELI weldments, MET TRANS, 3 (1972)
235

122   J K TIEN, S NAIR, R C BATES, O BUCK, Dislocation
sweeping model for hydrogen assisted subcritical
crack growth, SCRIPTA MET 14 (1980) 591

123   J K TIEN, O BUCK, R C BATES, S NAIR, On the role of
time delayed hydrogen assisted plastic zone growth
on subcritical crack growth in high strength
steels, SCRIPTA MET 14 (1980) 583

124   G M PRESSOUYRE, Trap theory of hydrogen embrittlement,
ACTA MET 28 (1980) 895

125   J K TIEN, A W THOMPSON, I M BERNSTEIN, R J RICHARDS,
Hydrogen transport by dislocations, MET TRANS 7A
(1976) 821

126   A INOVE, Y HOSOYA, T MASUMOTO, Effect of hydrogen
on the propagation of cracks and defect structure
around cracks in α iron, TRANS of Iron and Steel INST
of Japan 7 (1980) 433

127   R A ORANI, P H JOSEPHIC Equilibrium aspects of
hydrogen induced cracking of steels, ACTA MET
22 (1974) 1065

128   R B SCARLIN Some effects of microstructure and
environment on fatigue crack propagation, ASTM
STP 675 (1979) 396

129   S P LYNCH, Mechanisms of fatigue and environmentally
assisted fatigue, ASTM STP 675 (1979) 174

130   K SIERADZKI, P FICALORA Kinetic aspects on slow
crack growth in the gaseous hydrogen embrittlement
of steels, JOURN of MAT SCI 14 (1979) 2703

131   W W GERBERISH, Y T CHEN, C ST JOHN, Short time
diffusion correlation of hydrogen induced crack
growth kinetics, MET TRANS 6A (1975) 1485

132   D I GOLLAND, P L JAMES Fatigue crack initiation
       and propagation in iron and iron-silicon alloys,
       MET SCI JOURN 4(1970) 113

133   N M GRINBERG, E N ALEKSENKO Fatigue failure of
       silicon iron in air and in vaccum, PROBLEMY
       PROCHNOSTI 5 (1977) 40

134   R C BOETTNER, A J MCEVILY Fatigue slip band
       formation in silicon iron, ACTA MET 13 (1965) 937

135   C E RICHARDS The influence of material properties
       on fatigue crack propagation as demonstrated by
       experiments on silicon iron, ACTA MET 19 (1971)
       583

136   P NEUMANN New experiments concerning the slip
       processes at propagating fatigue cracks - I,
       ACTA MET 22 (1974) 1155

137   P NEUMANN The geometry of slip processes at a
       propagating fatigue crack - II, ACTA MET 22
       (1974) 1167

138   P NEUMANN, H VEHOFF, H FUHLROTT On the mechanisms
       of fatigue crack growth, CONF. PROC 'FRACT 77',
       Waterloo, Canada 2 (1977) 1313

139   H VEHOFF, P NEUMANN Crack propagation and cleavage
       initiation in Fe-2.6%Si single crystals under
       controlled plastic crack tip opening rate in various
       gaseous environments

140   W W GERBERICH, N R MOODY, K JATAVALLABHULA A proposed
       cyclic cleavage crack growth model for fatigue of
       BCC iron and its alloys, SCRIPTA MET 14 (1980)
       113

141   P NEUMANN, H FUHLROTT, H VEHOFF Experiments
       converning brittle, ductile, and environmentally
       controlled fatigue crack growth, ASTM STP 675
       (1979) 371

142   S SAXENA, S ANTOLOVICH Low cycle fatigue crack
       propagation and substructures in a series of
       polycrystaline Cu-Al alloys, MET TRANS 6 (1975)
       1809

143   J T EVANS, F X LU Plastic deformation and fatigue
       crack growth in grain orientated Fe-3.5 Si, ACTA
       MET 30 (1980) 751

144   D L DAVIDSON The study of fatigue mechanisms with
       electron channeling, ASTM STP 675 (1979) 254

145   F B PICKERING The basis of quantitative matallo-
        graphy, Institute of Metallurgical Technicians
        (1976)

146   O BUCK Characterisation of a propagating crack
        by ultrasonic techniques, INT JOURN of FRACT
        MECH 8 (1972) 121

147   S TAIRA, K TANAKA Study of fatigue crack propagation
        by X-ray diffraction approach, ENG FRACT MECH
        4 (1972) 925

148   I M AUSTEN, E F WALKER An assessment of the ability
        of various methods of fatigue crack growth rate
        determination, BSC Sheffield LABS, Report No
        SH/PT/7422/8/79/B (1979)

149   R O RICHIE, G G GARRETT, J F KNOTT Crack growth
        monitoring optimisation of the electrical potential
        technique using an analogue method, INT JOURN of
        FRACT MECH 7 (1971) 462

150   J M LOWES, G D FEARNEHOUGH The detection of slow
        crack growth in crack opening displacement
        specimens using an electrical potential technique,
        ENG FRACT MECH 3 (1971) 103

151   K JERRAM, E K PRIDDLE System for determining the
        critical range of stress intensity factor necessary
        for fatigue crack propagation, JOURN of MECH ENG
        SCI 15 (1973) 271

152   R O RICHIE, K J BATHE On the calibration of the
        electrical potential technique for monitoring
        crack growth using finite element methods, INT
        JOURN of FRACT 15 (1979) 47

152   I M AUSTEN, E F WALKER Calibration of the electrical
        resistance technique for crack growth monitoring in
        CKS type test pieces, BSC Sheffield Labs. Research
        Report No PMC/6795/6/76/B (1976)

153   J P BAILON, J I DICKSON, J MOSOUNAVE, C BATHIAS
        Technical note - comment on the threshold stress
        intensity range in fatigue, FAT of ENG MAT and
        STRUCT 3 (1980) 277

155   H DOLLE, J B COHEN Residual stresses in ground
        steels, 11A (1980) 159

156   J PETERS, R SNOEYS, M MARIS Residual stresses in
        grinding, CONF PROC ADVANCED FAB PROC, Florence
        September 79 March 80

157   A MISURA, U R K RAO, R NATARAJAN ibid,
       An analytical approach to the determination
       of residual stresses in surface grinding

158   CEGB Instruction manual for the GEGB air-abrasive
       system for measuring residual stresses, Research
       Division, Berkeley Nuclear Laboratories

159   E M BEANEY Accurate measurement of residual stress
       on any steel using the centre hole method, Strain
       July (1976) 99

160   E PROCTER Residual stress, Welding Institute
       (1981) 34

161   E M BEANEY, E PROCTER A critical evaluation of
       the centre hole technique for the measurement
       of residual stress, STRAIN (1979) 7

162   K M LAL, S B L GARG Plastic zones in fatigue
       ENG FRACT MECH 13 (1980) 407

163   G T HAHN, A R ROSENFIELD Sources of fracture
       toughness: The relation between K_{IC} and the
       and the ordinary properties of metals, ASTM
       STP 432 (1968) 5

164   C J BEEVERS Micromechanisms of fatigue crack
       growth at low stress intensities, MET SCIENCE
       14 (1980) 418

165   A OHTA, E SASAKI Fatigue crack closure at stress
       intensity threshold levels, INT JOURN of FRACT
       11 (1975) 1049

166   S SURESH, G F ZAMISKI, R O RICHIE Met Trans
       12A (1981) 1435

167   R O RICHIE, S SURESH Communications - Some con-
       siderations on fatigue crack closure at near
       threshold stress intensities due to fracture
       surface morphology, MET TRANS 13A (1982) 937

168   R A SCHMIDT, P C PARIS Threshold for fatigue crack
       propagation and the effects of load ratio and
       frequency, ASTM STP 536 (1973) 79

169   G A O HUA, M W BROWN, K J MILLER Mixed mode
       fatigue thresholds, FAT of ENGINEERING MAT
       and STRUCT 5 (1982) 1

170   P E IRVING, J L ROBINSON, C J BEEVERS, A study of
       the effects of mechanical and environmental
       variables on fatigue crack closure, ENG FRACT MECH
       7 (1975) 619

AN ASSESSMENT OF THE OVERALL ECONOMICS OF THE FABRICATION OF A SYSTEM GAS STORAGE

INTRODUCTION

Steels are used extensively in the containment of liquids, gases and liquid gas mixtures in vessels under pressure and often operated at elevated temperature. They provide a range of usable properties at a much lower cost than possible with alternative materials. It is also important in these applications that the material is capable of being welded.

In order to fulfil their function pressure vessel steels must have a number of properties:-

(i)   High yield strength and low impact transition temperature.

(ii)   High fracture toughness and good resistance to fatigue crack propagation.

(iii)   Resistance to corrosion and oxidation.

(iv)   Creep resistance in high temperature applications.

(v)   Good weldability.

(vi)   Good formability in plate or sheet form.

(vii)   Minimum cost.

It is worthwile, at this point, to give some consideration to the strengthening mechanisms operable in steel in order

to optimise properties and cost. The main strengthening
mechanisms are:-

(i)   Solid Solution Strengthening

Solute elements increase the yield strength and ultimate
tensile strength and the strengthening effect is mainly
due to the difference in atomic size between the solute
element and iron. The effect of both substitutional and
interstitial solutes has been shown to influence strength
by a factor proportional to the square root of their
concentration. In dilute solution, as in the case with
most steels, this relationship can be simplified to a
linear dependance of solid solution strengthening upon
the atomic percentage of solute. The strengthening effect
of interstitial solutes is between one and two orders of
magnitude greater than substitutional solutes. However
their solubility is limited and they cannot be used to any
greater extent.

Substitutional and interstitial solutes are detrimental
to steel toughness, with the exception of nickel. Other
effects may be achieved by the addition of solutes such
as the alteration of the ferrite-pearlite ratio, refining
the grain size by depressing the transformation
temperature, precipitation effects and withdrawing inter-
sitials from solution (ie Aliminium).

(ii)   Grain Size Effects

Refinement of the grain size leads to an increase in the
yield strength and also decreases the impact transition
temperature.   The dependance of yield stress on grain
size is given by the Hall Petch relationship

$$\sigma_{ys} = \sigma_i + K_y d^{-\frac{1}{2}}$$

Where d is the grain size, σ_{ys} is the yield stress, σ_i is
the friction stress and K_y is a constant.   This
combination of desirable properties accounts for the
extensive use of grain refined steels.   Refined by
additions of aluminium or niobium.

(iii)   Dislocation Strengthening

The flow stress can be related to the dislocation
density by the following relationship:-

$$\sigma_f = \sigma_o + K\sqrt{\rho}$$

Where σ_o is the flow stress due to other strengthening
mechanisms, ρ is the dislocation density and K is a
constant incorporating the shear modulus and the burgers
vector.   Flow stress increases as dislocation density
increases.   The work hardening rate is dependant upon the
way the dislocations are distributed and their inter-
actions .

(iv) Precipitation Strengthening

Precipitation of second phase particles can increase material strength but also lower impact resistance. The effectiveness of elements such as niobium titanium and vanadium depend upon their solubility in austenite. Grain refinement is also achieved by using small quantities of these elements. During cooling interphase precipitation occurs which produces fine precipitates which lead to strengthening.

(v) Transformation effects

Generally, the lower transformation temperature the greater the strengthening effect. Lower transformation temperatures produce a finer grain size. This is used in high strength low alloy steels of ferrite-pearlite structures and low carbon bainitic steels. The dislocation density is also increased by lowering transformation temperatures. Solid solution strengthening is also enhanced by lower transformation temperatures. Whilst these effects all contribute to strengthening, effects on ductility and toughness can be variable and combinations of these effects can lead to complex results.

A number of different steel types are available for consideration for gas storage applications and these are reviewed below.

(a) Carbon Manganese Steels

Manganese additions to steels have a number of beneficial effects. Combination of manganese and sulphur to form high melting point sulphide inclusions which when uniformly distributed throughout the steel do not greatly affect toughness. The alternative product is usually iron rich sulphides which have a very damaging effect on material properties. Manganese imports solid solution strengthening and also retards the austenite to ferrite/pearlite reaction which results in more uniform properties. Higher strength levels can be obtained for a given cooling rate.

The major advantages of C.Mn steel are their relative cheapness and their ease of production in large quantities. These steels include the mild steel boiler plate with yield strengths of about 230 MNm^{-2} and UTS of about 390 MNm^{-2}. They are extensively used in boiler and high pressure plant upto about 350°C. Above this temperature strength levels fall off rapidly. Corrosion properties and scaling resistance are also poor. Ambient temperature properties can be improved by normalising, controlled rolling and quenching and tempering.

(b)   Molybdenum,   Chromium-Molybdenum and Chromium-
      Molybdenum-Vanadium Steels

The addition of Molybdenum to C-Mn steels increases
strength levels slightly at ambient temperature but
has a marked effect at higher temperatures. Carbon
manganese steels containing 0.5% Mo are used
extensively in pressure vessel applications. The
creep ductility and high temperature oxidation is
limited in these steels and therefore chromium-
molybdenum type steels, containing upto 9% Cr and
1% Mo may be preferred.

For higher temperature applications properties can
be improved by further additions of Cr and Mo.
2.25% - 1% Mo steels are used for their superior hot
strength 5% Cr-Mo and 9% Cr-Mo steels are used
widely in the petrochemical industry for their
superior corrosion and oxidation resistance.

Creep strength can be improved by the addition of
vanadium in addition to chromium and molybdenum to
give nominal compositions such as 1% Cr - 1½% Mo -
¼% V and ½% Cr - ½% Mo - ¼% V. On air cooling or
oil quenching these steels are martensitic and good
combinations of properties can be achieved by
tempering. One of the principle factors promoting
high creep strength is the presence of small
vanadium cabide particles in the structure .

(c)   Complex Bainitic Steels

The addition of small quantities of elements such as
manganese, chromium, molybdenum and vanadium in the
right quanties promotes transformation to bainite.
The alloying elements retard the transformation from
austenite and therefore effectively move the TTT
diagram to the right.   The resulting structure is
relatively strong at ambient temperatures and it main-
tains its strength well at higher temperatures.
These steels are particularly suited to applications
where the required working temperatures are not
particularly high but a higher strength level, than
obtained with C-Mn steels, is required. Superior
fracture toughness and weldability are also achieved.

(d)   Quenched and Tempered Steels

The addition of combinations of alloying elements to
steel leads to a retardation in the transformation
kinetics and this allows harder structures to be
obtained at equivalent rates of cooling. Increasing
hardenability by correct addition of alloying
elements to produce a martensitic structure through-
out when quenched or air cooled produces an important
group of steels. These steels can then be tempered
to produce an adeuqate combination of properties.
The total quantity of alloying elements in these
steels may be high but it is possible to obtain a
good combination of high strength and toughness. They

128

are also relatively easy to weld since the carbon
content can be kept low.

Table 1 shows a number of commercial steels with
typical compositions and properties.

TABLE 1

ANALYSIS

TYPE	C	Si	Mn	Nb	Ni	Cr	Mo	V	B	HEAT TMT	YS MNm^{-2}	UTS MNm^{-2}
BS 4360-43C	0.18 (max)	–	1.5 (max)	–	–	–	–	–	–	AR	240	500
BS 4360-43D	0.16 (max)	–	1.5 (max)	0.1 (max)	–	–	–	–	–	N	270	500
QT 131 A	0.2 (max)	0.5 (max)	1.6 (max)	0.1 (max)	–	–	–	–	–	QT	400	560
QT 131 B	0.2 (max)	0.1 0.5	1.6 (max)	–	0.5 (max)	–	–	–	–	QT	430	590
QT 445 A	0.15 0.21	0.8 (max)	0.8 1.1	–	–	0.5 0.8	0.18 0.4	–	.0005 .0025	QT	695	803
QT 445 B	0.15 0.21	0.9 (max)	0.8 1.1	–	–	0.5 0.8	0.25 0.6	–	.0005 .0025	QT	695	803
BS 4360-55C	0.22 (max)	0.6 (max)	1.6 (max)	0.1 (max)	–	–	–	–	–	AR	430	600
BS4360-55E	0.22 (max)	0.6 (max)	1.6 (max)	0.1 (max)	–	–	–	–	–	N	430	600

Cylinderical pressure vessels are usually formed by a steel plate and welding along the seam. End plates can then be fitted and welded. The most likely site of failure of cylinderical vessels of this type is the welded seam. Consequently much time and expense is expended in ensuring that both weld and heat effected zone are of a suitably high quality.

For all the main seams mechanised processes are preferred to reduce the number of welding defects and reduce costs. A number of welding processes are used and it is worth-while reviewing these at this point.

Submerged arc welding is an automatic process capable of high deposition rates on straightforward joints. The process is limited to flat, horizontal and vertical welding positions and is restricted to steels. Careful joint alignment is also required. Increased usage of the submerged arc process is envisaged for further welds and butt welds on steels from 5 to 50 mm thick for weld lengths greater than one metre.

Manual metal arc (MMA) may be used to produce the required external weld profile. Manual metal arc is extremely versitile and is also a low cost process. Excellent joint properties can be obtained in mild, low alloy, stainless steels and copper and nickel based alloys. It is basically a manual technique requiring a skilled

operator for best results. Multirun welds are necessary
in thick plates and slag removal is required after each
pass together with frequent changes of electrodes.

Other welding processes are the MIG (Metal inert gas)
and TIG (Tungston inert gas) techniques which both rely
on gas shielding. In the MIG process the arc is made
between base filler wire and the workpiece and in the TIG
process the arc is made between a non-consumable tungston
electrode and the work piece with filler material being
added when necessary. The TIG process is relativly slow
but a high degree of control is possible. It is therefore
frequently used for root runs and other welds where a
good root bead shape is important. The MIG process is
capable of higher deposition rates and is easily
mechanised which produces welds or a more even quality.

Welding effects on microstructure

During welding the parent metal adjacent to the molten
weld pool is rapidly heated, the rate of heating being
dependent upon the rate of movement of the heat source
along the weld and the rate at which energy is supplied.
When the welding head has passed the parent metal adjacent
to the weld is rapidly cooled by conduction of heat into
the surrounding mass of cold parent material. The rate of
cooling is dependent upon the amount of material heated
in relation to the thickness and dimensions of the job.
The weld metal usually cools rapdily to form a chill
casting.

The parent metal is heated during welding to a temperature which depends upon the distance from the fusion boundary. A large temperature gradient is produced and peak temperatures adjacent to the fusion boundary are approaching the liquidus. A few millimeters away the temperature may only reach a few hundred degrees ^{o}C. Material heated below the lower critical temperatures is very little changed although properties may be affected by the combined effects of strain and temperature. Material heated above this undergoes a phase change to austenite and on cooling transforms to a structure which may differ considerably from the parent metal. This may lead to weld cracking or poor joint properties.

The effect of a local application of heat is to cause expansion on heating and contraction on subsequent cooling. However this expansion and contraction are constrained by the surrounding cold material and result of which is a tensile residual stress in the weld and heat affected zone. Tensile residual stresses exist approximately three weld widths on either side of the weld and are of yield stress magnitude. Plastic deformation also occurs in the region of the weld and may result in cracking if the ductility falls to a level where the plastic strain cannot be accommodated. Control of cracking problems is achieved by manipulating the plastic strain and the ducility.

Welding Defects

Welding can result in a number of defects which are outlined below:

Solidification cracking occurs as the growth of dendritic crystals occurs in the molten weld. Solute and impurity elements are rejected ahead of the growing crystals and become concentrated in the residual liquid lowering its freezing point. If the freezing point of the remaining liquid is sufficiently lowered then liquid films may persist. At the same time the weld and its immediate surroundings are contracting so a tensile strain is applied across the weld. If the ductility of the weld metal is lowered by the presence of a residual film then cracking may occur. Cracking will be affected by the impurity content of the weld material, parent metal and by the amount of strain occurring during solidification. Weld metals with a low susceptability to solidification cracking are available for most alloy steels. Incorrect setting of welding perameters in automatic processes may lead to problems with solidification cracking.

Heat effected zone liquation cracking may occur where high peak temperatures occur in the HAZ and local melting may occur at grain boundaries in ferritic steels due to the formation of eutectic sulphide. This phenomena in conjunction with plastic strains may cause microcracks to open up at the liquation boundaries. When the liquid solidifies the resulting grain boundary sulphide film

may reduce the fracture toughness of the heat effected zone to unacceptable levels. This problem may be overcome by specifying a low sulphur content of the parent metal. Phosphorus must also be maintained at a low level.

Hydrogen cracking may occur after welding if - hydrogen is introduced during welding, the weld metal or HAZ is susceptable and a high level of residual stress is present after welding. Cracking may then occur under the influence of the residual stress in the susceptable HAZ or weld metal. The extent to which the weld HAZ strength is reduced depends strongly upon the analysis of the parent and weld material. High strength steels are more susceptable than low strength steels.

If the through thickness ductility is low, lamellar tearing may result. Lamellar tearing most frequently occurs when long range stresses are present as well as local welding stresses. This phenomena occurs when planar inclusions (particularly large ones) are present parallel to the plate surface. Arrays of small inclusions can also have the same effect. The possibility of lamellar tearing also increases with increasing material strength. This phenomena can be avoided by the use of forged products as lammellar inclusion in plate are the result of large reductions occurring during rolling.

PRESSURE VESSEL CASE STUDY - A GAS STORAGE SYSTEM

This case involves the production of a number of storage vessels for a secondary shutdown system at a nuclear power station which, when activated, injects nitrogen into the reactor core. The system requires a large permanent storage capacity for high pressure gaseous nitrogen. The vessels were part of a contract proposal by a pressure vessel manufacturer for the CEGB in 1981.

The storage system is normally pressurised but inactive. When the system is activated the nitrogen is injected into the reactor until the store and reactor pressures equalise. Part of the storage capacity will be exhausted to reactor pressure in approximately one minute and the remainder will take several hours.

Specifications required by the CEGB were as follows:-

The design of the vessels must be in accordance with BS 5500 Category 1.

The design life is 30 years. All welded joints are to be designed to allow for full ultrasonic inspection.

The vessels are required for storing dry nitrogen gas and will be sited outdoors, possibly under cover. For a large part of the working life the system will be inactive and the vessels will be kept at a pressure which will vary with ambient temperatures. When the system is operated the store discharges into the reactor over a period of several hours.

During discharge of the nitrogen the vessels temperature falls to low values.

The ambient temperature range is $-13^{\circ}C$ to $+30^{\circ}C$. The corresponding maximum working pressures are 130.5 bar abs and 158.9 bar abs respectively. As the gas is discharged its pressure and temperature fall. For an ambient temperature of $-13^{\circ}C$ the lowest gas and vessel temperature is $-28^{\circ}C$. The number of these cycles is, for design purposes, 300. The minimum total vessel volume is 487 m^3 and a corrosion allowance of 1 mm is to be allowed on each metal surface.

The full length of all welds is to be examined by ultrasonics and by magnetic particle methods. The inside surface of the vessels are to be completely free of any scale or grit or corroded material which may become loose during service and possibly be carried into the system control valves.

In addition to being hydraulically tested the vessels are to be leak tested with a suitable search gas and are given a maximum leak rate of 1 insec at 0.1 times the design pressure. After testing and final inspection the vessels are to be sealed and filled with dry, oil free nitrogen.

MATERIALS

In order to illustrate this case study three steels have been selected as possible, suitable candidates for this application. This is not a complete list of suitable steels.

The selected steels are:- BS 1501 224, BS 1501 281 and HYPLUS 29. Analysis and mechanical properties are given in tables 2 and 3. Table 3 indicates the mechanical properties in the normalised condition and since mechanical properties are variable with thickness only the properties at the relevant vessel wall thickness are considered.

STRESSES ACTING ON A CYLINDRICAL VESSEL UNDER INTERNAL PRESSURE

Stresses acting on cylinderical bodies can be analysed in terms of the radial forces acting on the circumference of a circular ring. Hoop forces are produced which act in a tangential direction. An enlargement of the ring will occur if the forces are radial outwards and the opposite will occur if the forces are radial inwards. The magnitude of the force in a section of the ring can then be expressed as follows:-

$$F = qr$$

where q is the unit length of circumference and r is the radius of the ring.

The unit stress in the ring is then obtained by dividing the force F by the cross sectional area.

$$\sigma = \frac{qr}{A}$$

where A = Cross sectional area

r = Vessel radius

TABLE 2 CHEMICAL ANALYSIS

	C	Si	Mn	P	S	Cp
BS 1501 224	0.15 - 0.22	.10 - .55	.90 - 1.50	.050 max	0.050 max	.25
BS 1501 281	0.09 - 0.15	.40	.90 - 1.30	.040 max	0.040 max	.40 - .70
HYPLUS 29	0.22 max	.15 - .50	1.60 max	.050 max	.050 max	-

	Mo	Ni	Cu	V	N	Nb
BS 1501 224	.10	.30	.30	-	-	-
BS 1501 281	.20 - .28	.70 - 1.00	.30	0.04 - 0.12	.015	.10
HYPLUS 29	-	-	-	.20	-	-

TABLE 3 MECHANICAL PROPERTIES

	UTS (MNm^{-2})	YS (MNm^{-2})	Elongation (%)
BS 1501 224	490 - 600	310	16
BS 1501 281	590 - 680	415	16
HYPLUS 29	600 - 695	448	20

If the ring is considered to be a section of a cylindrical vessel of thickness, h, and stress in the vessel is:-

$$\sigma = \frac{pr}{h}$$

where p = internal pressure.

The longitudinal stress can then be determined by equating the total pressure acting against the end of the cylinders to the longitudinal forces acting on a transverse section of the cylinder:-

$$\sigma h 2\pi r = p\pi r^2$$

$$\sigma = \frac{pr}{2h}$$

FRACTURE MECHANICS CONSIDERATIONS

If it is assumed that steel contains defects which are sufficiently small so as to be undetectable by non-destructive testing methods then it is likely that these defects may grow, by fatigue, during service. It is therefore important in selecting materials and operating limits for pressure vessels that catastrophic failure does not occur by defects growing to critical sizes. A leak before break criterion may be applied. This is based on the fracture mechanics concept that a detectable leak can be supported by the vessel without catastrophic failure occurring. Some experience with thin walled pressure vessels shows that vessels containing through cracks perpendicular to the hoop stress of length twice the

thickness of the vessel will deform sufficiently under
pressure to permit leakage.

Critical crack sizes required to produce catastrophic
failure can be determined using suitable analysis.
Equations based upon the one below are commonly used:-

$$a_{crit} = \frac{K_{Ic}^2 \; Q}{1.21 \; \pi \; \sigma^2}$$

where Q is a flaw shape parameter
and σ is the hoop stress.

The flaw shape parameter, Q, is dependant upon the major
and minor axis dimensions, particularly of non metallic
inclusions. A knowledge of fracture toughness parameters
and inclusions sizes, therefore provides vital information
in determining critical crack sizes and the amount of
allowable growth before failure may occur.

The situation is further compounded if stress corrosion
cracking and/or fatigue are taking place. Sub-critical
crack growth may occur as a result of the presence of
either of these mechanisms and lead to growth of defects
to critical sizes.

Fatigue crack propagation studies in a number of materials
have shown that under steady loading conditions the rate of
crack growth is often a unique function of the stress
intensity range ΔK. A simple power law relationship sug-
gested by Paris has been shown to hold for intermediate
fatigue crack growth rates.

$$\frac{da}{\partial N} = C(\Delta K)^n$$

where C and n are constants.

Crack propagation data may be used to determine values of ΔK_I that may be tolerated or alternatively the number of cycles required to extend a crack of initial length, a_i, to a critical size, a_c, can be established.

Thus, the uses of linear elastic fracture mechanics data and fatigue data can be instrumental in providing detailed knowledge of defect tolerance in the pressure vessel field leading to more efficient use of materials and resources.

PRESSURE VESSEL FABRICATION

The fabrication of the pressure vessel is carried out in accordance with BS 5500:1982.

For cylindrical shells the minimum calculated thickness of shell plate excluding corrosion allowances is given by the design equation

$$e = \frac{pDi}{2f-p}$$

where p is the design pressure.

     Di is the inside diameter of the shell without

         corrosion allowance.

     f is the nominal design stress.

This equation produces the following material data.

Material	Vessel Length (mm)	Vessel Diameter (mm)	Thickness of Shell (mm)	Thickness of ends (mm)
BS 1501 224	15,000	508	16	25
BS 1501 281	15,000	508	14	21
HYPLUS 29	15,000	508	13	21

Vessel length and diameter are as prescribed by the vessel specification. The thickness of the end plates are derived from spherical shell formuli.

The reduction in shell thickness leads to some savings in material costs, however this may be balanced against the cost per tonne of a given steel.

The vessel material costs for the vessels of thickness indicated above are as follows:-

	£/Vessel
BS 1501 224	1364
BS 1501 281	2087
HYPLUS 29	1333

All cost data has been provided by a company working in the pressure vessel field and were correct in 7 June 1983.

In all three vessel cases welding is identical. A T.I.G. root run is made to produce high quality weld deposits and a good bead shape. This process is carried out automatically. The welding is completed by automatic multirun manual metal arc. Weld perheat and stress relief treatment

is necessary to avoid the possibility of cracking. The
costs of forming and welding are shown below.

	£/Vessel
BS 1501 224	3931
BS 1501 281	5126
HYPLUS 29	4738

In the case of pressure vessel manufacturer considered
cost of forming the vessels was increased by press tool
non-availability and the necessity of using non standard
press tools for the thinner shelled vessels.

The amount of non destructive testing required depends upon
the type and thickness of the shell being welded and is
carried out in accordance with BS 5500: 1982. BS 1501 224
requires ultrasonic inspection of the weldment at a cost
of £159.00 BS 1501 281 and Hyplus 29 have more stringent
requirements imposed upon them. Higher yield stress and
thinner vessel walls make the detection of small defects
very important and therefore a full X-ray is required and
ultrasonic inspection of the weld costing £778.

The total cost of production including finishing treatments
(painting etc) is as follows.

	£/Vessel
BS 1501 224	5454
BS 1501 281	8307
HYPLUS 29	7151

It must be noted at this point that in practice BS 1501 281
has a minimum quantity delivery from steel suppliers, of
3 tonnes and therefore material cost would increase from
£2,087 to 3,651. This increases the total cost of this
vessels fabrication to £9,871.

Clarely the cheapest vessel to produce is the BS 1501 224,
approximately 25% cheaper than Hyplus 29.

DISCUSSION

In this example there is a considerable difference in total
production costs between the vessels described. Had this
not been the case a number of other factors may have con-
tributed in the final decision. Fatigue, corrosion fatigue
or, more importantly, stress corrosion cracking properties
may be significant.

Corrosion below the paint layers can reduce fatigue life
through damage to surfaces causing roughening and also by
pitting which reduces the cross-sectional area, thereby
increasing the magnitude of the applied stress. During
corrosion fatigue corrosion occurs both on the surface
and in a crack once formed, accelerating growth rates by
corrosion products wedging open cracks to allow corrosion
to continue. Stress corrosion cracking is the most serious
problem in this example since the number of fatigue cycles
likely to be experienced by a vessel in this application
is probably less than 10^2. Stress corrosion properties
particularly in the suseptable heat affected zone may be

significant if high residual stresses remain in the HAZ and a corrosive environment is present. Preferential rusting has been observed adjacent to weld seams and illustrates the problems which may occur.

TABLE 1

SERIES 1   CAST ANALYSIS   (Wt%)

	C	Si	Mn	S	P	N_2	O_2
1S00 A	<.01	<.01	<.01	<.002	<.002	0.001	0.015
B	<.01	<.01	<.01	<.002	<.002	0.001	0.012
1S05 A	<.01	0.34	<.01	<.002	<.002	0.002	0.020
B	<.01	0.38	<.01	<.002	<.002	0.002	0.020
1S10 A	<.01	0.82	0.015	<.002	<.002	0.001	0.018
B	<.01	0.83	0.015	<.002	<.002	0.001	0.014
1S20 A	<.01	1.79	<.01	<.002	<.002	0.001	0.016
B	<.01	1.79	<.01	<.002	<.002	0.001	0.014
1S30 A	<.01	2.63	<.01	<.002	<.002	0.015	0.020
B	<.01	2.61	<.01	<.002	<.002	0.015	0.020
1S40 A	<.01	3.45	<.01	<.002	<.002	0.001	0.025
B	<.01	3.39	<.01	<.002	<.002	0.001	0.016

TABLE 2

SERIES 2   CAST ANALYSIS   (Wt%)

	C	Si	Mn	S	P	Al	O_2
1S05(2) A	<.01	0.46	0.015	0.003	<.002	0.57	0.018
B	<.01	0.47	0.015	0.003	<.002	0.42	0.016
1S10(2) A	<.01	0.94	0.010	0.003	<.002	0.86	0.015
B	<.01	0.89	0.010	0.004	<.002	0.62	0.015

TABLE 3

SERIES 3   CAST ANALYSIS (Wt%)

	C	Si	Mn	S	P	N_2	O_2
1S05(3) A	<.01	0.47	<.01	<.02	<.002	0.0015	0.020
(3) B	<.01	0.45	<.01	<.002	<.002	0.0065	0.015
1S10(3) A	<.01	0.84	<.01	<.002	<.002	0.0010	0.015
(3) B	<.01	0.88	<.01	<.002	<.002	0.0015	0.007
1S15(3) A	<.01	1.40	<.01	<.002	<.002	-	0.020
(3) B	<.01	1.48	<.01	<.002	<.002	0.0013	0.007
1S20(3) A	<.01	1.88	<.01	<.002	<.002	0.0019	0.015
(3) B	<.01	2.00	<.01	<.002	<.002	0.0023	0.008

TABLE 4

CAST ANALYSIS OF BASE ELEMENTS (Wt%)

	B	Ti	Fe	Ca	Al	Cu	P	S	Sb
SILICON	>10ppm	>10ppm	0.42	.19	.68	<.01	<.002	<.002	<10ppm
IRON	<5ppm	<10ppm	BAL	<50ppm	NIL	<.01	<.002	<.002	<10ppm

150

TABLE 5

ANALYSIS OF RESIDUAL ELEMENTS (Wt%)

	B	Ti	Cu	Al	Cu	P	S	Sb
IS00(1) A	<5ppm	<5ppm	<50ppm	<.002	<.01	<.002	<.002	<5ppm
IS05(3) A	<5ppm	<5ppm	<50ppm	NIL	<.01	<.002	<.002	<5ppm
IS05(3) B	<5ppm	<5ppm	<50ppm	NIL	<.01	<.002	<.002	<5ppm
IS10(3) A	10ppm	<5ppm	<50ppm	.003	<.01	<.002	<.002	<5ppm
IS10(3) B	10ppm	<5ppm	<50ppm	.004	<.01	<.002	<.002	<5ppm
IS15(3) A	<5ppm	<5ppm	<50ppm	.004	<.01	<.002	<.002	<5ppm
IS15(3) B	10ppm	<5ppm	<50ppm	.004	<.01	<.002	<.002	<5ppm
IS20(1) A	<5ppm	<5ppm	<50ppm	.008	<.01	<.002	<.002	<5ppm

TABLE 6

GRAIN SIZES FOR FATIGUE SPECIMENS

SPECIMEN	GRAIN SIZE μ	$d^{-\frac{1}{2}}$	95% CONFIDENCE LIMITS
ISOO(1) A 1	195	71.6	±10%
ISOO(1) A 2	200	70.7	"
ISOO(1) A 3	237	65.0	"
ISO5(3) A 1	110	95.3	±10%
ISO5(3) A 2	203	70.2	"
ISO5(3) A 3	276	60.2	"
ISO5(2) B 1	138	85.1	"
ISO5(3) B 2	210	69.0	"
IS1O(3) A 1	154	91.3	±10%
IS1O(3) A 2	215	68.2	"
IS1O(3) A 3	292	58.5	"
IS1O(3) B 1	159	79.3	"
IS1O(3) B 2	193	72.0	"
IS15(3) A 1	246	63.8	±15%
IS15(3) A 2	354	53.1	"
IS15(3) B 1	340	54.2	"
IS15(3) B 2	350		"
IS15(3) B 3	395	50.0	"
IS20(1) A 1	395	50.0	±15%
IS20(1) A 2	434	48.0	"
IS20(1) A 3	621	40.1	"

TABLE 7

TENSILE DATA FOR FATIGUE SPECIMENS

Specimen	0.1% Proof Stress MNm^{-2}	Ultimate Tensile Stress MNm^{-2}	% Elongation	% Reduction of Area
IS00(1)A 1	274.7	403.2	35.4	76
	–	269.8	16.3	15
IS00(1)A 2	231.7	348.1	36.2	69
	194.6	311.7	29.1	59
IS00(1)A 3	312.4	396.6	34.7	66
	–	–	–	–
IS05(3)A 1	387.1	450.0	36.9	72
	388.5	484.3	14.0	61
IS05(3)A 2	204.9	329.8	50.8	62
	254.9	338.3	49.8	52
IS05(3)A 3	254.9	340.8	35.1	69
	214.9	346.3	38.2	71
IS05(3)B 1	367.7	480.0	36.0	61
	344.1	462.1	35.8	74
IS05(3)B 2	194.9	341.3	38.5	68
	257.9	344.8	47.0	70
IS10(3)A 1	220.7	391.4	40.9	84
	–	401.2	36.6	76
IS10(3)A 2	267.6	330.4	40.0	80
	313.2	361.4	32.7	72
IS10(3)A 3	310.0	400.5	26.1	59
	348.2	460.7	24.4	66
IS10(3)B 1	270.0	421.3	36.7	80
	263.9	409.8	37.6	78
IS10(3)B 2	–	–	–	–
	364.4	–	13.2	11
IS15(3)A 1	314.8	400.8	38.8	60
	320.8	412.8	38.0	56
IS15(3)A 2	301.1	417.9	31.0	–
	302.1	415.0	42.1	–
IS15(3)B 1	–	–	–	–
	343.6	–	1.20	9
IS15(3)B 2	334.9	426.8	38.0	71
	329.8	422.8	37.4	71
IS15(3)B 3	324.8	439.8	26.2	62
	300.0	441.3	36.2	74
IS20(1)A 1	351.3	467.8	34.1	55
	408.8	468.3	29.7	68
IS20(1)A 2	345.2	399.7	29.6	67
	376.0	–	15.1	12
IS20(1)A 3	390.0	442.5	24.4	54
	401.4	467.6	20.1	50

TABLE 9

SHOWING MONOTONIC AND CYCLIC PLASTIC ZONE SIZES FOR

THRESHOLD STRESS INTENSITIES AND GRAIN SIZES

SERIES	SPECIMEN	MONOTONIC PZS (μm)	CYCLIC PZS (μm)	GRAIN SIZE μm
1	IS00(1)A1	238	38	195
	IS00(1)A2	324–459	51–73	200
	IS00(1)A3	198	32	237
2	IS05(3)A1	157–156	25–25	110
	IS05(3)A2	408–631	65–100	203
	IS05(3)A3	445–625	71–100	276
	IS05(3)B1	198–227	32–36	138
	IS05(3)B2	378–662	60–106	210
3	IS10(3)A1	795	127	154
	IS10(3)A2	454–331	53–73	215
	IS10(3)A3	256–323	41–52	292
	IS10(3)B1	542–776	86–90	159
	IS10(3)B2	285	46	193
4	IS15(3)A1	417–433	67–69	246
	IS15(3)A2	224–225	36–36	354
	IS15(3)B1	288	46	340
	IS15(3)B2	210–217	33–35	350
	IS15(3)B3	267–313	43–50	395
5	IS20(1)A1	190–257	30–41	395
	IS20(1)A2	190–320	30–36	434
	IS20(1)A3	101–107	16–17	621

NOTE: Values determined from 0.1% proof stress
in each case,

154

TABLE 8

FATIGUE THRESHOLD RESULTS

SERIES	SPECIMEN	THRESHOLD ΔK $MNm^{-3/2}$	THRESHOLD K_{MAX} $MNm^{-3/2}$
1	1S00(1)A1	10.4	13.0
	1S00(1)A2	10.2	12.8
	1S00(1)A3	10.8	13.5
2	1S05(3)A1	11.9	14.9
	1S05(3)A2	12.6	15.8
	1S05(3)A3	13.2	16.5
	1S05(3)B1	12.7	15.9
	1S05(3)B2	12.3	15.4
3	1S10(3)A1	15.3	19.1
	1S10(3)A2	14.0	17.5
	1S10(3)A3	13.7	17.1
	1S10(3)B1	15.4	19.3
	1S1O(3)B2	15.1	18.9
4	1S15(3)A1	16.1	20.1
	1S15(3)A2	11.1	13.9
	1S15(3)B1	14.3	17.9
	1S15(3)B2	11.9	14.9
	1S15(3)B3	13.0	16.3
5	1S20(1)A1	13.8	17.3
	1S20(1)A2	12.7	15.9
	1S20(1)A3	9.9	12.4
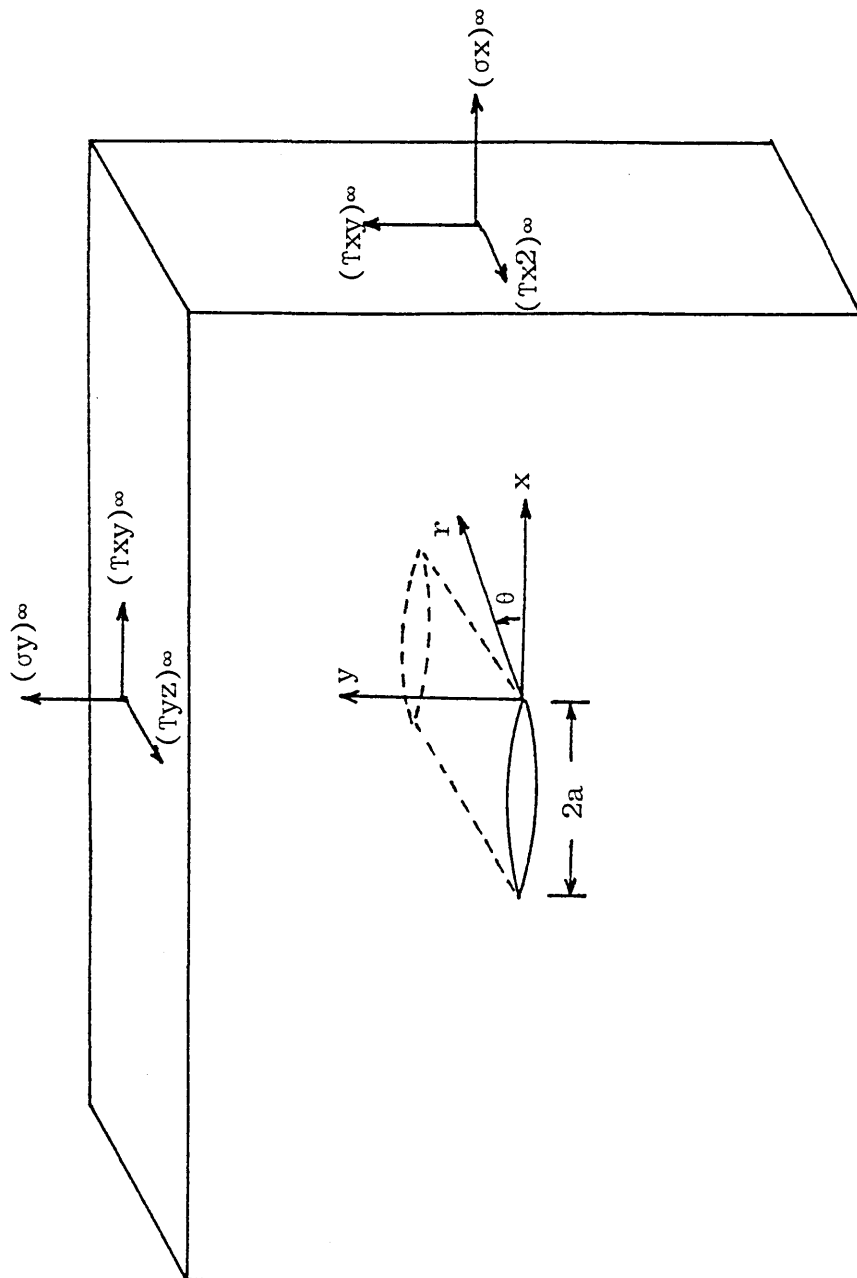
Figure 2

    (a)   Elastic stress distribution around a geometric
            stress concentration.

    (b)   Through thickness variation of σ_{zz}

(a)

(b)

159
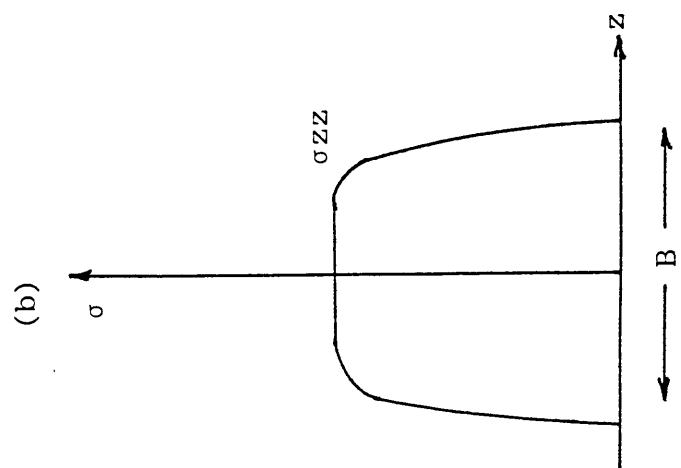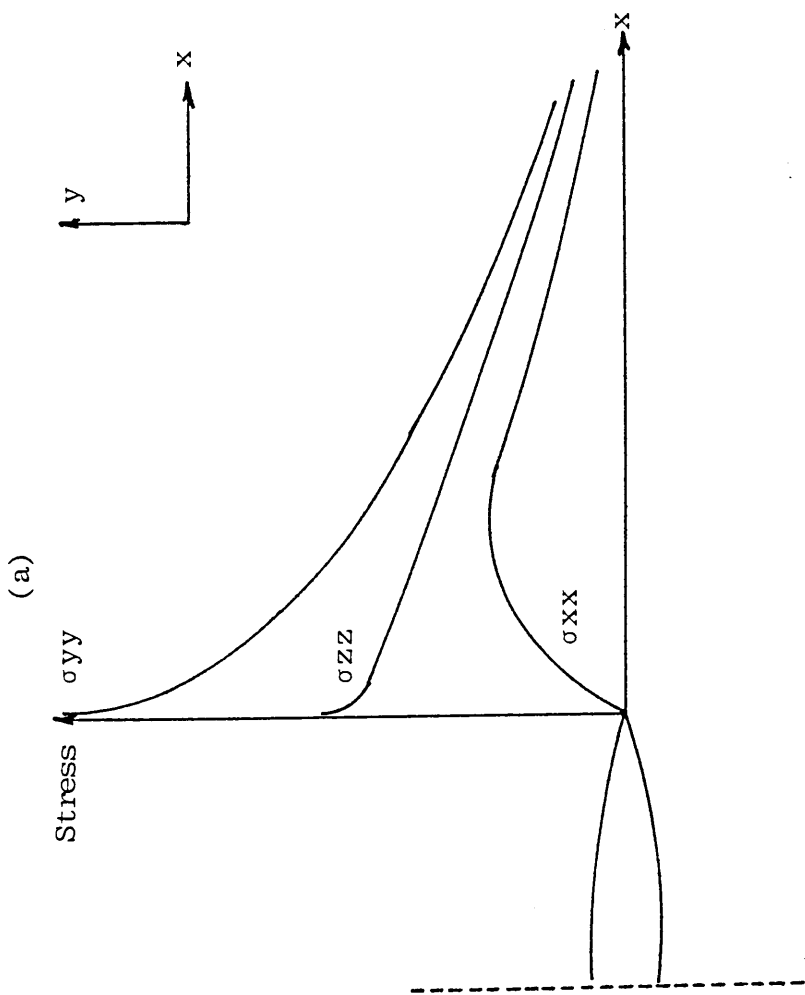
Figure 3

Schematic elastic/plastic stress distribution near a
crack under plane strain conditions.

$\sigma yy = K/(2\pi r)^{\frac{1}{2}}$

σyy

r

a

(c)

$\sigma yy = K/(2\pi r)^{\frac{1}{2}}$

σyy

σYS

ry

a

r

σyy

w

a

(d)

$\sigma yy = K*/(2\pi r)^{\frac{1}{2}}$

σyy

a

ry

r
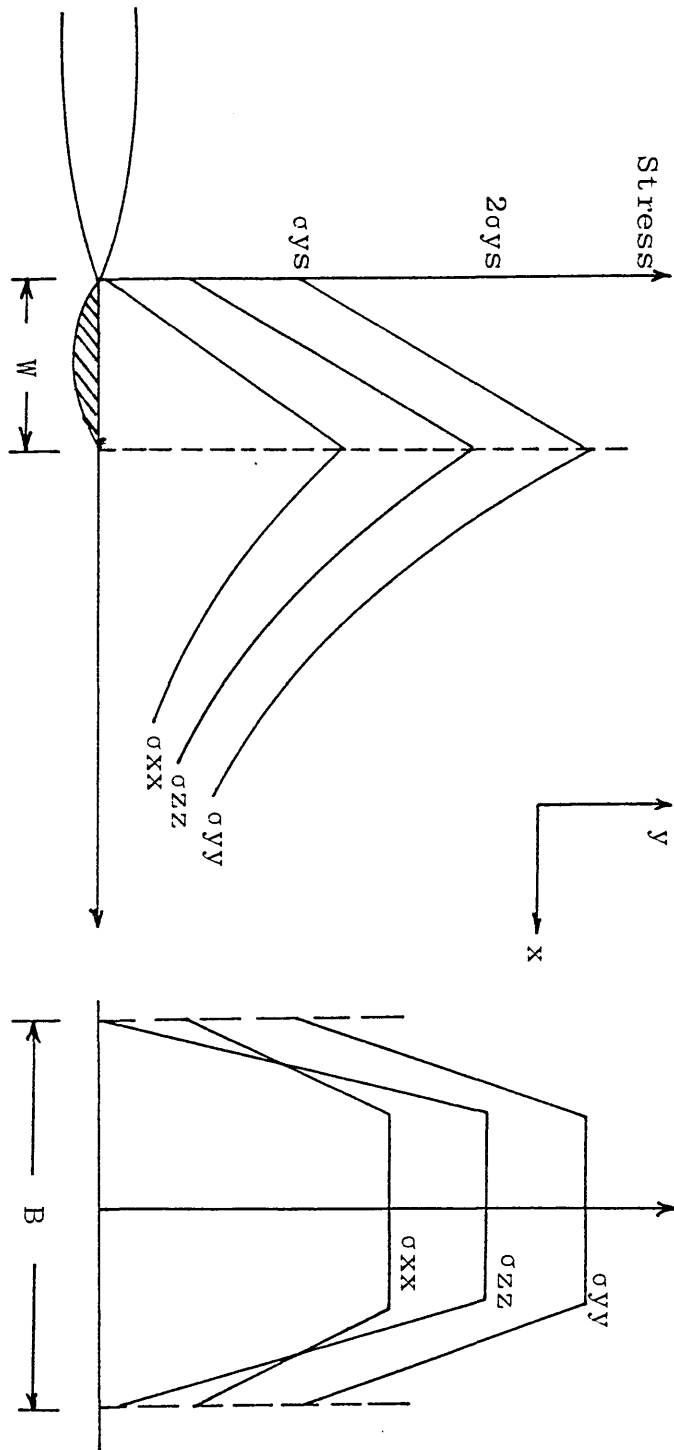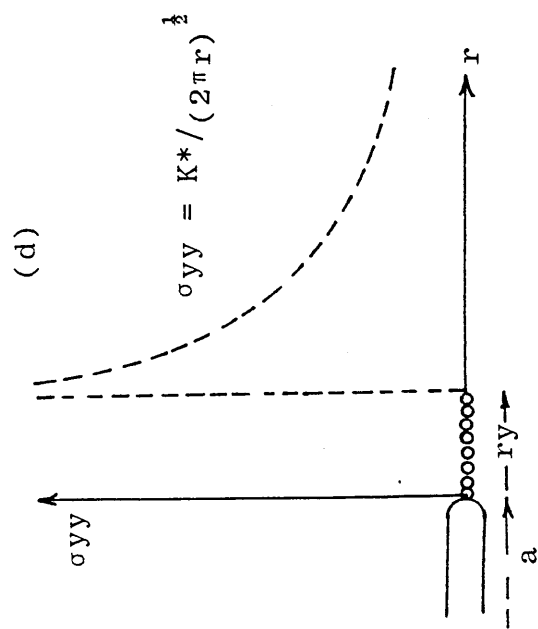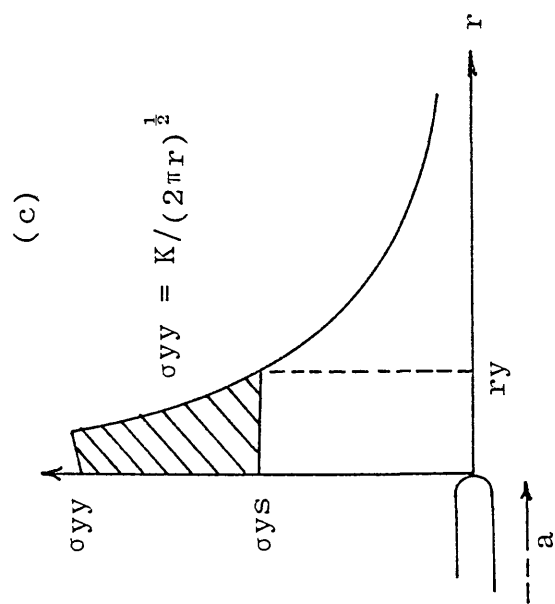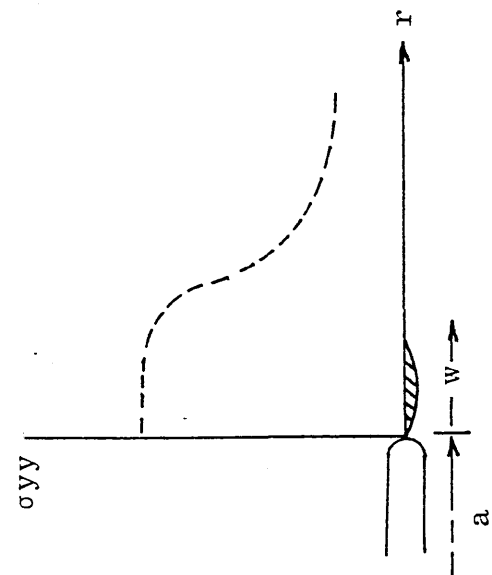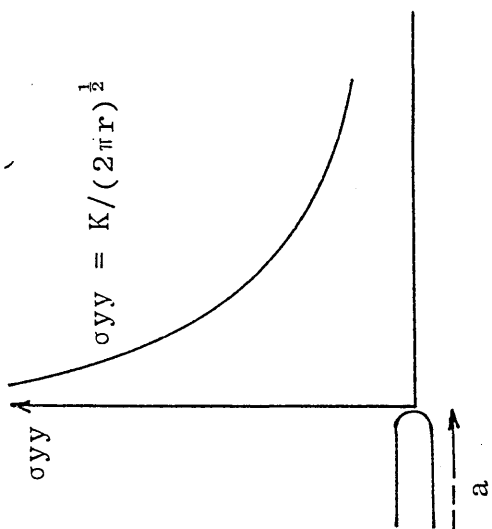
Figure 5

Schematic representation of a plastic zone across a crack of finite width.
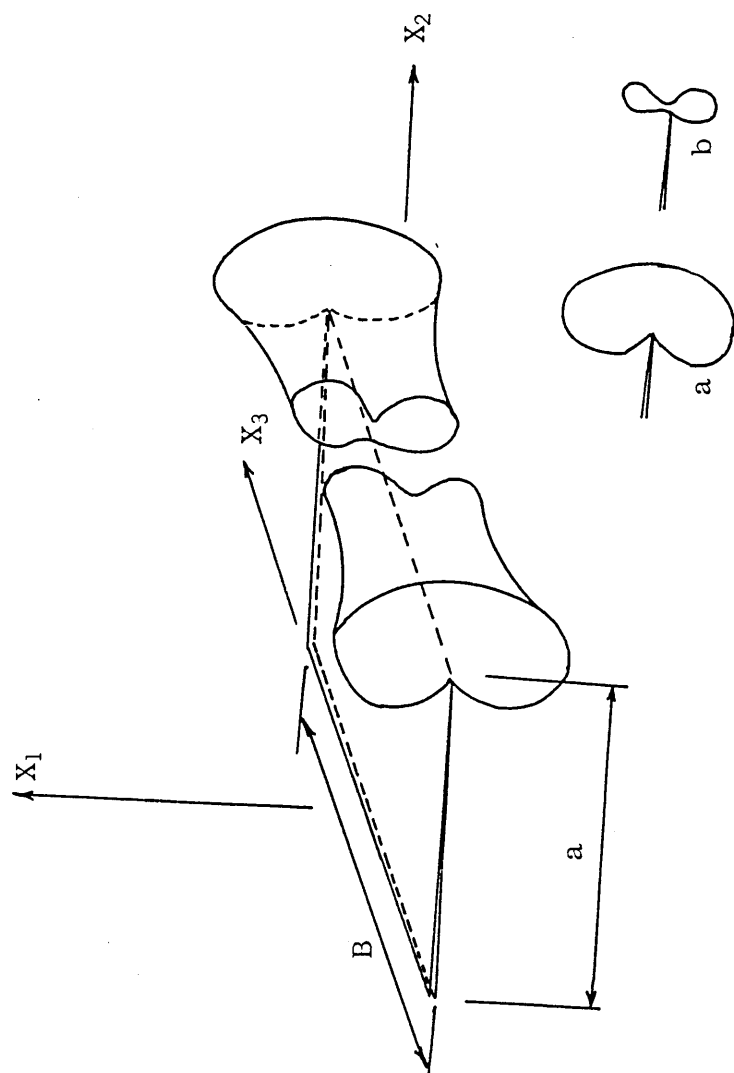
Figure 6

Schematic load displacement curve for region ahead
of crack tip.

(a)

(b)

(c)

Reversed flow plastic zone
Monotonic plastic zone
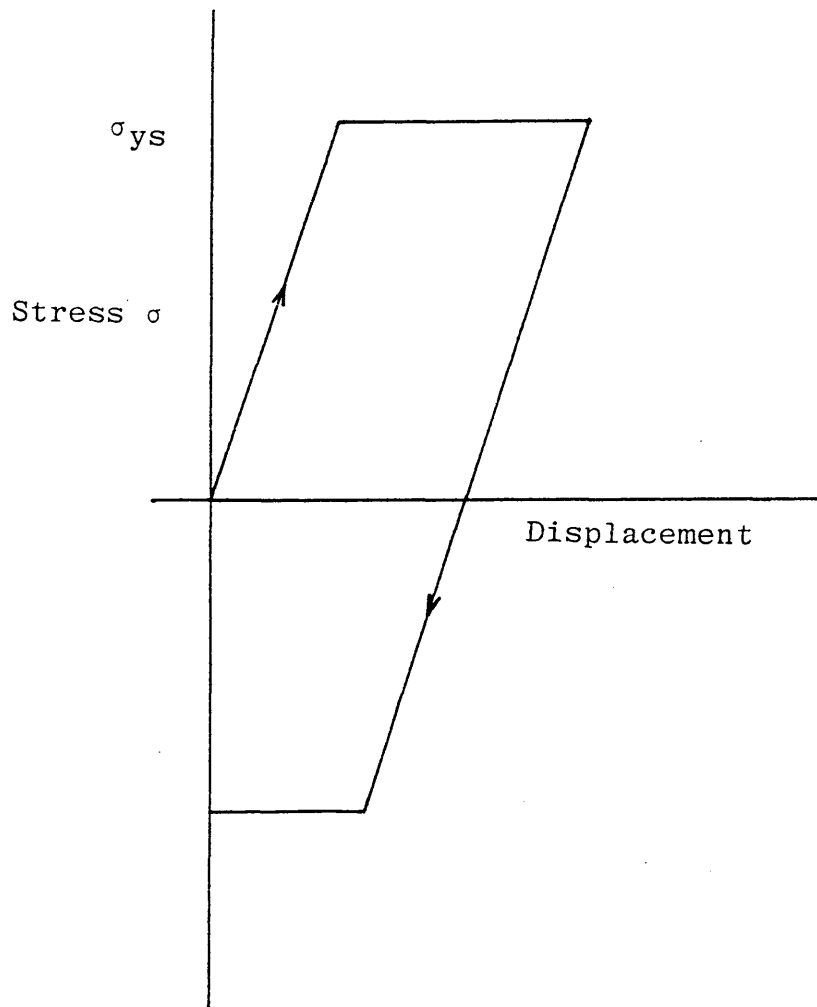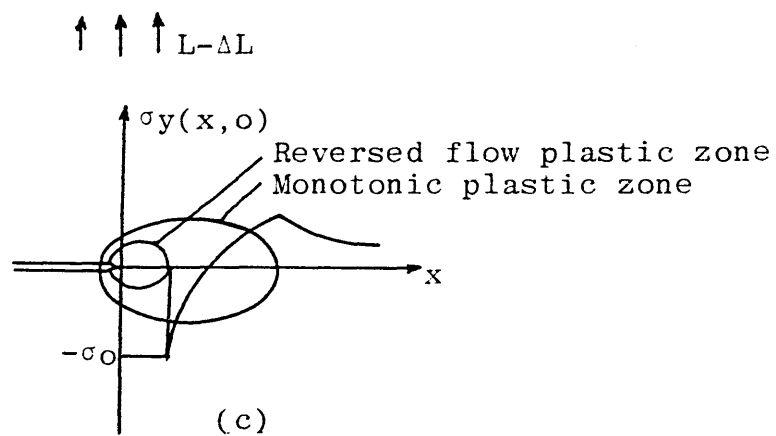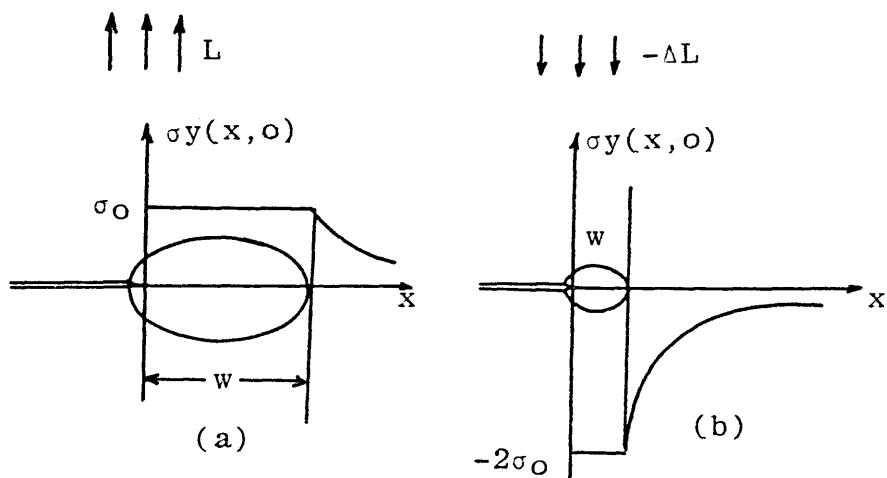
Figure 8

Schematic variation of fatigue crack growth rate with
alternating stress intensity, ΔK, in steels, showing
regimes of primary crack growth mechanisms.
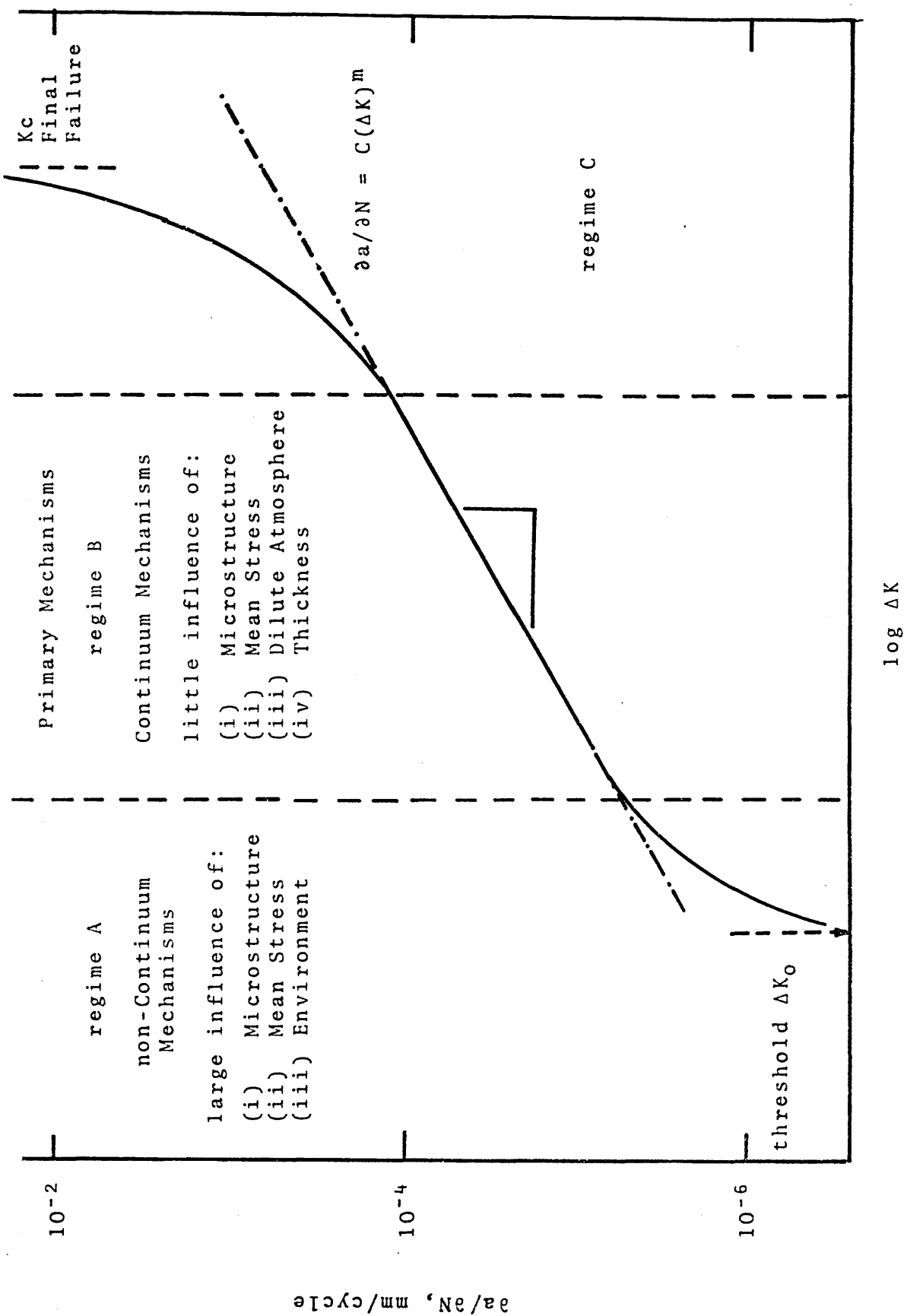
Figure 9

Schematic illustration of internal necking process;
represents increasing strain which causes crack
blunting, void growth, and eventual coalecence of
crack tip and void.

MnS
INCLUSIONS

δ_i
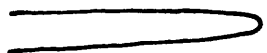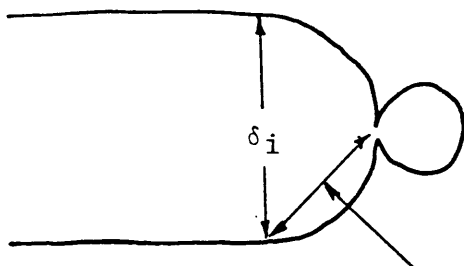
STRETCH ZONE

Figure 10

Schematic representation of dislocation arrangements
of plastic zones as compared to grain size.

(δ_S = static, δ_f = cyclic plastic zone)

(a) Stage I   (b) Stage II   (c) Transition II→II
(d) Stage III
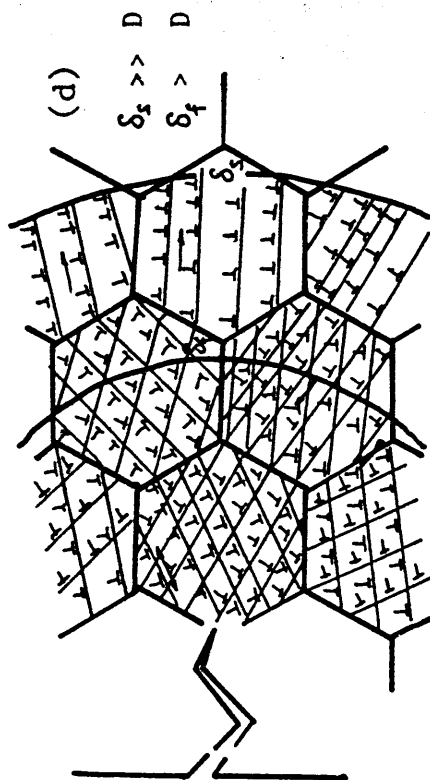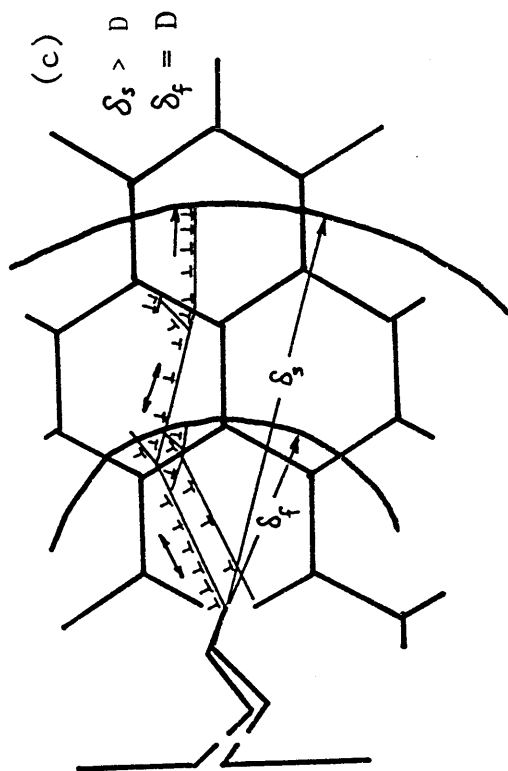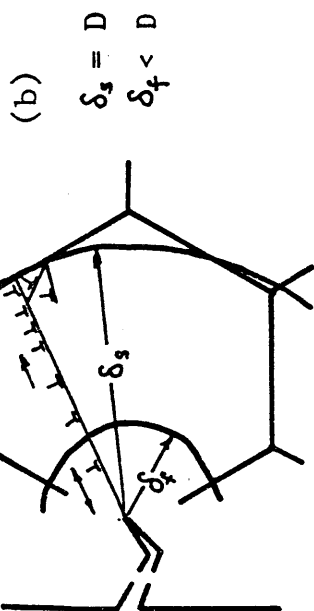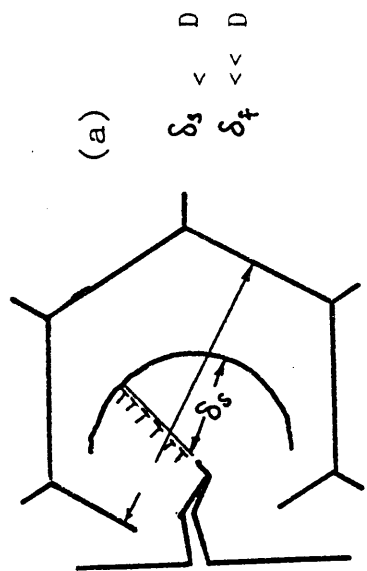
Figure 11

(a) Crystallographic geometry of fatigue crack propagation in BCC structures.

(b) Fatigue crack path in coarse grained ferrite.

(c) Fatigue crack path in finer grained ferrite.

(a)

CRACK

(110) SLIP PLANE

(100) MACROSCOPIC
FRACTURE PLANE

(110)

(b)

σ

A — — — — — — — B

C D F

E

σ

— CRACK PATH

(c)

σ

A — — — — — — — B

C E G H

D F I J

σ

177
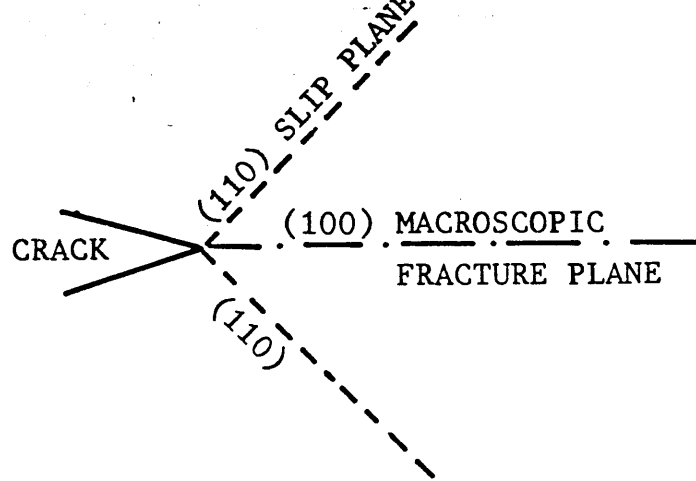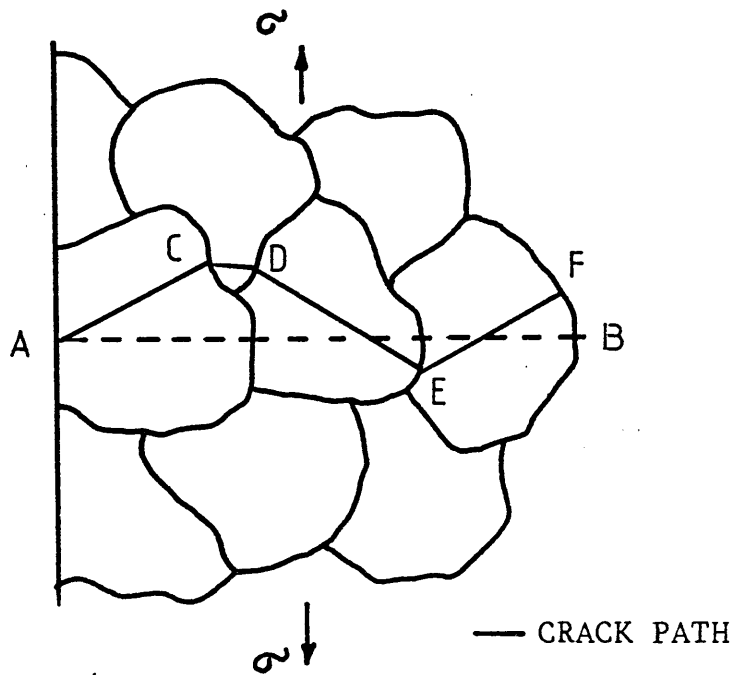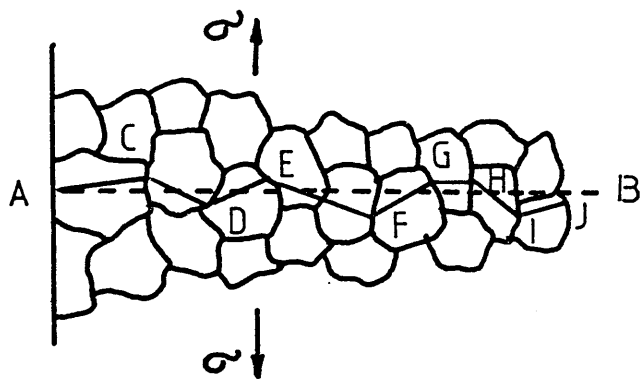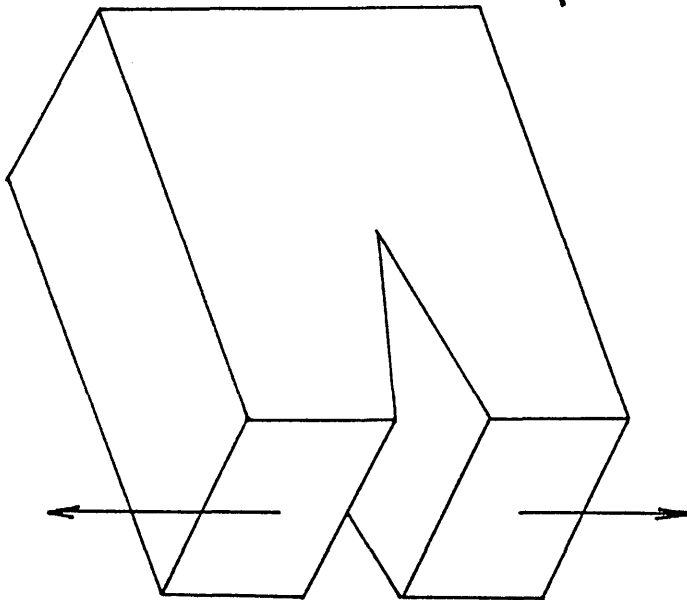
Mode III

Anti Plane Shear
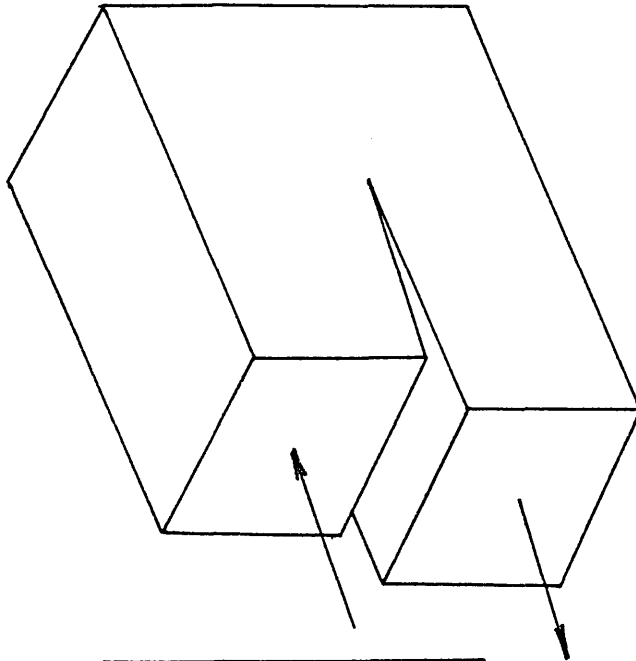
Mode II

in Plane Shear

Mode I

Tensile

179
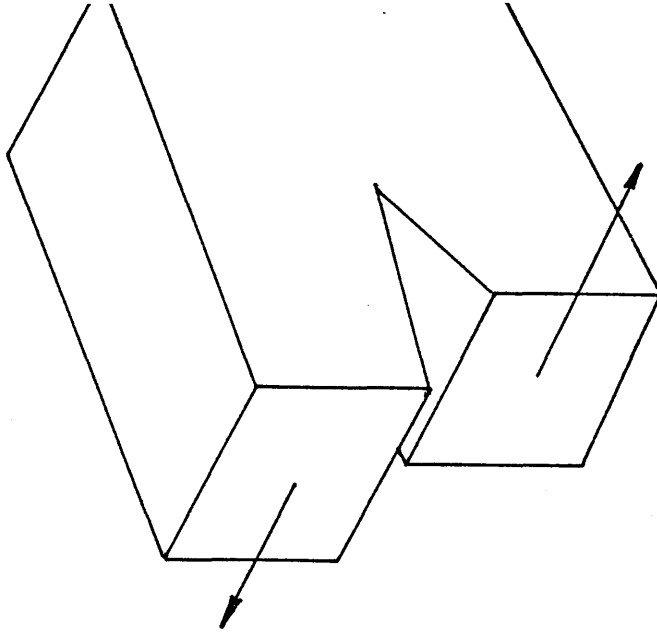
Figure 13

Schematic representation of fatigue crack advance
by a plastic blunting process.

(a)
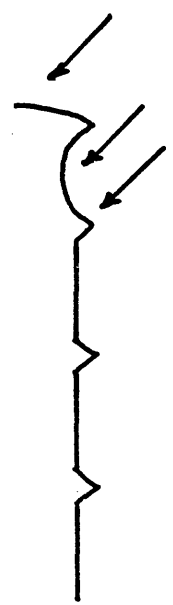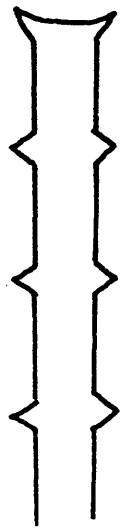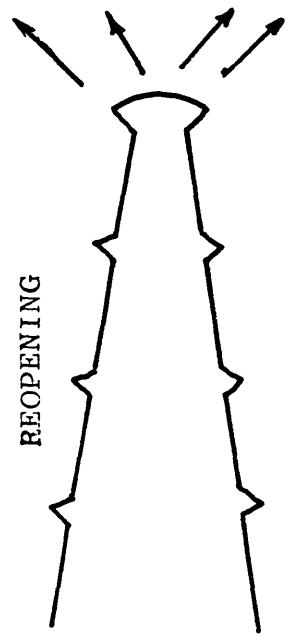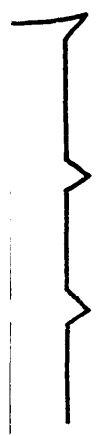
(b) CRACK OPENING
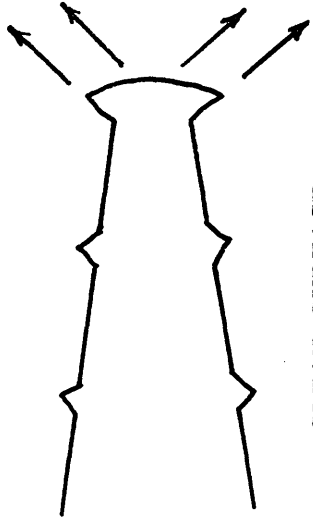
(c) CLEAN SURFACE PRODUCED

(d)

(e) FULLY CLOSED

(f) REOPENING
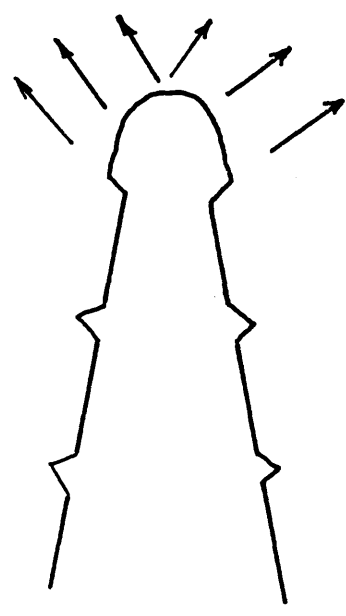
Figure 14

A shear decohesion mechanism for stage II fatigue
crack growth.

(a)

Maximum Compression
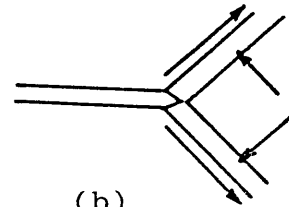
(b)
Small Tensile Stress

New Crack Surface
Formed by
Shear
Decohesion

(c)
Maximum Tensile
Strain
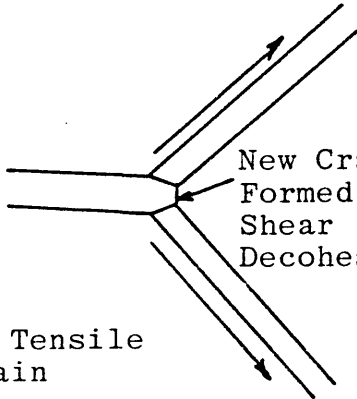
(d)
Small Compressive
Stress
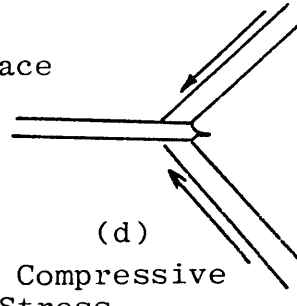
(c)
Maximum Compressive
Strain
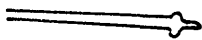
(f)
Maximum
Tensile Strain
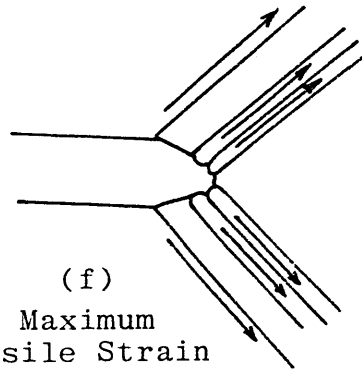
Figure 15

The influence of R ratio on fatigue crack growth for
a pearlitic steel tested in laboratory air.[37]

Crack growth rate, da/dN (mm/cycle)

10^{-4}

10^{-5}

10^{-6}

10^{-7}

10^{-8}

R=0.51   R=0.26
R=0.72   R=0.36   R=0.07

2   4   6   8   10   20   30

Stress intensity range ΔK (MNm$^{-3/2}$)
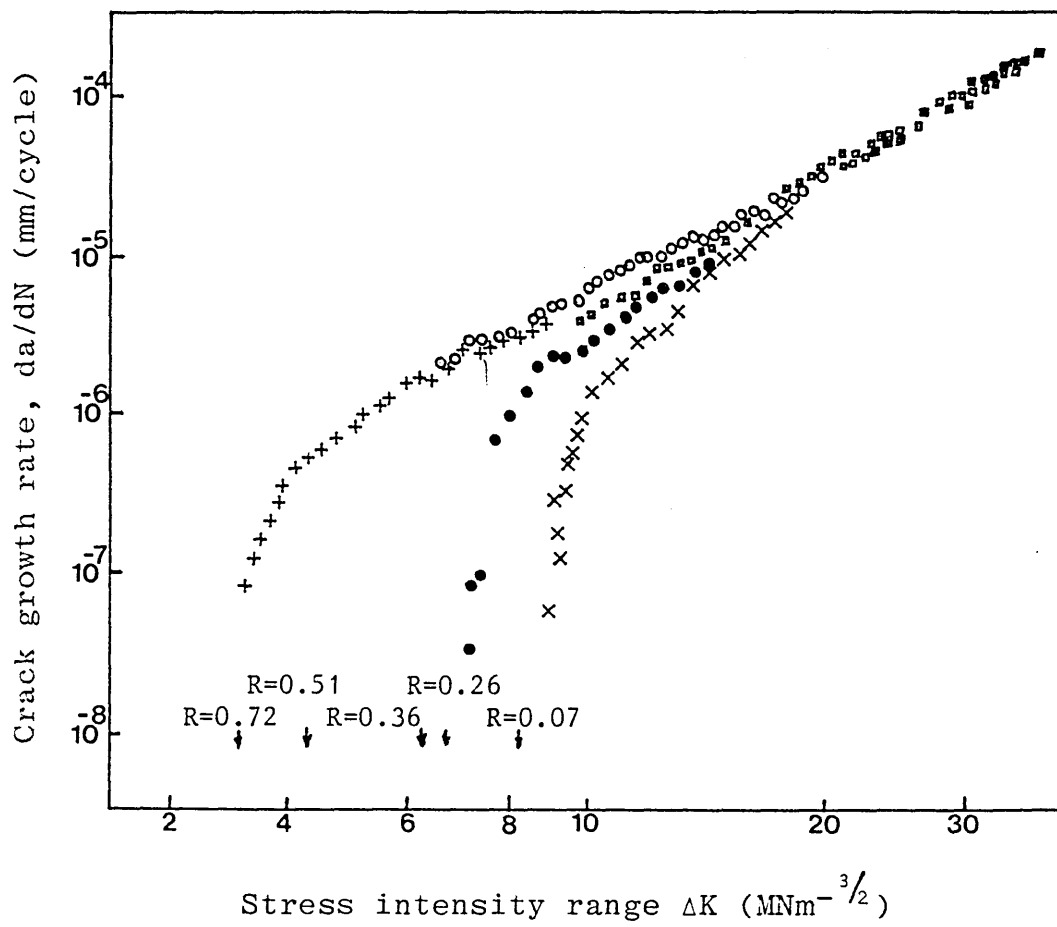
Figure 16

Orientation of maximum shear stress planes set up in
plane strain.

σ

Overall
Crack Growth
Direction

σ
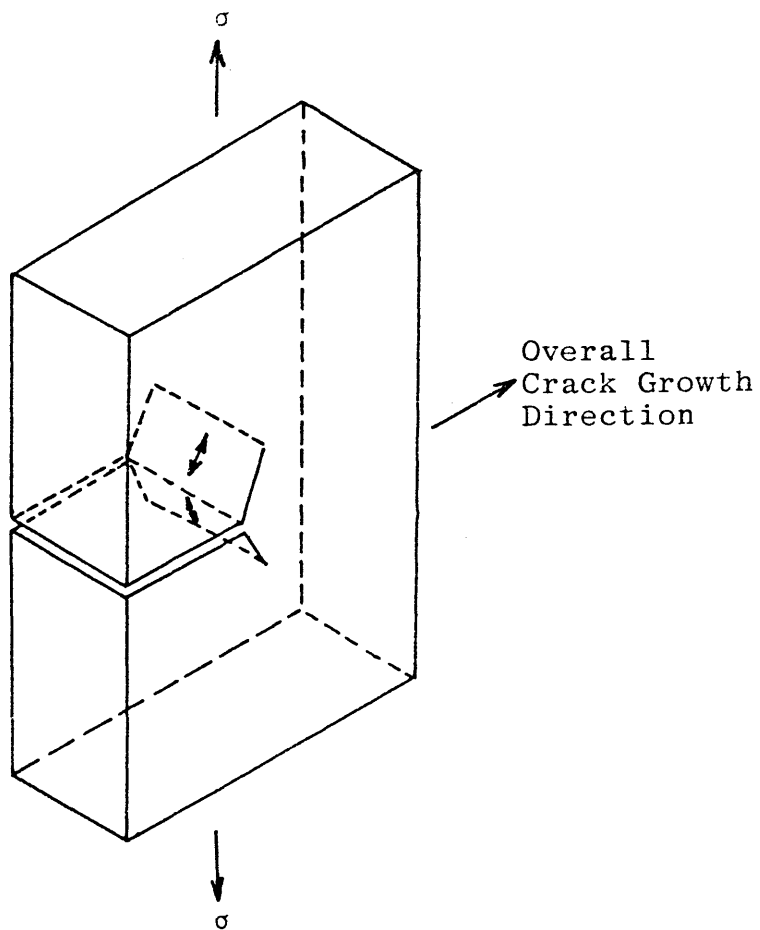
Figure 17

Fatigue crack growth rate versus stress intensity
range for a pearlitic steel.

Figure 18

    (a)   The influence of monotonic yield strength (σys) on threshold stress intensity for fatigue crack growth (ΔK_{Th}).
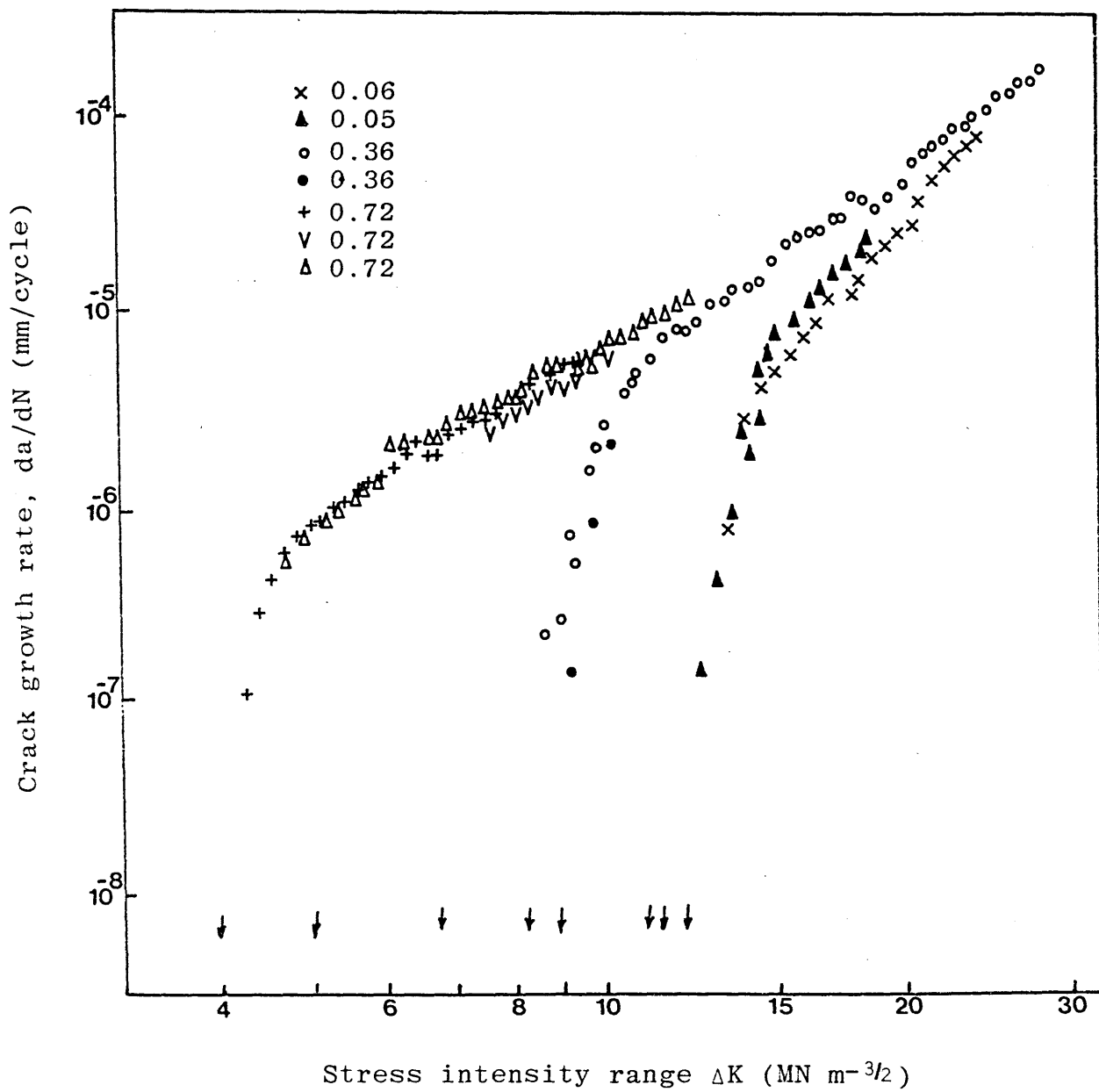
    (b)   The influence of U.T.S. on threshold for fatigue crack growth (ΔK_{Th}).

Threshold ΔK_{Th} $(MNm^{-3/2})$

— • — ΔK_T at R=0.05
– o – – ΔK_T at R=0.70

R = 0.05

R = 0.70

Yield Stress, σ_{ys} (MPa)

Threshold ΔK_T $(MNm^{-3/2})$

R = 0.05

R = 0.70

U.T.S., σ_{UTS} (MPa)
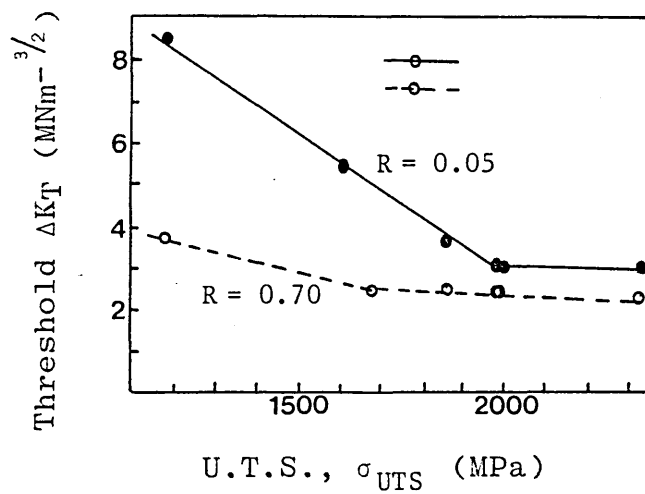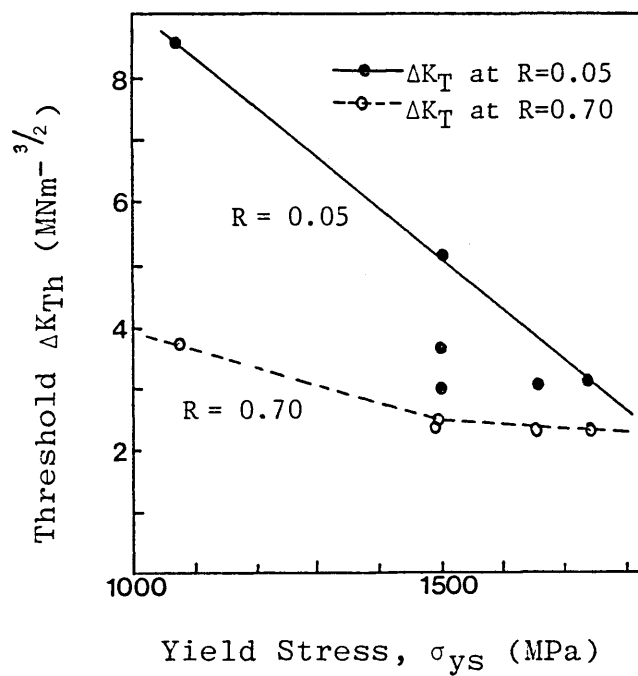
Figure 19

The variation of fatigue crack growth rate (da/dN)
with alternating stress intensity (ΔK) at R = 0.05
for 300.M steel, quenched and tempered between
$100^{\circ}C$ and $650^{\circ}C$, showing the influence of material
strength.[30]

Fatigue crack growth rate da/dN (mm/cycle)
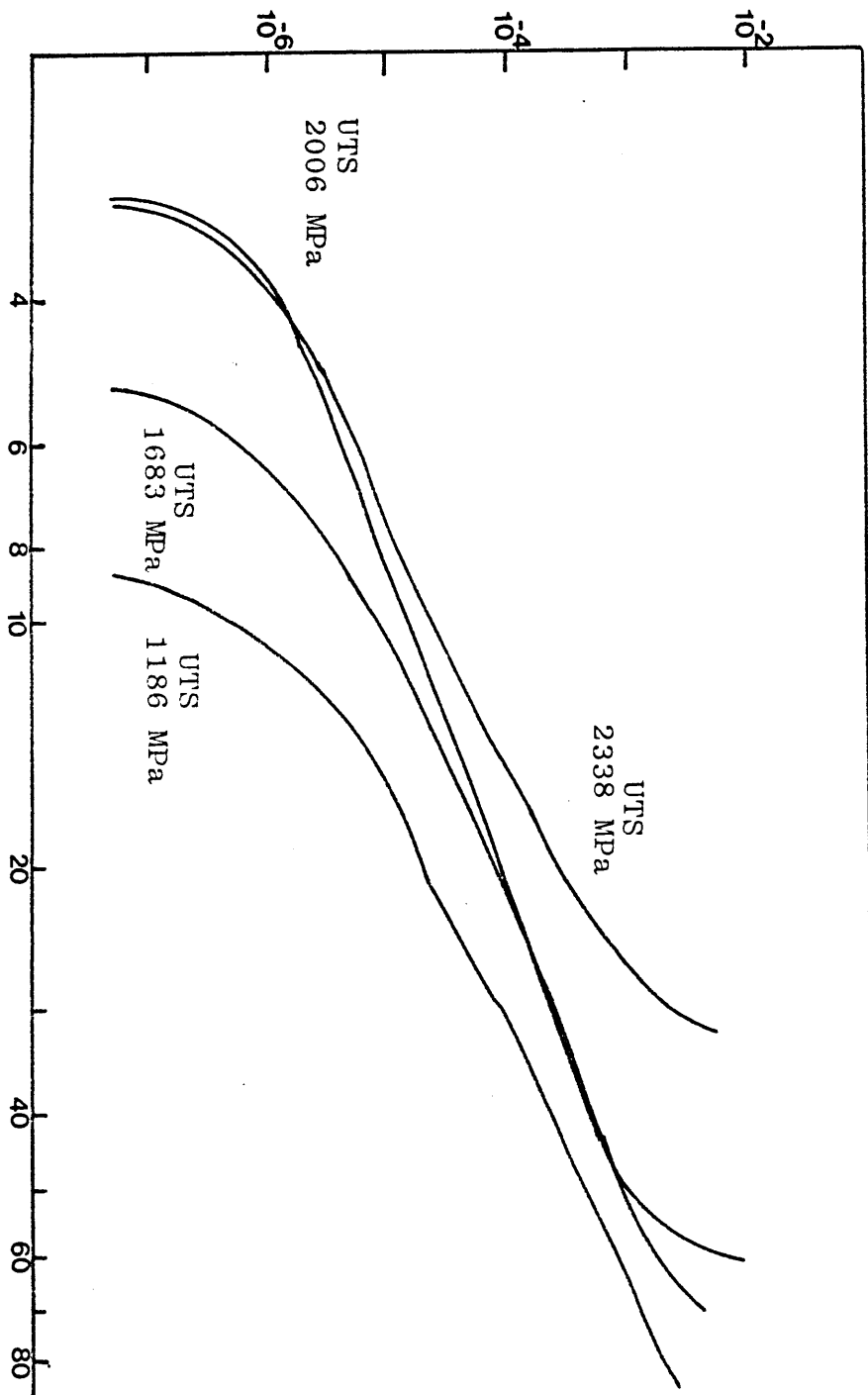
Figure 20

Results showing the variation of threshold for fatigue crack growth (ΔK_{Th}) at R = 0 with yield strength for steels.[29]
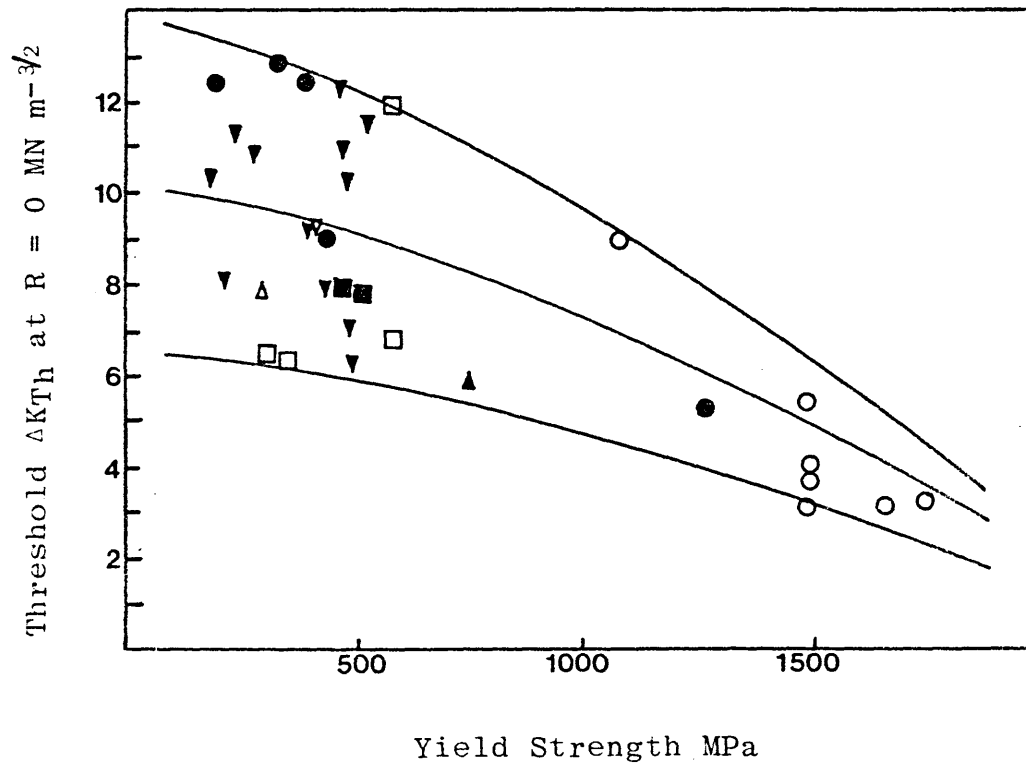
Figure 21

Effect of tempering temperature on threshold values.[8]
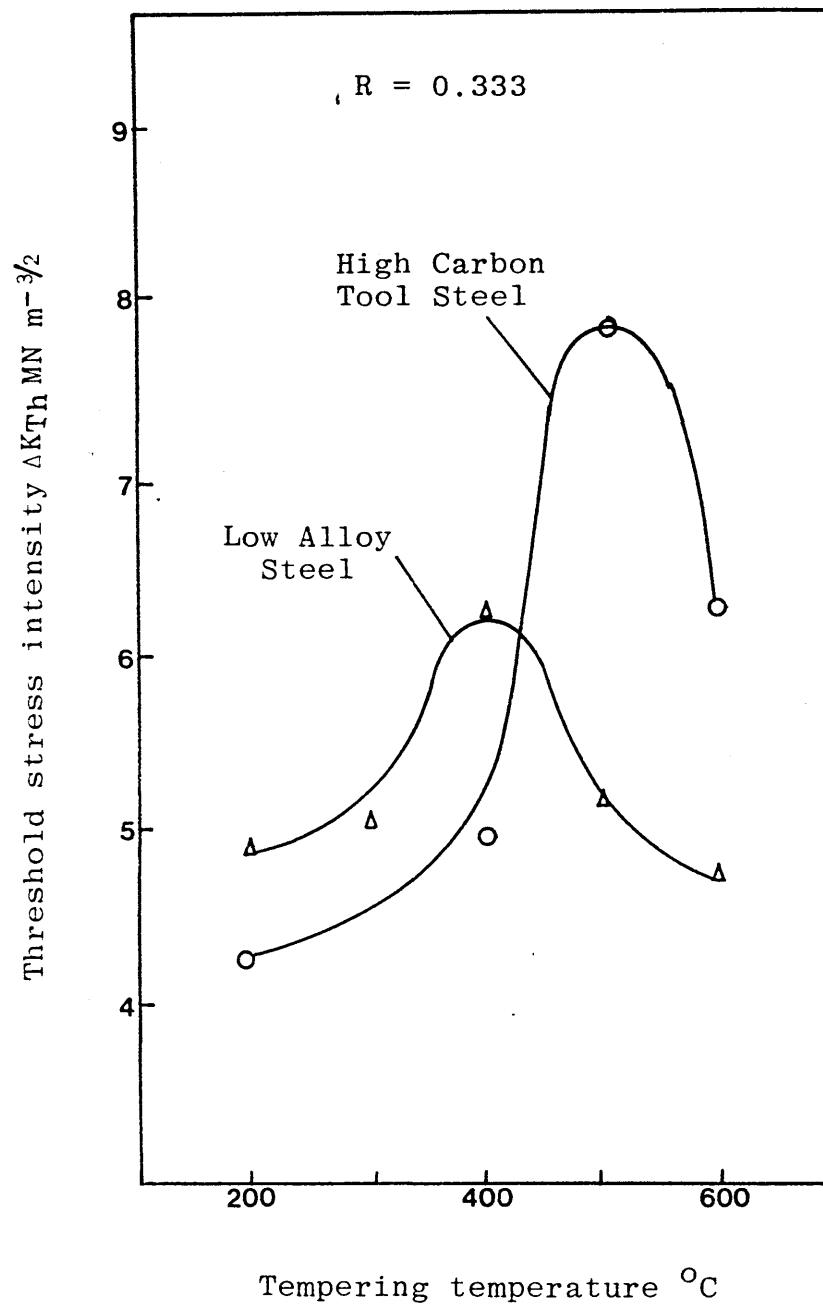
Figure 22

The effects of grain size and interstitial content on
fatigue crack propagation rates in α – titaninm at
R = 0.35.[20]
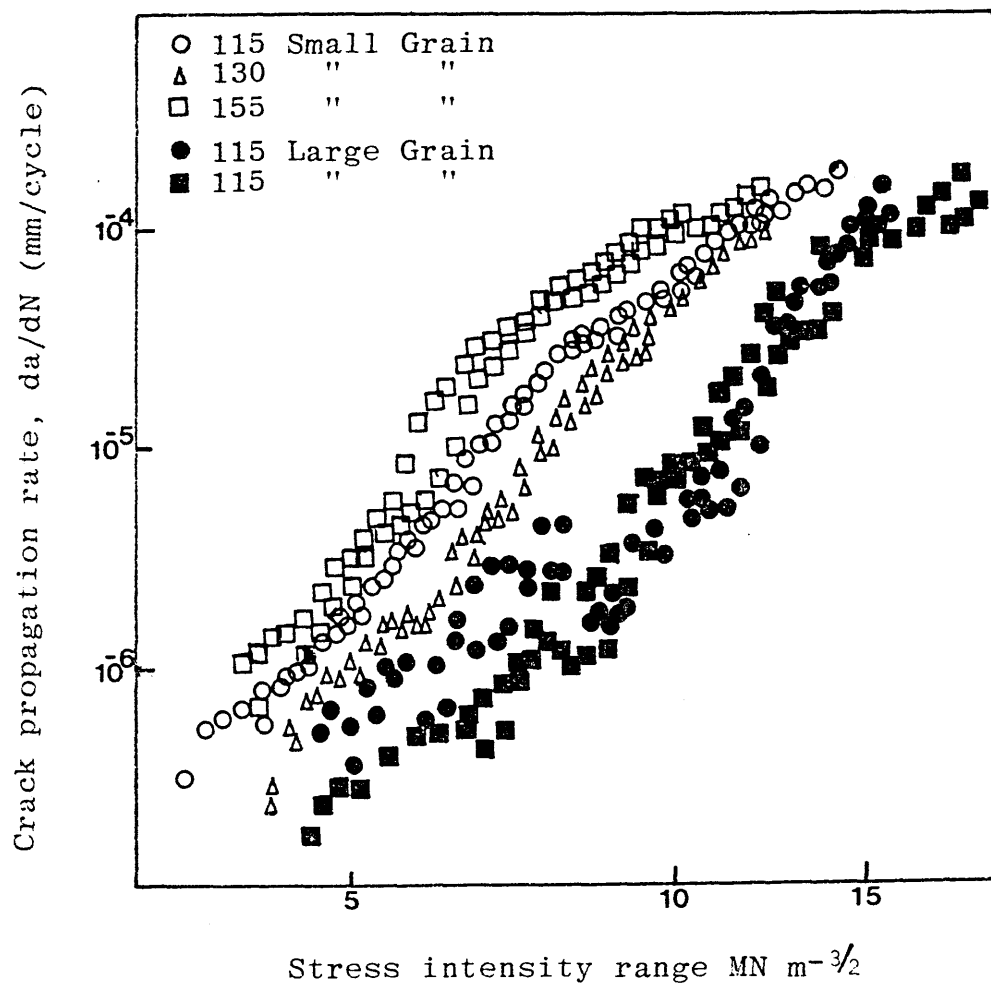
Figure 23

The variation of fatigue crack growth rate (da/dN)
with alternating stress intensity (ΔK) for 300.M
steel, austenitized at 870°C and 1200°C, showing
the influence of grain size.[30]

Crack growth rate, da/dN (mm/cycle)

Alternating stress intensity ΔK (MN m$^{-3/2}$)

R = 0.05

R = 0.70

20μm

20μm

160μm

10^{-2}

10^{-4}

10^{-6}

4

6

8

10

20

40

60

80
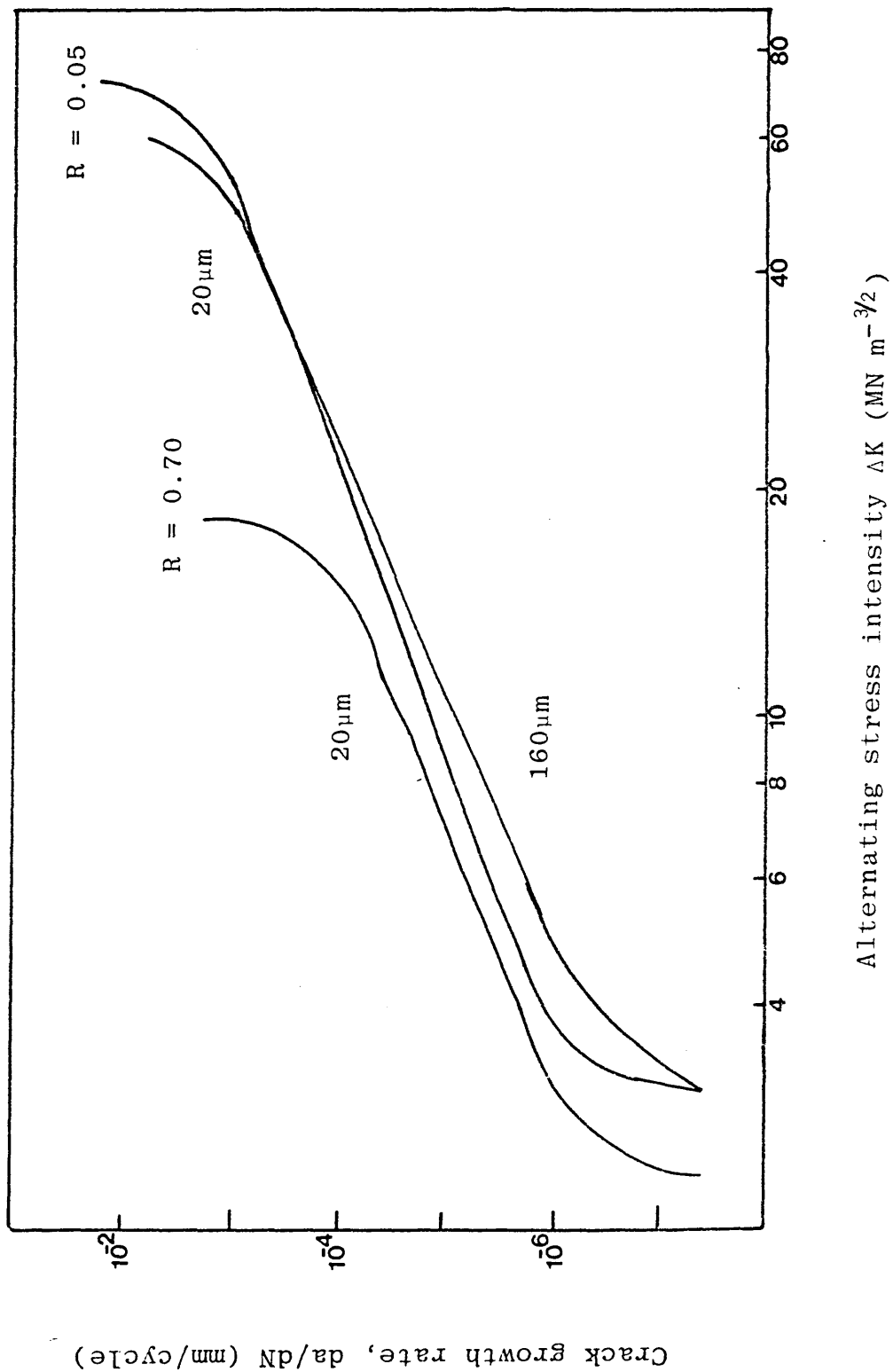
Figure 24

    The effect of grain size on the threshold stress
intensity factor for R = 0.

Figure axes: Threshold Stress intensity ΔK_{Th} (MN m$^{-3/2}$) versus $d^{-\frac{1}{2}}$ (10^{-3} m$^{-\frac{1}{2}}$)
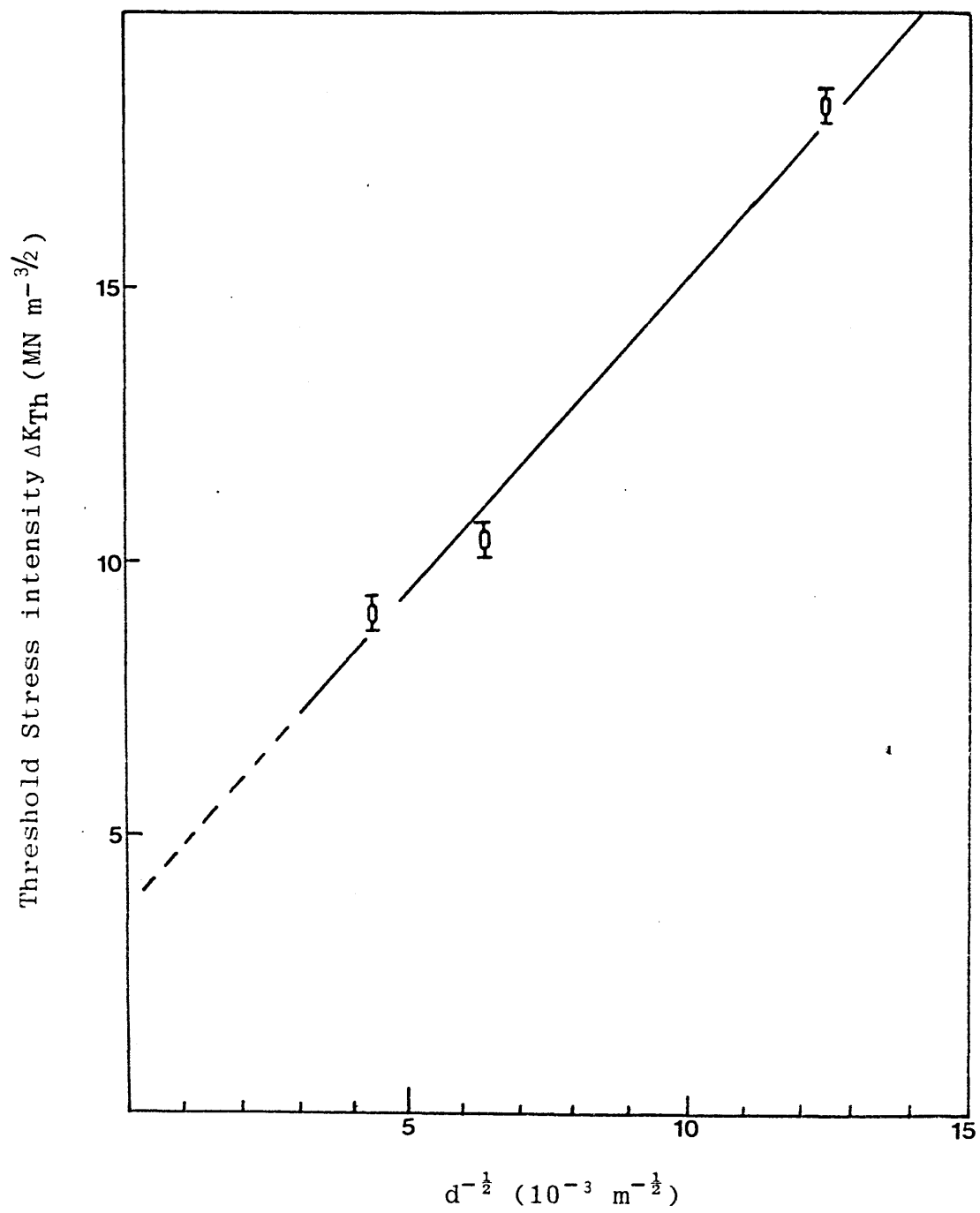
Figure 25

    (a)   Variation of threshold stress intensity range
           (ΔK_{Th}) with grain size.[89]

    (b)   Variation of threshold stress intensity range
           (ΔK_{Th}) with 0.1% proof stress.[89]
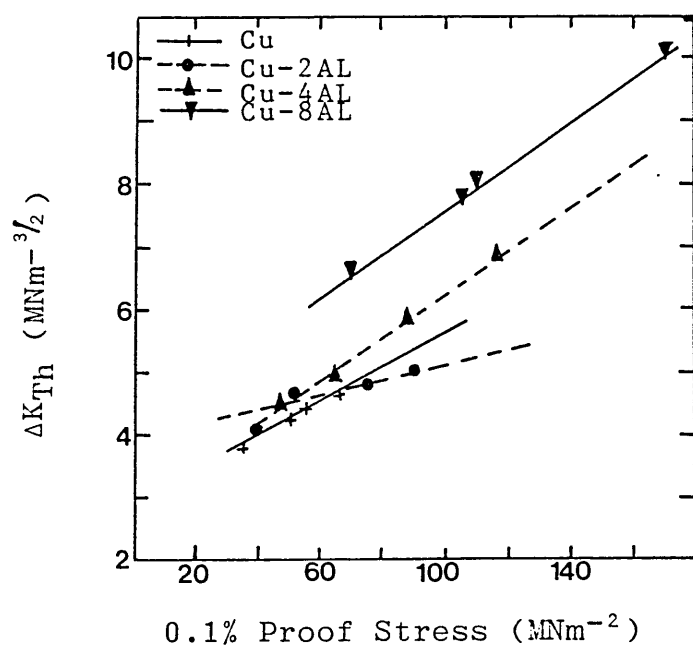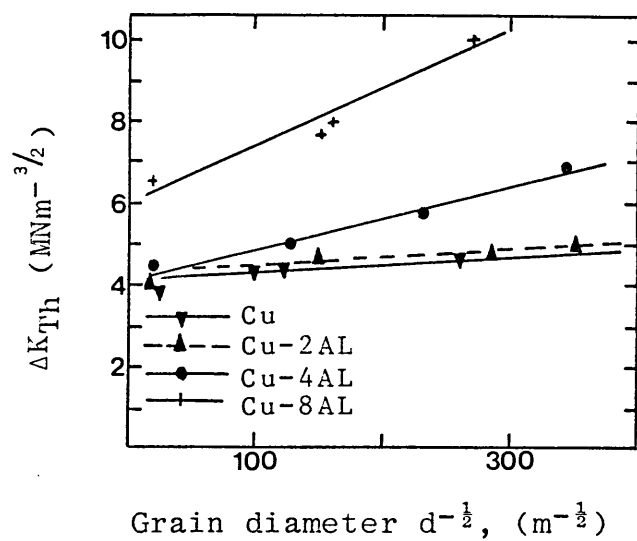
Figure 26

The effect of grain size on dislocation structure
at the crack tip. a) Small grain size, b) Large
grain size.[93]

Plastic zone size

(a)

(b)
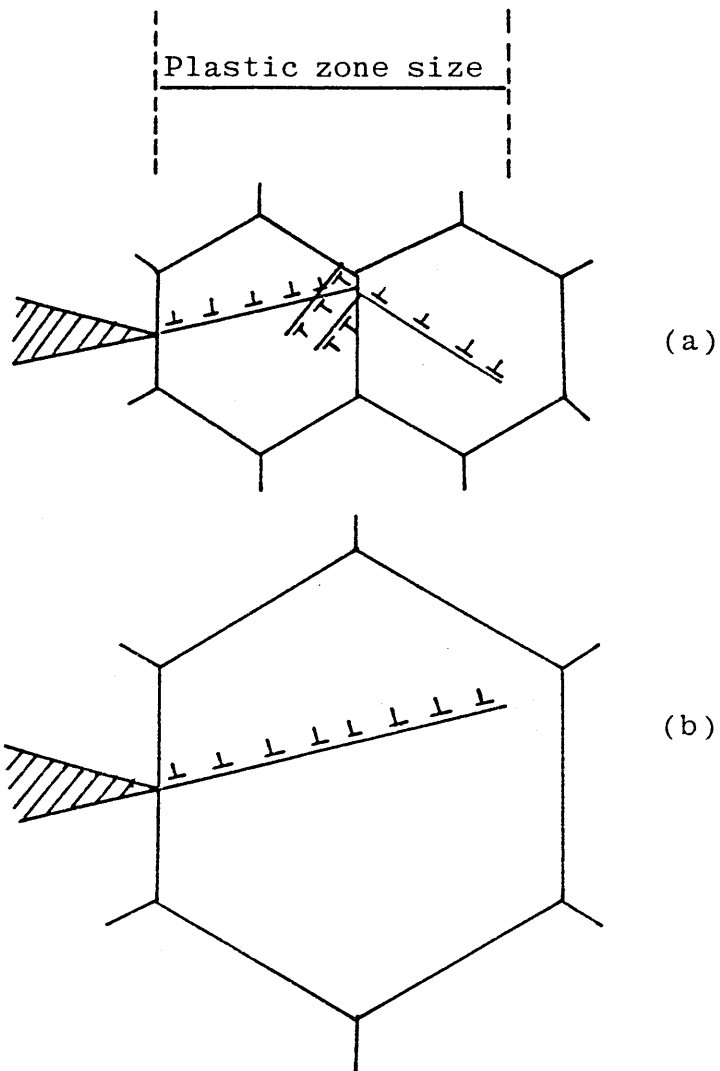
Figure 27

The prediction of grain size effects on the threshold
stress intensity range for low alloy steel.[67]
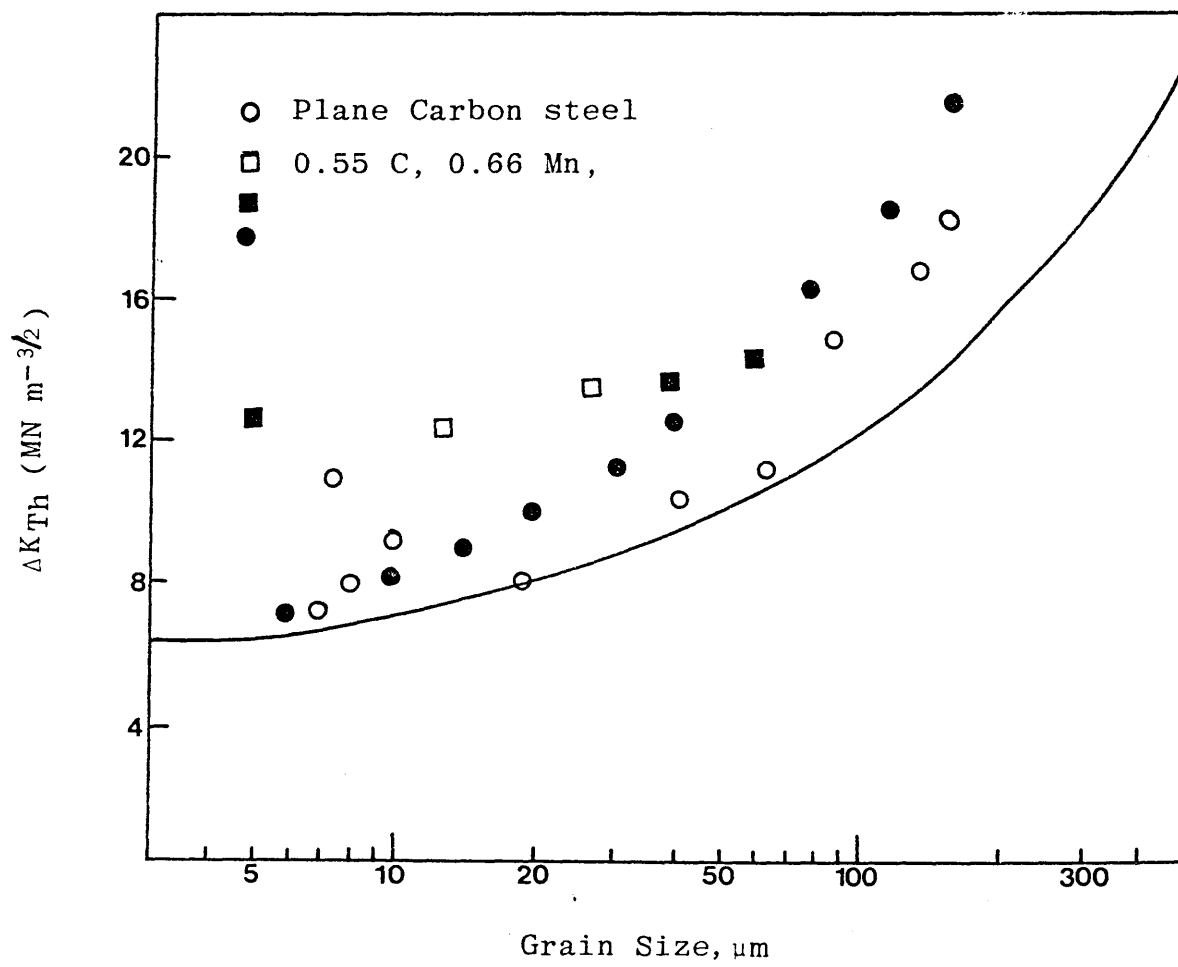
Figure 28

    Fatigue crack propagation results for 300.M, oil
    quenched and step cooled after tempering at 650°C
    showing the influence of inpurity induced
    embrittlement.[29]
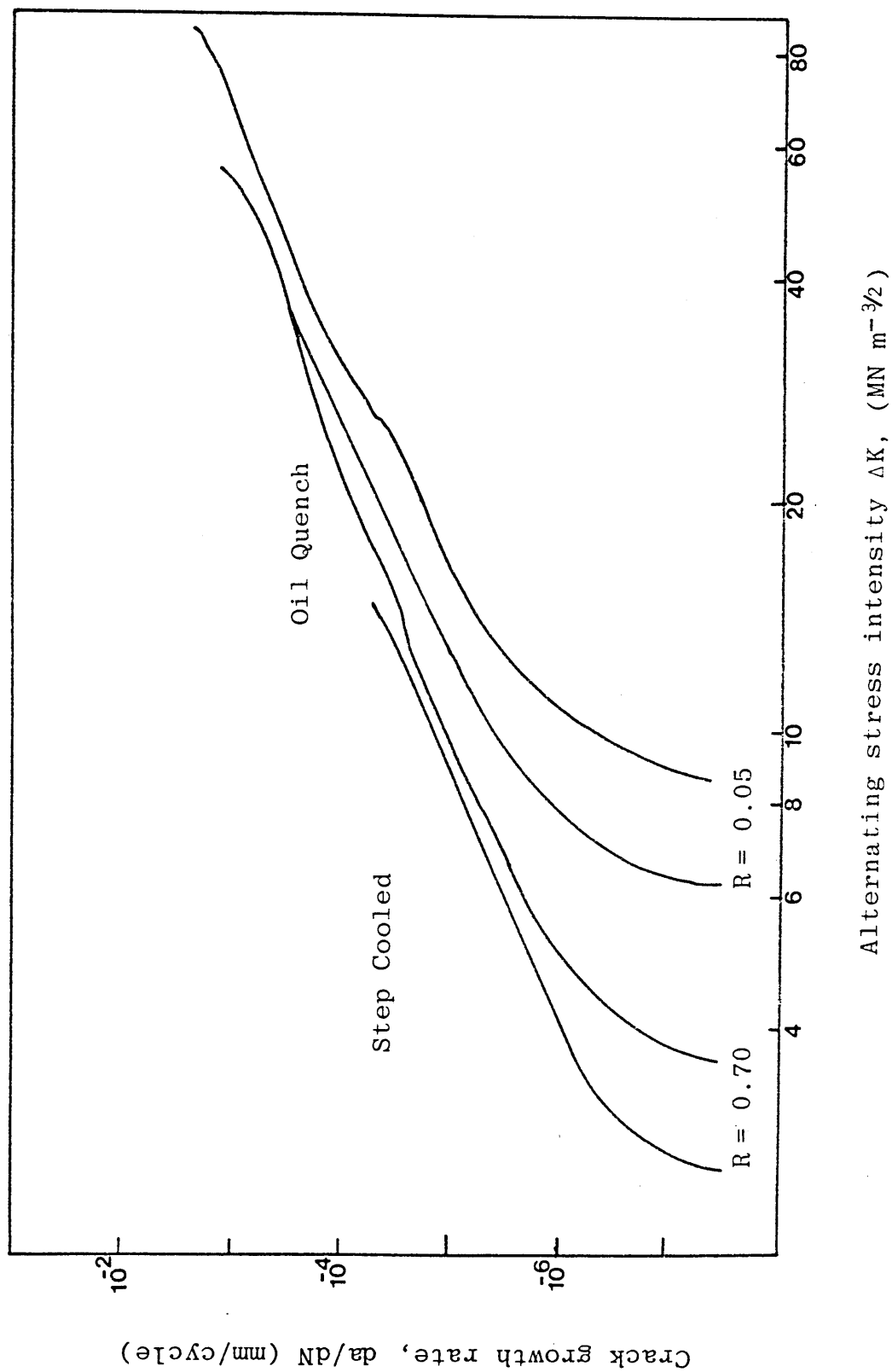
Figure 29

Percentage area of intergranular fracture versus ΔK
and K max, illustrating its transient nature and
dependance on ΔK in air.[46]
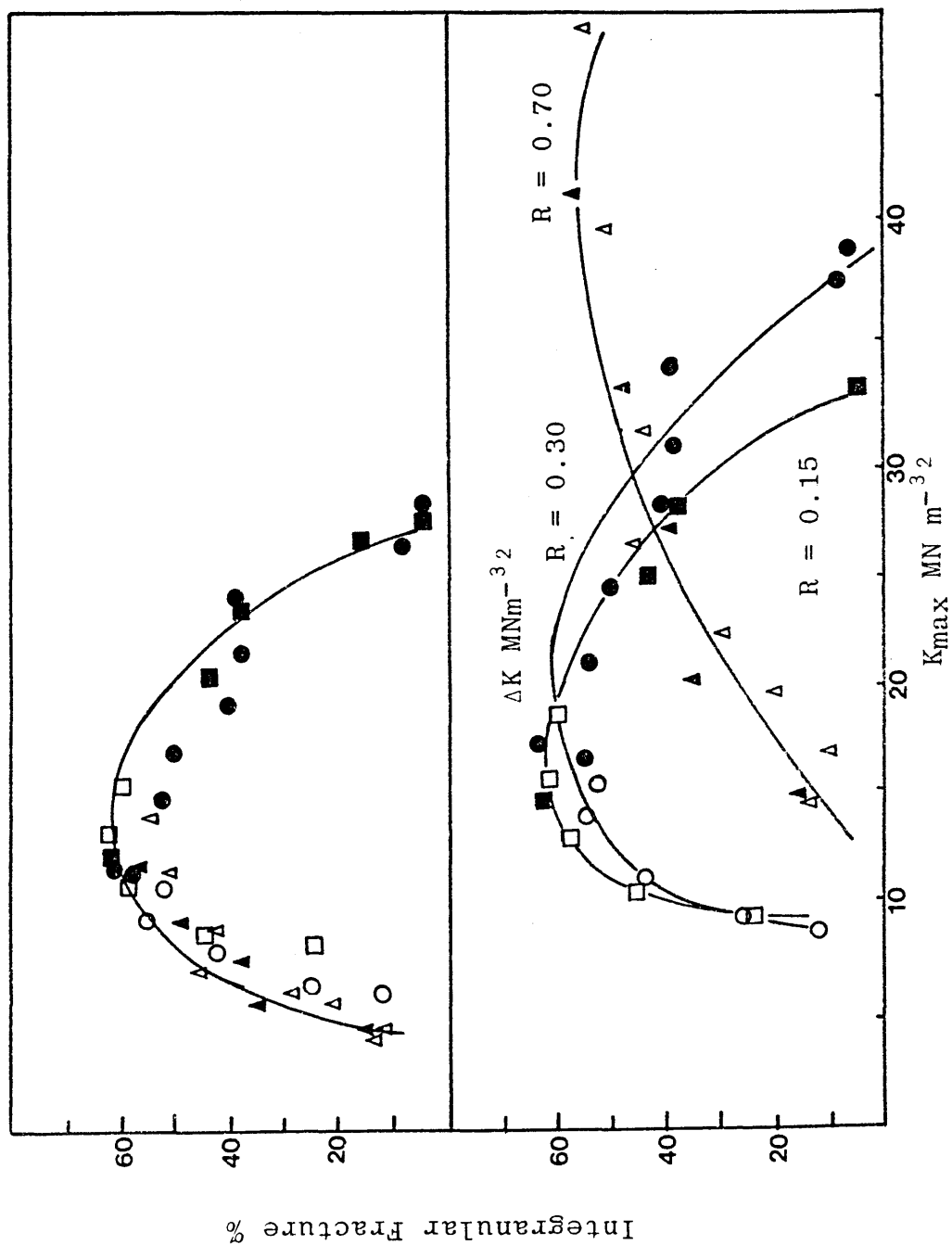
Figure 30

    Variation of fatigue crack growth rate with ampitude
stress intensity factor for high purity B.S. 817M40
steel tempered at 200°C and tested in vacuo in
Laboratory air.
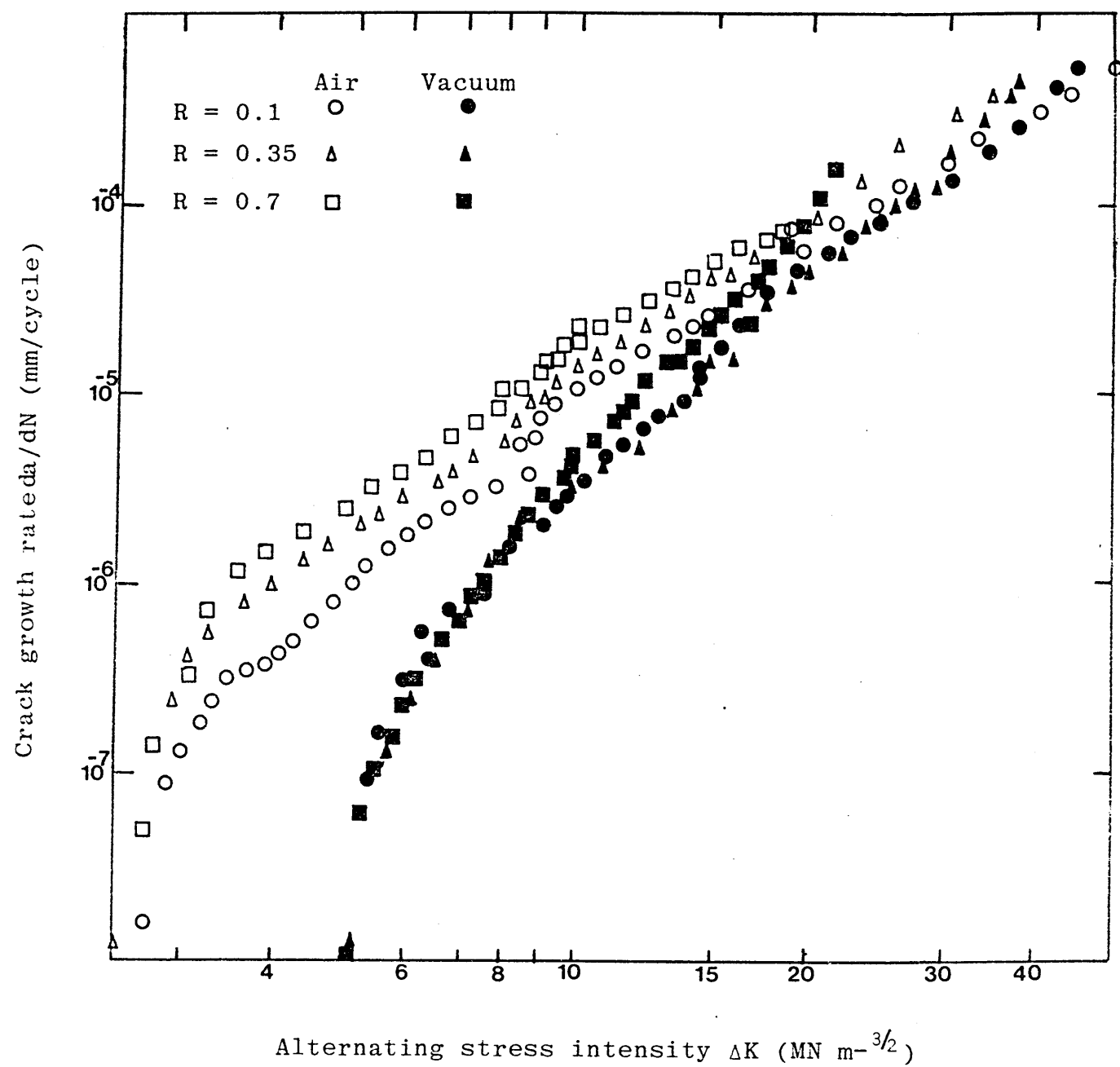
Figure 31

The relationship between threshold stress intensity range ΔK_{Th} and R for air and vacuum.[46]
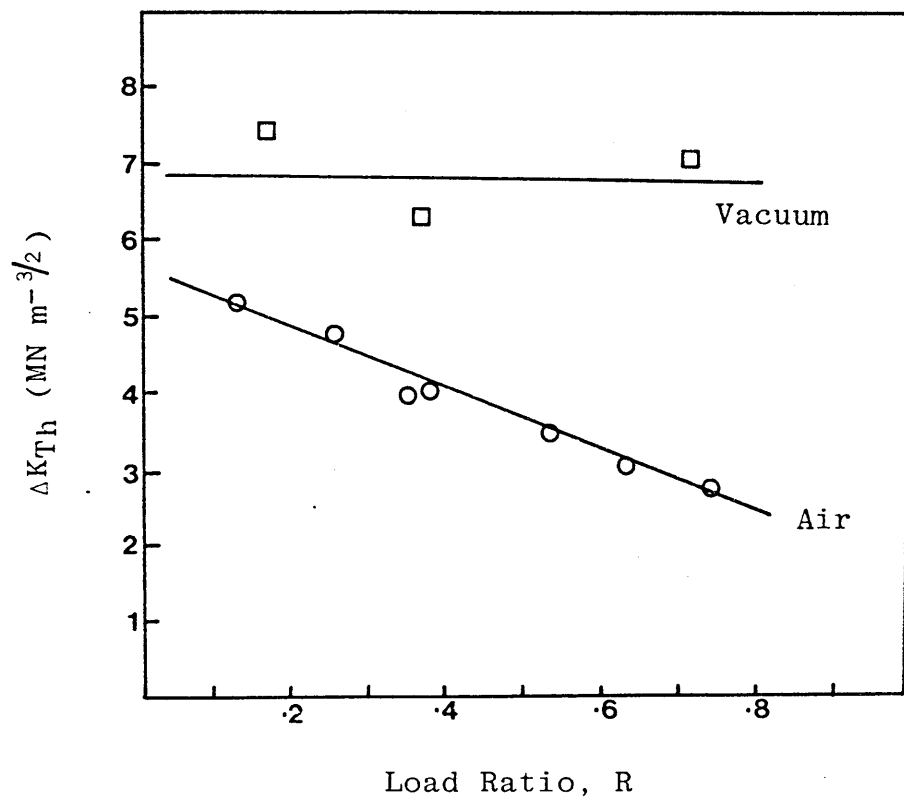
Figure 32

The increase in crack propagation rate and the
associated percentage of intergranular fracture
in a hydrogen environment over a range of stress
intensities.

R = 0.10
2 Hz
273° K
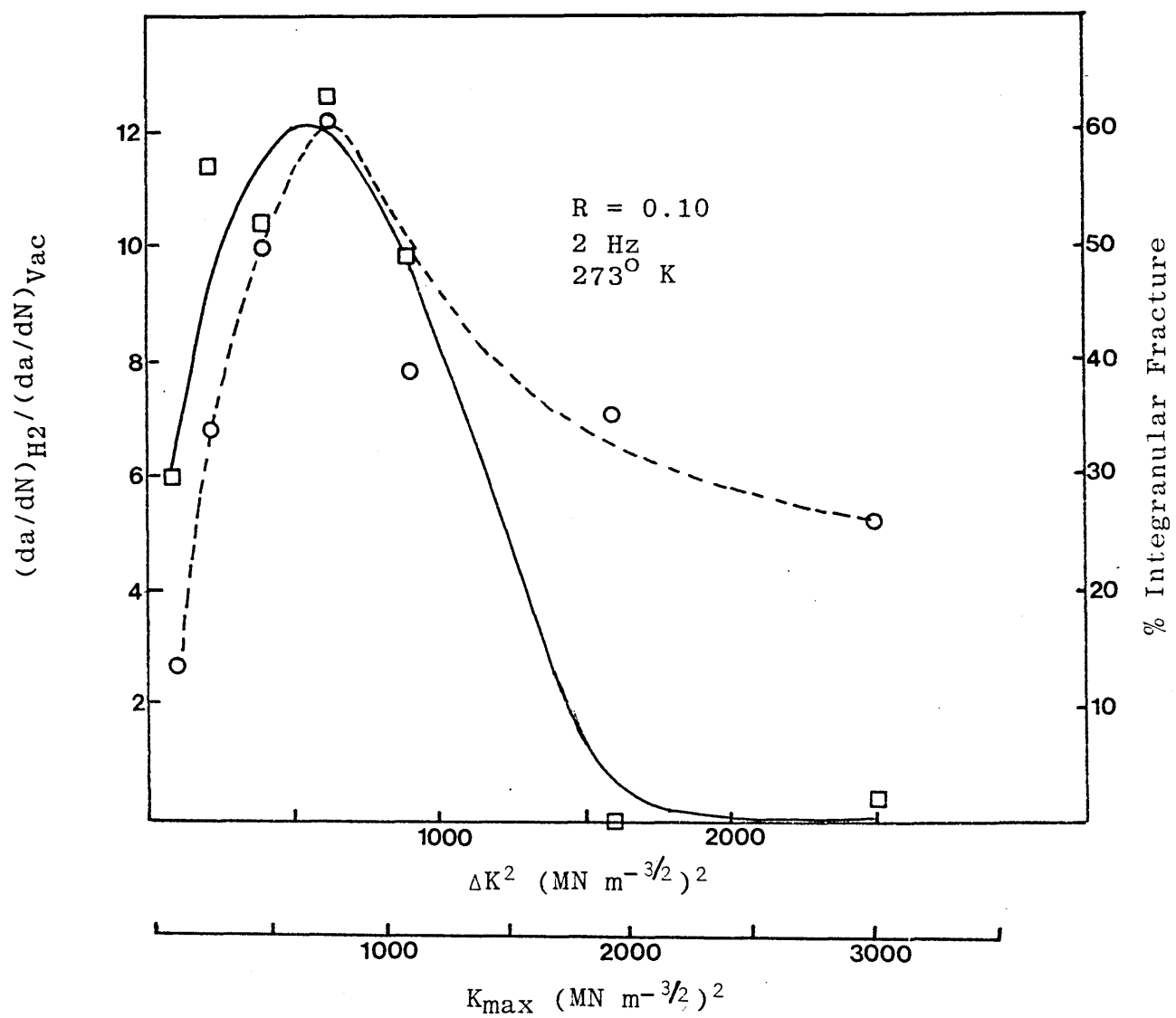
Figure 33

Solute concentration effects on fatigue crack growth
rates for the Fe-Si system.

173 K

- - Fe

□ Fe - 1% Si

● Fe - 2.5% Si

■ Fe - 4% Si

Crack growth rate da/dN (mm/cycle)

10^{-7}

10^{-8}

Stress intensity range (MN m$^{-3/2}$)

15   20   25   30
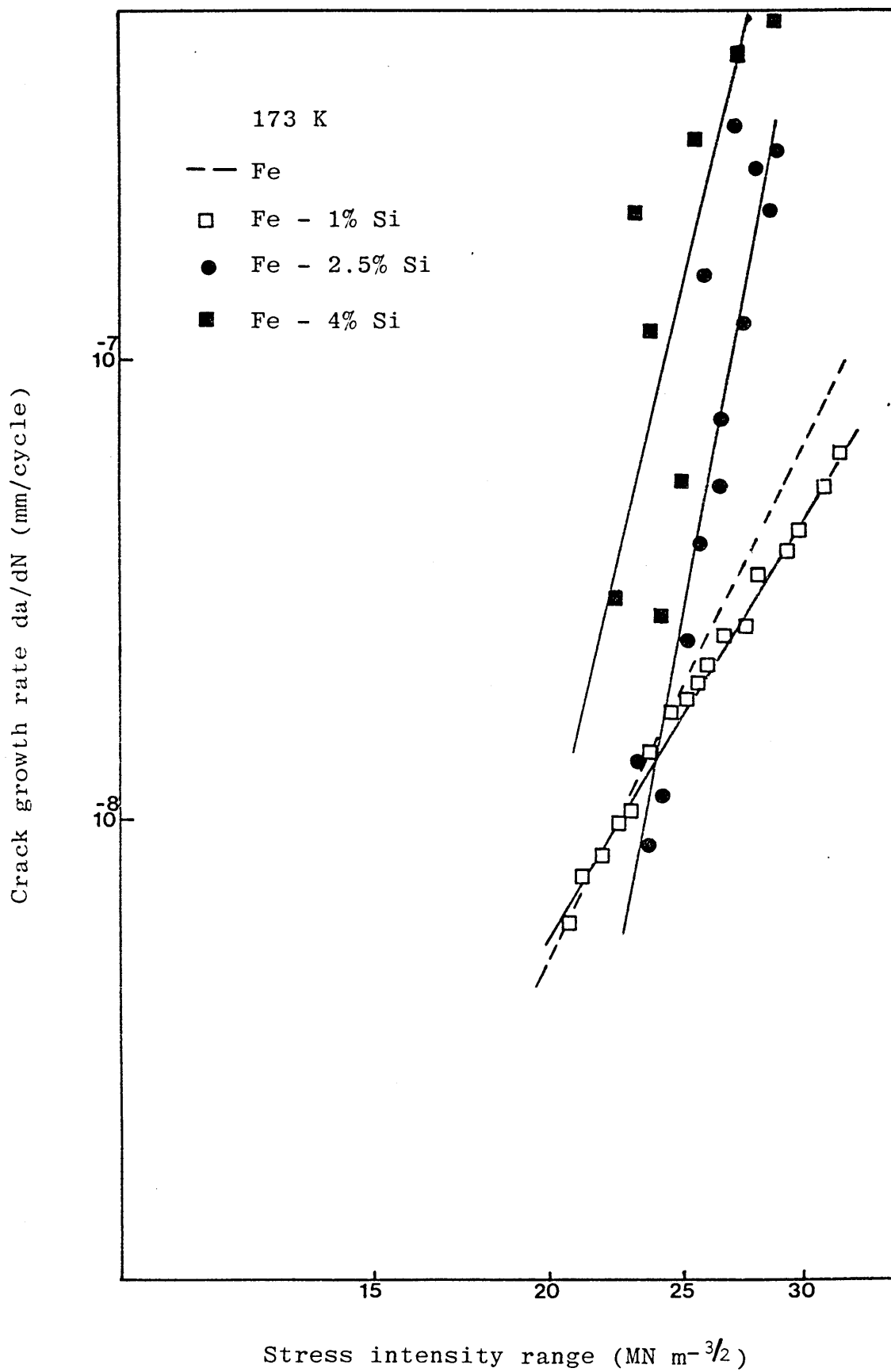
Figure 34

    Variation of grain size with holding time at

1100°C in IS10A
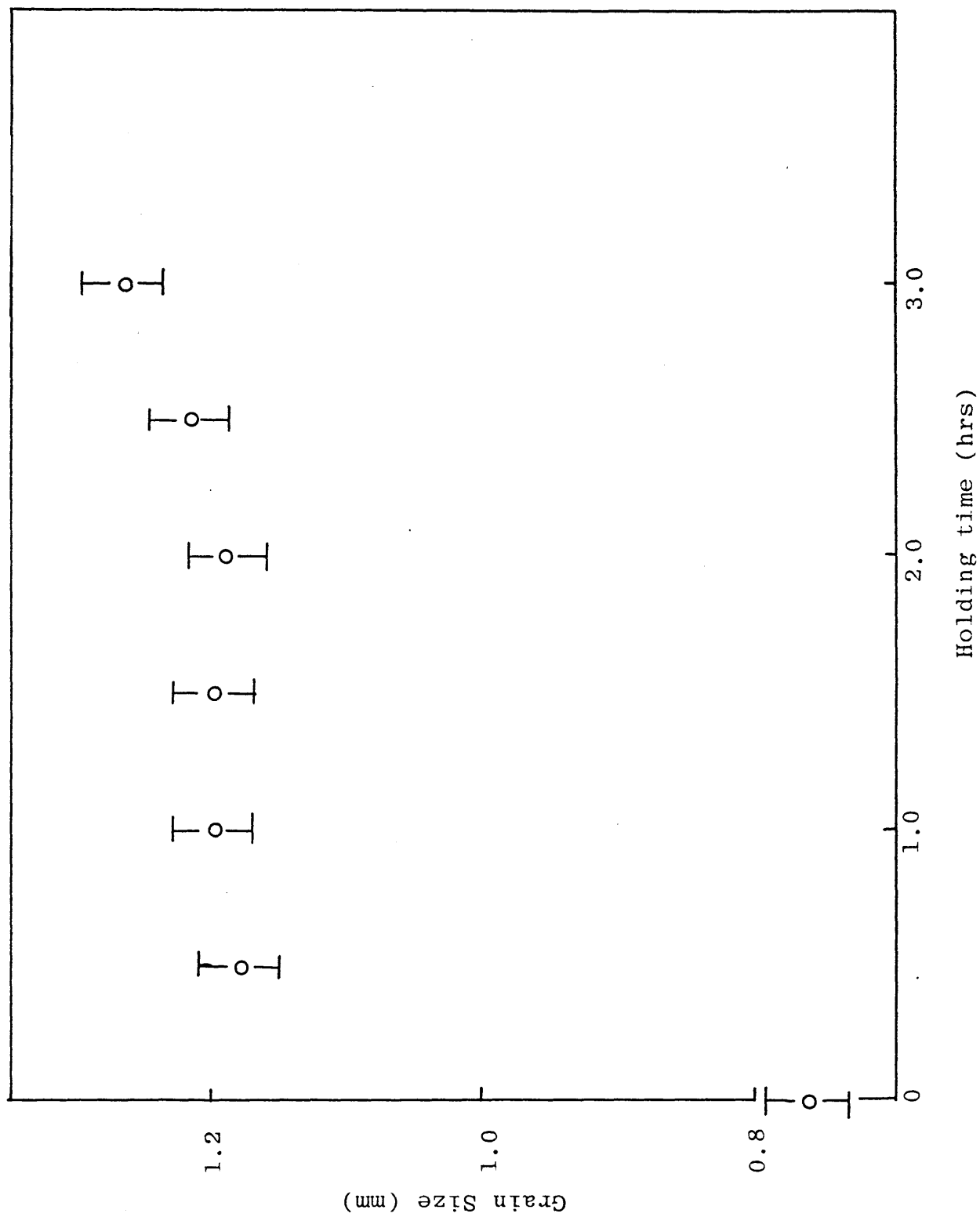
Figure 35

    Variation of grain size with holding time at

900°C in IS10A
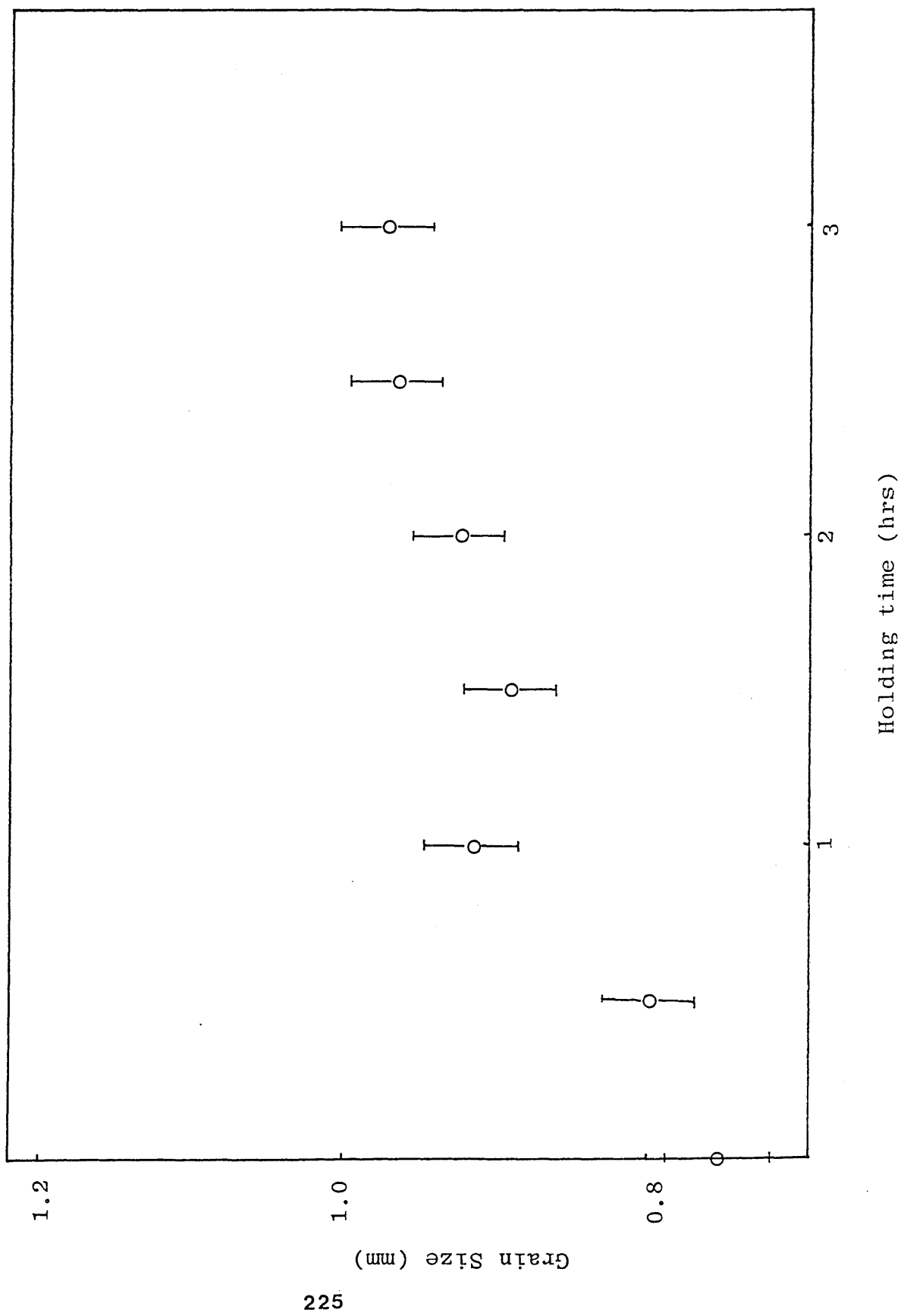
Figure 36

Variation of grain size with 5 (mm) cycles

(α−γ−α) at 950°C in IS20A

227

All Dimensions in mm.

60°

30.0

13.75

←12·5→

←25·0→

62.5

25.4

Position of tensile
specimen

All Dimensions in mm.

V/V$_o$

1.8

1.6

1.4

1.2

1.0

0.3   0.4   0.5   0.6   0.7   0.8   0.9

$V/V_o = a/W + 0.62$
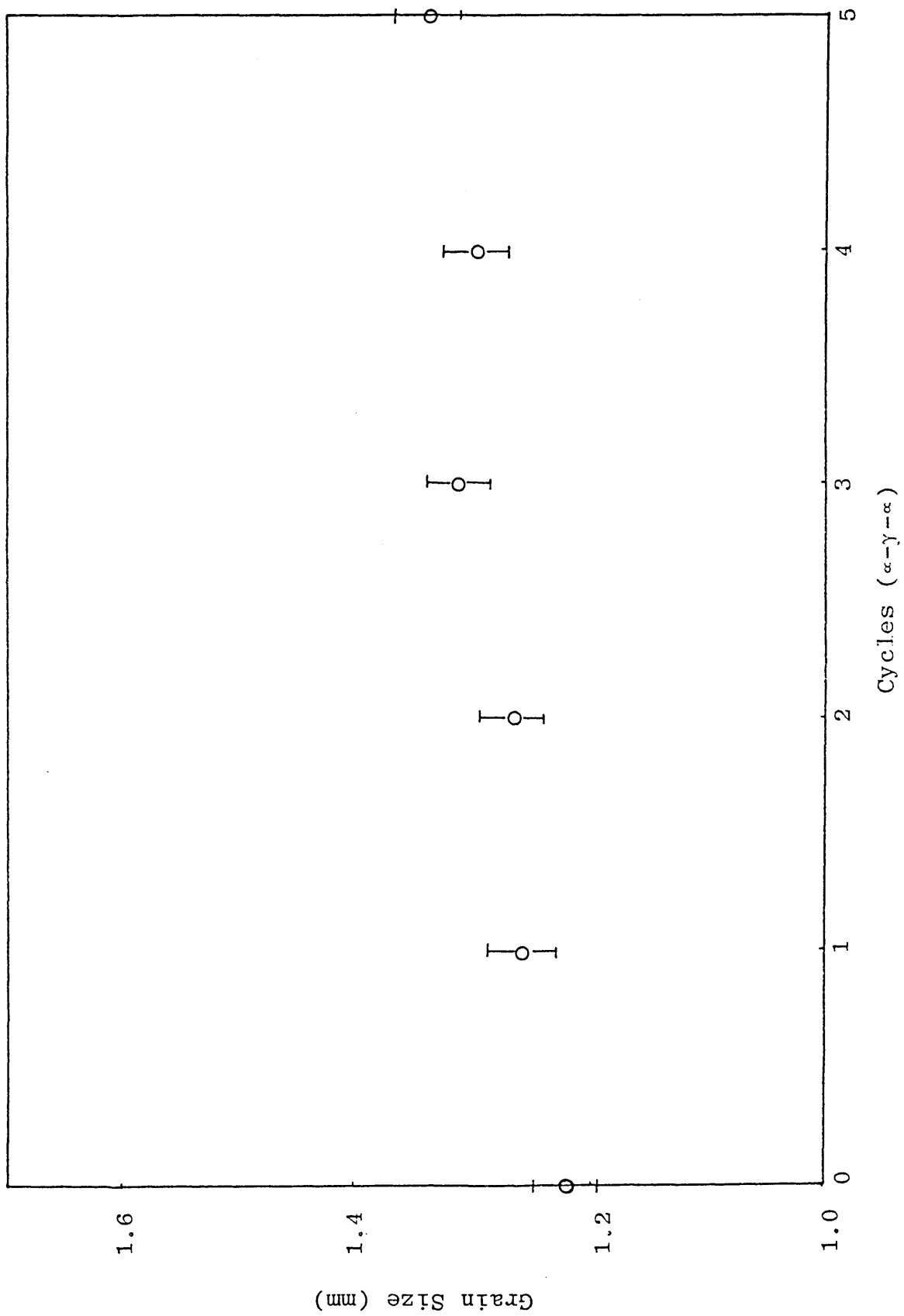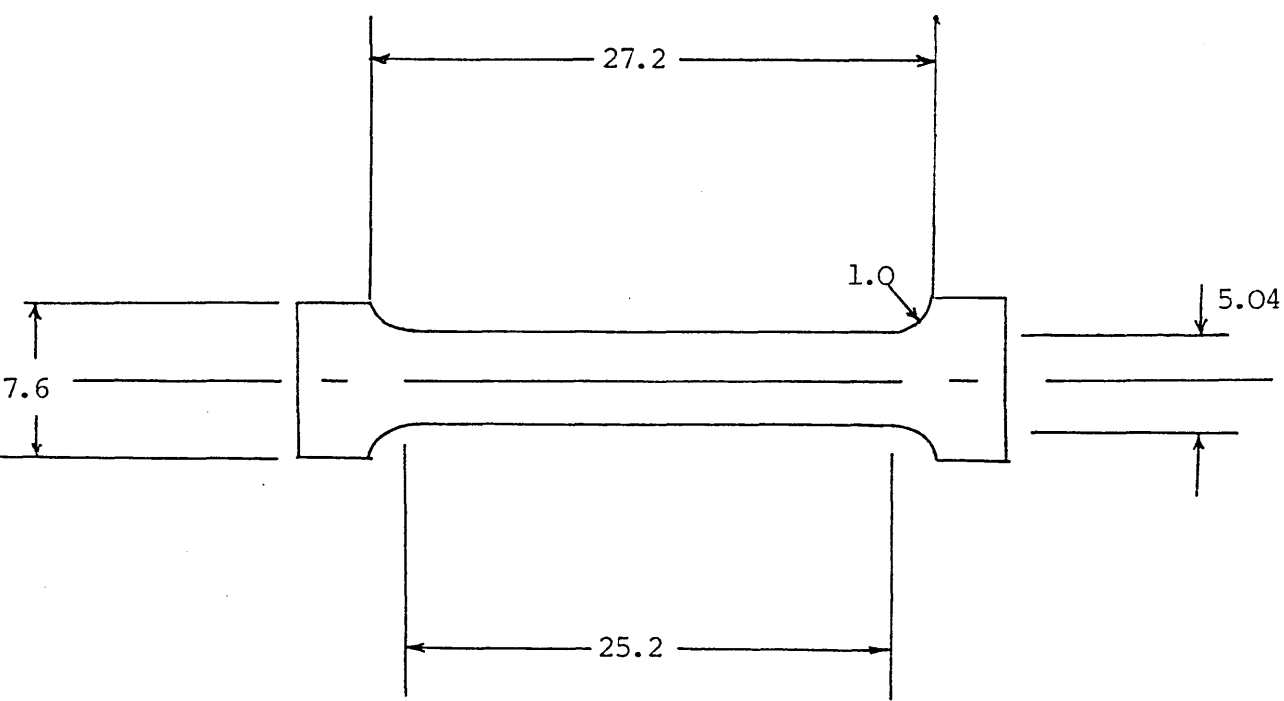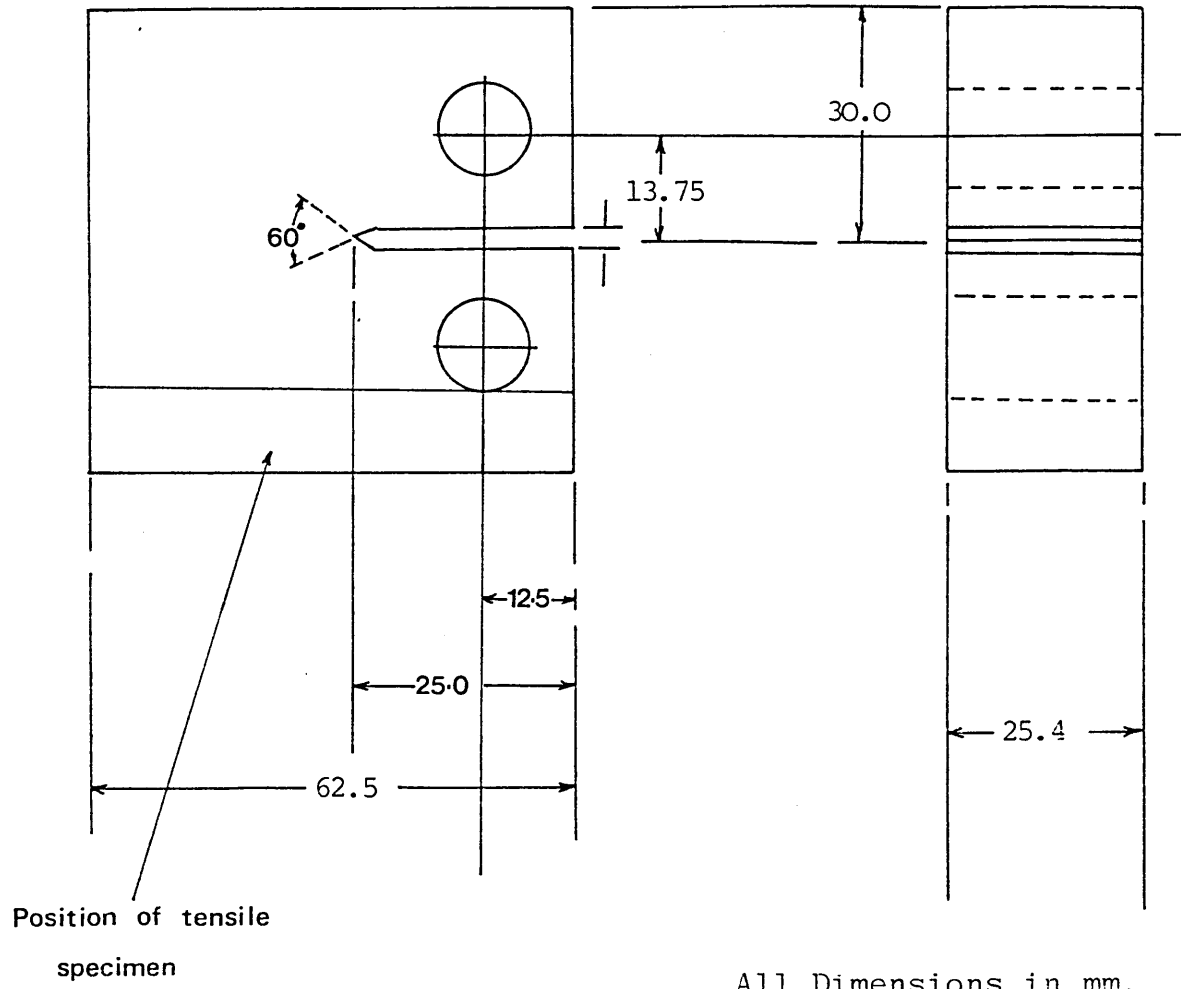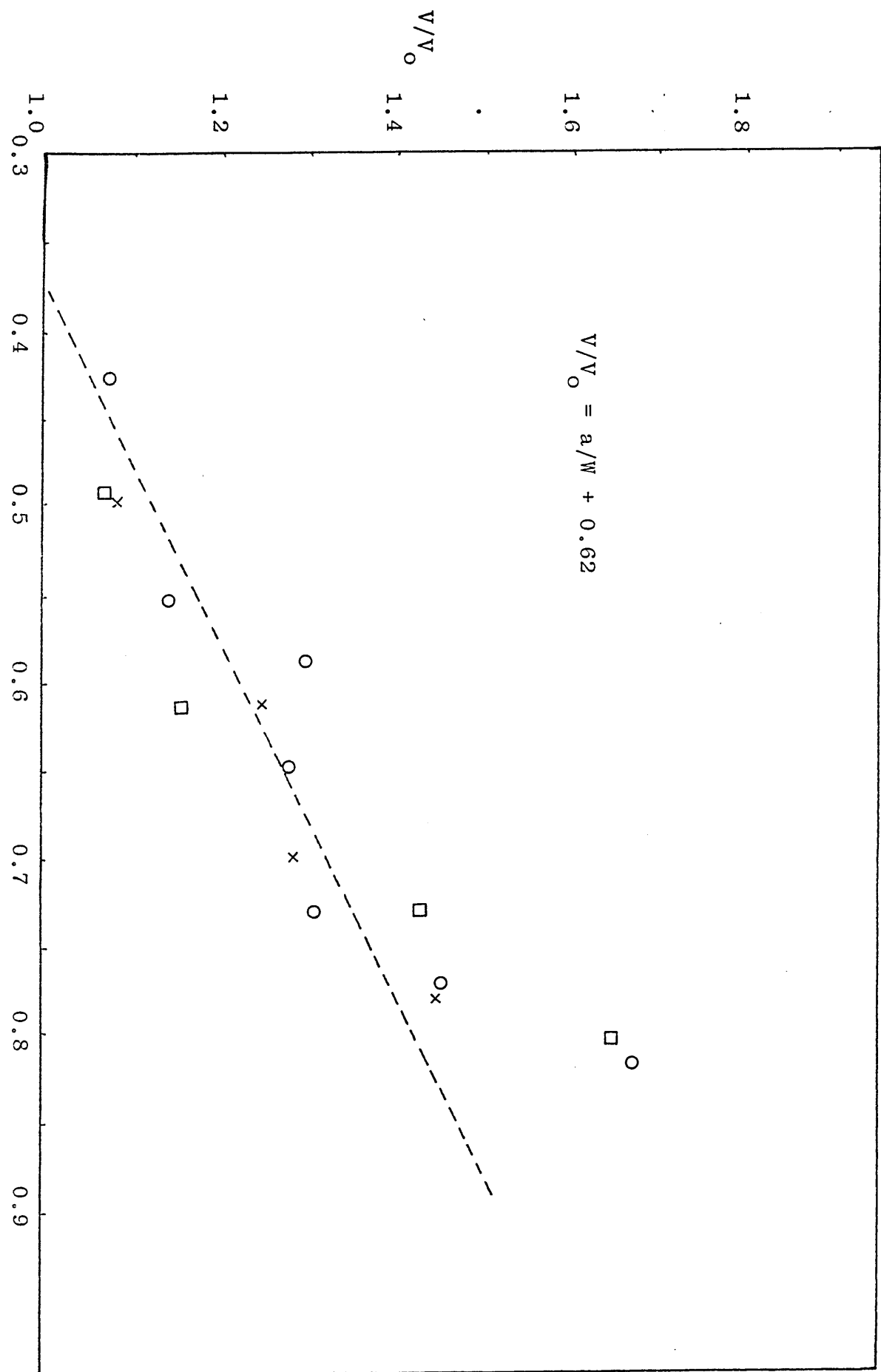
Figure 40

Schematic circuit diagram for fatigue threshold
testing equipment.

CONTROL
ERMOCOUPLE

THERMOCOUPLE

HEATING ELEMENT

TEMP
MONITOR

SOFT IRON
JUNCTION

Fe/Cu JUNCTION

MICROVOLT
SOURCE   5

3
2
1
4

MICROVOLT
METER   6

CONSTANT
CURRENT
SUPPLY   8'

TEMP
CONTROLLER

VOLTAGE
STABILISER

CHART
RECORDER   7
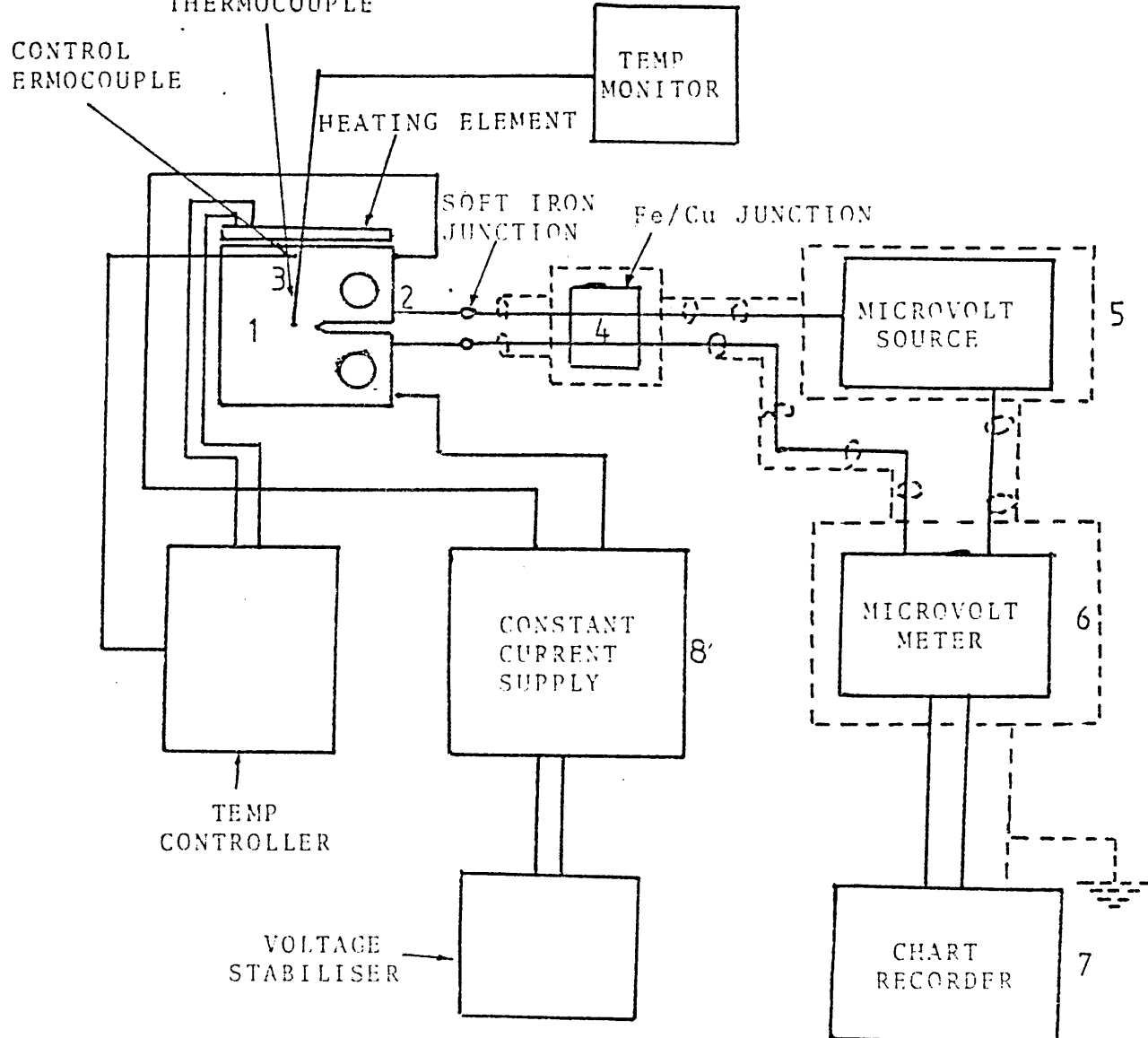
1   TEST PIECE AT CONSTANT TEMPERATURE, ELECTRICALLY INSULATED
     FROM TEST FRAME.

2   IRON WIRES SPOT WELDED TO TEST PIECE.

3   THERMOCOUPLES SPOT WELDED TO TEST PIECE.

4   Fe/Cu WIRE JUNCTIONS SUNK IN Al BLOCK TO ELIMINATE ELECTRICALLY
     GENERATED TEMPERATURE DIFFERENTIALS.

5   STABLE MICROVOLT SOURCE, SCREENED AND ISOLATED FROM MAINS SUPPLY.

6   STABLE MICROVOLT METER SCREENED AND BATTERY POWERED.

7   EARTHING POINT.

8   FEEDBACK STABILISED CONSTANT CURRENT SUPPLY.

Figure 41

    Fatigue specimen wired for threshold testing.

Heating
Element

Control
Thermocouple

Current
Cable

Monitoring   Thermocouple

Iron   P D   wires

$$\Delta K_1 = K_{max_1} - K_{min_1}$$

$$\Delta K_2 = K_{max_2} - K_{min_2}$$

$$R_1 = \frac{K_{min_1}}{K_{max_1}}$$

$$R_2 = \frac{K_{min_2}}{K_{max_2}}$$

Time

K_{max_1}

K_{max_2}

K_{min_1}

K_{min_2}

239
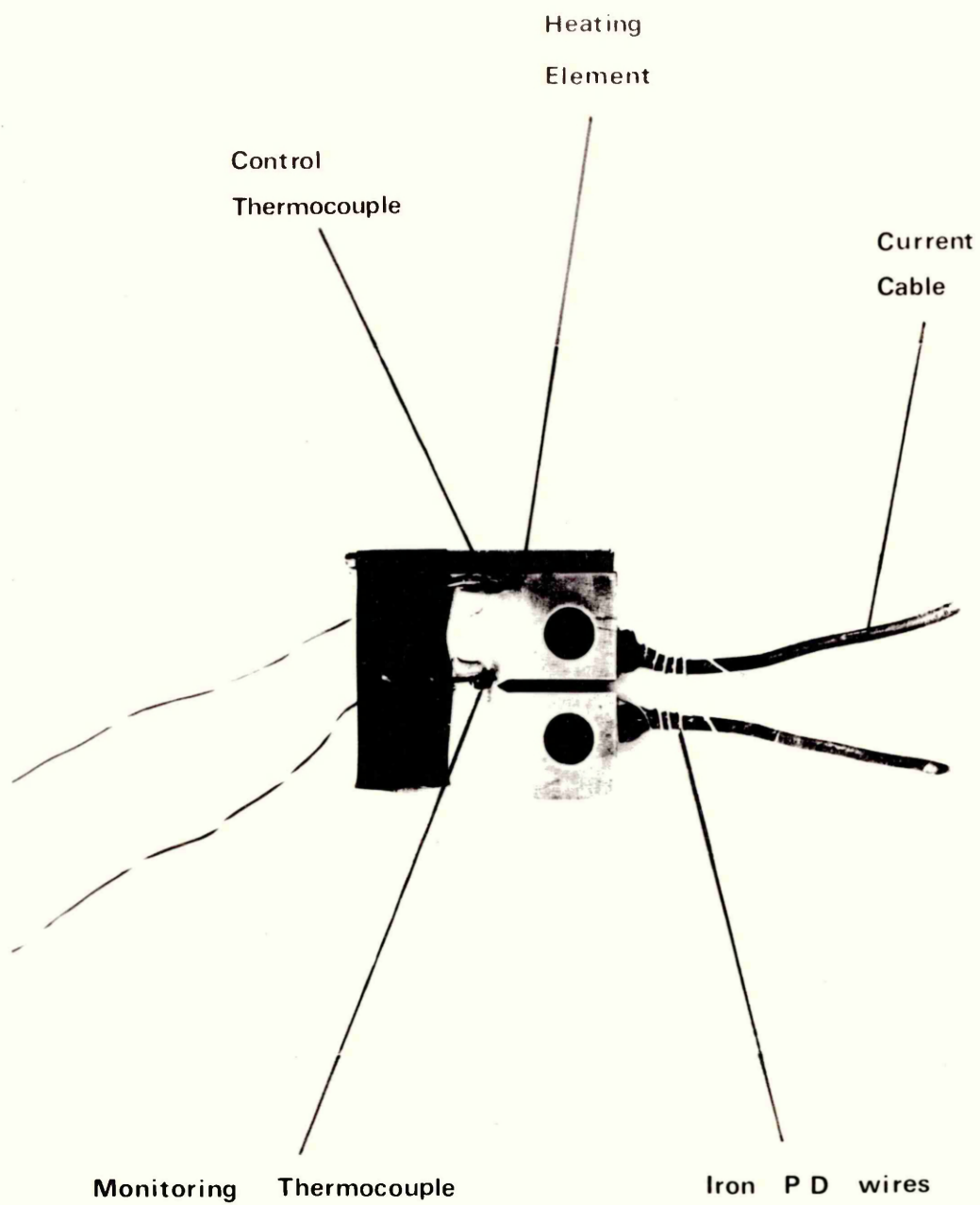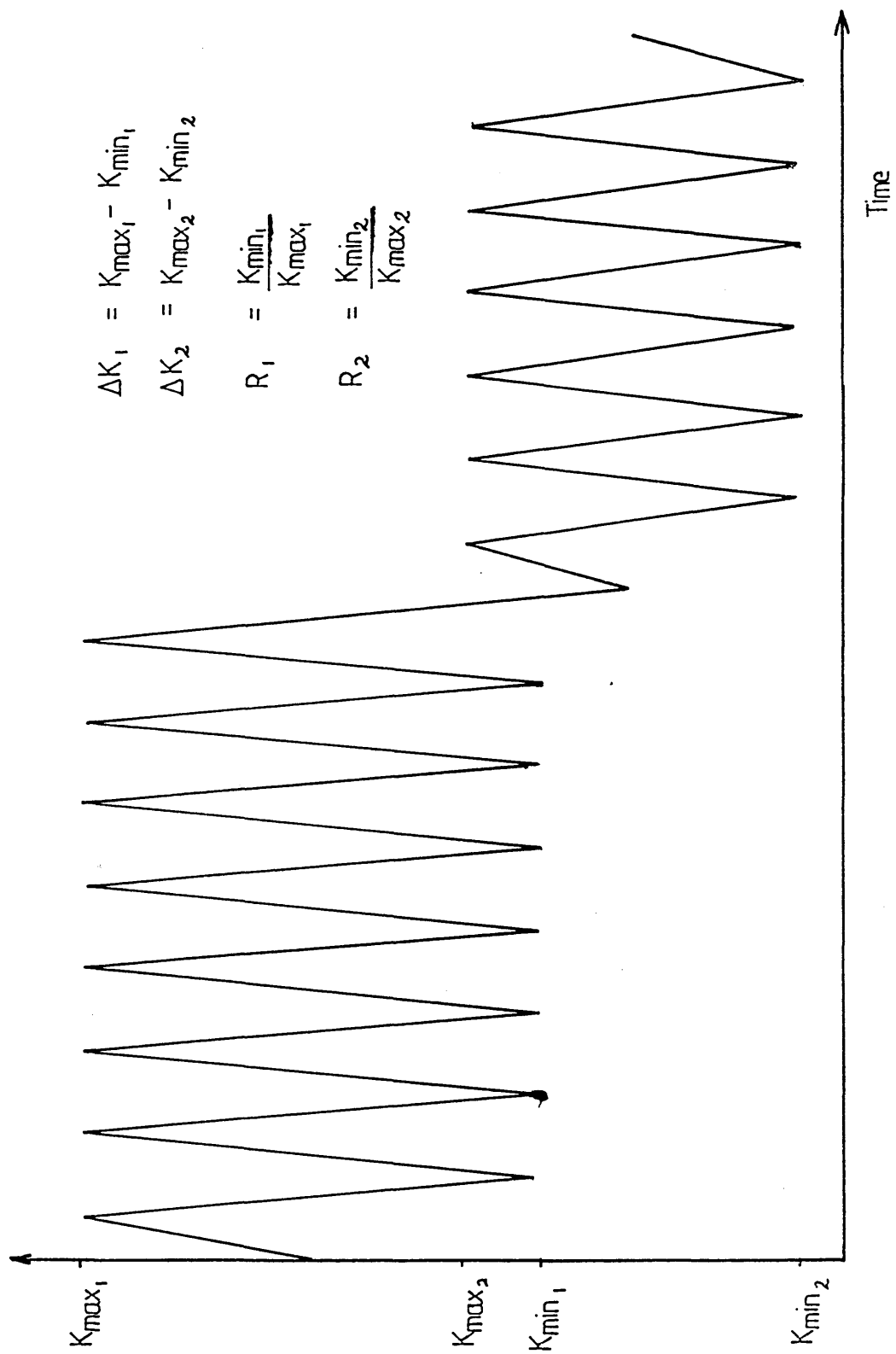
Figure 43

Rectangular rosette for residual stress
measurements.

3 Strain gauge elements
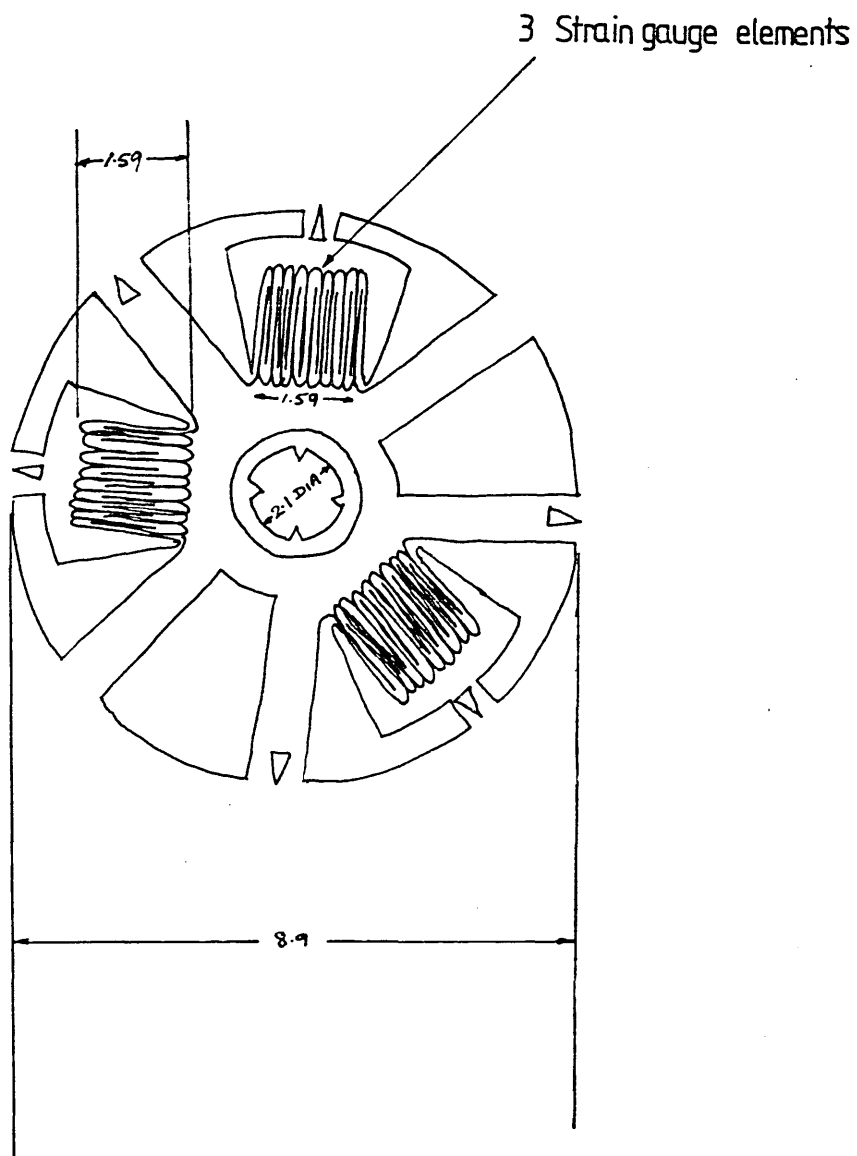
Figure 44

Positioning of strain gauge for residual stress

measurement.

Machined
Notch

Fatigue
Crack

Strain
Gauge

243
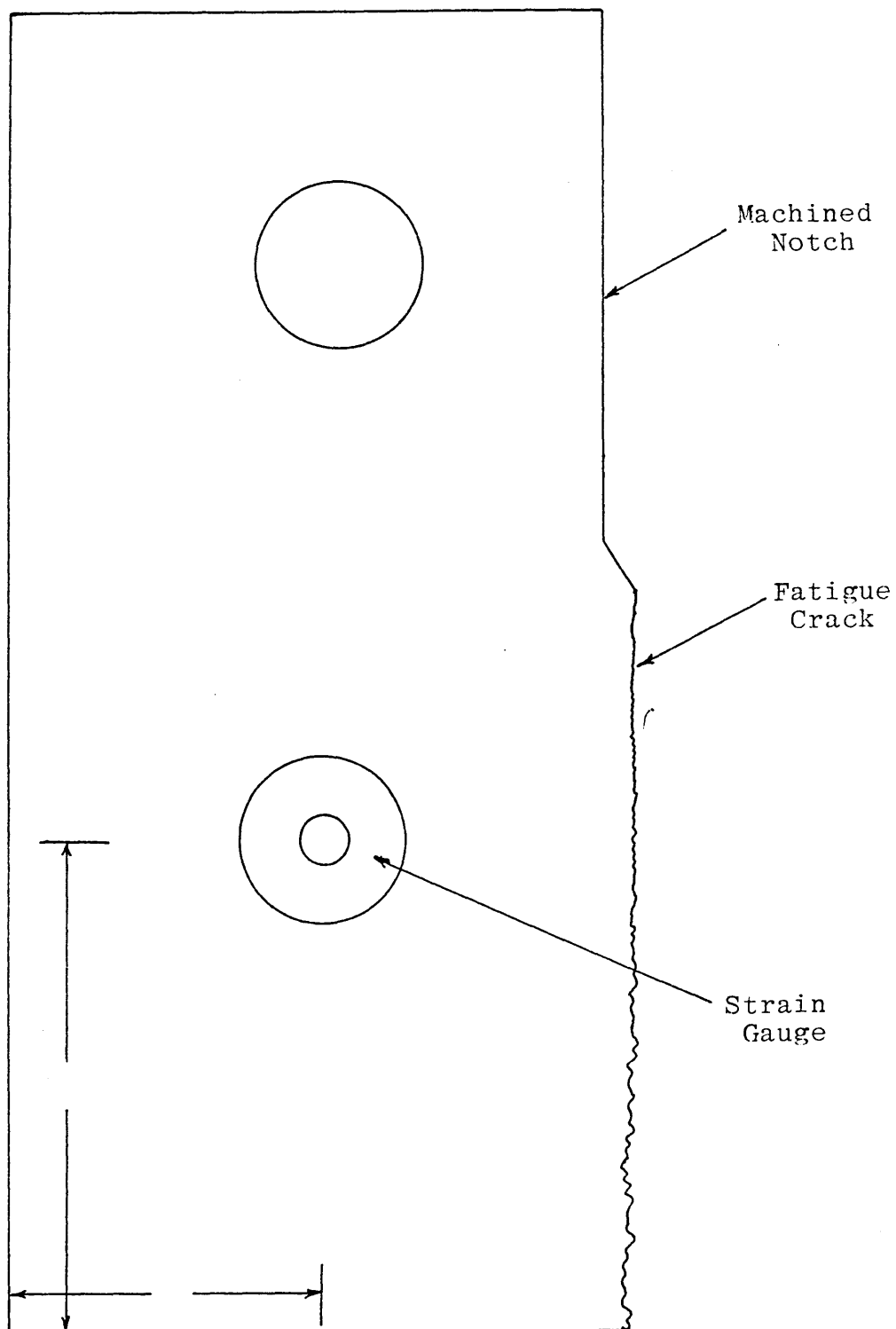
Figure 45

   Fatigue crack growth results for specimen
ISOO(1) A2.

GROWTH RATE mm/cycle

10^{-4}

10^{-5}

10^{-6}

10^{-7}

10^{-8}

4   6   8   10   15   20

$\triangle K$ $MNm^{-3/2}$

245
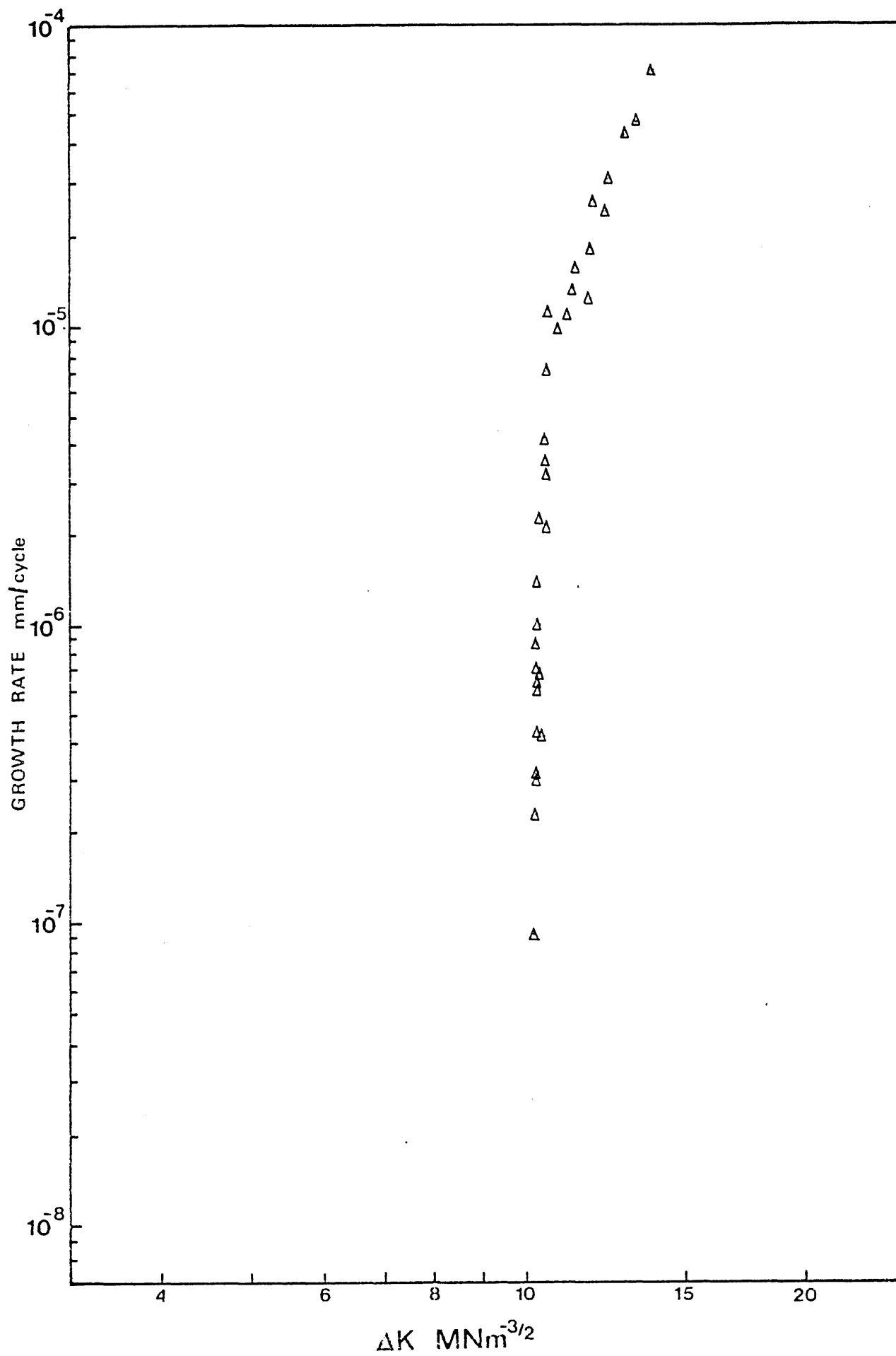
Figure 46

Fatigue crack growth results for specimen
IS00(1) A1.

GROWTH RATE mm/cycle

ΔK MNm$^{-3/2}$

247
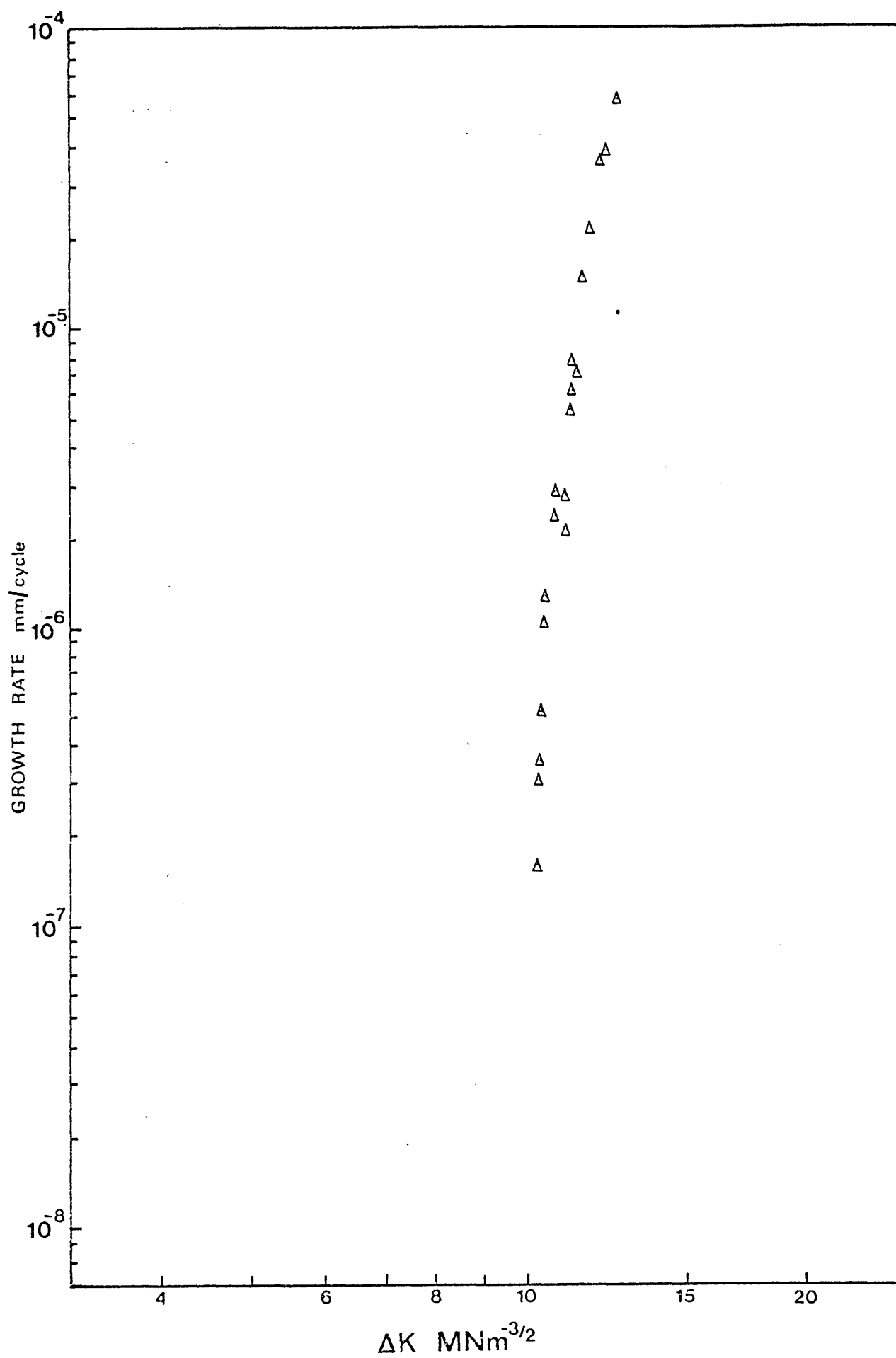
Figure 47

   Fatigue crack growth results for specimen
ISOO(1) A3.

GROWTH RATE mm/cycle

ΔK MNm$^{-3/2}$

249
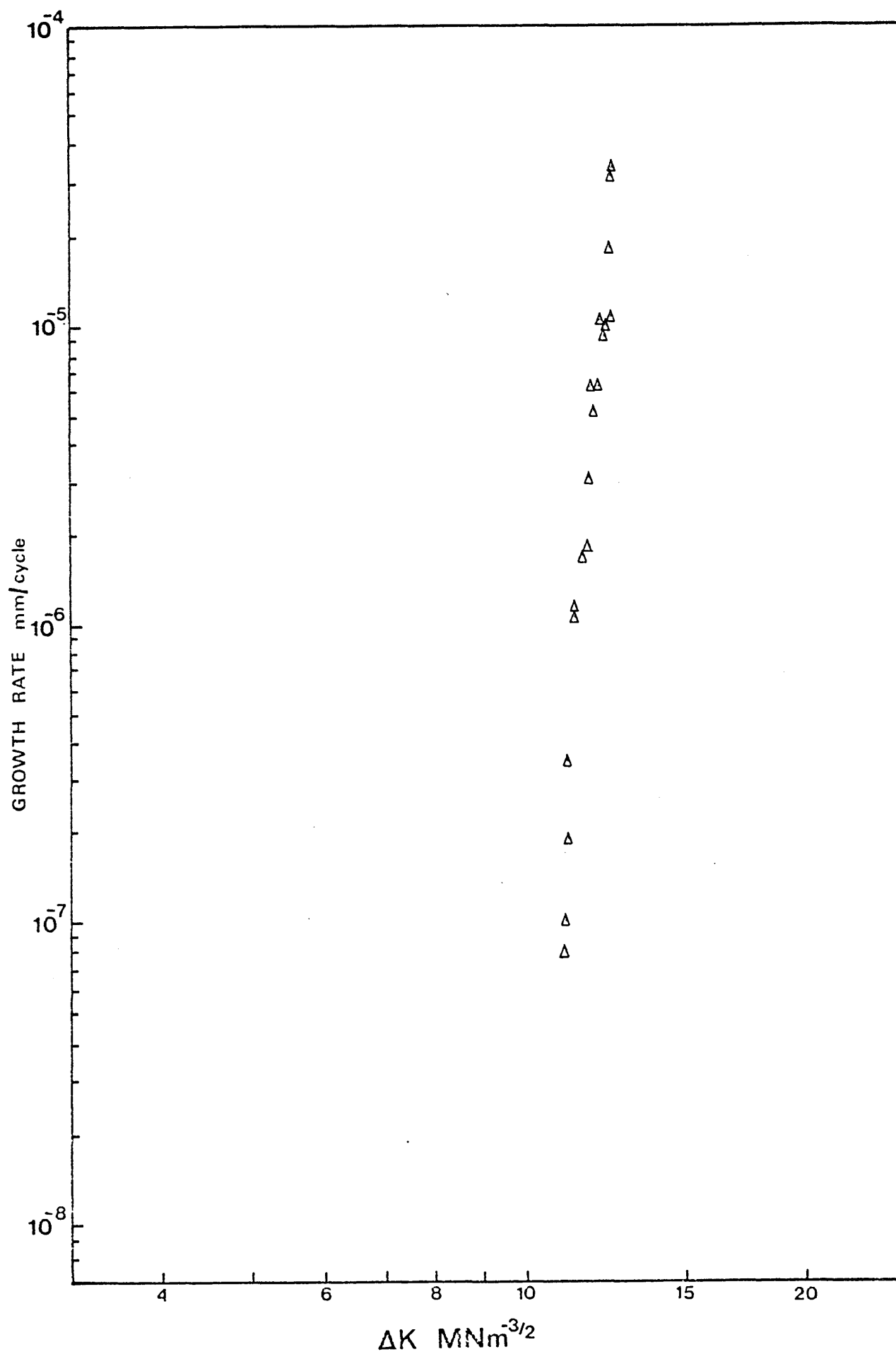
Figure 48

Fatigue crack growth results for specimen
IS05(3) A3.

GROWTH RATE $mm/cycle$

10^{-4}

10^{-5}

10^{-6}

10^{-7}

10^{-8}

4   6   8   10   15   20

ΔK $MNm^{-3/2}$

251
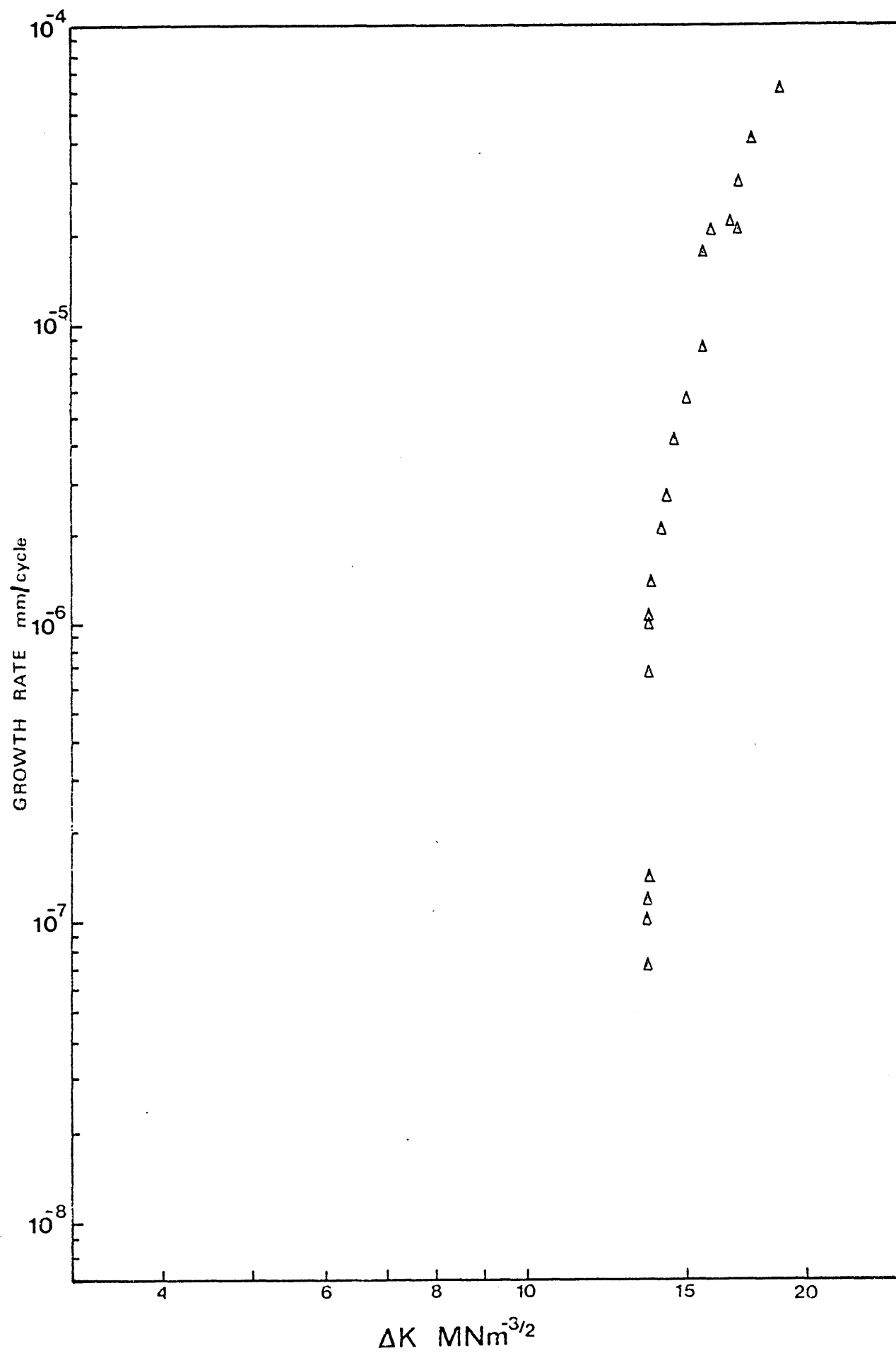
Figure 49

Fatigue crack growth results for specimen
IS05(3) B1.

GROWTH RATE mm/cycle

10^{-4}

10^{-5}

10^{-6}

10^{-7}

10^{-8}

4   6   8   10   15   20

ΔK MNm$^{-3/2}$
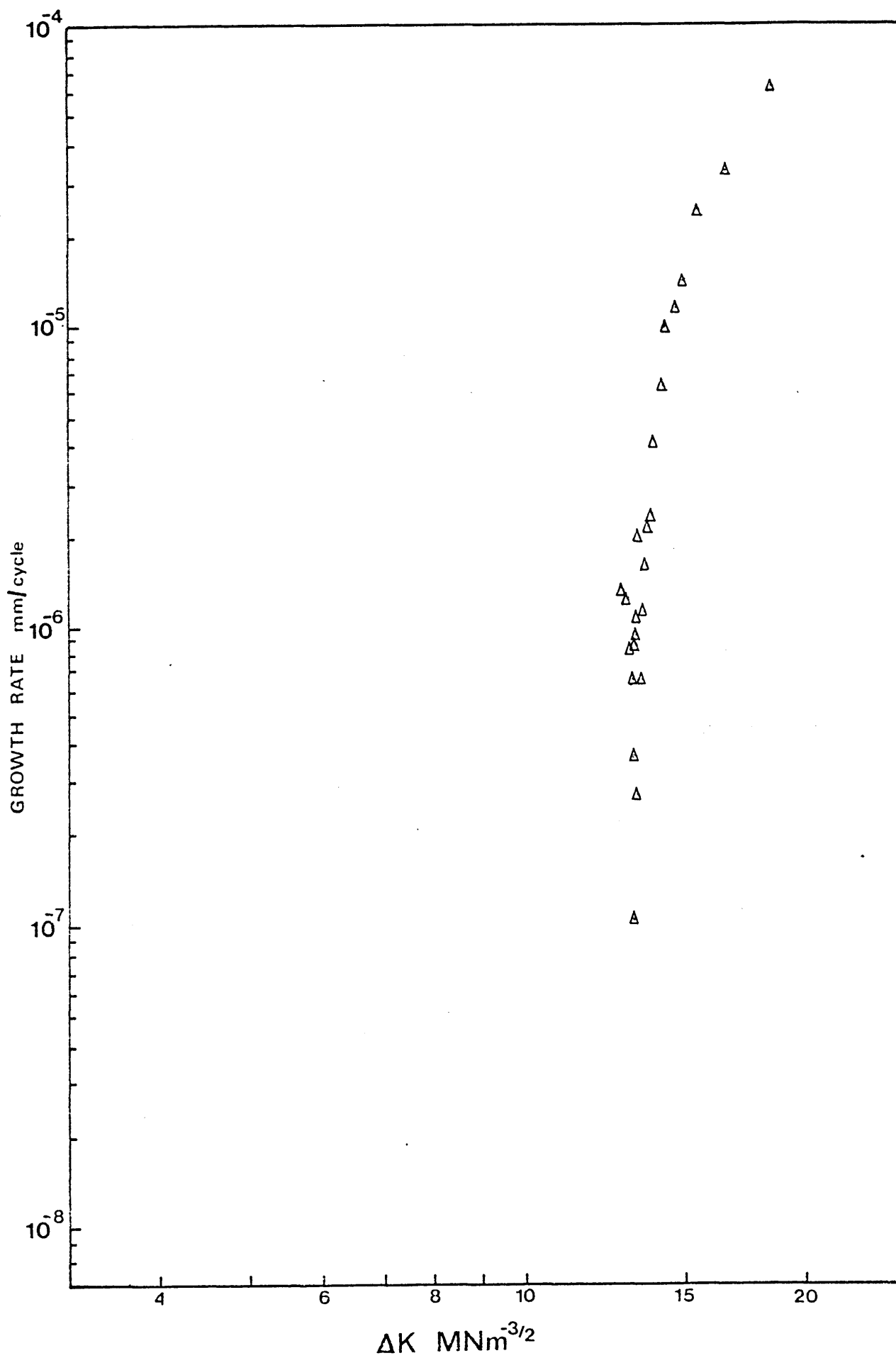
Figure 50

    Fatigue crack growth results for specimen
IS05(3) A1.
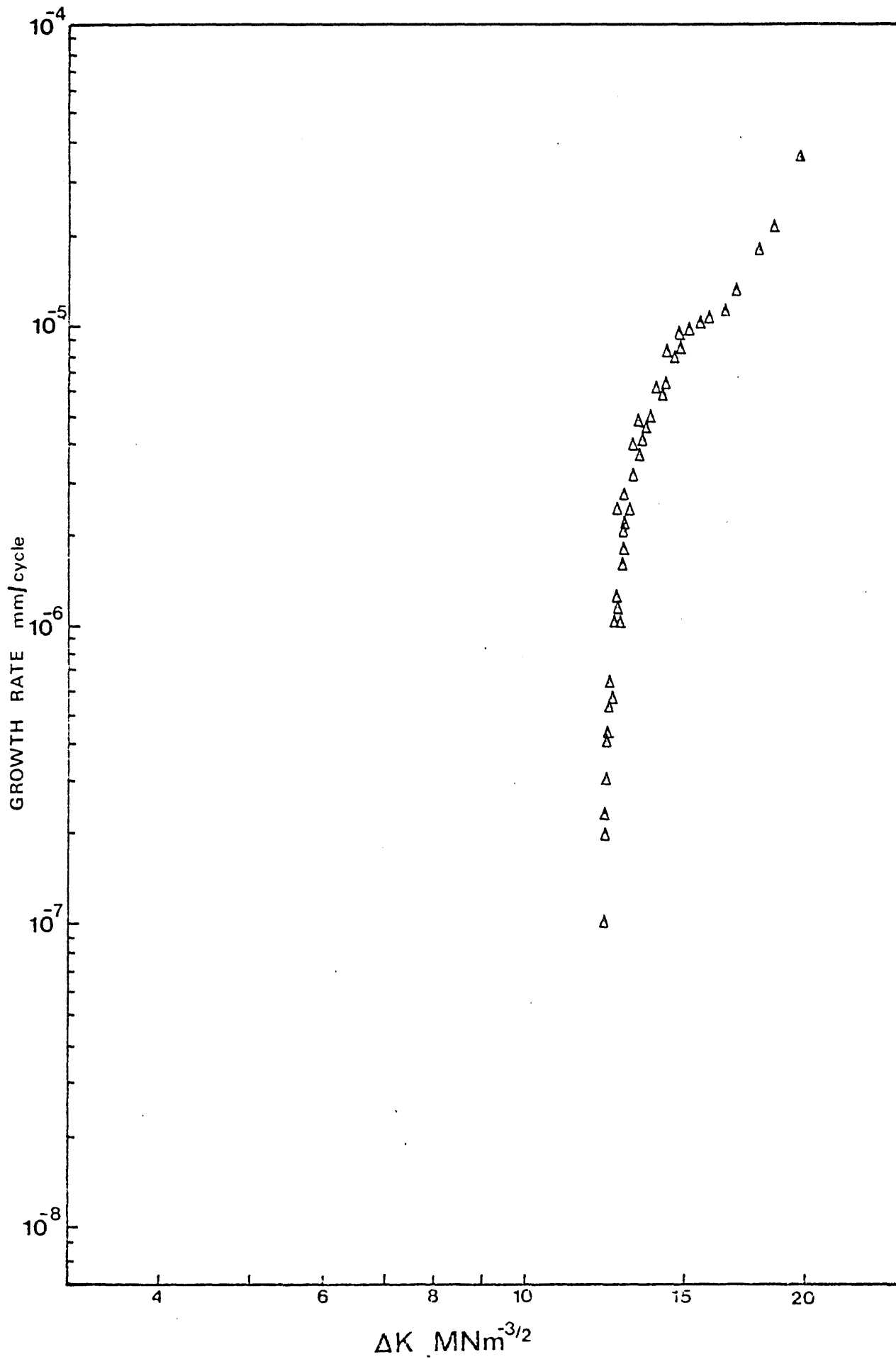
<u>Figure 51</u>

Fatigue crack growth results for specimen
IS05(3) B2.

257
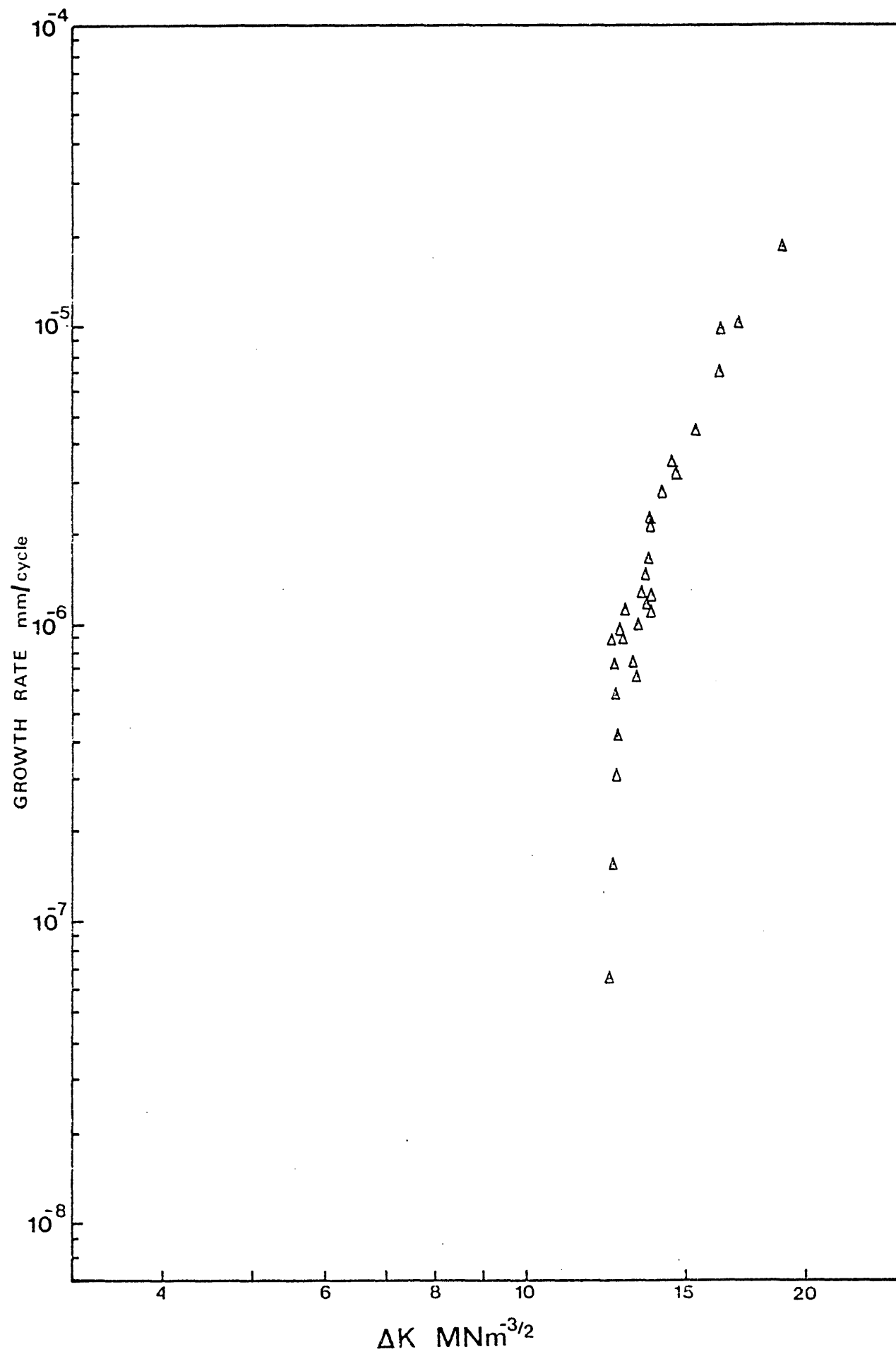
Figure 52

Fatigue crack growth results for specimen
IS05(3) A2.
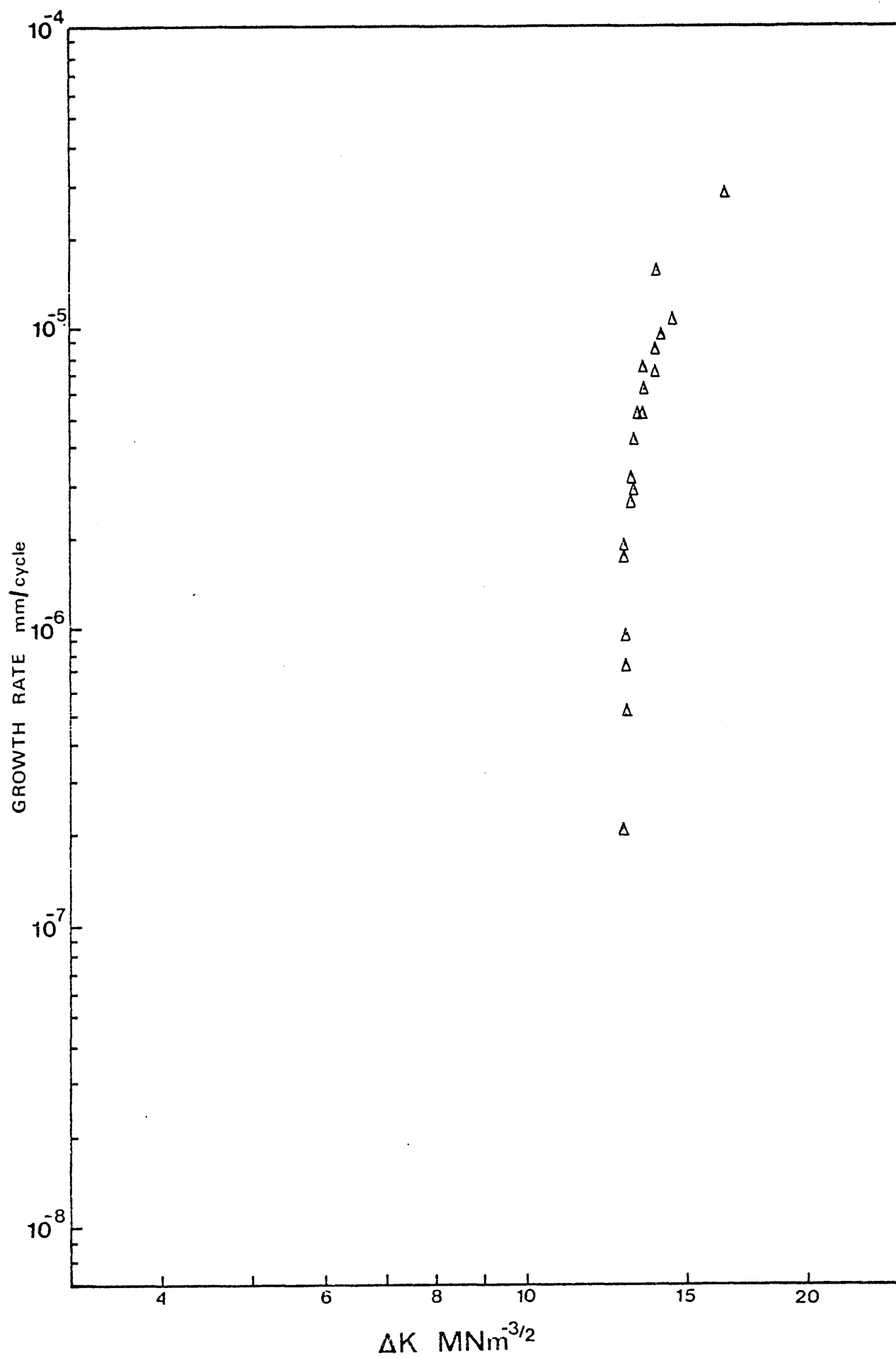
<u>Figure 53</u>

Fatigue crack growth results for specimen IS10(3) B2.

261
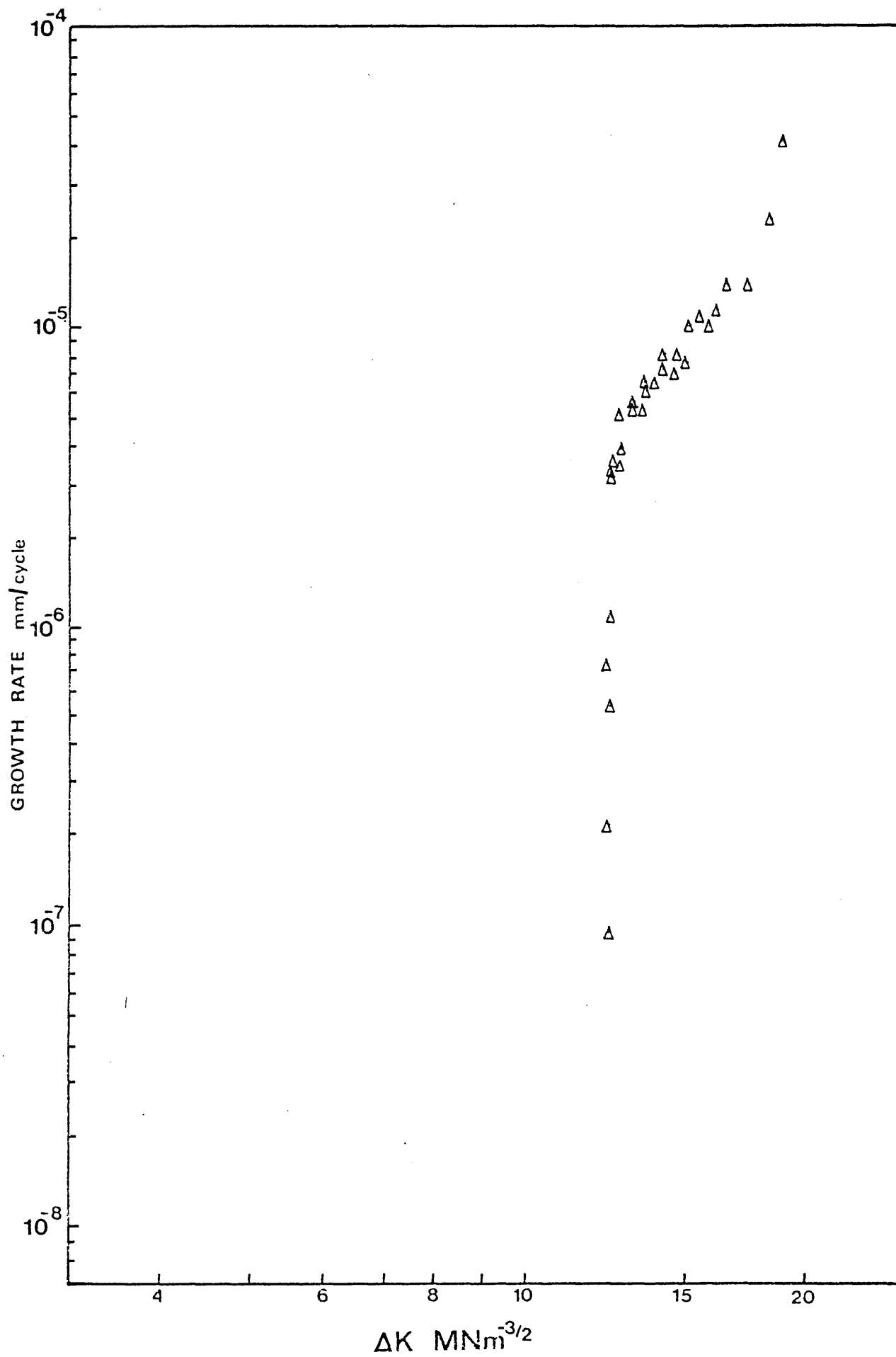
Figure 54

Fatigue crack growth results for specimen
IS10(3) A2.

263
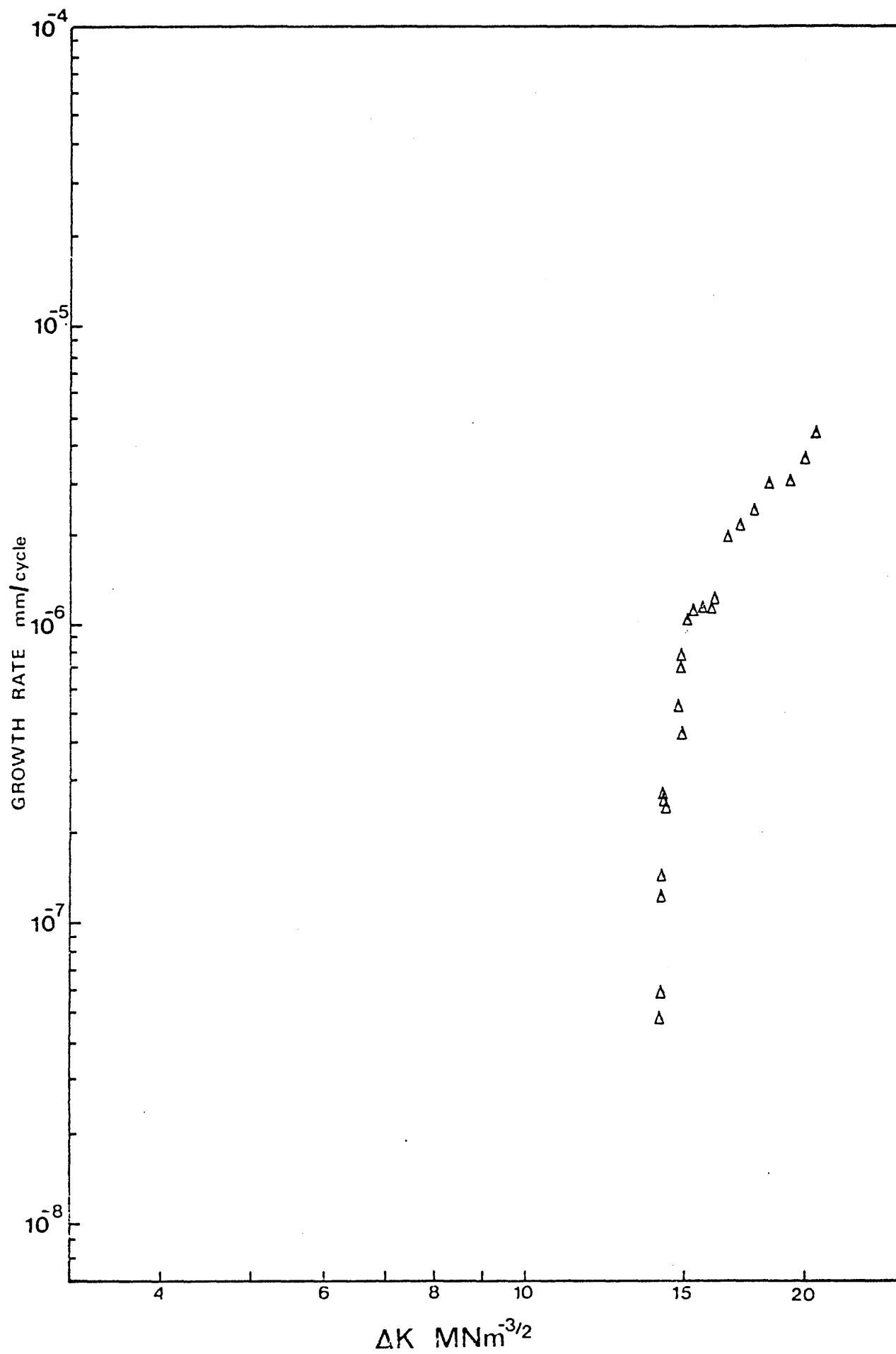
Figure 55

Fatigue crack growth results for specimen
IS10(3) A3.

GROWTH RATE mm/cycle

ΔK MNm$^{-3/2}$

265
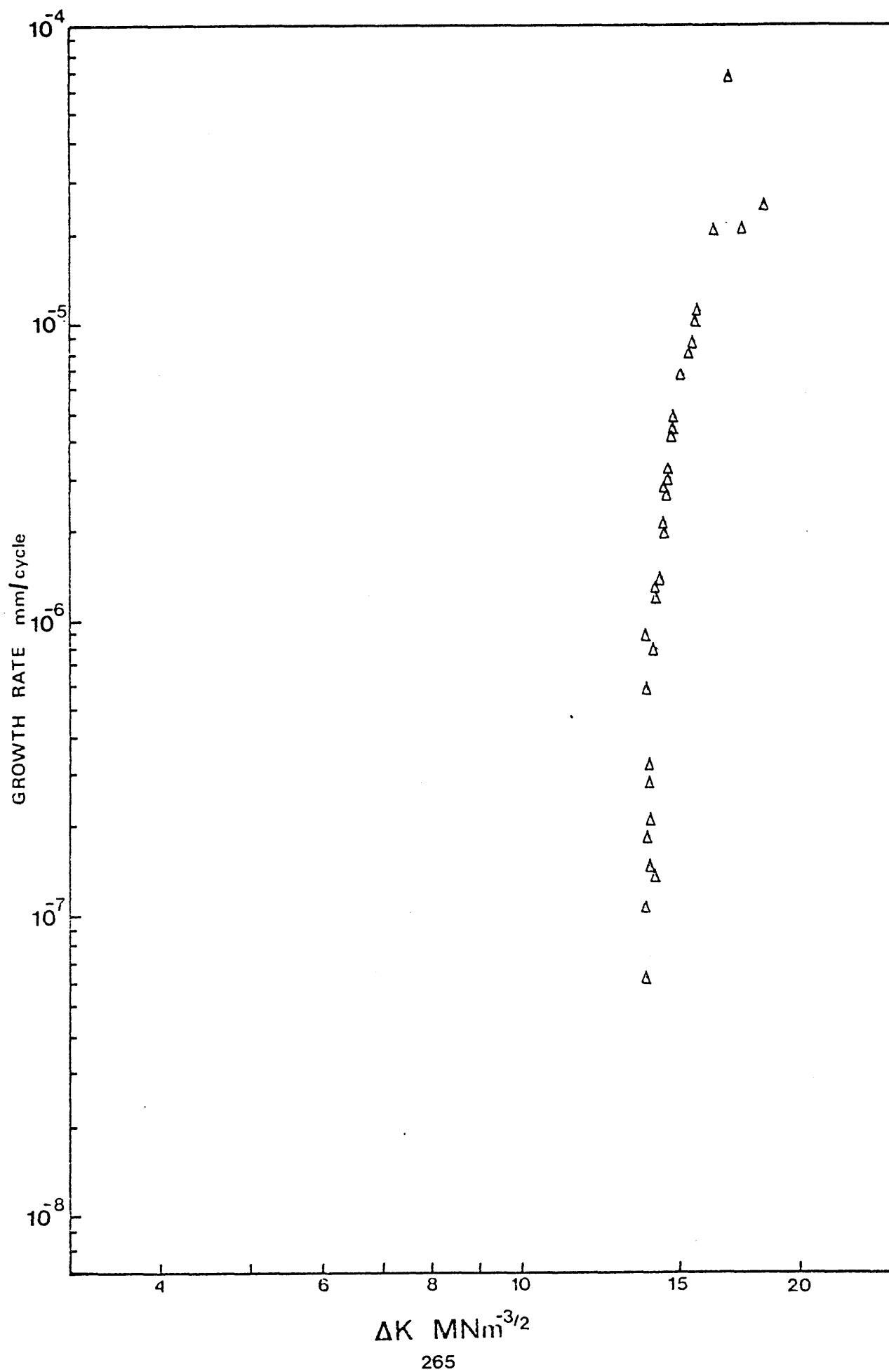
<u>Figure 56</u>

    Fatigue crack growth results for specimen
IS10(3) B1.
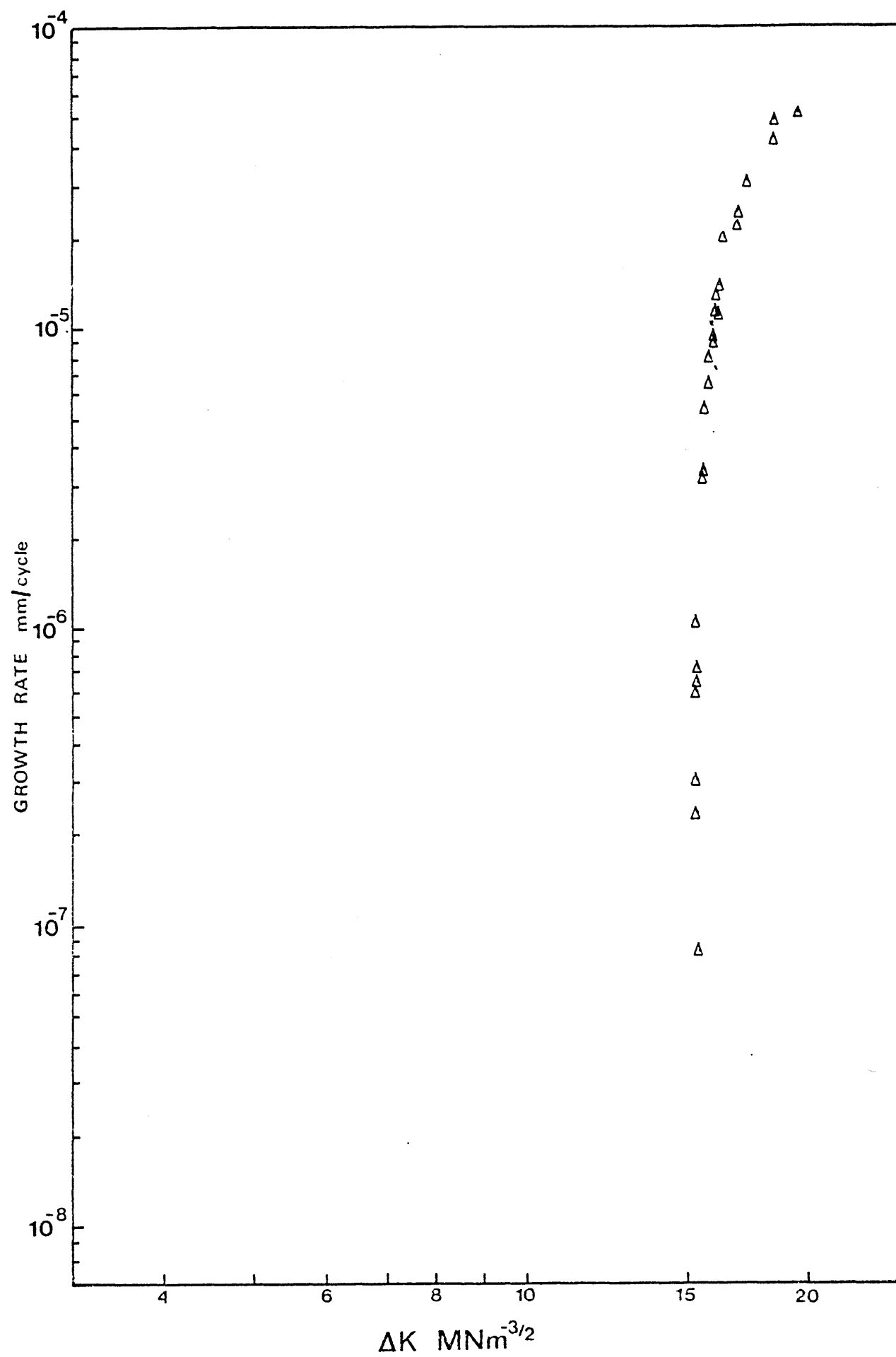
Figure 57

Fatigue crack growth results for specimen
IS10(3) A1.

GROWTH RATE mm/cycle

10^{-4}

10^{-5}

10^{-6}

10^{-7}

10^{-8}

4   6   8   10   15   20

ΔK MNm$^{-3/2}$

269
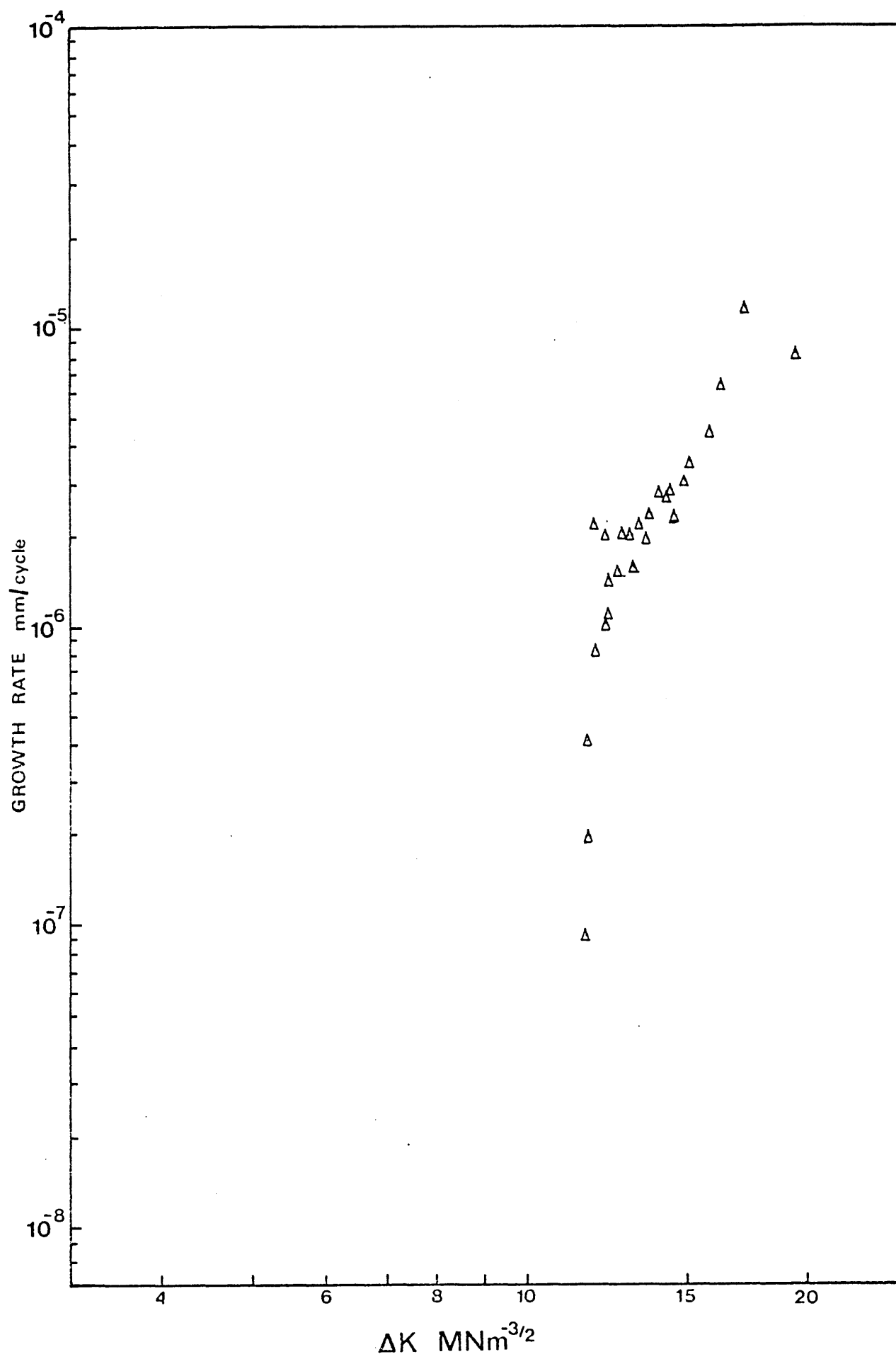
Figure 58

Fatigue crack growth results for specimen
IS15(3) A1.

The x-axis is labeled $\Delta K \ \ MNm^{-3/2}$ and the y-axis is labeled GROWTH RATE $mm/cycle$.
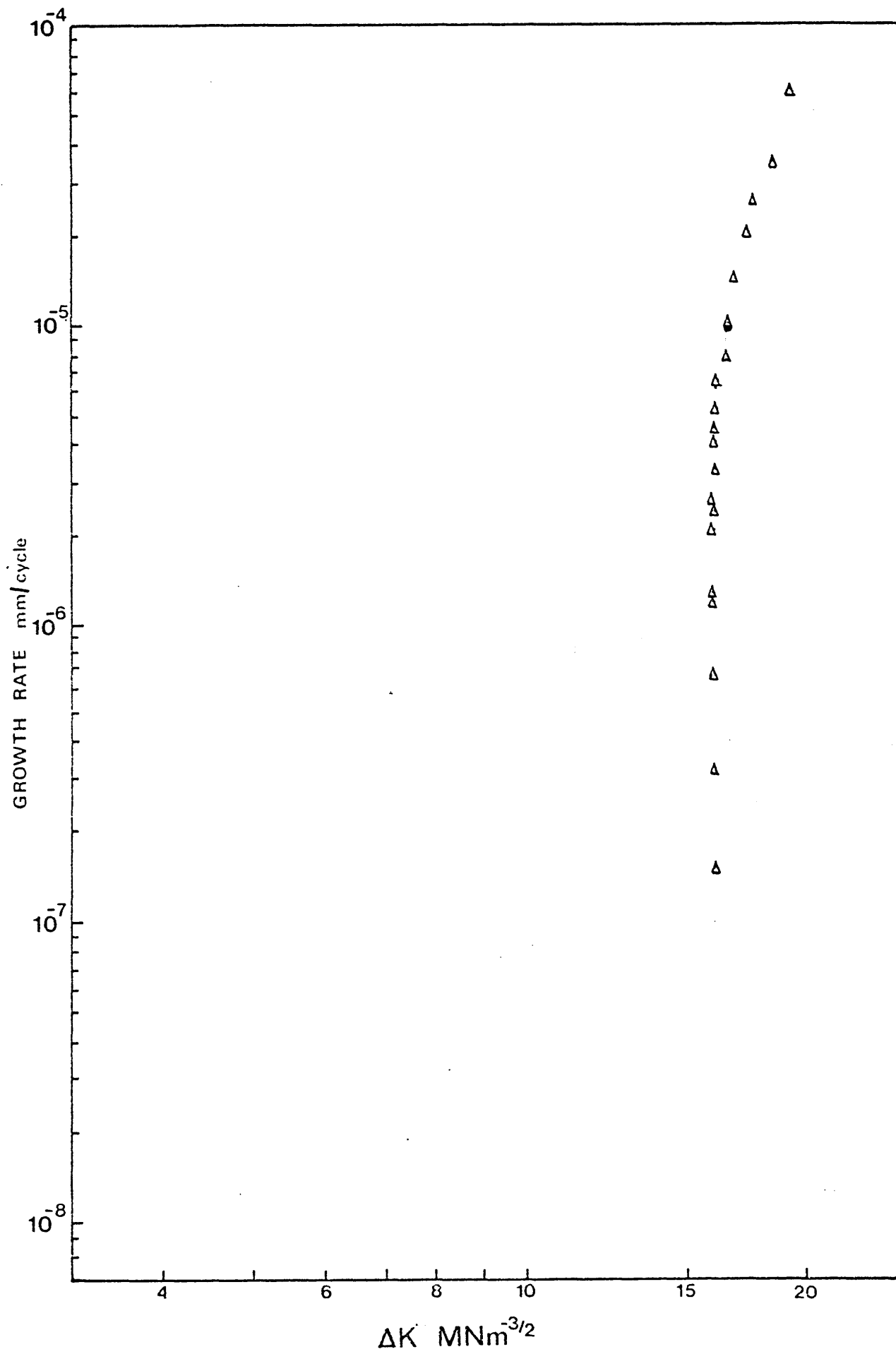
Figure 59

    Fatigue crack growth results for specimen
IS15(3) A2.

273
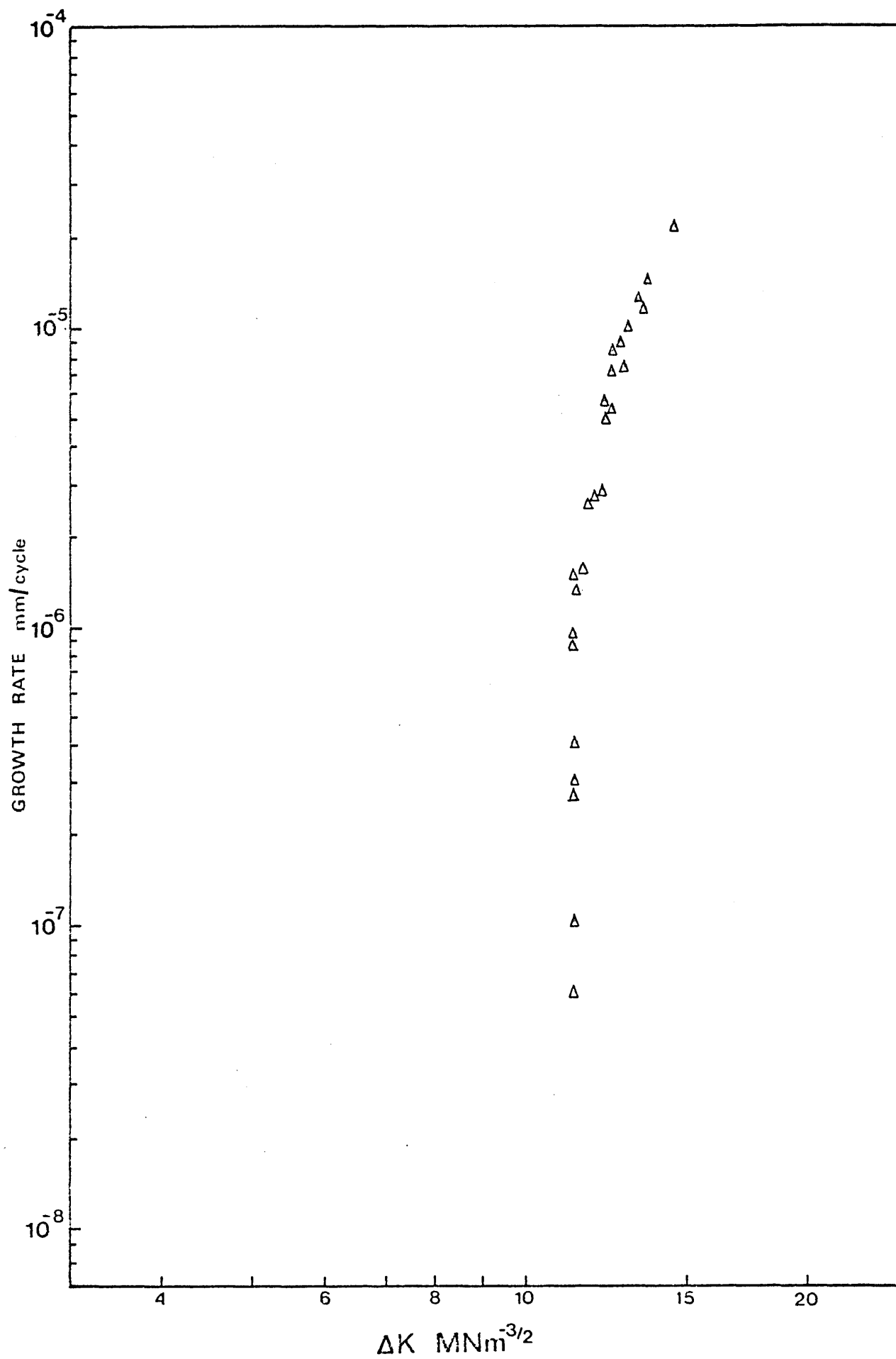
Figure 60

Fatigue crack growth results for specimen
IS15(3) B3.

GROWTH RATE mm/cycle

ΔK MNm$^{-3/2}$
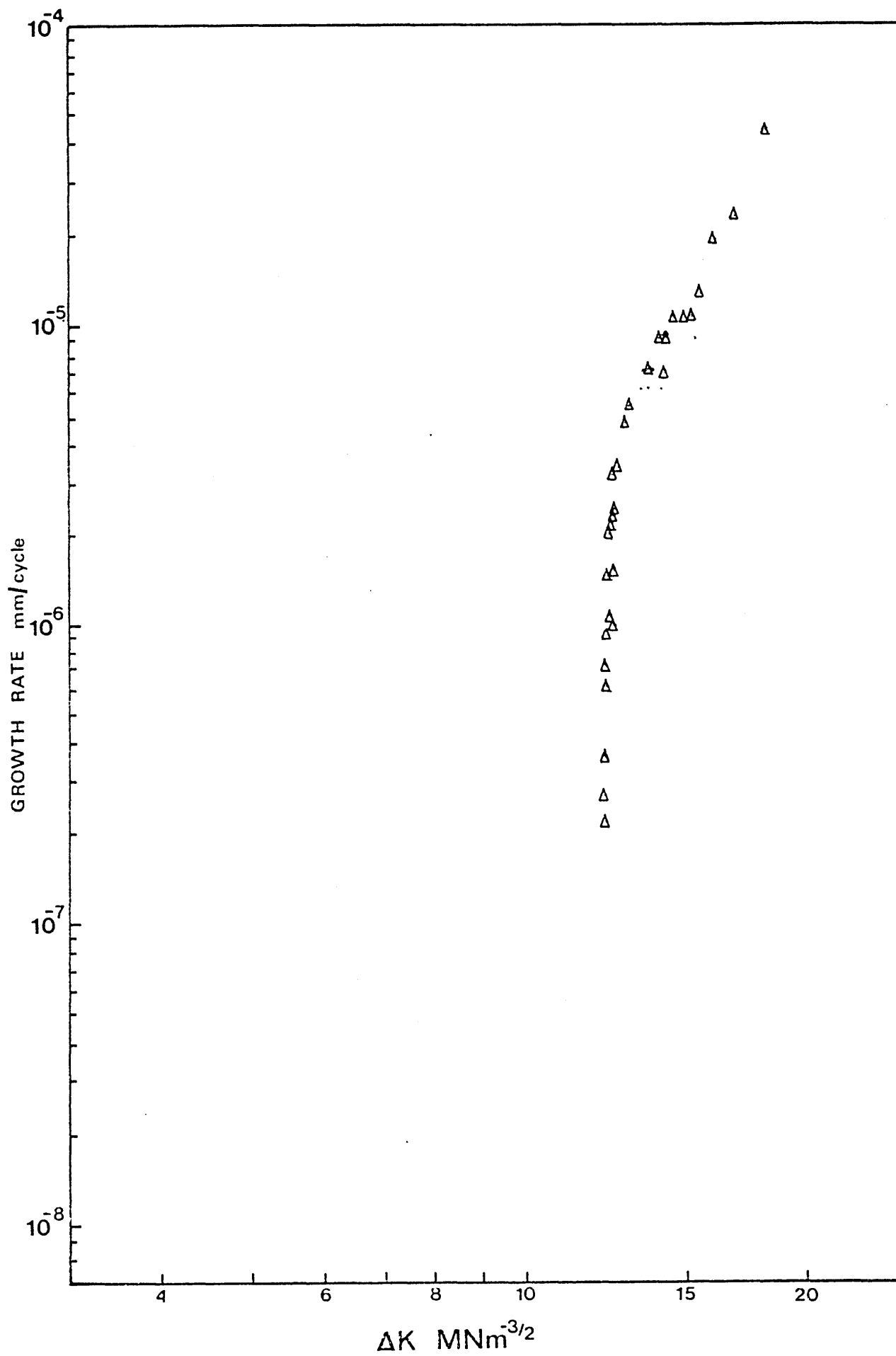
Figure 61

Fatigue crack growth results for specimen
IS15(B) B2.

GROWTH RATE mm/cycle

10^{-4}

10^{-5}

10^{-6}

10^{-7}

10^{-8}

4   6   8   10   15   20

ΔK MNm$^{-3/2}$

277
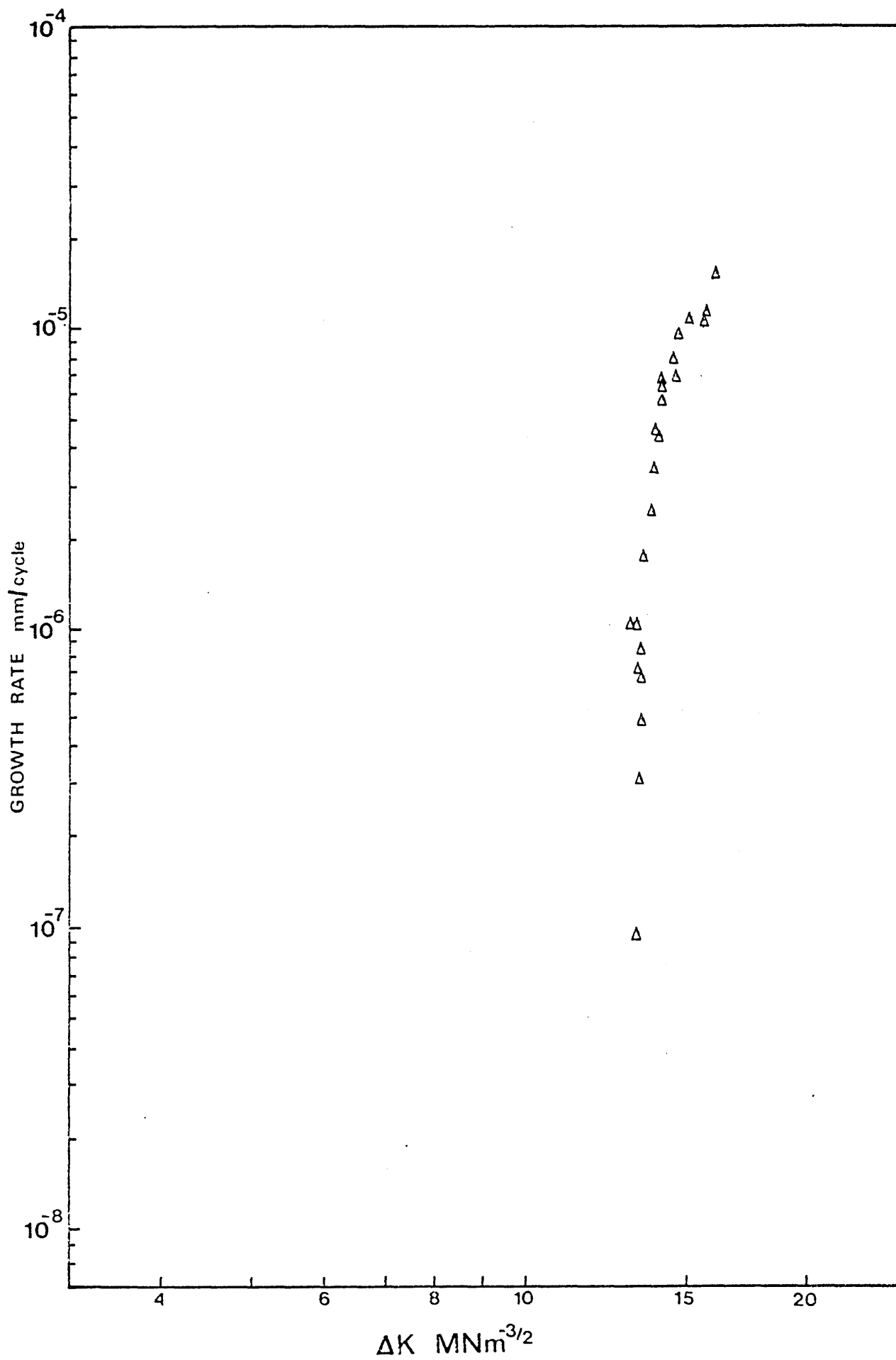
Figure 62

    Fatigue crack growth results for specimen
IS15(3) B1.

Figure 63

Fatigue crack growth results for specimen
IS20(1) A1.
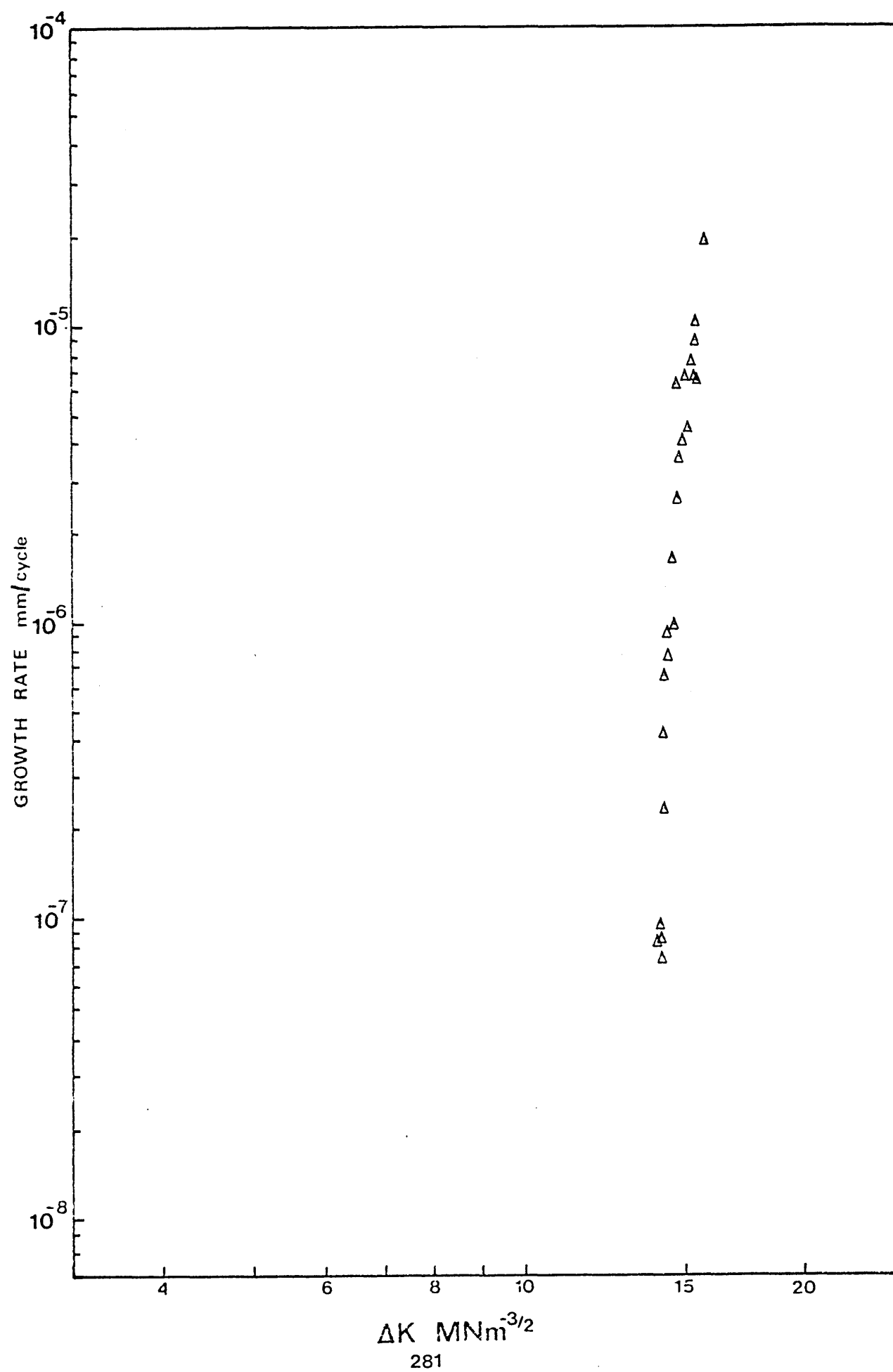
Figure 64

    Fatigue crack growth results for specimen
IS20(1) A2.

GROWTH RATE mm/cycle

10^{-4}

10^{-5}

10^{-6}

10^{-7}

10^{-8}

4   6   8   10   15   20

ΔK $MNm^{-3/2}$
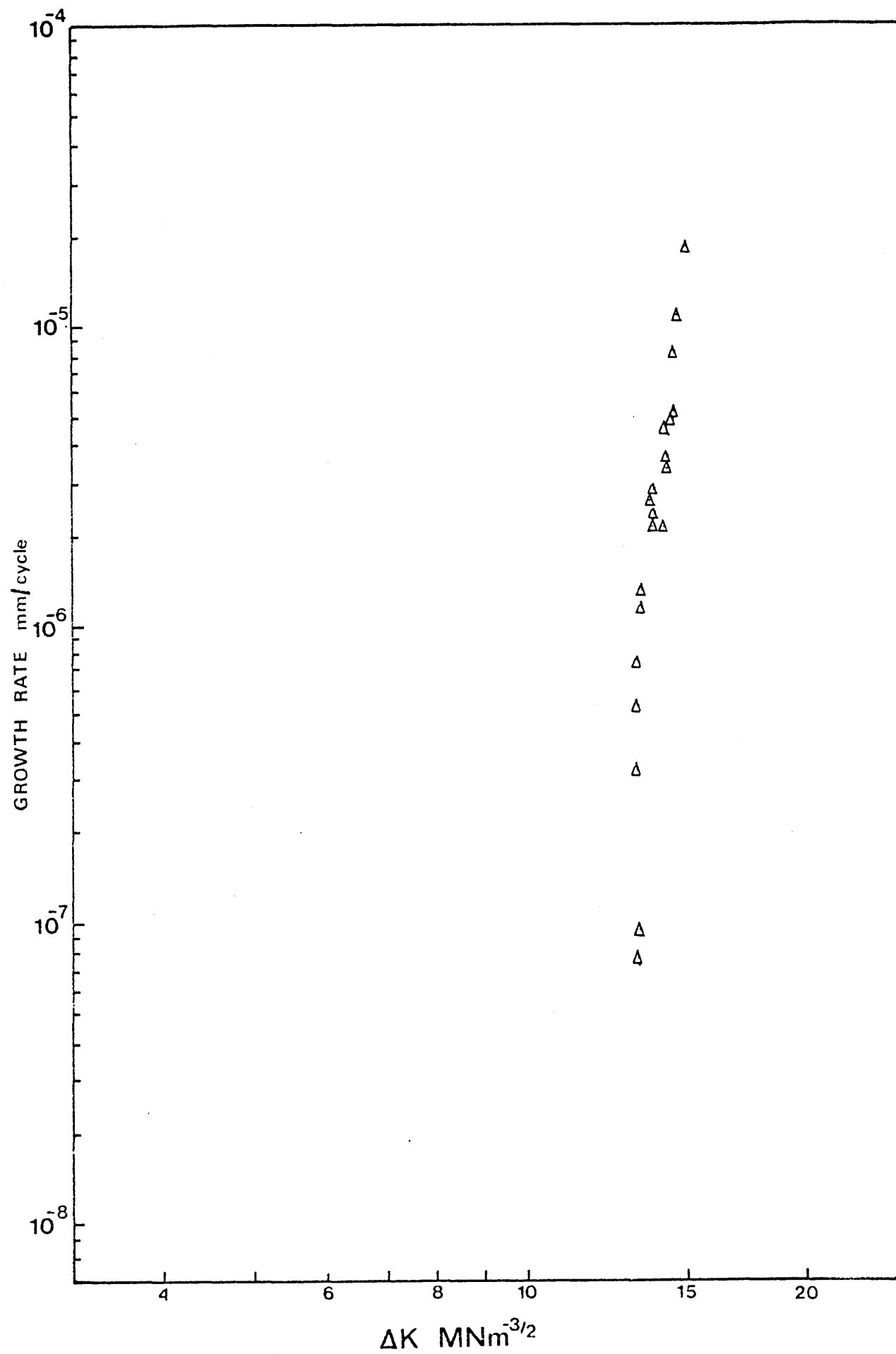
<u>Figure 65</u>

Fatigue crack growth results for specimen IS20(1) A3.

285
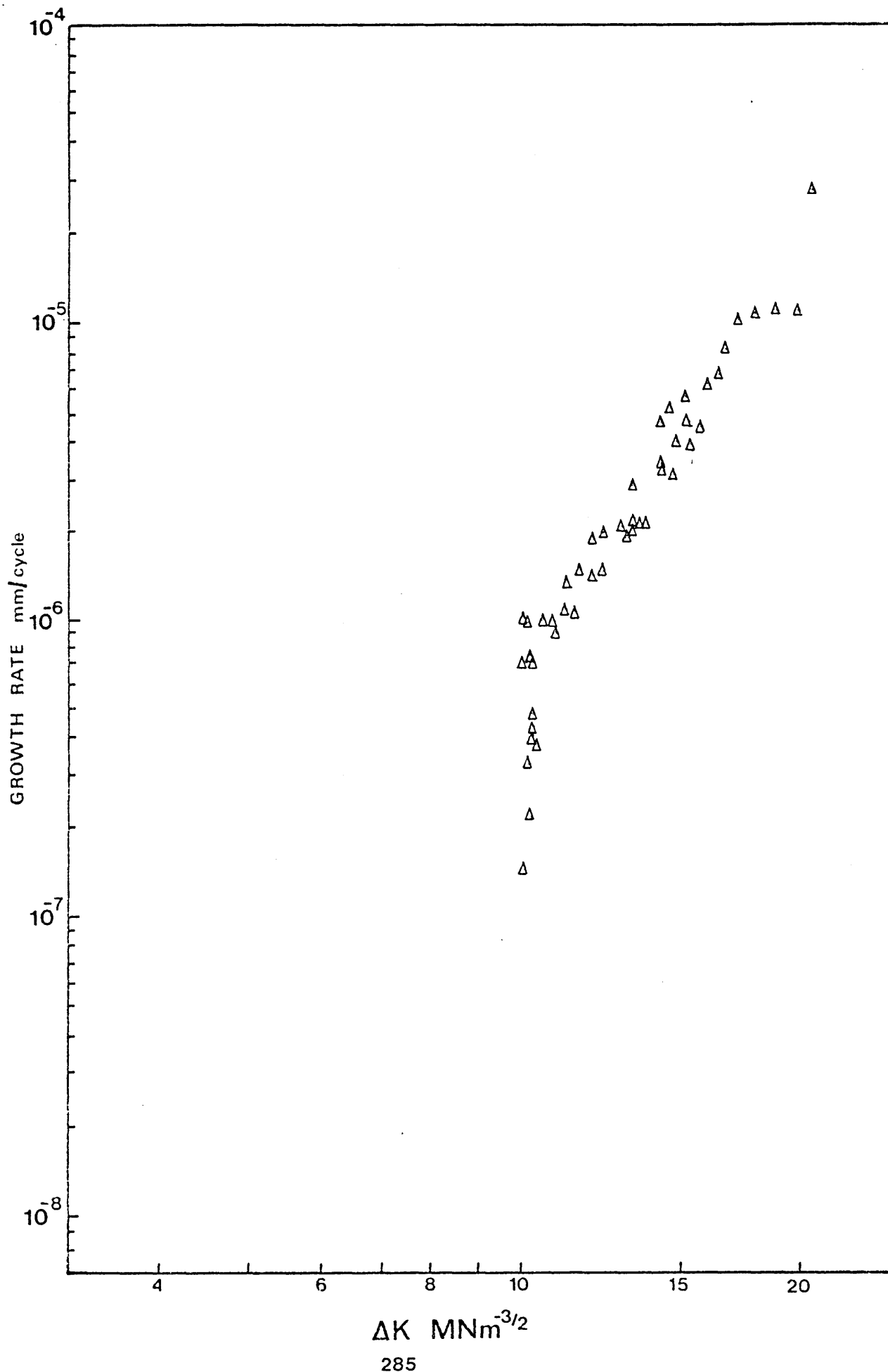
Figure 66

Fatigue crack growth results for series IS00(1)
specimens.

GROWTH RATE mm/cycle

10^{-4}

10^{-5}

10^{-6}

10^{-7}

10^{-8}

IS00 1 A1	○
IS00 1 A2	□
IS00 1 A3	△

4   6   8   10   15   20

ΔK MNm$^{-3/2}$

28.7
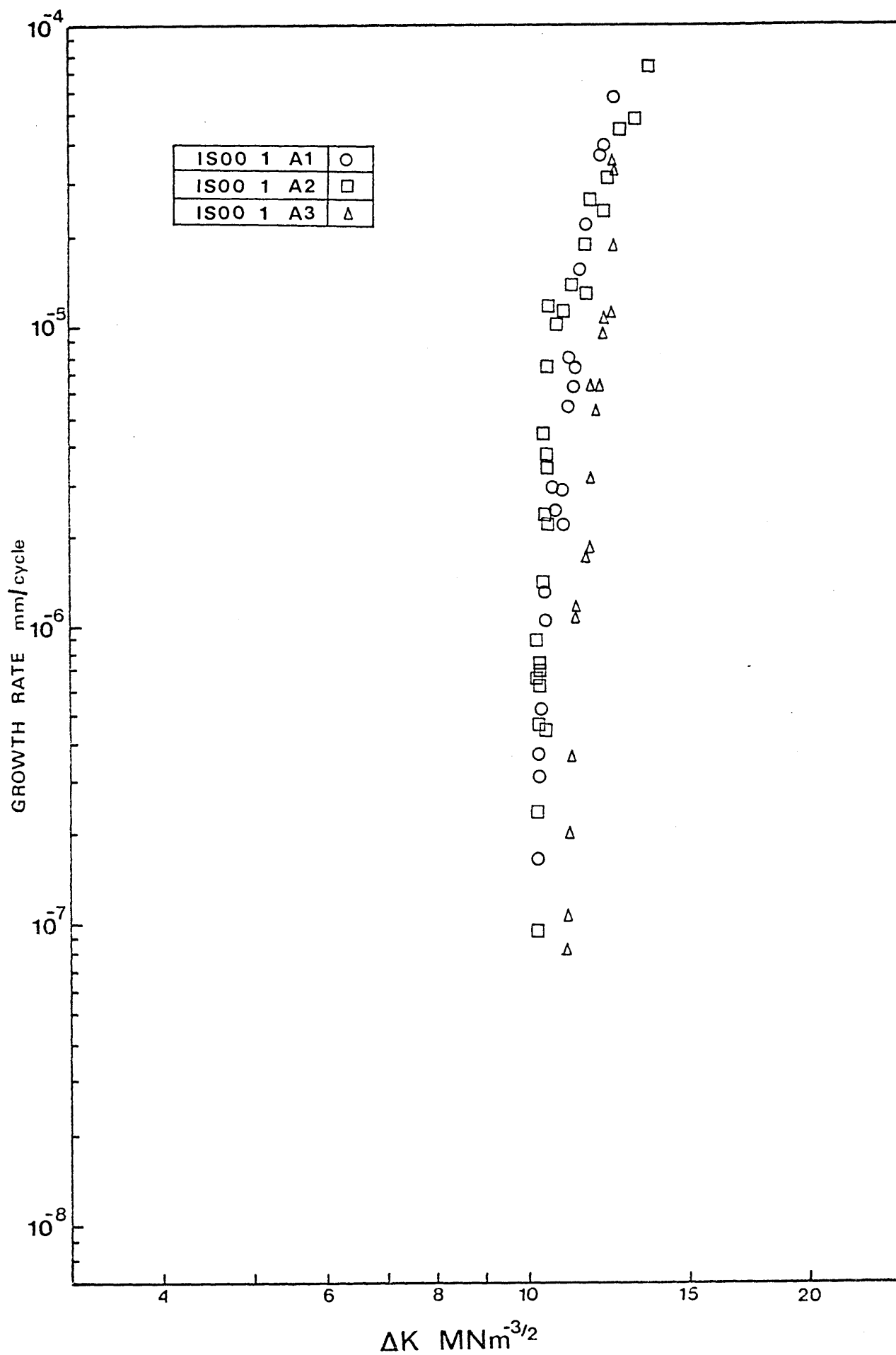
Figure 67

    Fatigue crack growth results for series IS05(3)
specimens.

289
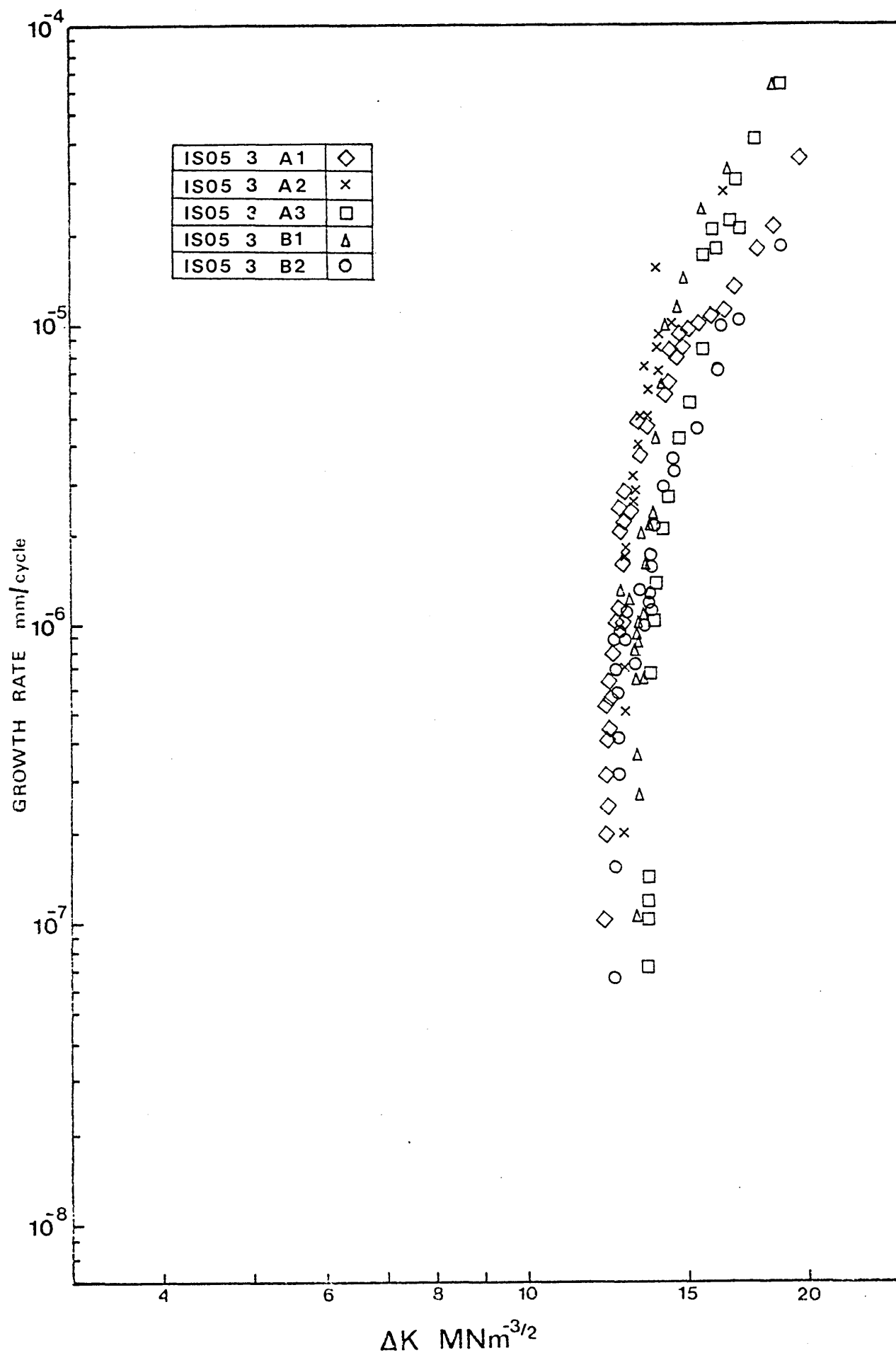
Figure 68

    Fatigue crack growth results for series IS10(3)

specimens.
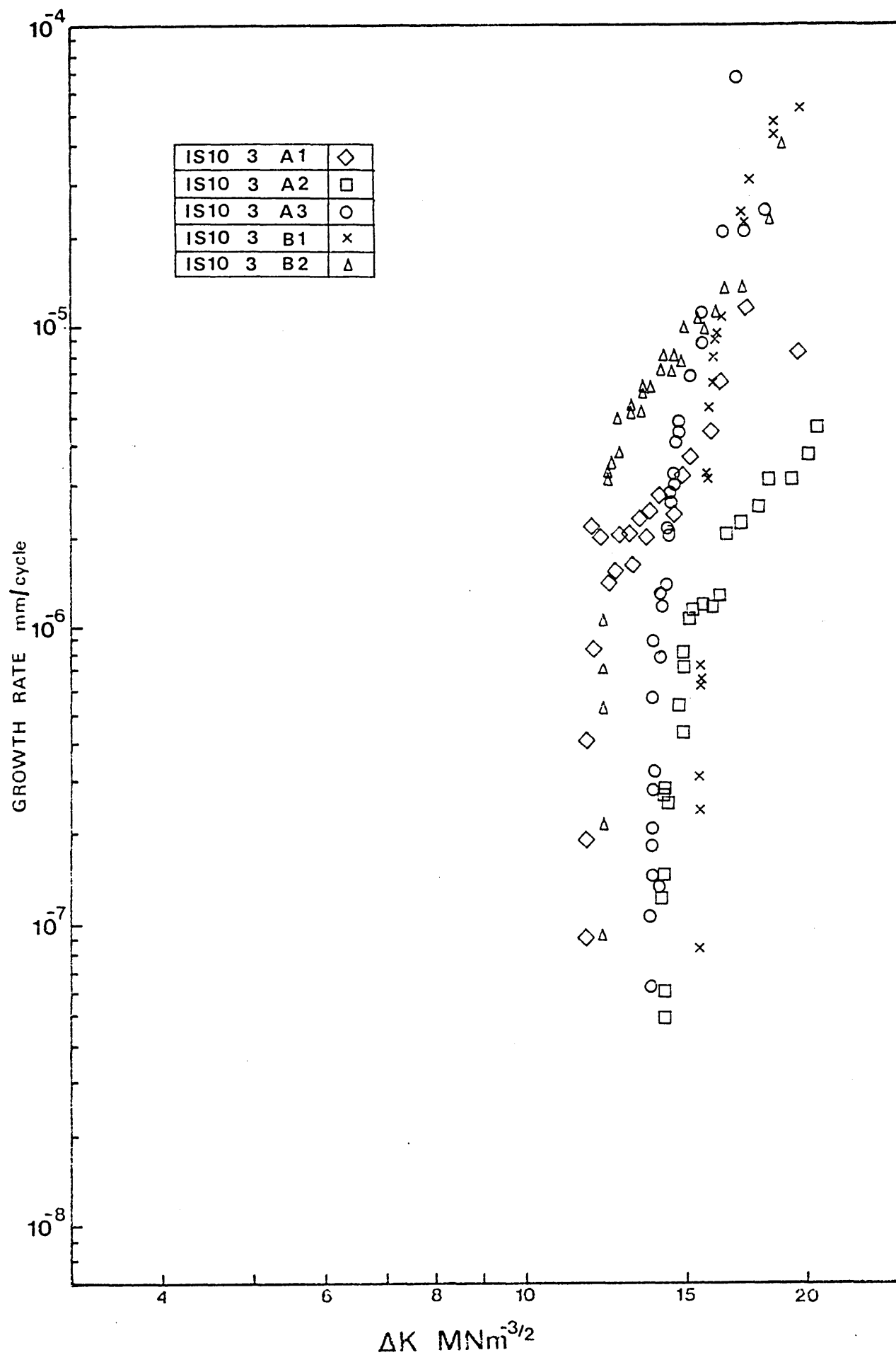
Figure 69

Fatigue crack growth results for series IS15(3)
specimens.

293
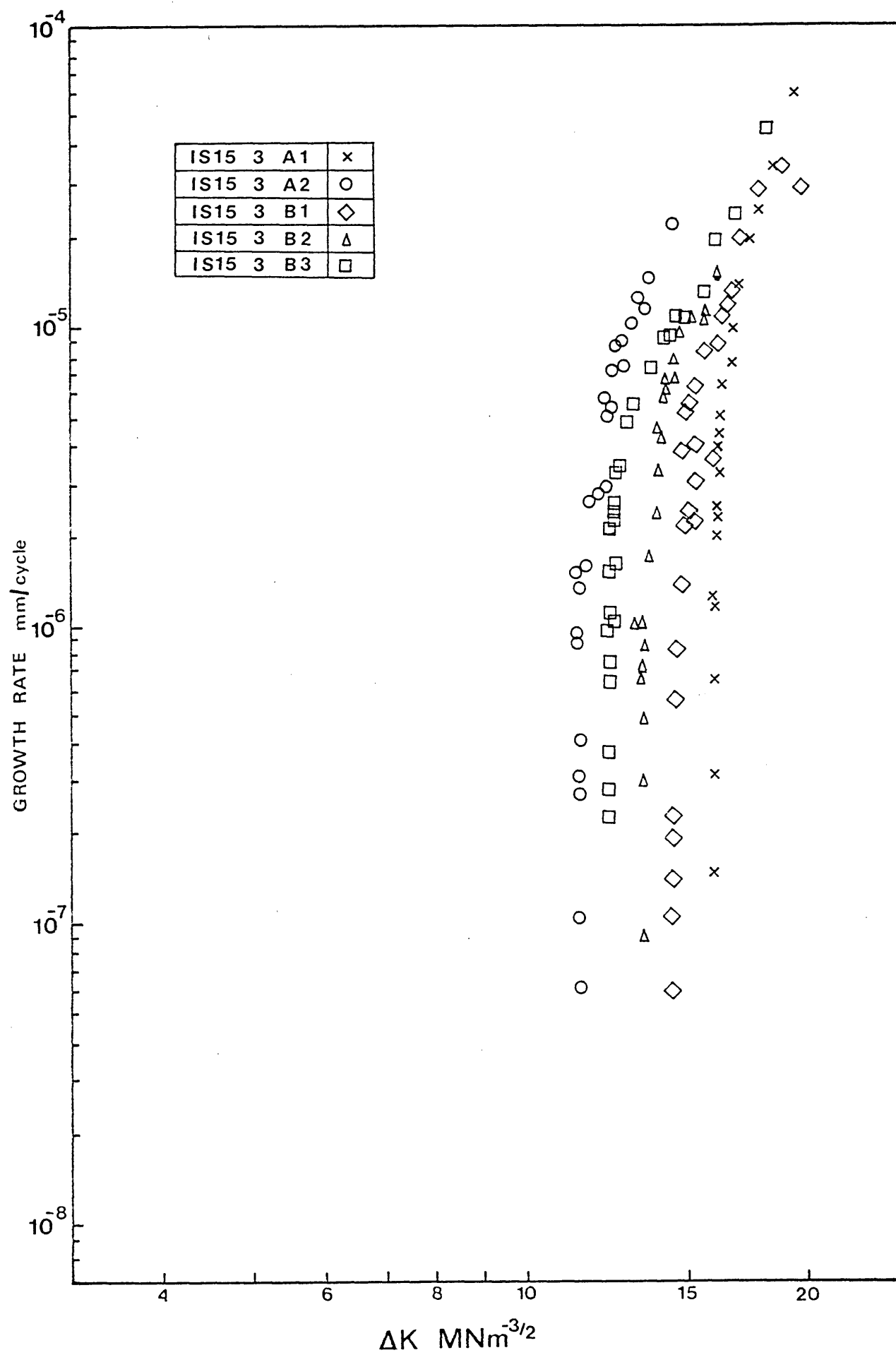
Figure 70

Fatigue crack growth results for series IS20(1)
specimens,
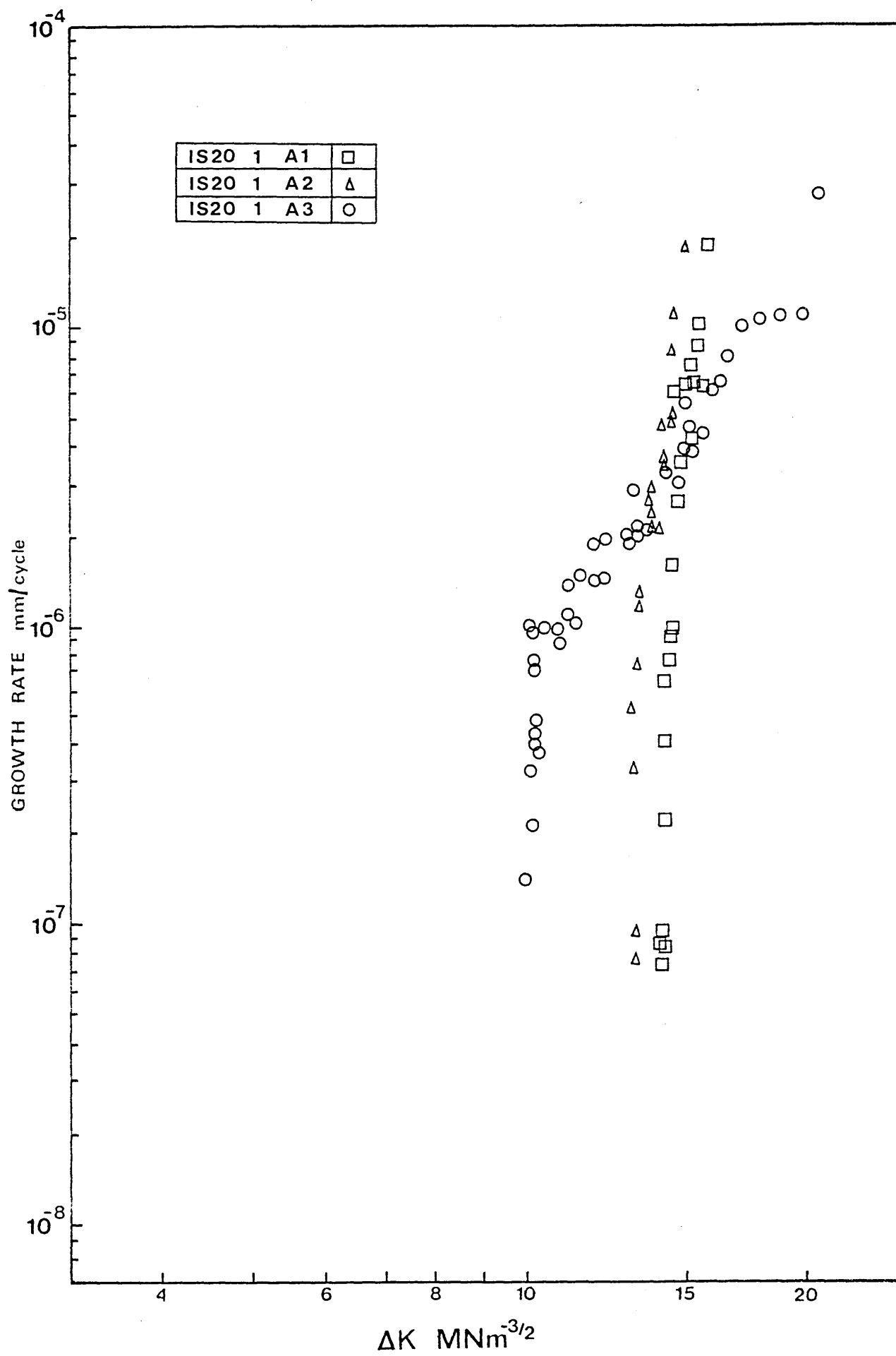
Figure 71

Fatigue threshold results as a function of grain size ($d^{-\frac{1}{2}}$)

Threshold stress intensity range, ΔK_{Th} (MNm$^{-\frac{3}{2}}$)

1S20(1)A3

1S10(2)A2

1S20(1)A1

1S15(3)A2

1S15(3)B3

1S15(3)B2

1S15(3)B1

1S10(3)A3

1S05(3)A3

1S00(1)A3

1S05(3)B2

1S00(1)A2

1S00(1)A1

1S05(3)A2

1S10(3)A2

1S10(3)B2

1S15(3)A1

1S10(3)B1

1S10(3)A1

1S05(3)B1

1S05(3)A1
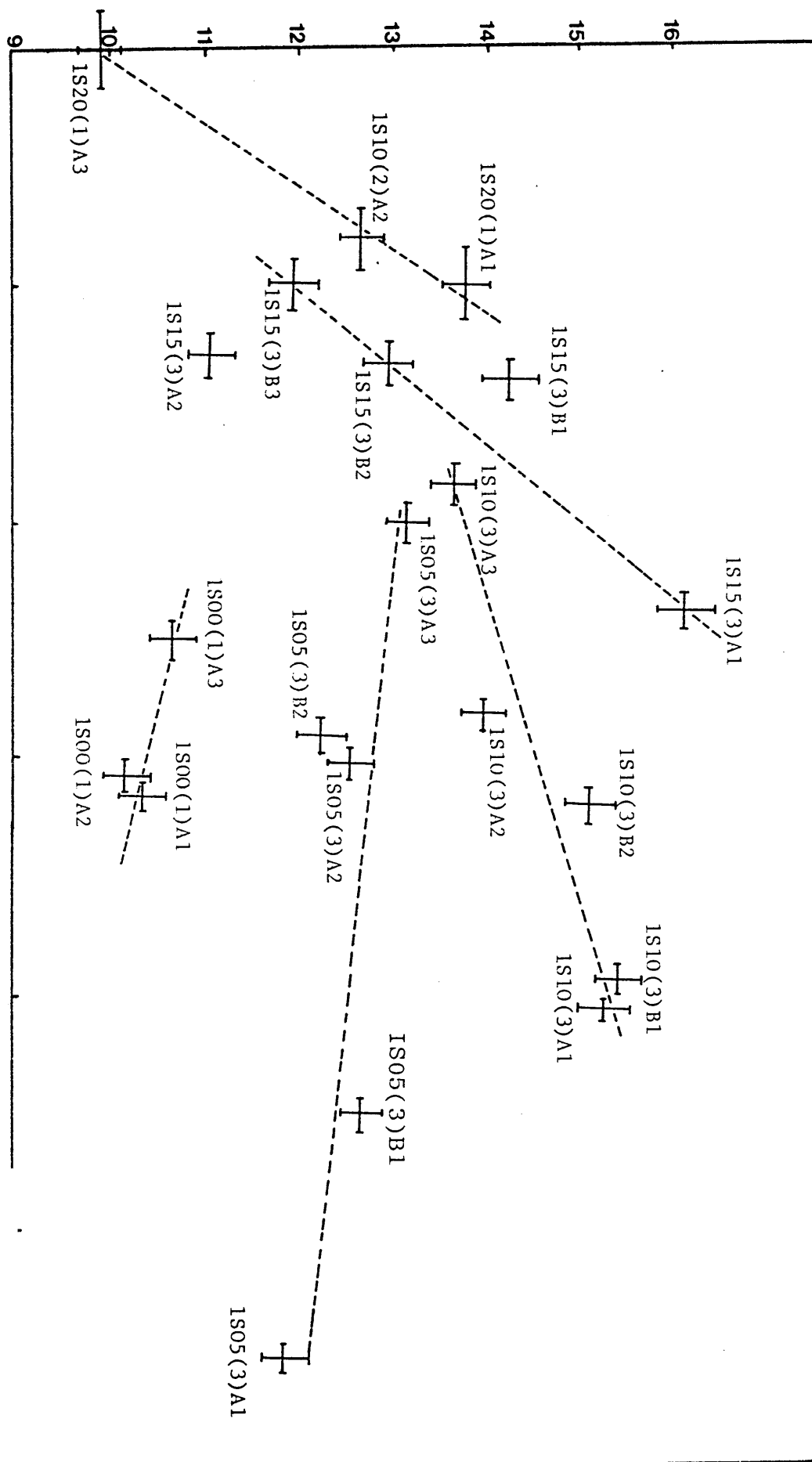
Figure 72

Relationship between strain hardening exponent, n, and silicon content.

Strain hardening exponent,
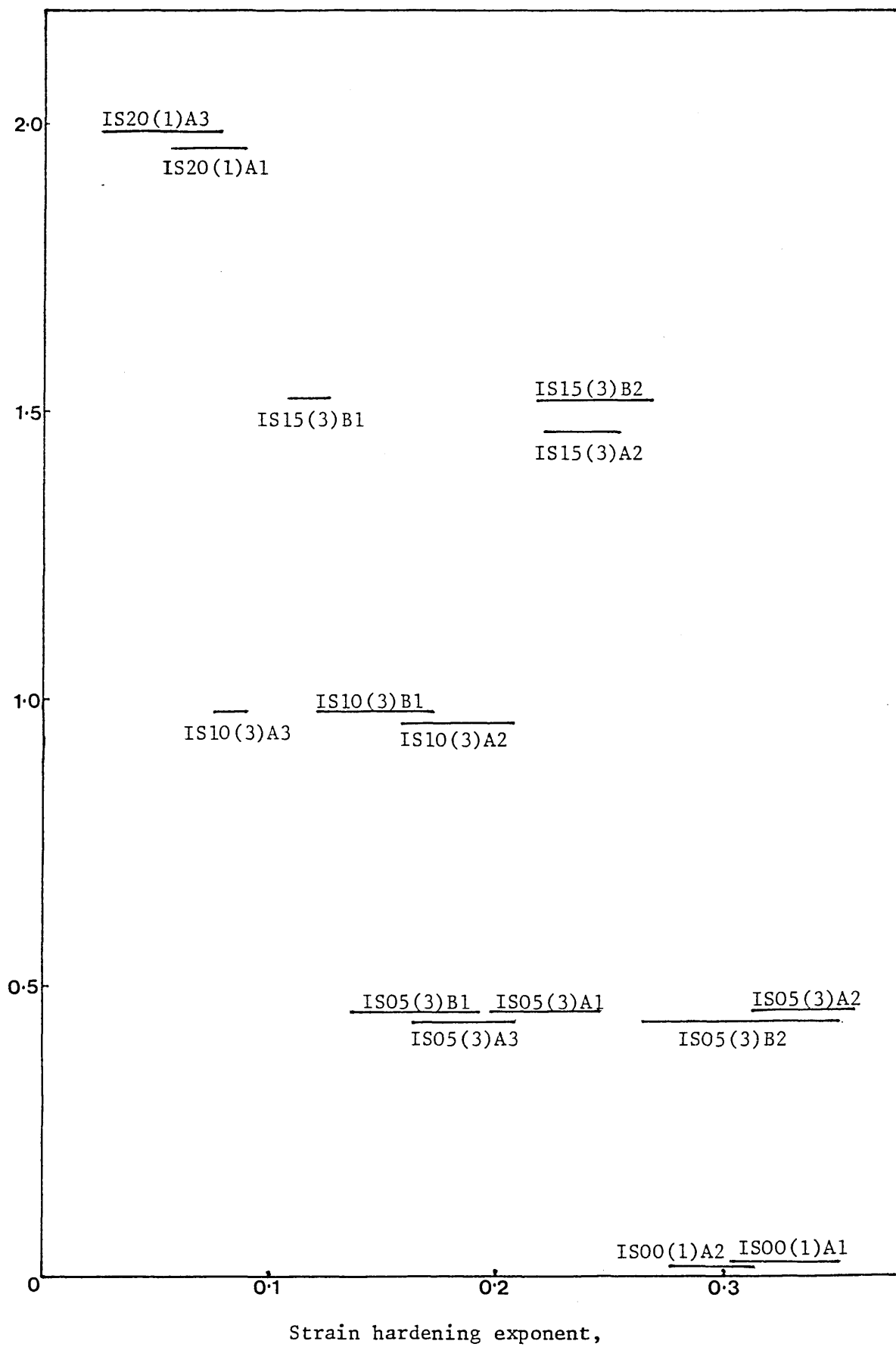
Figure 73

Transmission electron micrographs of the plastic zone attending a propagating fatigue crack.

x 42·5 k
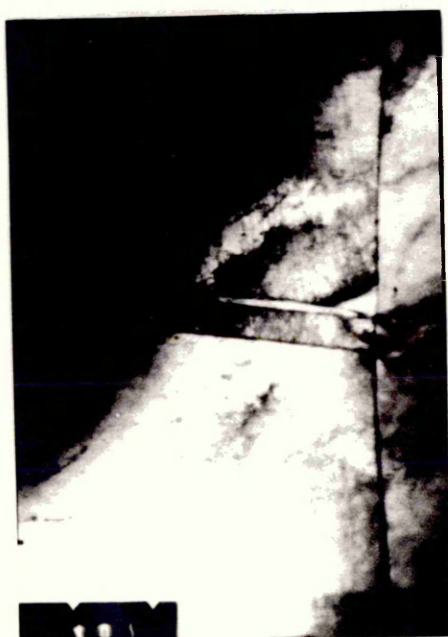
x 1·64 k

IS2O I A2

x 3·85 k

Figure 74

Intergranular fatigue fracture surface in
material IS00(1)A1

Threshold

Direction of Propagation
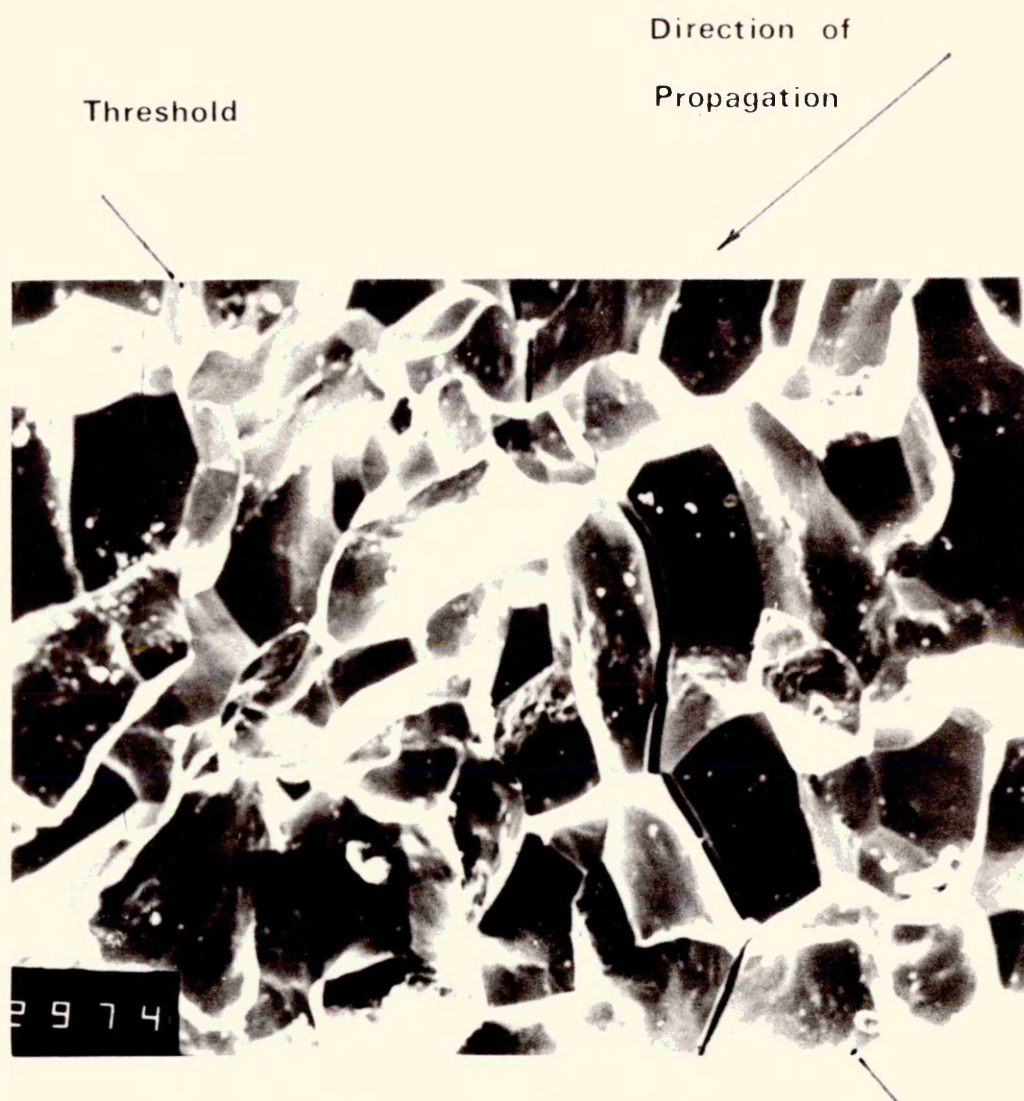
x 150

IS00 1 A1

Figure 75

Threshold and near treshold fatigue crack

propagation in material IS05(3)A3.

x 400

IS05 3 A3

Direction of
Propagation

Threshold condition reached

305
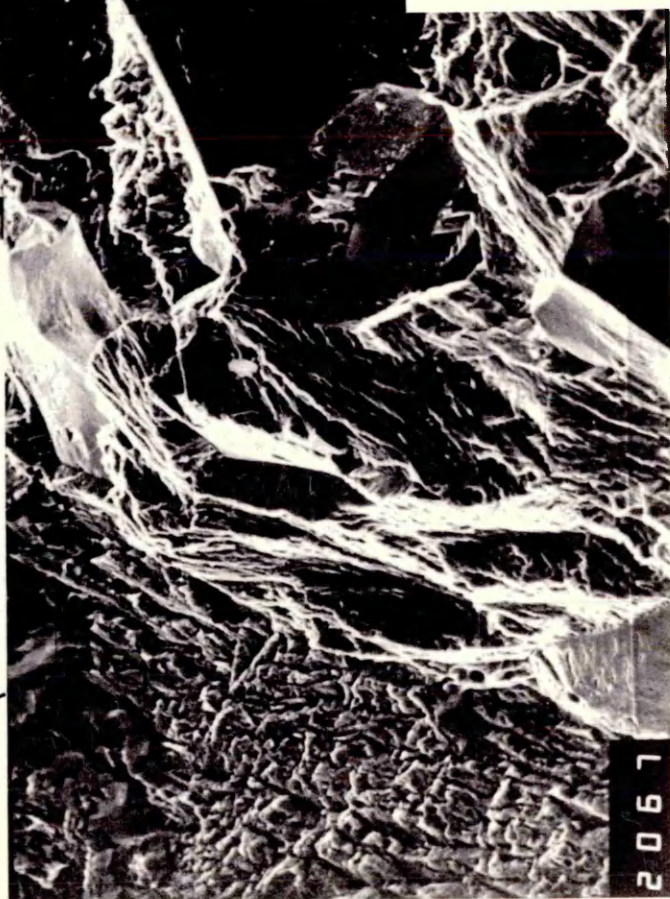
Figure 76

Near threshold fatigue crack propagation in

material IS05(3)A3.

Direction of Propagation

x 400

IS05 3 A3

307
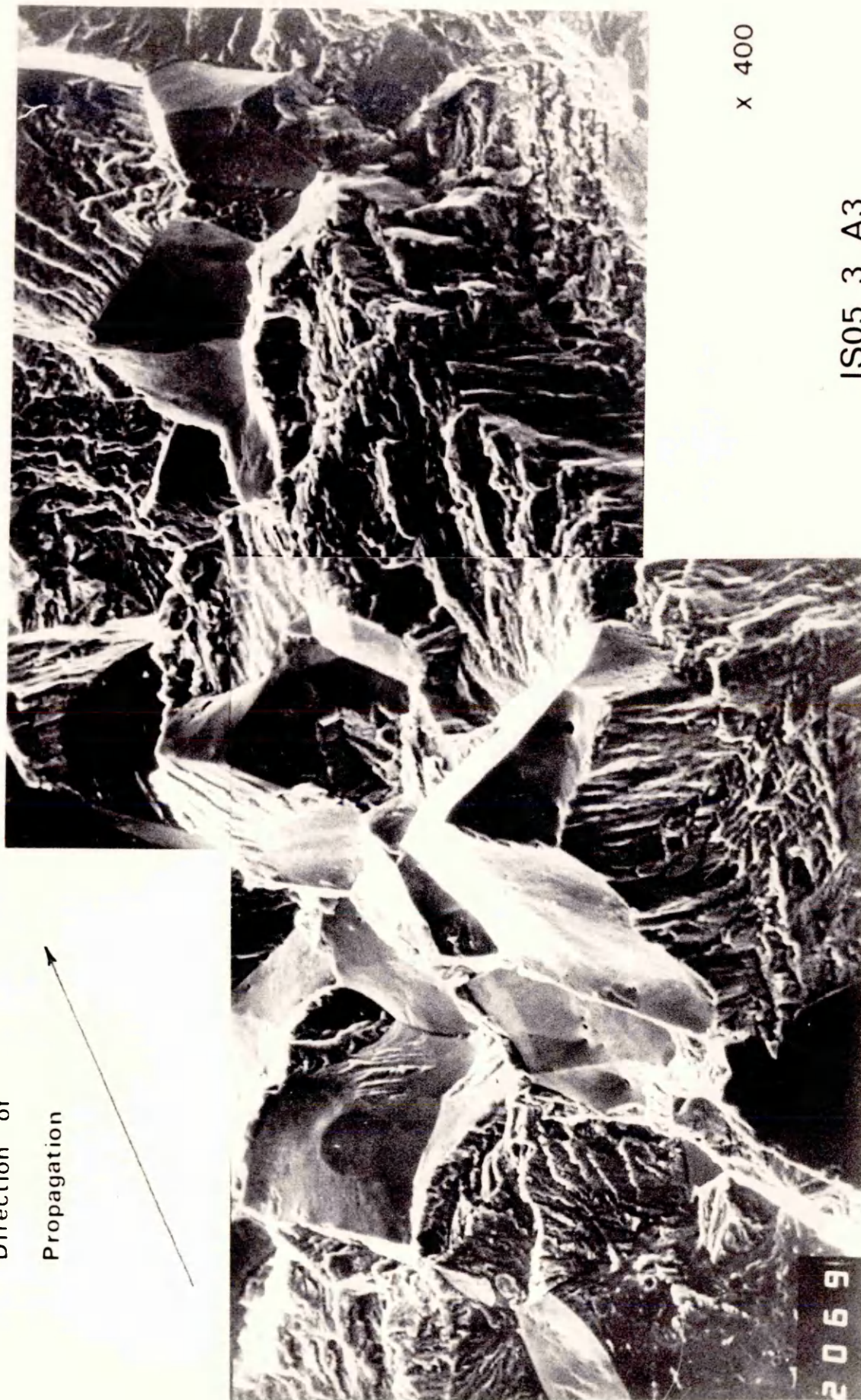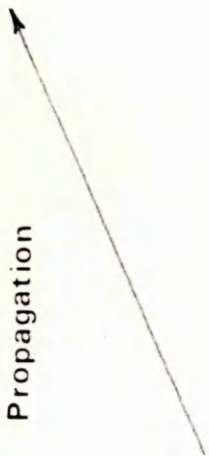
Figure 77

    (a)   Fatigue fracture surface at near threshold
         growth rates in material IS05(3)Al.

    (b)   Fatigue fracture surface at a higher stress
         intensity range in IS05(3)Al.

IS05 3 A1   x 300

Direction of

Propagation
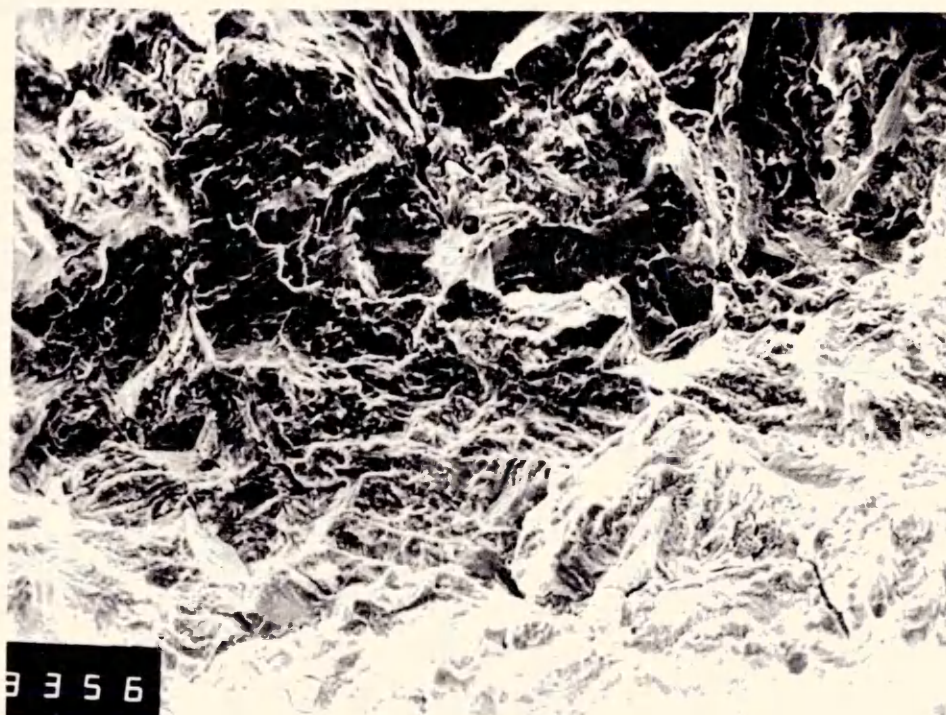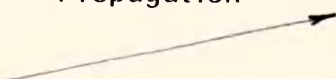
IS05 3 A1   x 300

Figure 78

Mixed intergranular/transgranular failure in

material IS05(3)B2.
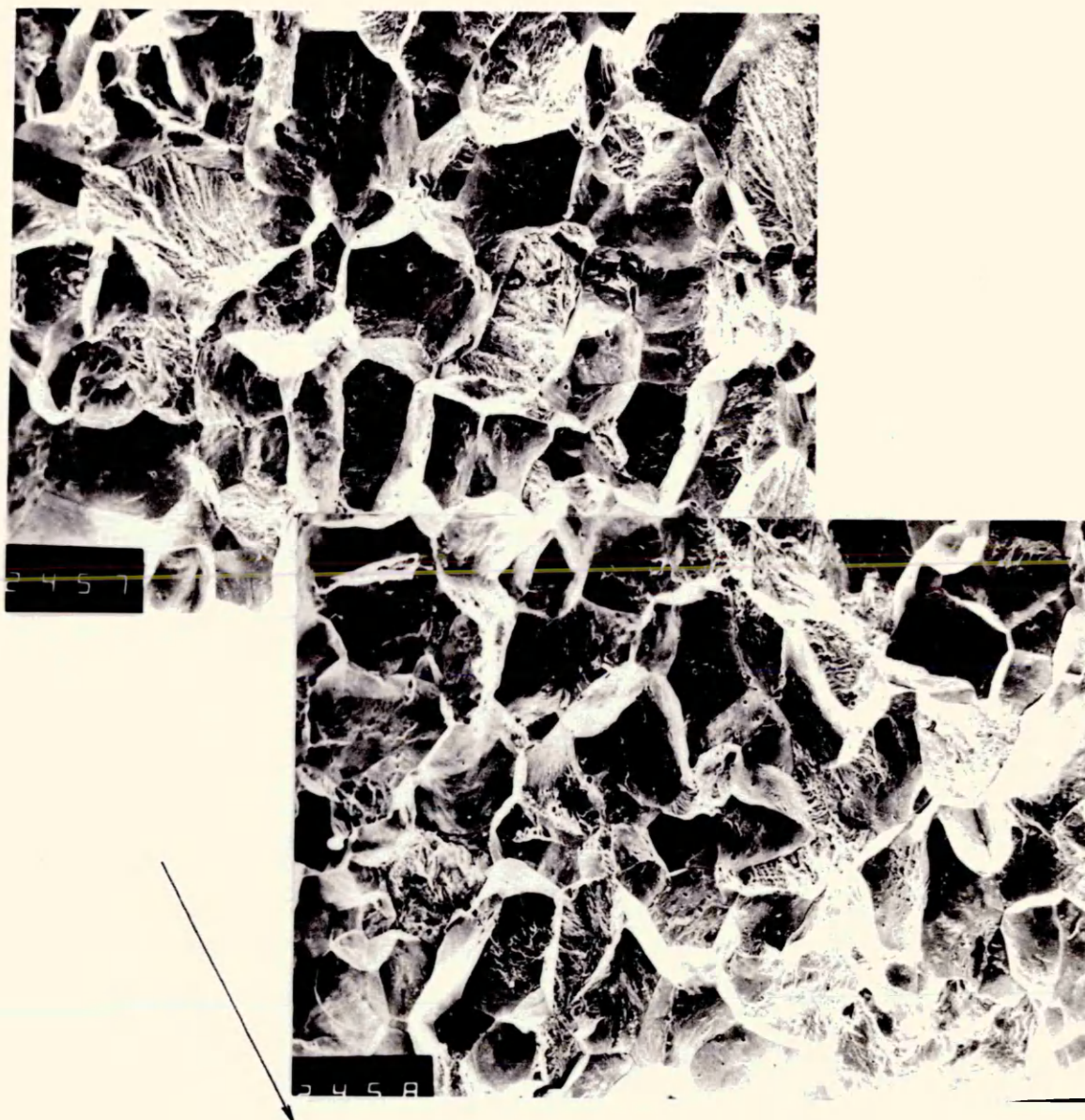
Direction of
Propagation

x 100

IS05 3 B2

<u>Figure 79</u>

Transgranular fatigue crack propragation observed in
IS10(3)A2.

Direction of Propagation

IS10 3 A2

Δk_{th}

x 300

313
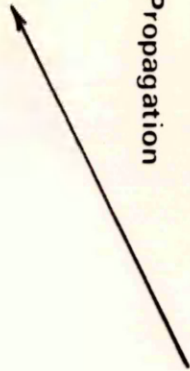
Figure 80

    (a)   Near threshold fatigue crack propagation in
           material IS10(3)A1.

    (b)   Near threshold prapagation in material IS10(3)A1.

ΔK_{th}
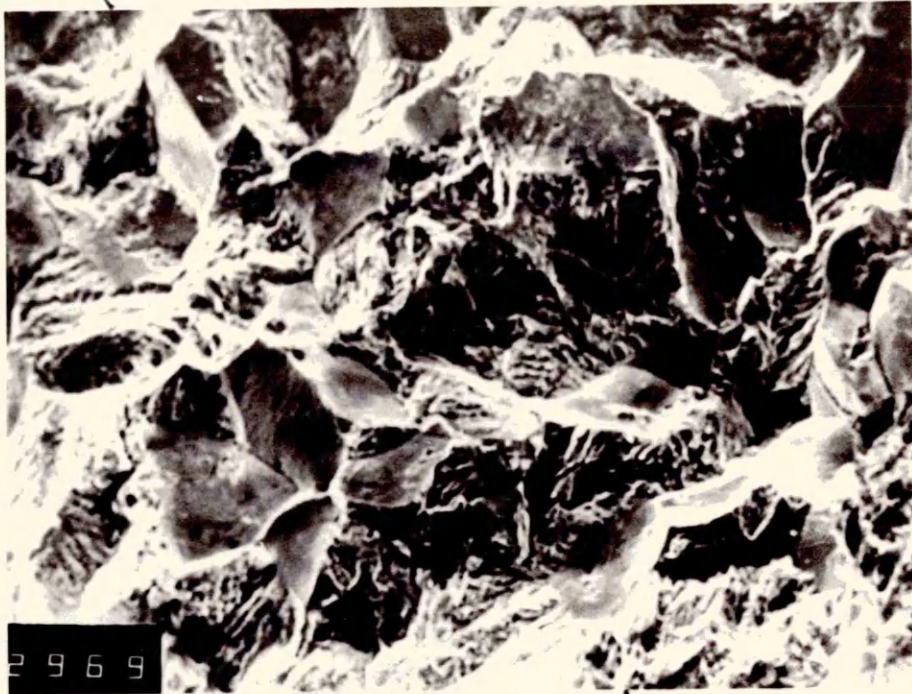
x 250

Direction of

Propagation

IS10 3 A1

x 500

IS10 3 A1

Figure 81

Near threshold fatigue crack propagation in material
IS10(3)B2.

ΔK_{th}

Direction of
Propagation

x 300

IS10 3 B2

317

Figure 82

Transgranular fatigue crack propagation in
material IS15(3)B1.

ΔK_{th}
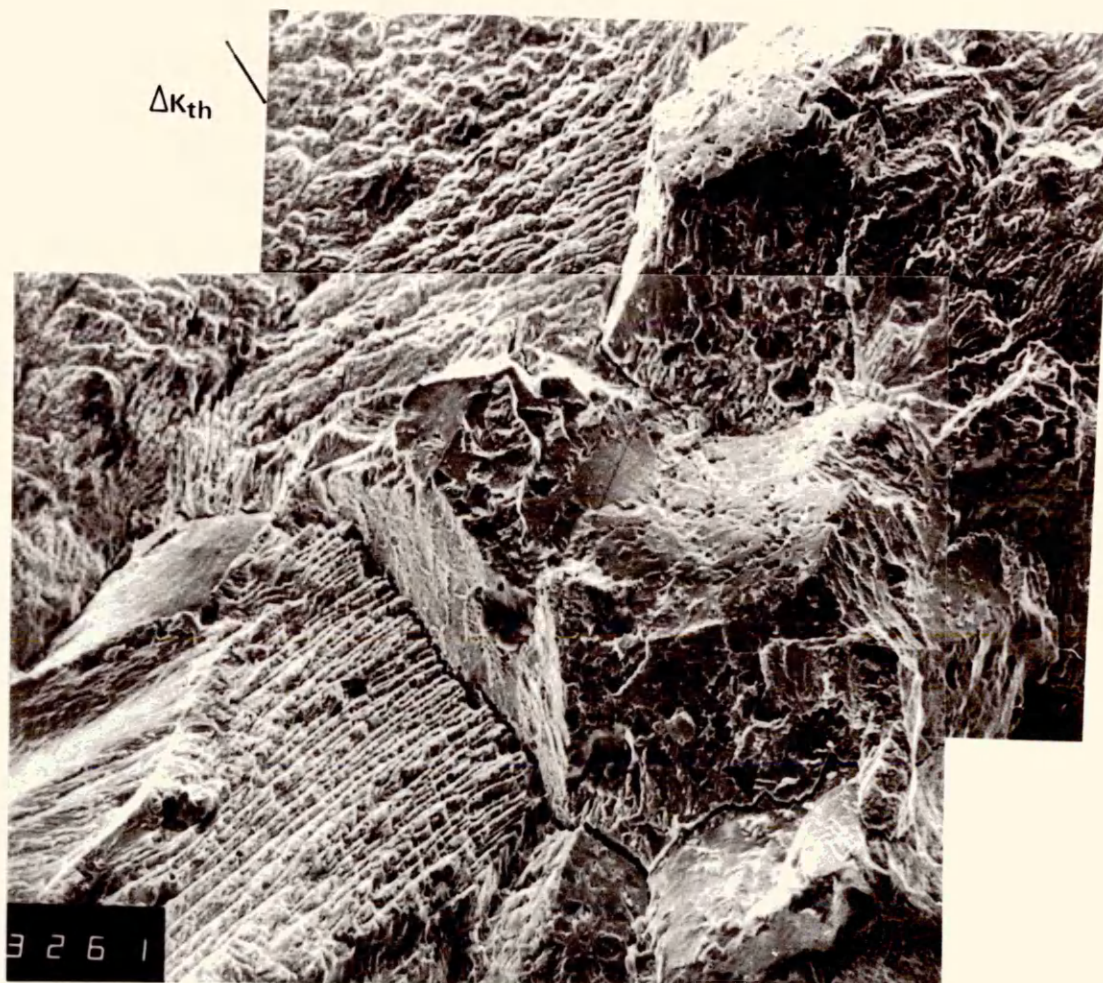
x 250

Direction of

Propagation

IS15 3 B1

Figure 83

Near threshold fatigue crack propagation in
material IS15(3)B3

Direction of Propagation

ΔK_{th}

x 250

IS15 3 B3

321

Figure 84

Near threshold fatigue crack propagation in
material IS20(1)A3.

Direction of Propagation

ΔK_{th}

IS20 1 A3

x 50
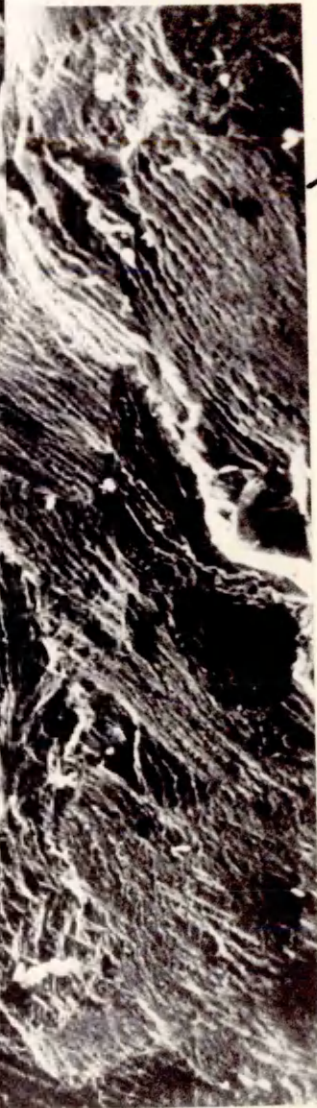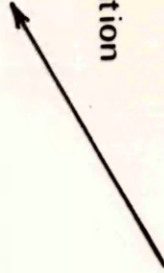
323

Figure 85

Near threshold fatigue crack propagation in
material IS20(1)A2.

ΔK_{th}

Direction of
Propagation
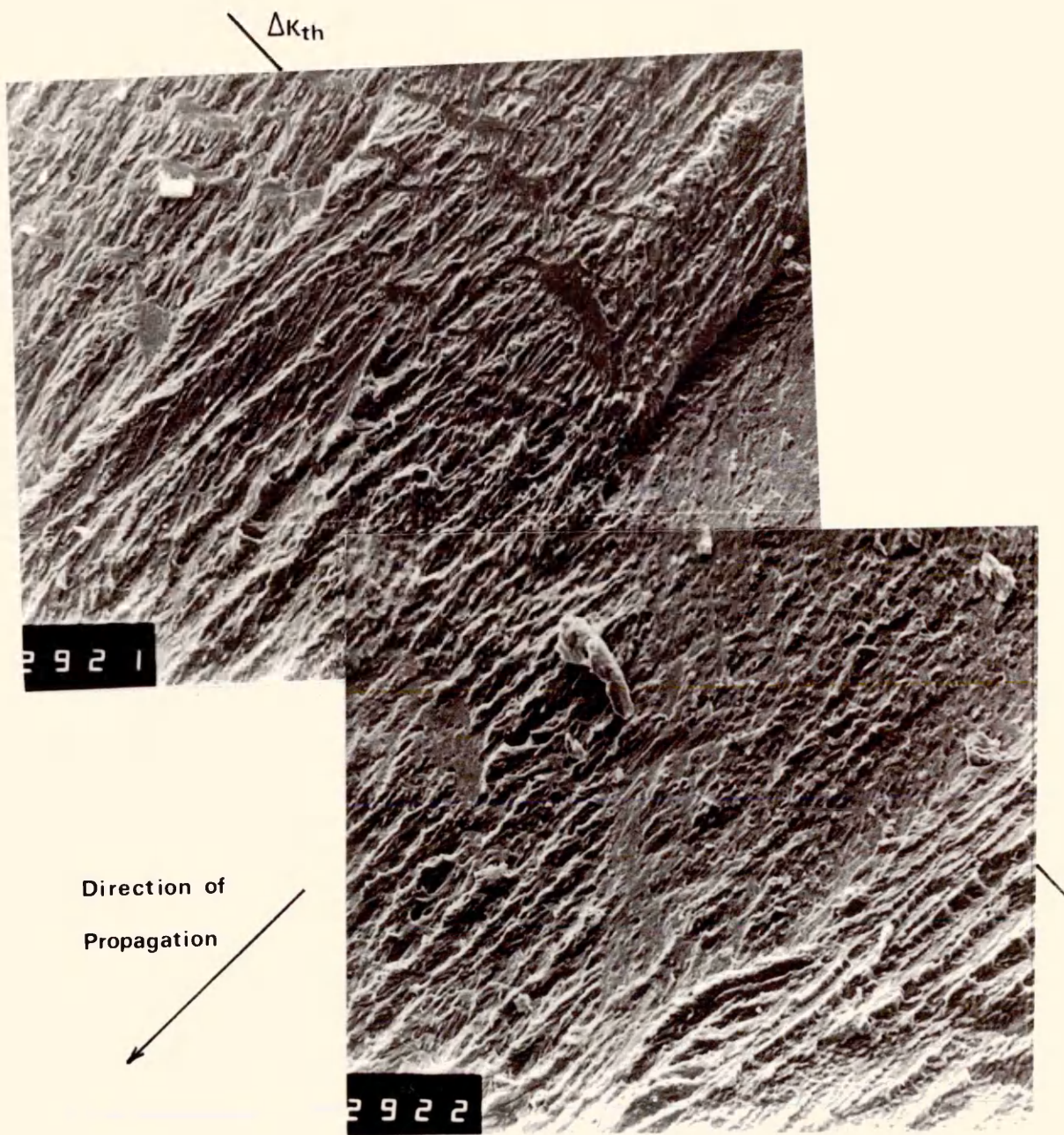
x 250

IS20 1 A2

Figure 86

Macroscopic features observed on material IS05(3)B2.
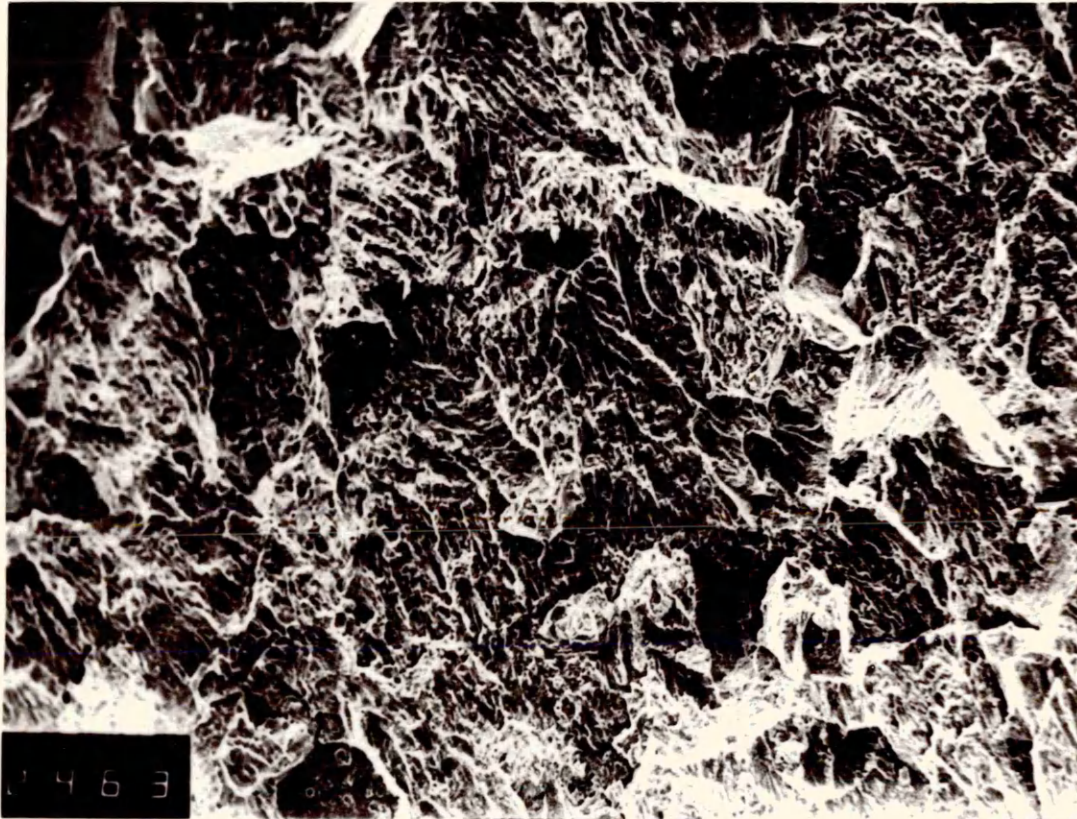
ΔK 16·0 MNm$^{-3/2}$ x150

IS05 3 B2

<u>Figure 87</u>

(a) Fatigue crack propagation profile observed at
     $\Delta K = 17$ MNm$^{-\frac{3}{2}}$ in material IS10(3)B2.

(b) Fatigue crack propagation profile observed at
     $\Delta K = 18$ MNm$^{-\frac{3}{2}}$ in material IS10(3)B1.
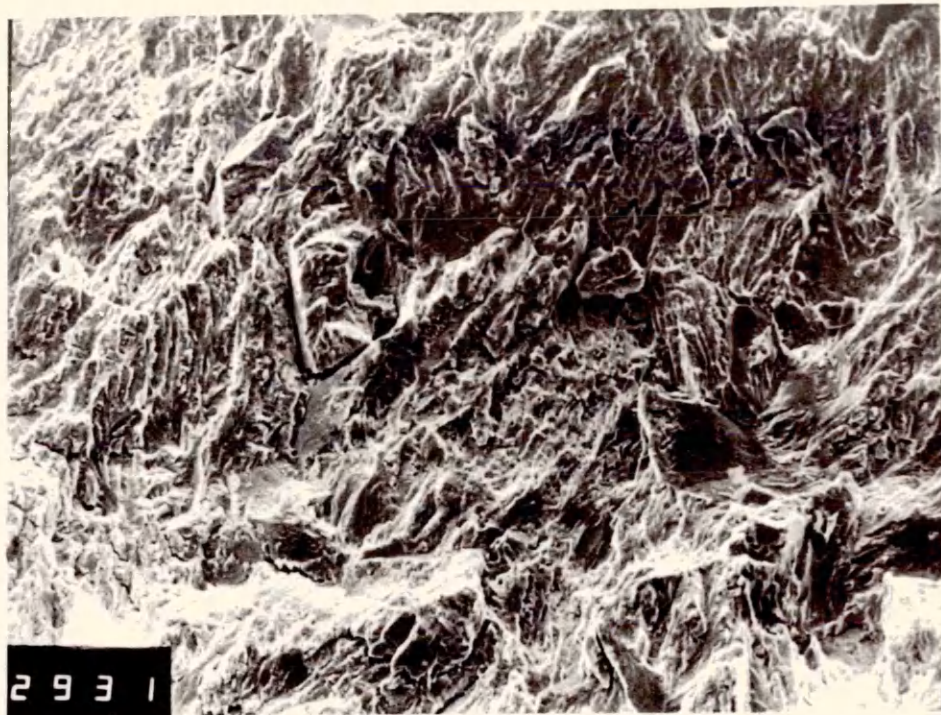
x250

IS10 3 B2
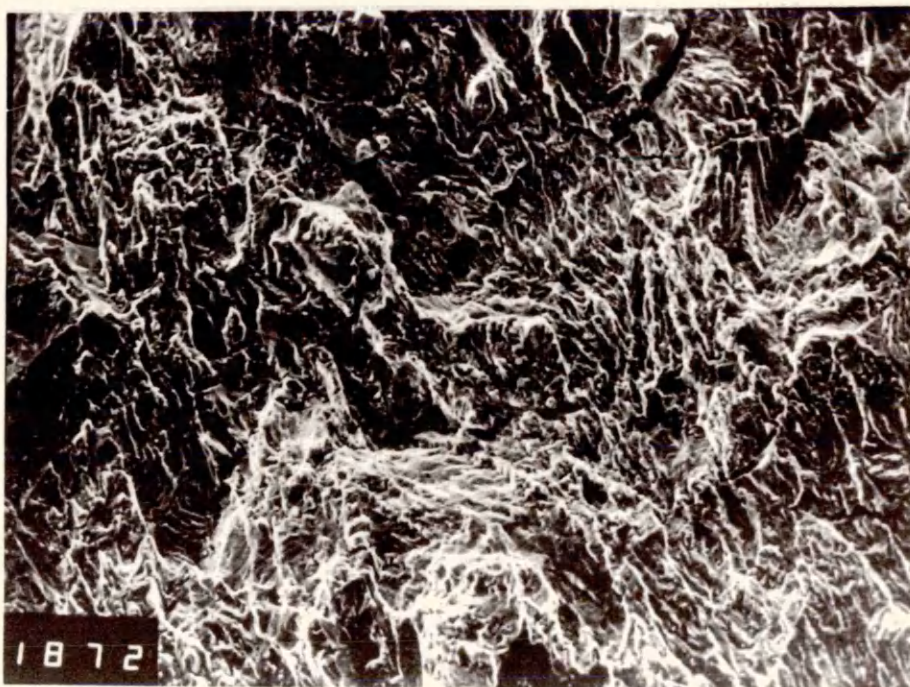
x 250

IS10 3 B1

Figure 88

(a) Features observed an fatigue freactue surface at
$\Delta K = 14.5$ MNm$^{-\frac{3}{2}}$ in material IS15(3)A2.

(b) Features observed on fatigue fracture surface at
$\Delta K = 19.4$ MNm$^{-\frac{3}{2}}$ in material IS15(3)B1.

x 250

IS15 3 A2
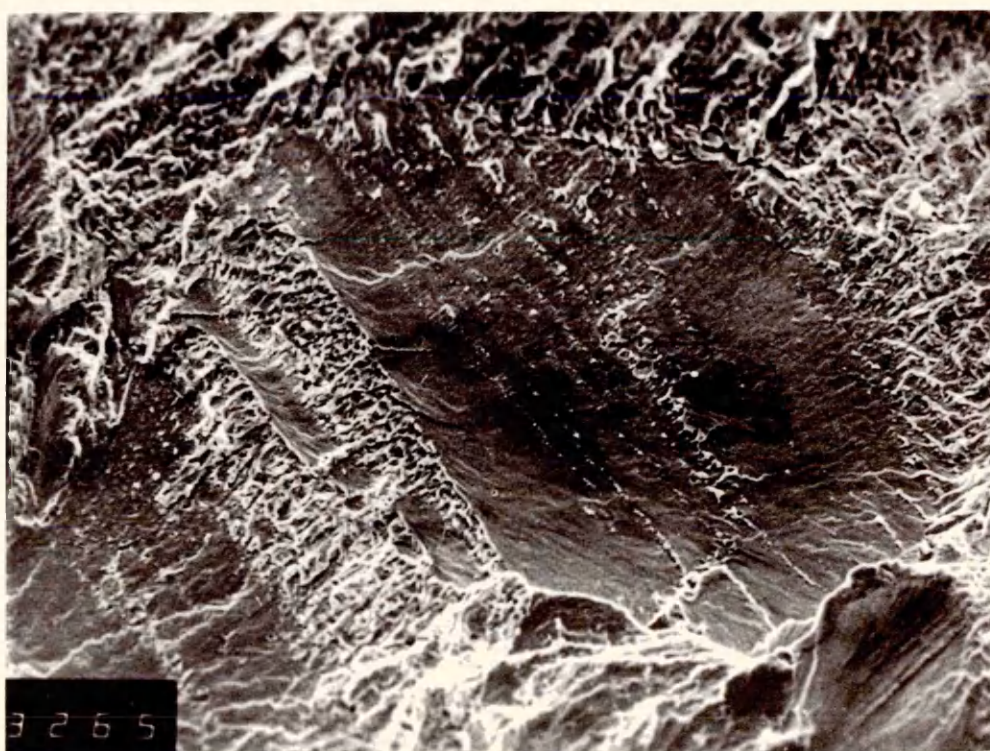
x 250

IS15 3 BI

Figure 89

    (a) Features observed on fatigue fracture surface
at $\Delta K = 14.0$ MNm$^{-\frac{3}{2}}$ in material IS20(1)A3.

    (b) Features observed on fatigue fracture surface
at $\Delta K = 14.0$ MNm$^{-\frac{3}{2}}$ in material IS20(1)A3.
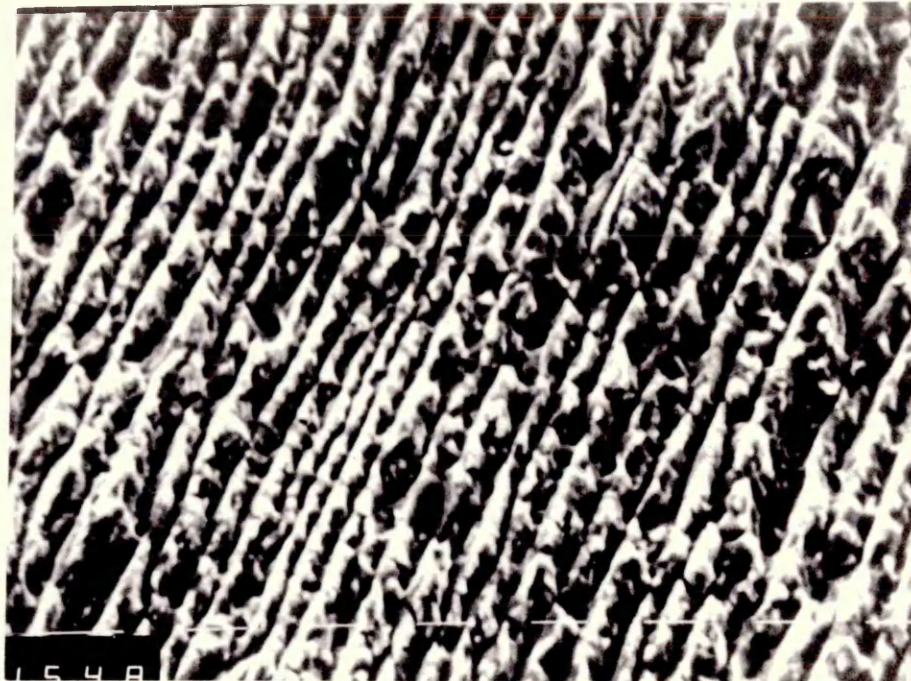
x 1600

IS20 I A3
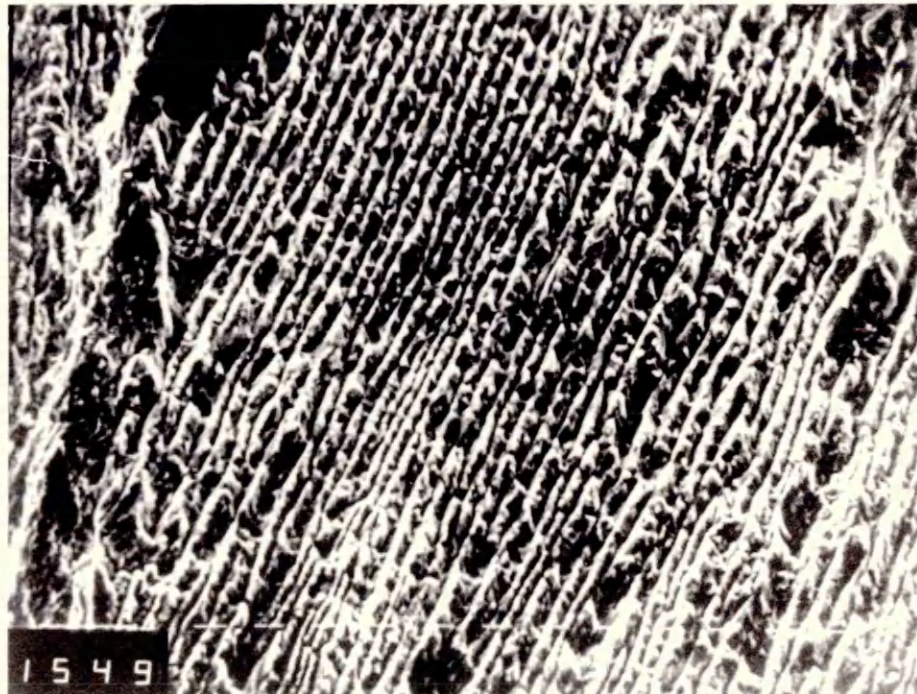
x 800

IS20 I A3

Figure 90

    (a)   Features observed on fatigue fracture surface at $\Delta K = 14.0$ MNm$^{-\frac{3}{2}}$ in material IS20(1)A2.

    (b)   Features observed on fatigue fracture surface at 14.0 MNm$^{-\frac{3}{2}}$ in material IS20(1)A2.

x 500

Direction of

Propagation

x 500

IS20 I A2

335
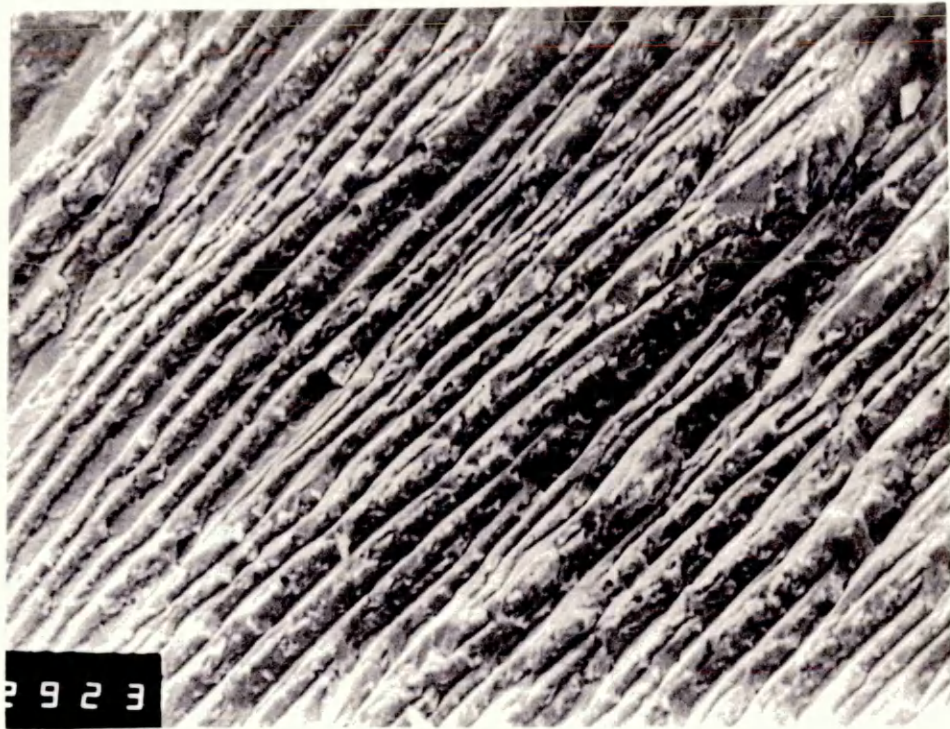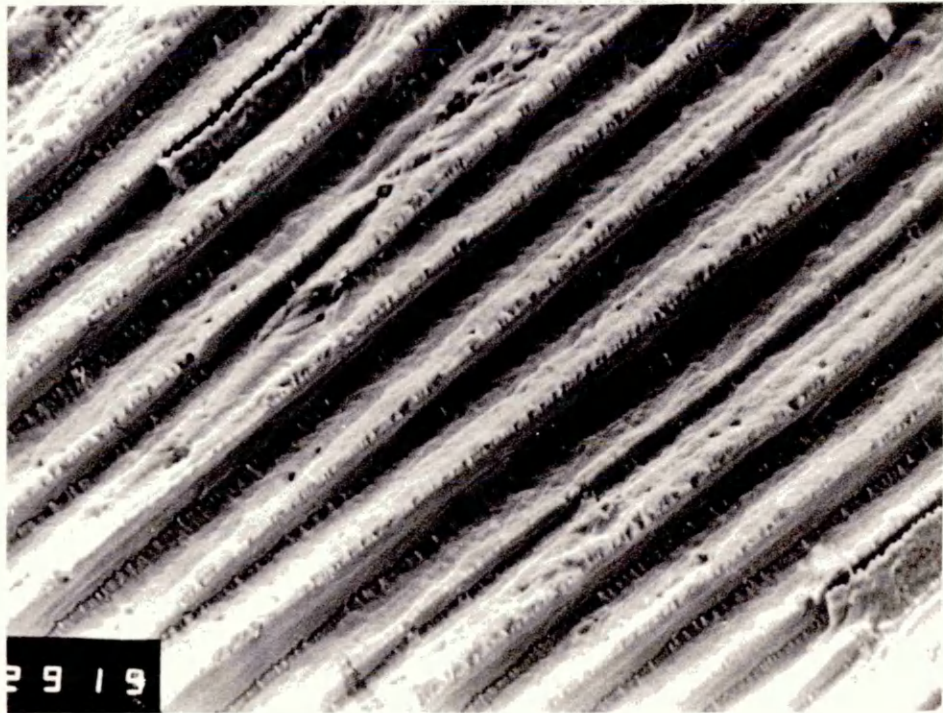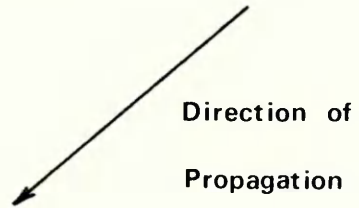
Figure 91

    (a)   Crack branching observed in material IS00(1)A1.

    (b)   Crack branching observed in material IS05(3)A1.
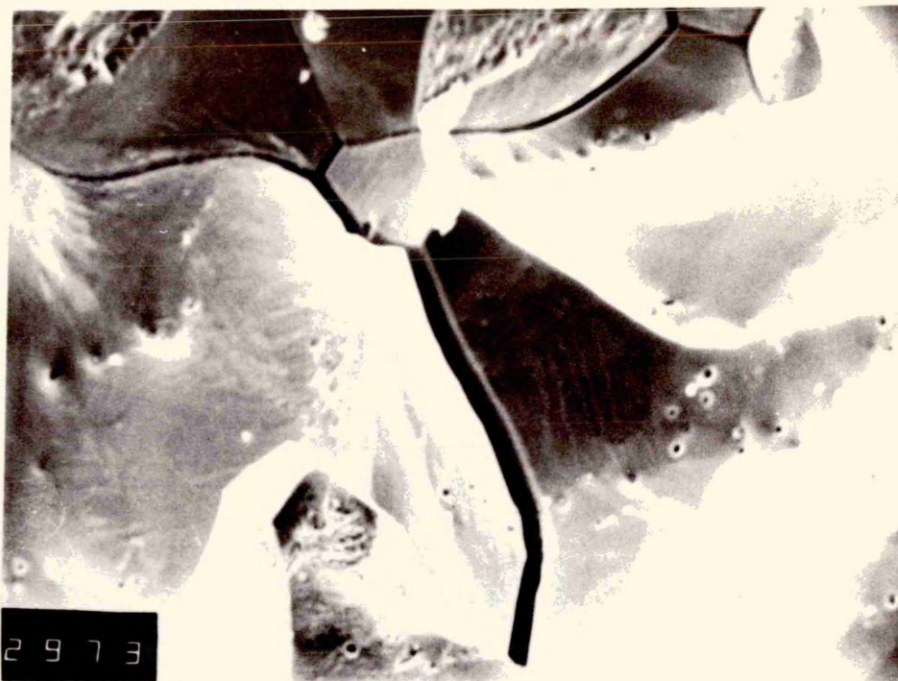
Direction of
Propagation

ΔK 10·6 MNm$^{-3/2}$ x 1000

IS00 1 A1
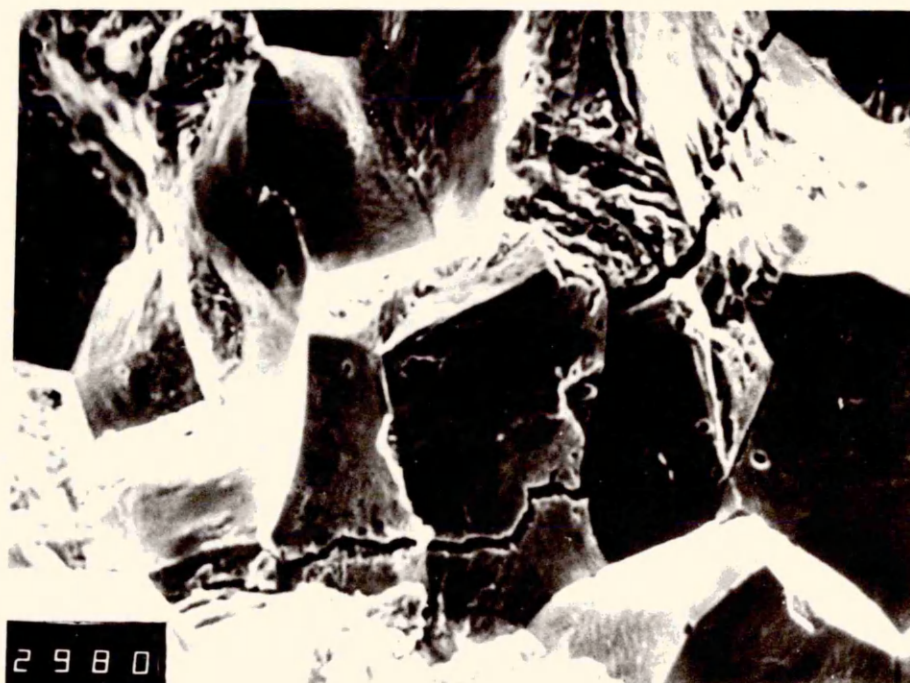
ΔK 12·0 MNm$^{-3/2}$ x 500

IS05 3 A1

337

Figure 92

    (a)   Crack branching observed at near threshold

          growth rates in material IS05(3)A3.

          $\Delta K = 13.2$ MNm$^{-\frac{3}{2}}$

    (b)   Crack branching observed at near threshold

          growth rates in material IS05(3)A3.

          $\Delta K = 13.4$ MNm$^{-\frac{3}{2}}$

x 400

Direction of

Propagation
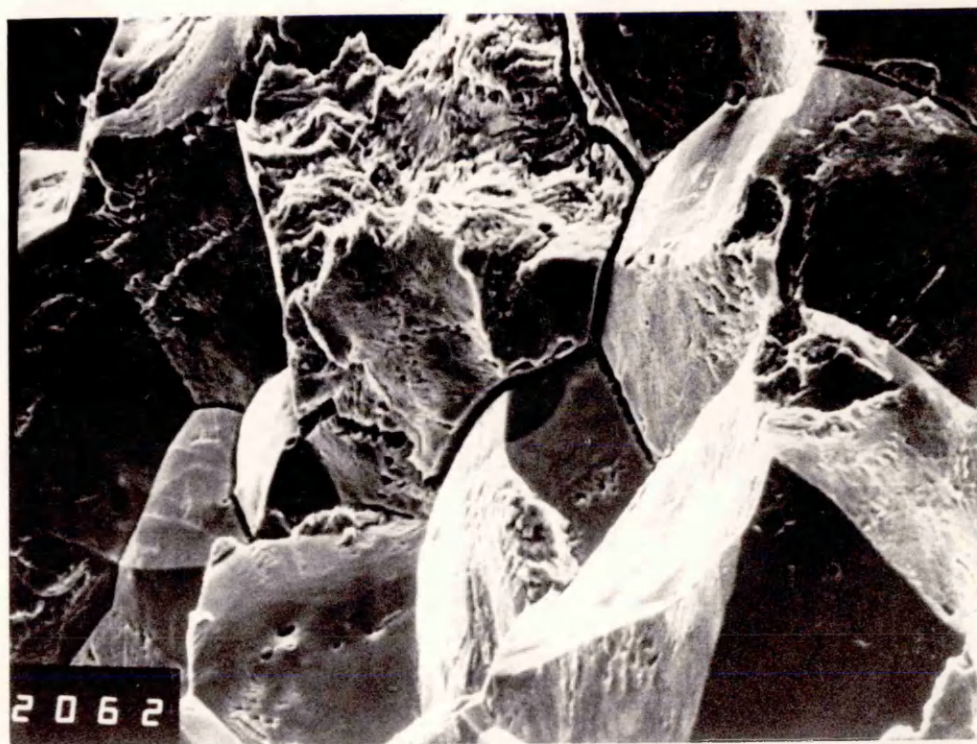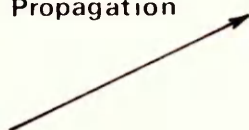
x 800

ISO5 3 A3

Figure 93

    (a)   Secondary cracking observed near the threshold

            in material IS15(3)B1.

    (b)   Secondary cracking observed at $\Delta K = 17$ MNm$^{-\frac{3}{2}}$

            in material IS10(3)B2.
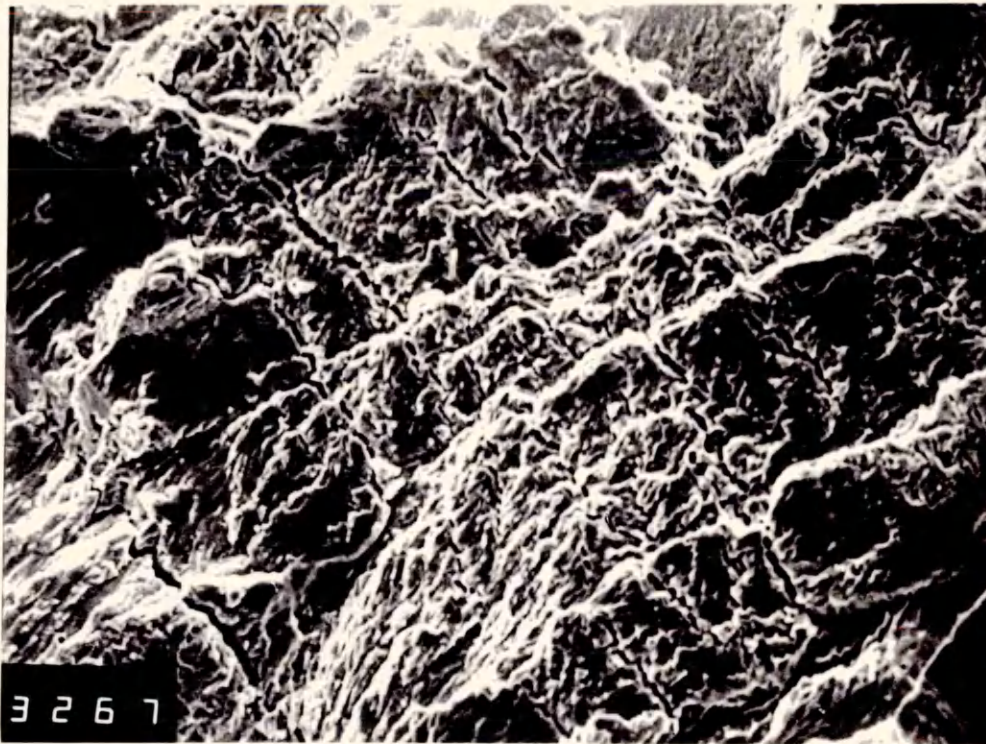
x 500

Direction of

Propagation

ISI5 3 BI
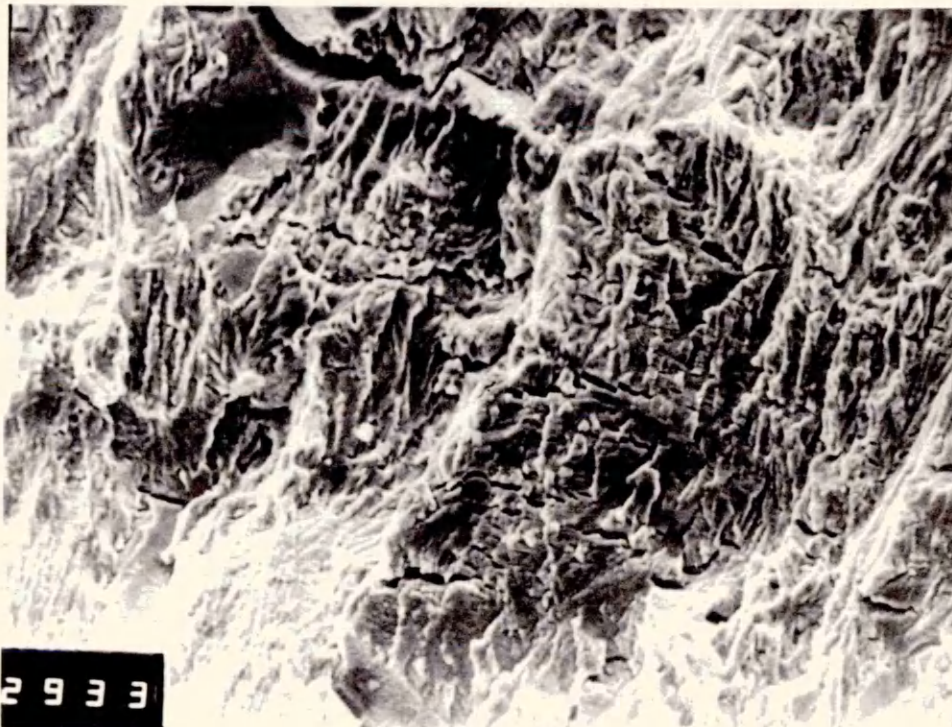
x 500

ISIO 3 B2

Figure 94

    (a)   Secondary cracking occurring both inter-
             granulary and transgranulary near the threshold
             in material IS10(3)B2.

    (b)   Secondary cracking occurring transgranulary
             at $\Delta K = 16.6$ MNm$^{-3/2}$ in material IS10(3)B2.
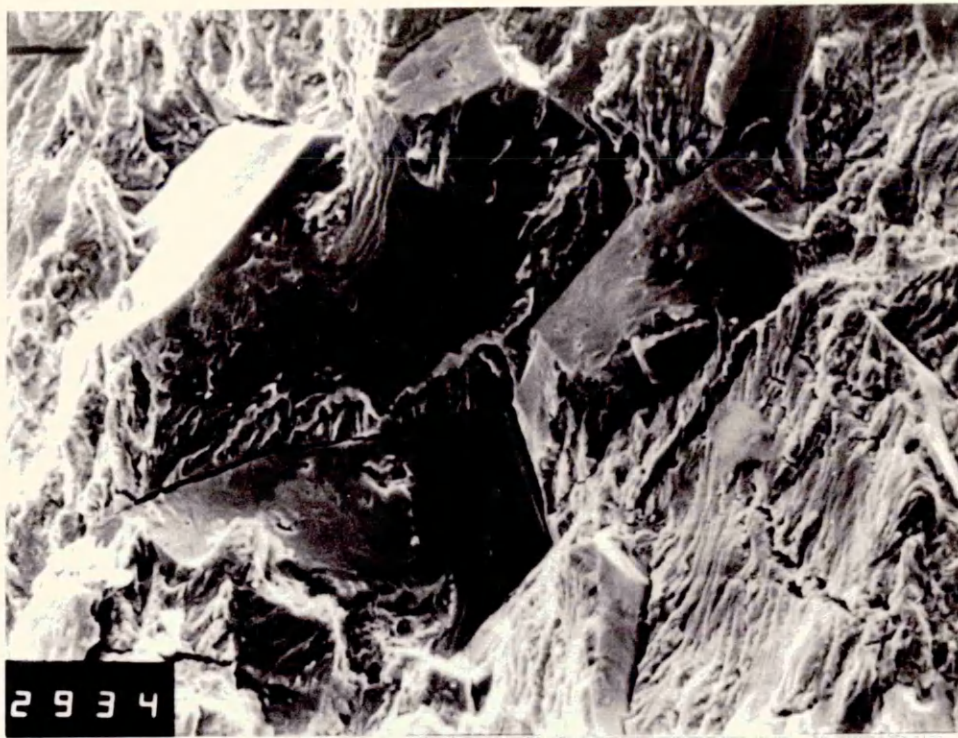
x 500

Direction of
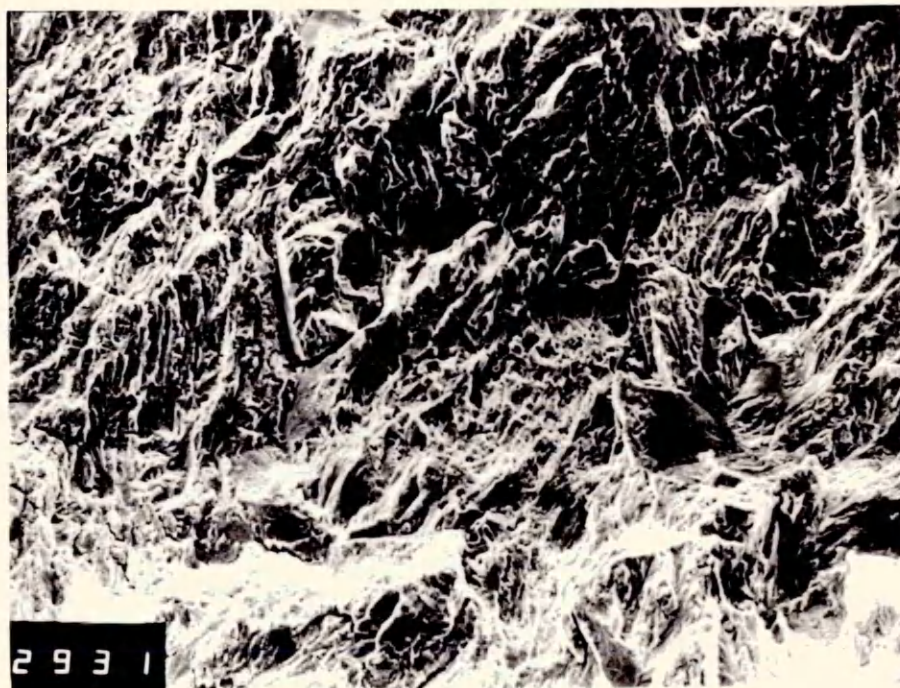
Propagation

x 300

ISIO 3 B2

Figure 95

    (a)   Crack profile observed in material IS00(1)A2.

    (b)   Complex crack profile observed in material
         IS00(1)B2.
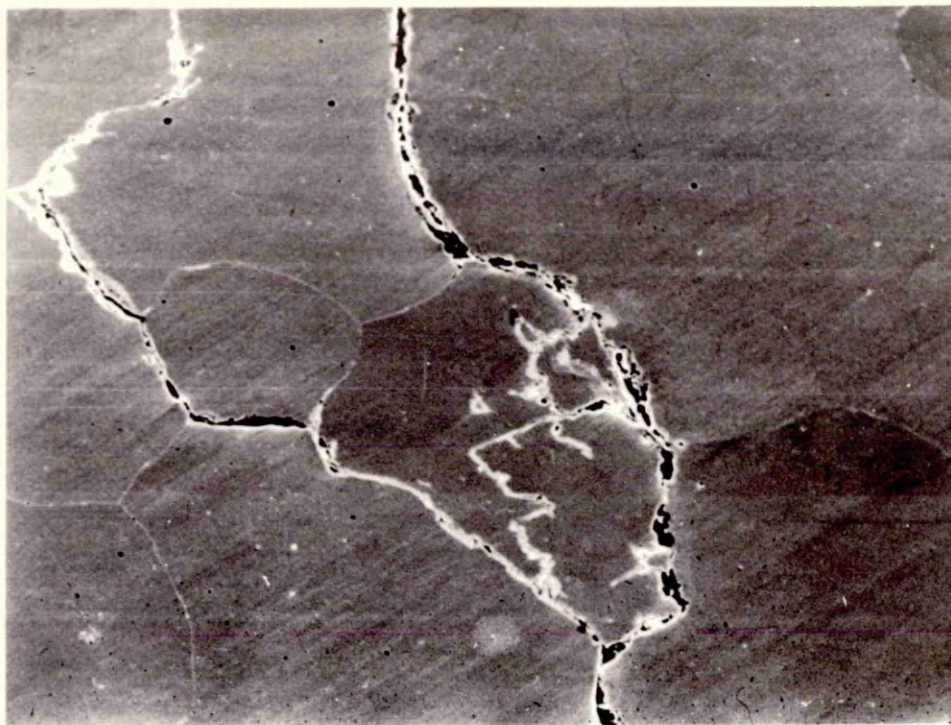
Direction of

Propagation

x150

ISOO I A2

x150

ISOO I B2

345
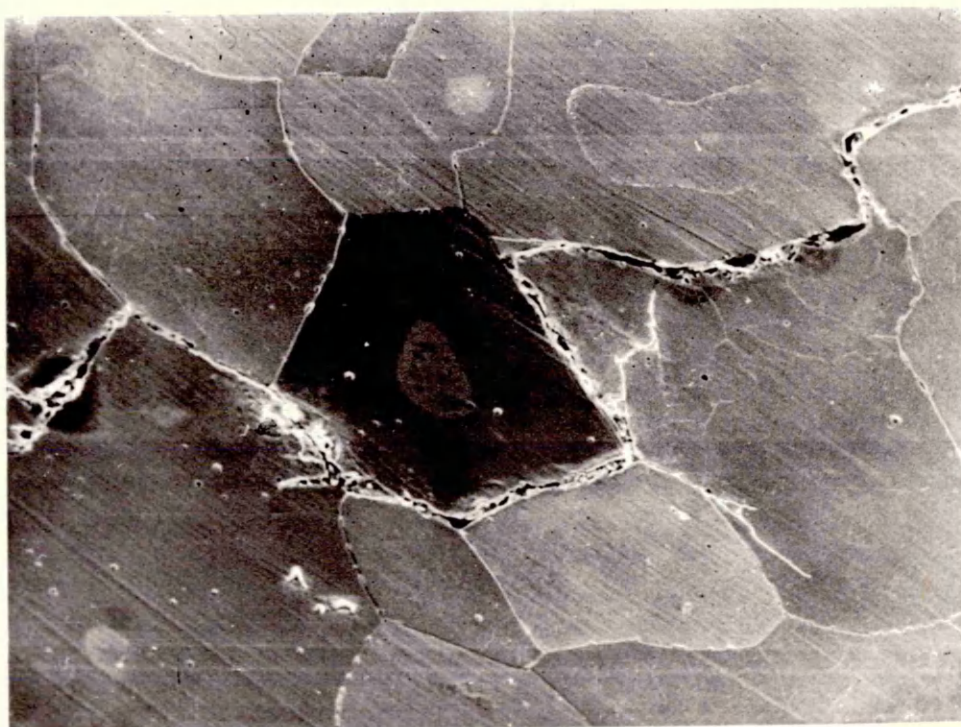
Figure 96

(a) Fatigue crack sensitivity to the presence of grain boundaries observed at $\Delta K = 16.4$ MNm$^{-\frac{3}{2}}$ in material IS15(3)A1.

(b) Fatigue crack sensitivity to the presence of gain boundaries observed at $\Delta K = 18.0$ MNm$^{-\frac{3}{2}}$ in material IS15(3)A1.

x 600

Direction of
Propagation
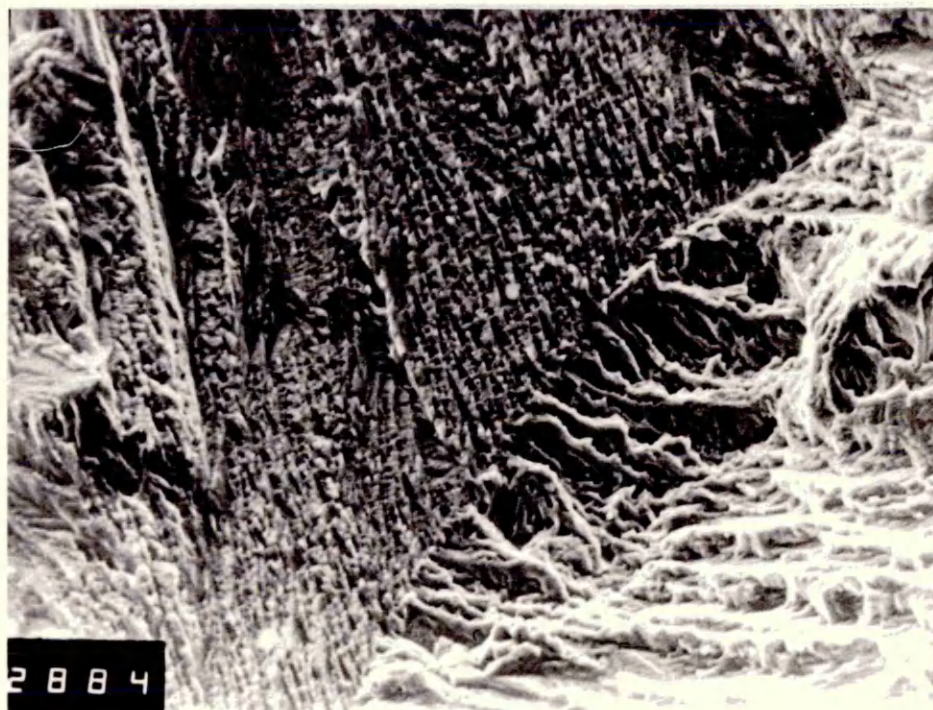
x 600

ISI5 3 AI

<u>FIGURE 97</u>

(a)   Striations observed at $\Delta K = 14.1$ MNm$^{-3/2}$
      in material IS20(1)A2.

(b)   Striations observed at $\Delta K = 14.1$ MNm$^{-3/2}$
      in material IS20(1)A2.
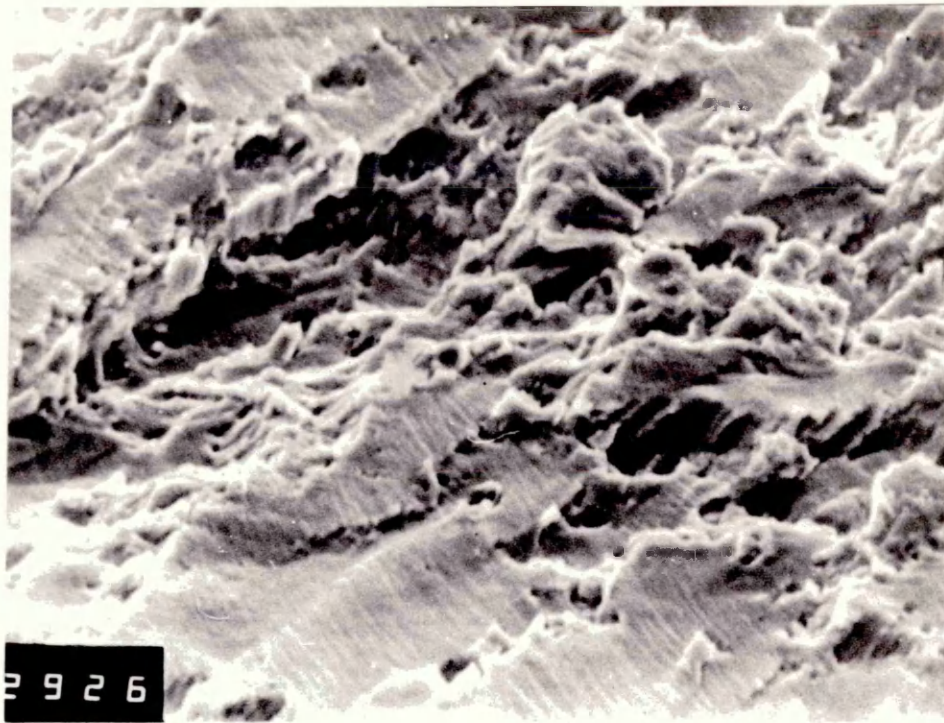
x 2100

Direction of

Propagation
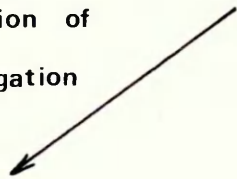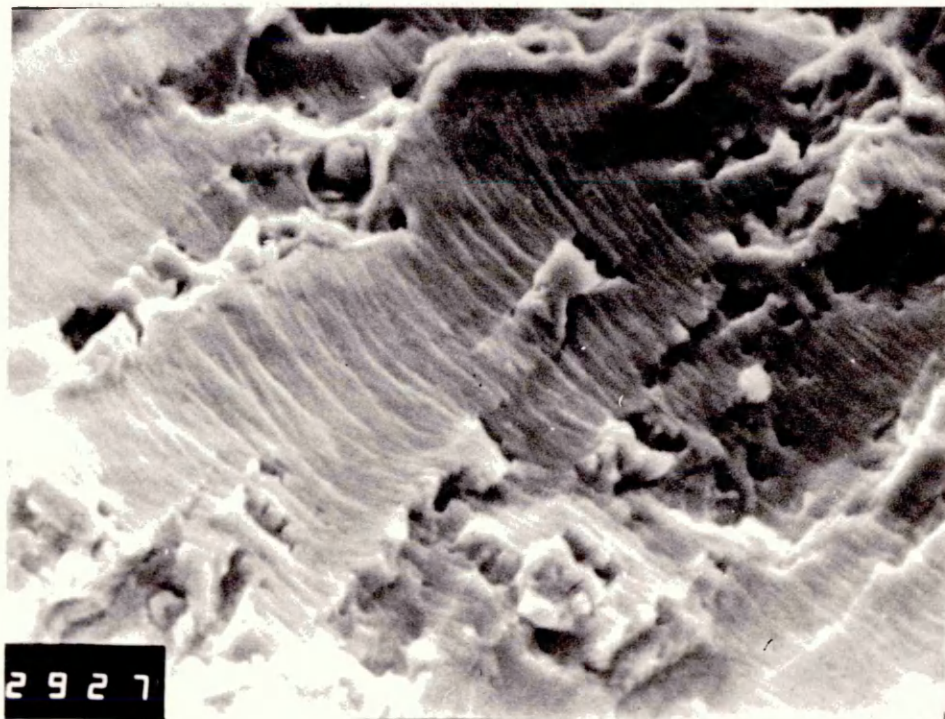
x 4200

IS20 I A2

FIGURE 98

    (a)   Detached particles of material observed on
fracture surface at near threshold values in
material IS20(1)A2.

    (b)   Detached particles of material observed on
fracture surface at higher ΔK values in
material IS15(3)B3.
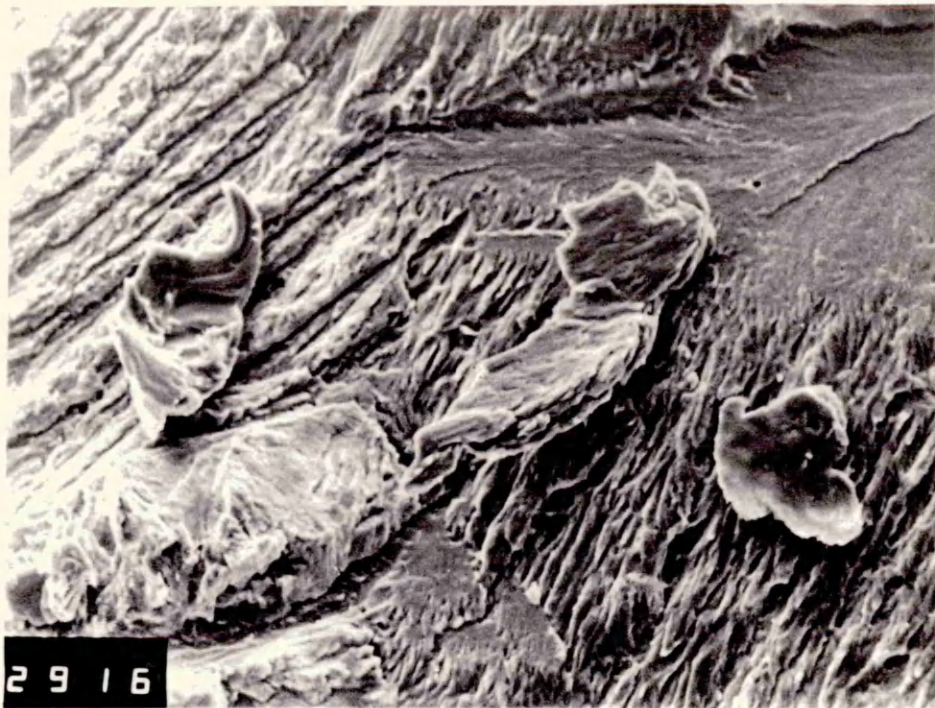
x 500

Direction of

Propagation

IS20 I A2

x 500

IS15 3 B3

351

Figure 99

    (a) Rough intergranular facets observed in material
          IS15(3)A1.

    (b) Rough intergranular facets observed in material
          IS15(3)B1.
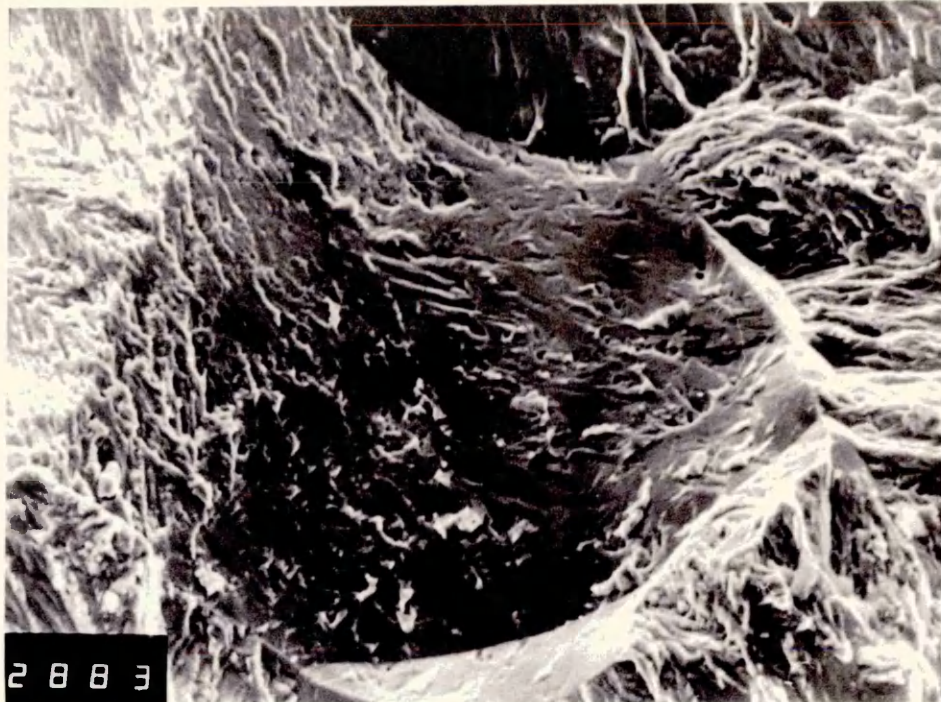
x 600

Direction of

Propagation

ISI5 3 AI

x 1000

ISI5 3 BI

Figure 100

Proportion of transgranular failure produced during
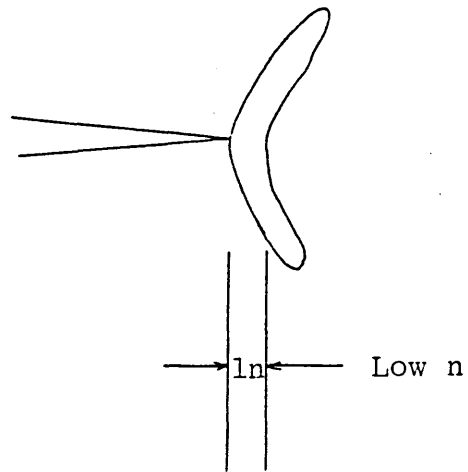fatigue testing as a function of stress intensity
range, ΔK.
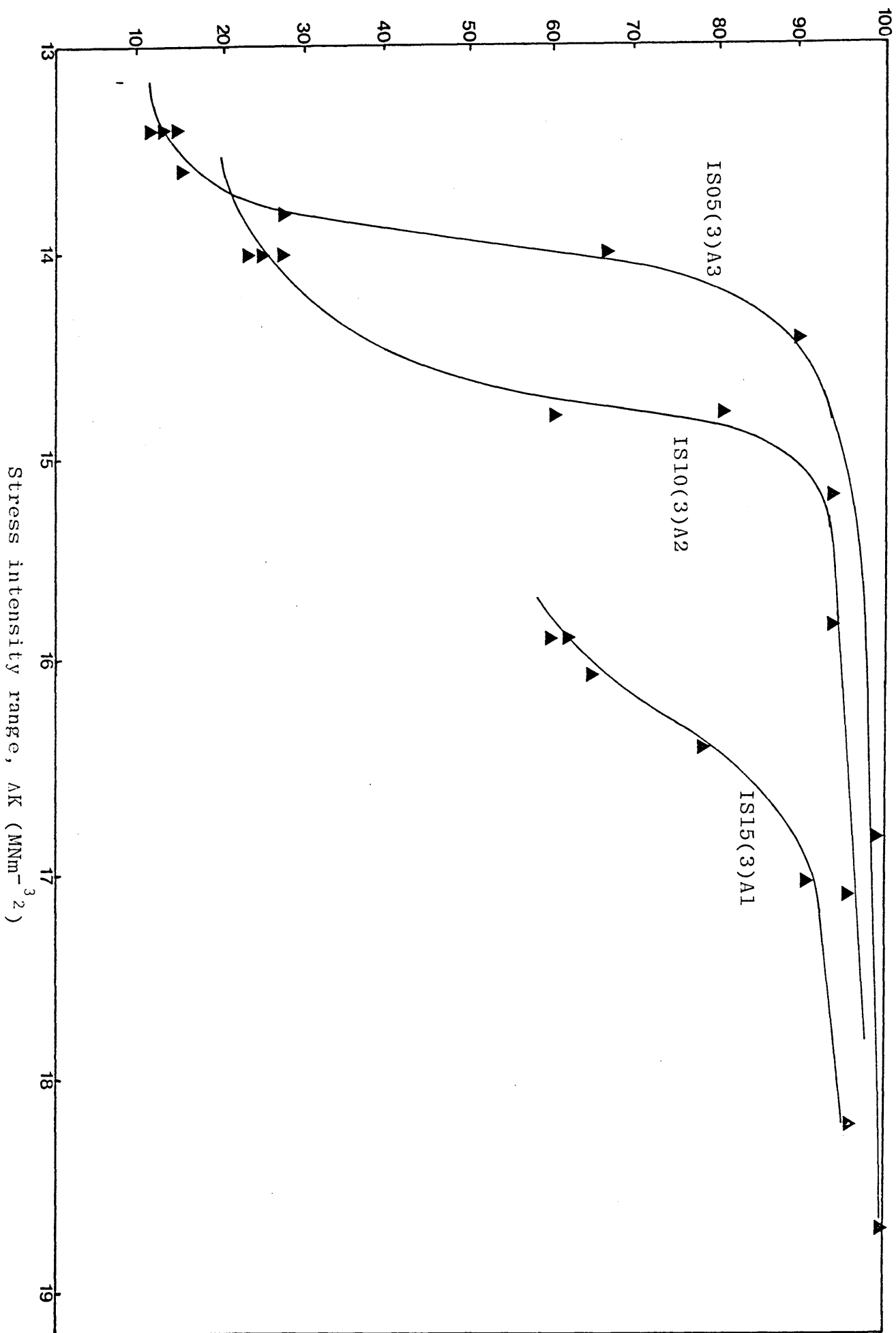
Figure 101

Relationship between strain hardening exponent, n
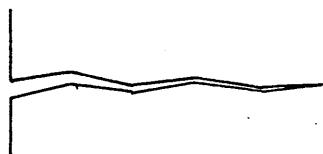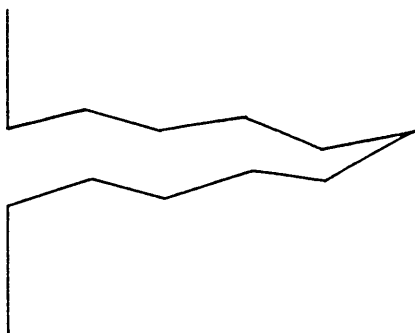and the width of the yield zone, ln.

Low n

High n
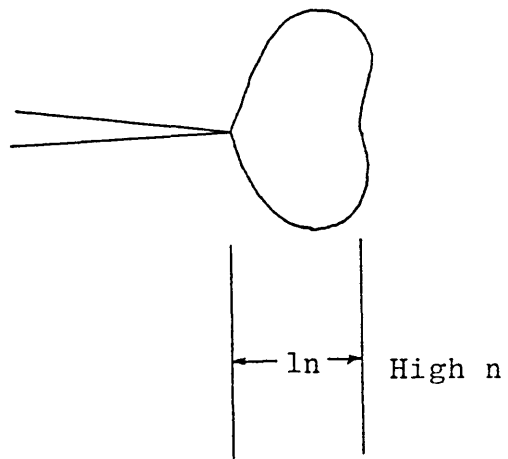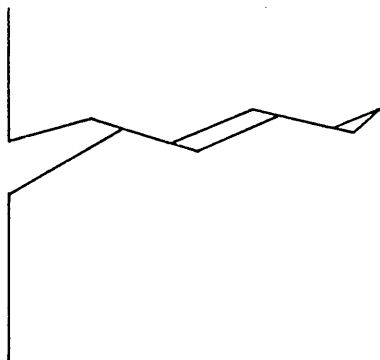
ln proportional to n

Figure 102

    Mode II displacements leading to wedging open of

the crack.

K min

Crack opening and
Contribution of mode
II opening.

K min
Crack wedged open
at contact points.